HEAT TRANSFER AND THE UNIDIRECTIONAL SOLIDIFICATION OF METALS AND ALLOYS

A thesis
presented for the
Diploma of Imperial College

by

ELIEZER SPINAT

SEPTEMBER 1971

John Percy Research Group in
Process Metallurgy,
Royal School of Mines,
Imperial College of Science
and Technology,
LONDON, S.W.7.

ABSTRACT

A pure metal, eutectic alloys and alloys which freeze over a range of temperatures were solidified in an apparatus which was designed to ensure that one dimensional heat flow occurred during solidification. Heat was removed from the casting by convection and the heat transfer coefficient was assumed to be constant.

The rates of solidification and the temperature variations in each system were determined at various degrees of superheat over a range of heat transfer coefficients.

The systems investigated were:

1) Aluminium; 2) Al-$CUAl_2$; Al-si and Fe-C-P eutectics; 3) Al-4% cu, Al-8% cu and Al-30% cu binary alloys.

The experimental results for the pure metal and for the eutectic alloys were compared with predictions from an integral profile solutions. The results for binary alloys which freeze over a range of temperatures were compared with a modified integral profile solution. This solution assumed a Scheil type distribution of the solid fraction in the liquid and used this distribution to develop an enthalpy function describing the latent heat effect in the two phase region. The theoretical predictions from both types of solution agreed satisfactorily with the experimental results.

The effects of constant growth rates during unidirectional solidification of eutectic alloys on the structure and properties of the ingots were observed. This study involved solidification of lead-tin eutectic in addition to the three eutectic alloys mentioned above.

TABLE OF CONTENTS

LIST OF FIGURES

LIST OF TABLES

LIST OF PLATES

CHAPTER 1

INTRODUCTION

CHAPTER 1

INTRODUCTION

Problems associated with heat flow during casting processes have long been the subject of reasearch, both fundamental and applied and this investigation is similarly divided.

The fundamental part of the work presented here is concerned with unidirectional solidification under conditions where heat is removed from the cooled surface of the solidifying metal by convection, the heat-transfer coefficient between the cooled surface and the cooling media remaining constant. The fundamental part can be further divided into three sections.

1) Investigations involving the determination of solidification rates and temperature distributions in metalic systems, the results being compared with predictions made by an integral profile solution to the unsteady state heat transfer equation.

   The systems investigated were pure aluminium, aluminium-cuAl_2 and aluminium-silicon binary eutectics and the iron-carbon-phosphorus ternary eutectic.

2) The development of an extended integral profile solution to predict the rate at which the solidus and liquidus of a binary-freezing-range alloy move through the melt, with and without superheats and to predict the resulting temperature distribution in an ingot. The binary alloys investigated were aluminium-copper alloys of three compositions: 4%.,8% and 30% copper. The equations were solved numerically using Fortran IV language . The computer programme used is presented in Section 3.4 of the thesis and the computations were carried out on the Imperial College I.B.M. 7094 computer.

3) The determination of heat transfer coefficients in an independent experimental investigation is reported in Chapters 4 and 5 of the thesis.

Applied research is usually concerned with the effect that the rate of heat removed from the mould has on the structural changes that occur during and after solidification and on the resulting mechanical properties and soundness of a casting.

In the investigation presented here, eutectic alloys were unidirectionally solidified at constant rates without superheat, theoretically predicted variations in heat transfer coefficient at the cooled surface being used to control the growth rates. The solidified ingots were subsequently sectioned an examined microscopically and specimens were tested in tension. Lead-tin eutectic was used in this part of the work in addition to the three other eutectic systems mentioned above.

In the following Chapter, a brief review of previous work on the subject is presented. Chapter 3 deals with the development of the theories and with the methods of solution. The experimental apparatus is described in Chapter 4 and results are reported in Chapter 5. The whole project is discussed in Chapter 6 and conclusions are drawn in Chapter 7.

CHAPTER 2

REVIEW OF PREVIOUS WORK

CHAPTER 2

REVIEW OF PREVIOUS WORK

2.1 Theoretical Solutions

Stefan's problem, which deals with one dimensional heat flow during solidification or melting of a material, has been the subject of numerous theoretical investigations. These can be divided into two broad categories.

a) Approximate mathematical solutions using realistic or almost realistic solidification conditions, and

b) Exact solutions under conditions rarely achieved in practice.

2.1.1 Approximate solutions

The approximate solutions to problems of solidification involve the use of an integral profile approach or a finite differences method. Hills' (1) integral profile solution for solidification of pure metals has been used in the development of the theory presented in Chapter 3 and a full account of it is given below.

An integral profile approach to the solidification of alloys was used by Tien and Geiger (23) who assumed in their treatment that the cooled surface remained at a constant temperature below the solidus through out the solidification process. This unrealistic boundary condition has been replaced in a subsequent solution given by the same authors (10) and by Koump and Tien (22), by a time dependent surface temperature. In all of their solutions, a combination of finite differences method with Goodmans' heat balance integral (25) is used. A heat generation term is

employed to account for the heat liberated in the partially solidified layer. This term includes a polynomial of the nth order describing the variations of solid fraction with distance across the layer. The coefficients of the polynomial are evaluated by a curve fitting procedure using a least square method. Pfans' equation is used to evaluate the constant-FSU. All the solutions mentioned so far apply only to solidification at zero superheat and assume constant physical and thermal properties. In comparing the theoretical predictions with measured values, using a series of aluminium-copper alloys (9), only qualitative agreement was established. In a recent theoretical treatment they attributed some of the differences between theory and practice to flow of liquid during solidification (24). This flow results from density differences between the solid and the liquid in the two phase region. In the solutions where density differences are taken into account, temperature distributions are higher than in those where solid and liquid densities are equal at any given time. A finite differences solution to alloy solidification has been given recently by Campagna (26), who has assumed the solid fraction, and hence the latent heat to vary linearly across the partial layer. The concept of 'moving boundaries' is used, permitting to take into the account heat released at the eutectic. Finite difference methods used in previous solutions (21, 27, 28, 29) have treated the latent heat as an effective addition to the specific heat of the alloy and assumed also a uniform distribution of the solid fraction across the partial layer. Heat released at discreet temperatures cannot be treated directly in those solutions. Malhotra (16) has also modified his thermal capacity term to indluce the latent heat using a linear solid fraction distribution in a modification to Hills' integral profile solution. An integral profile technique (30) was developed by Goodman and Shea for problems involving melting with a

constant surface heat flux. The metal slab considered could either have its remote surface insulated or maintained at a constant temperature. This solution could be modified to solve solidification problems of pure metals with superheat.

2.1.1.1 Hills' generalised integral profile solution

Hills developed this solution for predicting solid thickness and surface temperature variations during solidification of pure metals. The solution presented in Chapter 3, for solidification problems involving alloys, uses Hills' integral profile solution to predict the rate at which the solidus moves. For clarity Hills' solution is presented here in full.

Consider the solid layer presented in Fig. 3.1. The temperature variations within it must satisfy the unsteady state heat conduction equation:

$$K_s \frac{\partial^2 \theta}{\partial x^2} = \rho_s C_s \frac{\partial \theta}{\partial T} \qquad (2.1.1.1)$$

Integrating equation (2.1.1.1) across the solid layer:

$$K \left(\frac{\partial \theta}{\partial x}\right)_{s,t} - K \left(\frac{\partial \theta}{\partial x}\right)_{s,o} = \frac{d}{dT} \left\{ \int_{x=o}^{x=ts} \rho_s C_s \theta \, dx \right\} - \rho_s C_s \frac{dt_s}{dT} \theta(s,t) \qquad (2.1.1.2)$$

conservation of heat at the boundaries yields:

$$K \left(\frac{\partial \theta}{\partial x}\right)_{s,o} = - \dot{q}''(s,o) = - \dot{q}''_o \qquad (2.1.1.3)$$

and

$$K \left(\frac{\partial \theta}{\partial x}\right)_{s,t} = - \dot{q}''(s,t) + \rho_s H_s \frac{dts}{dT} \qquad (2.1.1.4)$$

The boundary conditions are:

at $x = 0$: $\theta = \theta_o$

at $x = ts$: $\theta = \theta_s$ = constant.

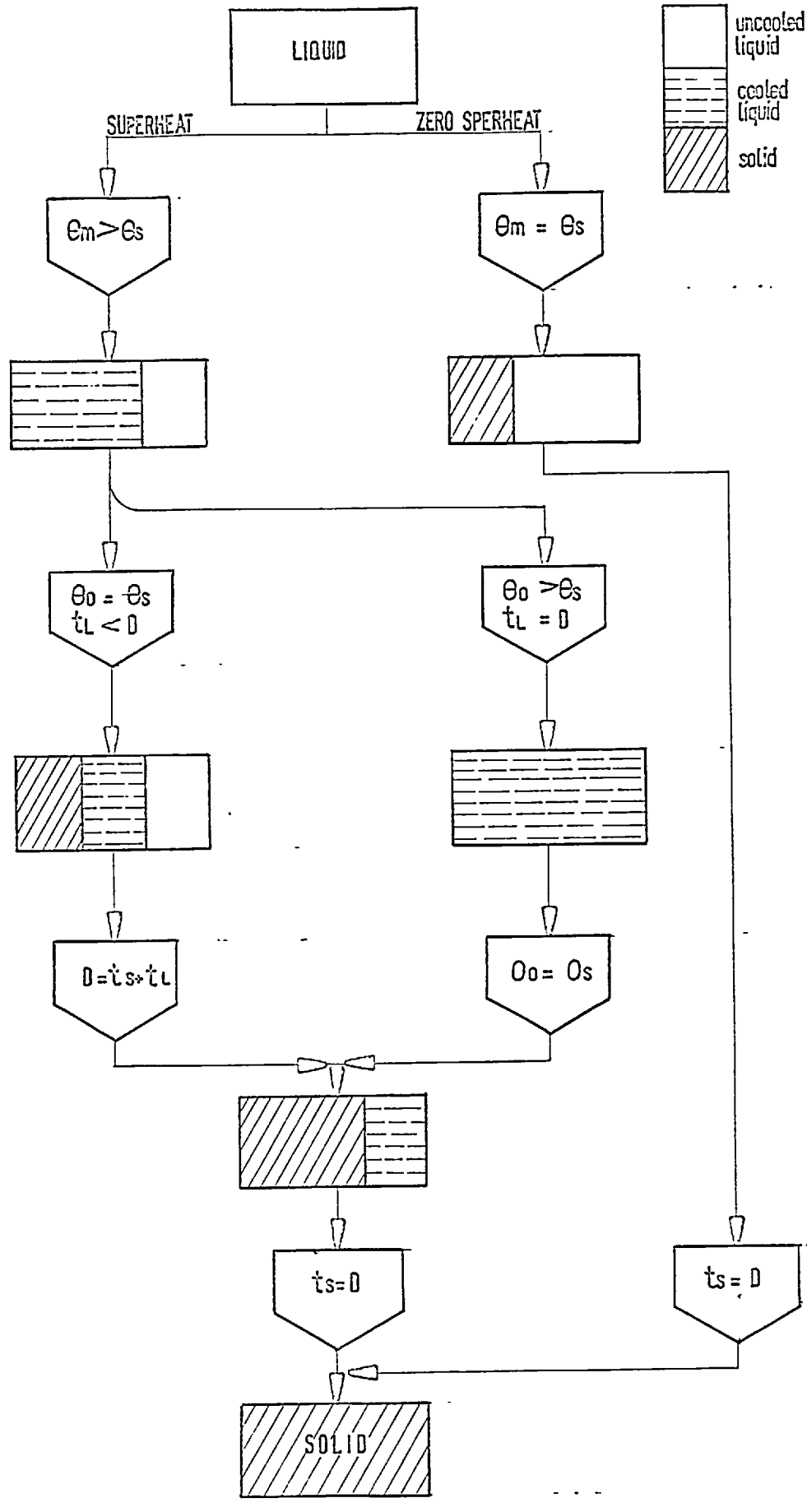

Fig 2.1 SOLIDIFICATION ALGORITHM FOR PURE METALS

The temperature distribution appearing in the integral in equation (2.1.1.2) is unknown, but it can be represented approximately by an auxiliary function chosen to satisfy the boundary conditions given above and so that it's differential will satisfy equation (2.1.1.3) i.e.

$$\theta = \theta_o - \frac{\dot{q}''_o}{K_s}\left(\frac{x}{t}\right) + \left[\theta_s - \theta_o + \frac{\dot{q}''_o}{K_s}\, t_s\right]\left(\frac{x}{t}\right)^2 \qquad (2.1.1.5)$$

Substituting from equations (2.1.1.5), (2.1.1.3) and (2.1.1.4) into equation (2.1.1.2), integrating and rearranging:

$$\left\{\rho_s H_s + \tfrac{1}{3}\rho_s C_s\left[2(\theta_s - \theta_o) + \frac{\dot{q}''_o t_s}{K_s}\right]\right\}\frac{dt_s}{dT} - \frac{2}{3}t_s C_s \rho_s \frac{d\theta_o}{dT} +$$

$$\frac{\frac{1}{6}t_s^2 \rho_s C_s}{K_s} \cdot \frac{dq^*_o}{dT} = -(\dot{q}''_o - \dot{q}''_s) \qquad (2.1.1.6)$$

Equation (2.1.1.6) can be re-written in dimensionless terms i.e.

$$\left\{H^* + \tfrac{2}{3}(\theta^*_o - 1) - \tfrac{1}{3}(t^*_s q^*_o)\right\}\frac{dt^*_s}{d\xi} - \tfrac{2}{3}t^*_s \frac{d\theta^*_o}{d\xi} - \frac{1}{6}t^{*2}_s \frac{dq^*_o}{d\xi} = q^*_o - q^*_s \qquad (2.1.1.7)$$

An additional equation for the cooled surface temperature variations is derived by considering the variations of $\frac{\partial\theta}{\partial T}$ across the solidified layer. At the stationery surface $x = 0$

$$\left(\frac{\partial\theta}{\partial T}\right)_{s,o} = \frac{d\theta_o}{dT} \qquad (2.1.1.8)$$

At the moving boundary $x = t$: $\theta = \theta_s$ = constant

hence:

$$\frac{d}{dT}\left[\theta(t,T)\right] = \left(\frac{\partial\theta}{\partial x}\right)_{s,t}\frac{dt_s}{dT} + \left(\frac{\partial\theta}{\partial T}\right)_{s,t} = 0 \qquad (2.1.1.9)$$

Substituting into equation (2.1.1.9) from equation (2.1.1.4) and rearranging

$$\left(\frac{\partial\theta}{\partial T}\right)_{s,t} = -\frac{dt_s}{dT}\left[\rho_s H_s \frac{dt_s}{dT} - \frac{\dot{q}''_o}{k_s}\right] \qquad (2.1.1.10)$$

Differentiating equation (2.1.1.1) yields:

$$\left(\frac{\partial \theta}{\partial T}\right)_{s,t} - \left(\frac{\partial \theta}{\partial T}\right)_{s,o} = \frac{k_s}{\rho_s c_s} \left\{\left(\frac{\partial^2 \theta}{\partial x^2}\right)_{s,t} - \left(\frac{\partial^2 \theta}{\partial x^2}\right)_{s,o}\right\}$$

$$= \frac{k_s}{\rho_s c_s} \int_{x=o}^{x=t_s} \frac{\partial^3 \theta}{\partial x^3}\, dx \qquad (2.1.1.11)$$

Without sudden changes in cooling conditions, $\frac{\partial \theta}{\partial x}$ will not change very much across the layer and its variations are assumed to be linear. Hence $\frac{\partial^3 \theta}{\partial x^3}$ is a constant and we have

$$\int_{x=o}^{x=ts} \left(\frac{\partial 3\theta}{\partial x^3}\right) dx = \left(\frac{\partial^3 \theta}{\partial x^3}\right)_{s,o} \int_{x=o}^{x=ts} dx = t_s \left(\frac{\partial^3 \theta}{\partial x^3}\right)_{s,o} \qquad (2.1.1.12)$$

Differentiating equation (2.1.1.1) with respect to x yields

$$-\frac{dt_s}{dT}\left(\frac{\rho_s H_s}{k_s} - \frac{\dot{q}''_s}{k_s}\right) - \frac{d\theta_o}{dT} = \frac{t_s}{k_s}\frac{d\dot{q}''_o}{dT} \qquad (2.1.1.15)$$

Equation (2.1.1.15) can be re-written in dimensionless terms to give

$$\frac{d\theta^*_s}{d\xi} = -H^*\left(\frac{dt^*_s}{d\xi}\right)^2 - q^*_s\left(\frac{dt^*_s}{d\xi}\right) - t^*_s \frac{dq^*_o}{d\xi} \qquad (2.1.1.16)$$

In general, the heat flux from the cooled surface will be a function of surface temperature or of time or of both i.e.

$$q^*_o = f(\theta^*_o : \xi) \qquad (2.1.1.17)$$

and

$$\frac{dq^*_o}{d\xi} = \frac{\partial q^*_o}{\partial \theta^*_o} \cdot \frac{d\theta^*_o}{d\xi} + \frac{\partial q^*_o}{\partial \xi} = f'\theta \frac{d\theta^*_o}{d\xi} + f'\xi \qquad (2.1.1.18)$$

Rearranging equations (2.1.1.16) and (2.1.1.18):

$$\frac{d\theta^*_s}{d\xi} = -\frac{H^*\left(\frac{dt^*_s}{d\xi}\right)^2 + q^*_s \frac{dt^*_s}{d\xi} + t^*_s f'\xi}{1 + t^*_s f'\theta} \qquad (2.1.1.19)$$

and

$$\frac{dt^*_s}{d\xi} = \frac{2\Lambda}{\Gamma + \sqrt{\Gamma^2 + 4\Lambda\vartheta}} \qquad (2.1.1.20)$$

where

$$\mathcal{R} = H^*_s t^*_s \left(4 + t^*_s f'\theta\right) \qquad (2.1.1.21)$$

$$\Gamma = \left[6H^*_s + 4(1-\theta^*_o) - 2t^*_s q^*_o\right]\left(1+t^*_s f'\theta\right)+q^*_s t^*_s\left(4+t^*_s f'\theta\right) \qquad (2.1.1.22)$$

$$\Delta = 6(q^*_o - q^*_s)(1-t^*_s f'\theta)-3t^{*2}_s f'\xi \qquad (2.1.1.23)$$

2.1.1.2 Exact Solutions

A review covering several exact solutions is given by Ruddle (4). Some solutions, the most important of which is Neuman's are discussed by Carslow and Jaeger (13). As already mentioned, all the exact solutions employ simplifying assumptions. Neuman's solution concerns a semi-infinite body. Goddman (31), gives a solution where the surface temperature is constant. Other solutions consider the temperature to vary by some empirical function of time. Recently Cho and Sunderland (11) presented an exact solution to heat conduction problems with melting and freezing of alloys. They give solutions to the temperature distribution and to the rate of change of phases for a semi-infinite body. The surface temperature drops instantaneously to a value at which it is kept constant.

2.2 Experimental Techniques

2.2.1 Experimental techniques used in the study of the progress of solidification.

The most common experimental techniques used to study the progress of solidification are: 'Dip-Stick', 'pour-out', ultrasonic testing, X-ray observations, thermal analysis and foreign additives.

In the dip stick method, a rod is dipped into the molten metal at various time intervals and the position of the solid liquid interface is determined from the direct contact with the rod.

The pour out technique involves decanting of the liquid at measured time intervals. The solid left in the mould indicates the position of the solidification front at the time of pour out.

In the former method, interferences due to the sticks' motion may introduce errors, and in the latter case only pure metals can be investigated. The ultrasonic method uses the different sound effect produced by the waves when travelling through solid and liquid regions.

X-ray techniques are used to enable the direct observation of the interface between solid and liquid and its motion during the process of solidification.

The addition of isotopes or foreign substances, metallic or non-metallic, to the melt, followed by subsequent sectioning is a technique that is also commonly used.

Thermal analysis was used in this work .It is a useful method as it gives direct information about the temperature distribution at any time during the process, from which the thermal and physical histories of the ingot can be determined. It is relatively cheap and accurate. A review of various techniques has been given by Ruddle (4), and more recently, Malhotra (16) discussed their relative merits.

2.2.2 Experimental techniques in controlling the growth of eutectics

The controlled growth of eutectics at constant solidification rates is normally achieved by relative motion between the furnace and the mould. The rate of relative motion controls the rate of solidification the metal being quenched by water cooled chills. The temperature gradient imposed in the melt in front of the moving interface is controlled by the distance between the heating device and the quench (34). Most designs involve vertical moulds but horizontal solidification techniques are also used (35). The moulds are usually made of graphite, the eutectics prepared from super pure metals, and the experiments conducted under an inert atmosphere (argon or helium).

Ingot lengths vary considerably, the cross section is either square or round and normally does not exceed one inch in thickness.

Structural studies relating to eutectics have been carried out under a microscope (36) in which organic systems analogous to metallic systems have been solidified in transparent cells. The results of these experiments have been used to explain the structures of metallic eutectics.

2.3 The Structure of Eutectics

Eutectic alloys are usually subdivided into three groups according to their microstructure i.e.

a) continuous microstructure.

The phases that constitute the eutectics in this category are continuous in the growth direction. i.e. lamellar and rod like structures. The Al-$CUAl_2$ structure is an example of a lamellar eutectic and Pb-Sn eutectic alloys usually possess a rod-like mictrostructure.

b) discontinuous microstructure (apparent)*

The structure of Al-Si eutectics is an example of this type of microstructure, where one phase is continuous in all directions and the other phase id dispersed through it. A similar type of structure is displayed by iron-carbon alloys.

* the phases are continuous in three dimensions

c) spiral microstructure.

Zn-Mg eutectic alloys (42) exhibit a growth structure in which the two phases constitute the loops of a spiral. Spiral eutectic structures are rare.

A strong dependence of the structure on nucleation was shown to exist (43). Lammelar eutectics result when one phase nucleates the others and random structures appear as a result of the nucleation of both phases by foreign impurities. The relative solid/liquid interfacial energy of the two phases is the controlling factor for the heterogenous nucleation (46).

The effects of undercooling were described by Tiller (19) who related the lamellar spacing for maximum growth rate at a given undercooling to the square root of the inverse growth rate. Hunt and Chilton (44) have similarly found that the growth rate is proportional to the square of the undercooling. Modes of growth were also proposed to depend on the interplay between the diffusion required for phase separation and

the formation of interphase boundaries (32). A classification of eutectics different from that given above, and based on the entropy of melting of the two phases was also proposed (36).

CHAPTER 3

THEORETICAL TREATMENT

CHAPTER 3

THEORETICAL TREATMENT

3.1 Mathematical Solutions

This section presents solution to mathematical problems involved in the unidirectional solidifcation of alloys.

Considerations is limited to alloys which freeze over a range of temperatures and have a eutectic in their system, and to the solidification of a stagnant liquid of finite extent cooled from one side only.

The integral profile approach is used to derive equations for the growth of the solid, partially solid and cooled liquid layers.

These equations have been solved, using a specially written computer programme, to predict the rates of freezing and the temperature distribution during the solidifcation of a series of aluminium copper alloys.

3.1.1. Method of Solution

The various distinct layers that exist in an ingot solidifying under unidirectional heat flow conitions are represented schematically in Fig. 3.1.

At any given time, the solidus isotherm acts as the boundary between the solid metal layer and the layer of metal that has not yet completely solidified.

Similarly the liquidus isotherm acts as a boundary between the liquid metal and the partially solidified layer.

The integral profile method postulates the existence of a third, imaginary boundary between liquid that has been cooled and liquid that has not yet been cooled.

The unsteady state heat transfer equations are integrated across each of the layers, and heat balances are established at the boundaries.

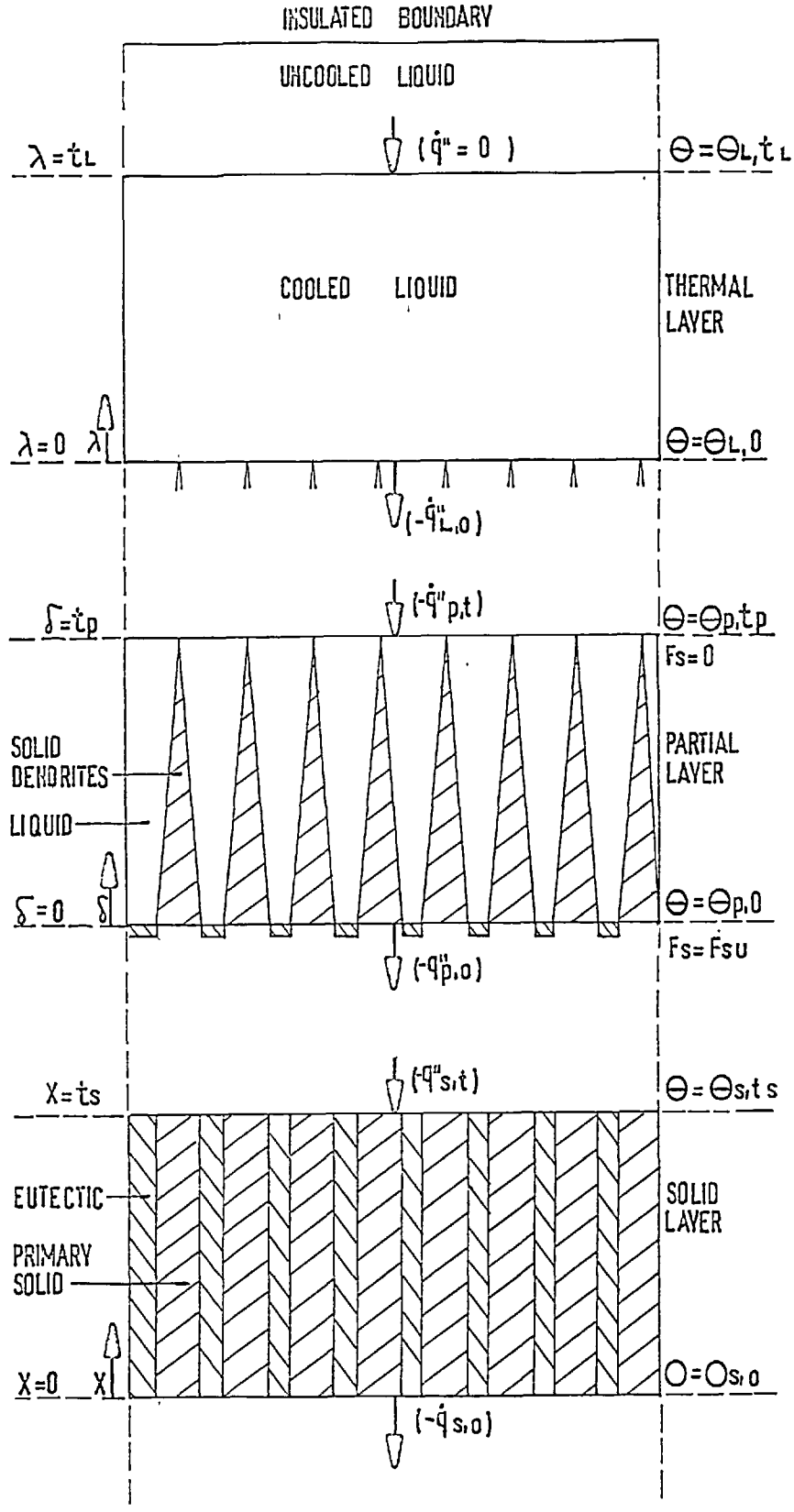

Fig 3.1 THE LAYERS RELATIVE TO THEIR COORDINATE SYSTEMS

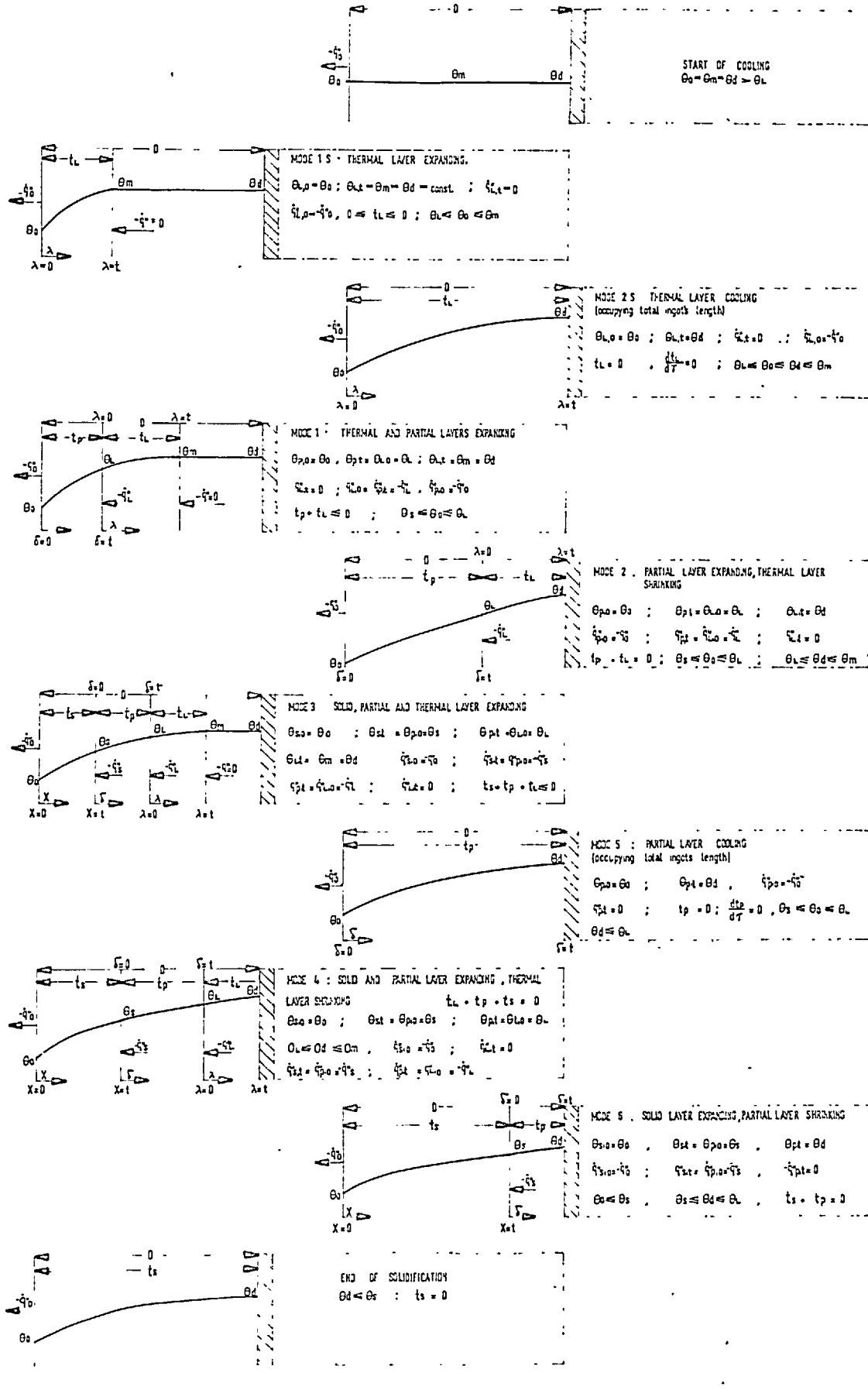

Fig 3.2 : SOLIDIFICATION MODES

Hills' integral profile solution (Chapter 2) is used to treat the solid layer, and a modification of it is used in the thermal layer.

An original integral profile solution is developed for the partial layer.

The equations derived separately for each layer are subsequently combined to represent the interaction between the layers and to follow a sequence of solidification modes which are shown schematically in Fig. 3.2.

3.1.2 The Equations for the Partial Layer

The co-ordinate system describing the partial layer has its origin in the cooled surface, until the temperature of the latter reaches that of the solidus, when the origin moves through the metal with the solidus.

Relative to this origin, the heat transfer equation within the partial layer must be modified to account for the liberation of latent heat, and for the movement of the origin through the metal.

$$\frac{\partial}{\partial \delta}\left(K_p \frac{\partial \theta}{\partial \delta}\right) + V_s \rho_p C_p \frac{\partial \theta}{\partial \delta} = \rho_p C_p \frac{\partial \theta}{\partial \tau} - \rho_p H_p \frac{\partial F_s}{\partial \tau} + V_s \rho_p H_p \frac{\partial F_s}{\partial \delta} \qquad (3.1.2.1)$$

Integrating equation (3.1.2.1) across the partial layer:

$$\int_{\delta=0}^{\delta=t_p} \left[\frac{\partial}{\partial \delta}\left(K_p \frac{\partial \theta}{\partial \delta}\right)\right] d\delta + \int_{\delta=0}^{\delta=t_p} \left[V_s\left(\rho_p C_p \frac{\partial \theta}{\partial \delta} - \rho_p H_p \frac{\partial F_s}{\partial \delta}\right)\right] d\delta =$$

$$\int_{\delta=0}^{\delta=t_p} \rho_p C_p \frac{\partial \theta}{\partial \tau} d\delta - \int_{\delta=0}^{\delta=t_p} \rho_p H_p \frac{\partial F_s}{\partial \tau} d\delta \qquad (3.1.2.2)$$

Applying Leibnitz integral formula to the right hand sideof equation (3.1.2.2):

$$\left[K_p \frac{\partial \theta}{\partial \delta}\right]_{p,t} - K_p \left[\frac{\partial \theta}{\partial \delta}\right]_{p,o} + V_s \left[\rho_p C_p \theta - \rho_p H_p Fs\right]_{p,t} - V_s \left[\rho_p C_p \theta - \rho_p H_p Fs\right]_{p,o} =$$

$$\frac{d}{dT}\left\{\int_{\delta=o}^{\delta=t_p} \theta \rho_p C_p \, d\delta\right\} - \rho_p C_p \frac{dt_p}{dT} \theta_{(p,t)} - \frac{d}{dT}\left\{\int_{\delta=o}^{\delta=t_p} \rho_p H_p Fs \, d\delta\right\} + \rho_p H_p \frac{dt_p}{dT} Fs_{(p,t)}$$

(3.1.2.3)

Rearranging and substituting $\frac{dts}{dT}$ for Vs :

$$\left[K_p \frac{\partial \theta}{\partial \delta}\right]_{p,t} - \left[K_p \frac{\partial \theta}{\partial \delta}\right]_{p,o} = \frac{d}{dT}\left\{\int_{\delta=o}^{\delta=t_p} (\rho_p C_p \theta - \rho_p H_p Fs) d\delta\right\} -$$

$$\left[\frac{dts}{dT} + \frac{dt_p}{dT}\right] \left[\rho_p C_p \theta - \rho_p H_p Fs\right]_{p,t} + \left[\frac{dts}{dT}\right] \left[\rho_p C_p \theta - \rho_p H_p Fs\right]_{p,o} \qquad (3.1.2.4)$$

The further development of equation (3.1.2.4) is facilitated by the definition of a series of effective thermal properties.

3.1.2.1. Effective thermal properties

The function appearing in the integral in equation (3.1.2.4) will be defined the effective enthalpy of the partial layer:

$$* \quad E = \rho_p C_p \theta - \rho_p H_p Fs \qquad (3.1.2.5)$$

differentiating equation (3.1.2.5) with respect to distance:

$$\frac{\partial E}{\partial \delta} = \rho_p C_p \frac{\partial \theta}{\partial \delta} - \rho_p H_p \frac{\partial Fs}{\partial \delta} \qquad (3.1.2.6)$$

---

* Strictly speaking E is not the true enthalpy in the partial layer because complete equilibrium does not exist between the solid and liquid phases. However, E behaves in the way that the true enthalpy would behave were equilibrium to exist.

but

$$\frac{\partial Fs}{\partial \delta} = \frac{dFs}{d\theta} \cdot \frac{\partial \theta}{\partial \delta} \qquad (3.1.2.7)$$

and equation (3.1.2.6) becomes:

$$\frac{\partial E}{\partial \delta} = \gamma_p \frac{\partial \theta}{\partial \delta} \qquad (3.1.2.8)$$

where

$$\gamma_p = \rho_p c_p - \rho_p H_p \frac{dFs}{d\theta} \qquad (3.1.2.9)$$

The function γ_p will be defined as the effective thermal capacity of the thermal layer.

The conservation of heat at the boundaries yields:

$$-\dot{q}''_{(p,t)} = \left[K_p \frac{\partial \theta}{\partial \delta}\right]_{P,t} \qquad (3.1.2.10)$$

and

$$-\dot{q}''_{(P,o)} = \left[K_p \frac{\partial \theta}{\partial \delta}\right]_{P,o} \qquad (3.1.2.11)$$

substituting $\frac{\partial \theta}{\partial \delta}$ from equation (3.1.2.8) into (3.1.2.10):

$$-\dot{q}''_{(P,t)} = \left[\frac{K_p}{\gamma_p} \frac{\partial E}{\partial \delta}\right]_{P,t} = \left[\alpha_p \frac{\partial E}{\partial \delta}\right]_{P,t} \qquad (3.1.2.12)$$

similarly

$$-\dot{q}''_{(P,o)} = \left[\alpha_p \frac{\partial E}{\partial \delta}\right]_{P,o} \qquad (3.1.2.13)$$

where

$$\alpha_p = \frac{K_p}{\gamma_p} \qquad (3.1.2.14)$$

The function α_p is the effective - thermal diffusivity of the partial layer.

3.1.2.2 The enthalpy profile

The effective - enthalpy, - thermal capacity, and - thermal diffusivity can now be used in the further development of equation (3.1.2.4) which becomes

$$\dot{q}''_{(P,O)} - \dot{q}''_{(P,t)} = \frac{d}{dT}\left\{\int_{\delta=o}^{\delta=t_p} E\, d\delta\right\} - \left[\frac{dt_s}{dT} + \frac{dt_p}{dT}\right] E_{(P,t)} + \left[\frac{dt_s}{dT}\right] E_{(p,o)} \qquad (3.1.2.15)$$

The distribution of the effective enthalpy across the partial layer is unknown. However, an estimated distribution can be obtained in the form of a polynomial and its coefficients can be evaluated using the known boundary conditions:

at $\delta = 0$; $E_p = E(p,o)$; $\dot{q}''_p = \dot{q}''(p,o)$

at $\delta = t$; $E_p = E(P,t)$; $\dot{q}''_p = \dot{q}''(P,t)$

A quadratic polynomial, correct at the above boundaries is:

$$E = E(P,o) + 2\left[E(p,t) - E(p,o) + \left(\frac{\dot{q}''}{\alpha}\right)(p,t)\,t_p\right]\left(\frac{\delta}{t_p}\right) - \left[E(p,t) - E(p,o) + \left(\frac{\dot{q}''}{\alpha}\right)(p,t)\,t_p\right]\left(\frac{\delta}{t_p}\right)^2 \qquad (3.1.2.16)$$

integrating equation (3.1.2.16) :

$$\int_{\delta=o}^{\delta=t_p} E\,d\delta = \left[\frac{1}{3}E(p,o) + \frac{2}{3}E(p,t) + \frac{1}{6}\left(\frac{\dot{q}''}{\alpha}\right)(p,t)\,t_p\right] t_p \qquad (3.1.2.17)$$

Since errors which are introduced in using an approximate function are reduced when the function is integrated, the integral given by equation (3.1.2.17) can be substituted into equation (3.1.2.15) without introducing too great an error.

3.1.2.3 The differential equations for the partial layer

The equation resulting from the above substitution is:

$$\dot{q}''(p,o) - \dot{q}''(p,t) = \frac{d}{dT}\left\{\left[\frac{1}{3}E(p,o) + \frac{2}{3}E(p,t) + \frac{1}{6}\left(\frac{\dot{q}''}{\alpha}\right)(p,t)\right] t_p\right\} - \left[\frac{dt_s}{dt} + \frac{dt_p}{dt}\right] E(p,t) + \left[\frac{dt_s}{dt}\right] E(p,o) \qquad (3.1.2.18)$$

Differentiating equation (3.1.2.16) at the boundary $\delta = o$

$$\left[\frac{\partial E}{\partial \delta}\right]_{\delta=0} = \frac{2(E(p,t) - E(p,o))}{t_p} + \left(\frac{\dot{q}''}{\alpha}\right)(p,t) \qquad (3.1.2.19)$$

Substituting from equation (3.1.2.13) into (3.1.2.19) and rearranging :

$$-\left[\left(\frac{\dot{q}''}{\alpha}\right)(p,o) + \left(\frac{\dot{q}''}{\alpha}\right)(p,t)\right] = \frac{2(E(p,t) - E(p,o))}{t_p} \qquad (3.1.2.20)$$

Expressing equations (3.1.2.18) and (3.1.2.20) in dimensionless terms :

$$q^*(p,o) - q^{*'}(p,t) = \left[E^*(p,t) - E^*(p,o)\right]\frac{dt^*_s}{d\xi} + \left[E^*(p,t)\right]\frac{dt^*_p}{d\xi}$$
$$- \frac{d}{d\xi}\left\{\left[\frac{2}{3}E^*(p,t) + \frac{1}{3}E^*(p,o) - \frac{1}{6}\left(\frac{q^*}{\alpha^*}\right)(p,t)\, t^*_p\right] t^*_p\right\} \qquad (3..1.2.21)$$

and

$$\left(\frac{q^*}{\alpha^*}\right)(p,o) + \left(\frac{q^*}{\alpha^*}\right)(p,t) = \frac{2(E^*(p,t) - E^*(p,o))}{t^*_p} \qquad (3.1.2.22)$$

Equations (3.1.2.21) and (3.1.2.22) are the required equations for the partial layer.

3.1.3 The Equations for the thermal layer

The co-ordinate system describing this layer has its origin in the cooled surface until this surface attains the liquidus termperature. Subsequently it moves with the liquidus through the metal.

The boundary conditions of the layer as represented in Fig. (3.1) are:

at $\lambda = 0$; $\quad \theta_L = \theta(L,o)$; $\quad \mathring{q}''_L = \mathring{q}''(L,o)$

at $\lambda = t$; $\quad \theta_L = \theta(L,t)$; $\quad \mathring{q}''_L = \mathring{q}''(L,t) = 0$

The unsteady state heat transfer equation in the liquid relative to this origin is:

$$K_L \frac{\partial^2 \theta}{\partial \lambda^2} - V_L \gamma_L \frac{\partial \vartheta}{\partial \lambda} = \gamma_L \frac{\partial \vartheta}{\partial T} \qquad (3.1.3.1)$$

The mathematical treatment of this equation is similar to that of the partial layer, except that

a) the boundary at $\lambda = t_L$ is adiabatic i.e. $q^*_{(L,t)} = 0$

b) the only heat liberated inside the layer is sensible heat.

i.e.

$$E_L = \gamma_L \vartheta_L; \qquad \alpha_L = \frac{k_L}{\gamma_L} \qquad (3.1.3.2)$$

Integration of equation (3.1.3.1) across the layer yields:

$$- \dot{q}''_{(L,o)} = \gamma_L \left[\vartheta_{(L,t)} \frac{dt_L}{dT} - V_L \left[\theta_{(L,t)} - \theta_{(L,o)} \right] - \frac{d}{dT} \left[\int_{\lambda=o}^{\lambda=t_L} \theta \, d\lambda \right] \right] \qquad (3.1.3.3)$$

The temperature distribution can be estimated in a similar manner to the enthalpy estimation given in section 3.1.2.2 by fitting a quadratic polynomial, to the temperatures at both boundaries, and to fit the heat flux equation at the boundary $\lambda = t_L$. i.e.

$$\theta = \theta_{(L,t)} - \left[\theta_{(L,t)} - \theta_{(L,o)} \right] \left[1 - \frac{\lambda}{t_L} \right]^2 \qquad (3.1.3.4)$$

Substituting equation (3.1.3.4) into (3.1.3.3), integrating and rearranging in dimensionless terms:

$$\frac{\dot{q}''_{(L,o)}}{\gamma^*_L} = \left[\theta^*_{(L,t)} - \theta^*_{(L,o)} \right] \left[\frac{dt^*_s}{d\xi} + \frac{dt^*_p}{d\xi} \right] + \theta^*_{(L,t)} \left[\frac{dt^*_t}{d\xi} \right] - \frac{d}{d\xi} \left[\left(\frac{2}{3} \vartheta^*_{(L,t)} + \frac{1}{3} \vartheta^*_{(L,o)} \right) t^*_L \right] \qquad (3.1.3.5)$$

where $V_L = \left(\frac{dt^*}{d\xi}_p + \frac{dt^*}{d\xi}_s \right)$

and

$$\frac{q^*(L,o)}{K^*_L} = \frac{2\left[\vartheta^*(L,t) - \vartheta^*(L,o)\right]}{t^*_L} \qquad (3.1.3.6)$$

Equations (3.1.3.5) and (3.1.3.6) are the two equations for the thermal layers.

3.1.4 The Equations for the Solid Layer

As discussed earlier, Hills equations are applied to the solid layer.

In this layer the solidification of liquid at eutectic composition occurs. The following boundary conditions, shown schematically in Fig. (3.1) exist:

at $x = 0$; $\theta = \vartheta_{(s,o)}$; $\mathring{q}'' = \mathring{q}''(s,o)$

at $x = t_s$; $\theta = \theta_{(s,t)} = \vartheta_s$; $\mathring{q}'' = \mathring{q}''_{(s,t)} = \mathring{q}''_s$

and the two differential equations are given by (2.1.1.19) and (2.1.1.20) describing the rate of change in surface temperature and solid thickness respectively.

3.1.5. Convenient Forms of Solution

The possible sequences of modes that may occur during the solidification of an alloy is illustrated schematically in Fig. (3.2)

The conditions for switching from one mode to another are represented schematically in Fig. (3.3).

3.1.5.1 Mode 1S - Semi infinite cooling of liquid

This mode is the first to occur and represents the cooling of a superheated liquid as a semi-infinite body. The cooled surface temperature drops towards the liquidus while the layer of cooled liquid expands towards the insulated boundary.

The boundary between cooled and uncooled liquid at $\lambda = t_L$ is adiabatic, and stays at the initial temperature.

The following conditions exist

$$\theta^*(L,t) = \theta^*_m > \theta^*_L = \text{constant}$$

$$\theta^*(L,o) = \theta^*_o \geq \theta^*_L \quad ; \quad q^*_{(L,o)} = q^* \quad ; \quad q^*_{(L,t)} = 0$$

$$0 \leq t^*_L \leq D^*$$

The differential equation (3.1.3.5) becomes

$$q^*_o = \frac{1}{3}\gamma^*_L (\theta^*_m - \theta^*_o) \frac{dt^*_L}{d\xi} - \frac{1}{3}\gamma^*_L t^*_L \frac{d\theta_o}{d\xi} \qquad (3.1.5.1)$$

q^*_o is a function of either temperature or of time or of both, hence:

$$\frac{dq^*_o}{d\xi} = \frac{\partial q^*_o}{\partial \theta^*_o} \cdot \frac{d\theta^*_o}{d\xi} + \frac{\partial q^*_o}{\partial \xi} = f'\theta \frac{d\theta^*_o}{d\xi} + f'\xi \qquad (3.1.5.2)$$

Differentiating equation (3.1.3.6) and substituting for $\frac{dq^*_o}{d\xi}$ from (3.1.5.2):

$$\frac{dt^*_L}{d\xi} = -\frac{1}{q^*_o}\left[(2K^*_L + t^*_L f'\theta)\frac{d\theta^*_o}{d\xi} + t^*_L f'\xi\right] \qquad (3.1.5.3)$$

rearranging equations (3.1.5.1) and (3.1.5.3) using equation (3.1.3.6) gives:

$$\frac{d\theta^*_o}{d\xi} = \frac{3q^{*3}_o + 2\gamma^*_L K^*_L (\theta^*_m - \theta^*_o)^2 f'\xi}{2\gamma^*_L K^*_L (\theta^*_m - \theta^*_o)\left[2q^*_o + (\theta^*_m - \theta^*_o) f'\theta\right]} \qquad (3.1.5.4)$$

and

$$\frac{dt^*_L}{d\Xi} = \frac{3\,q^*_o + \gamma^*_L t^*_L \frac{d\vartheta^*_o}{d\Xi}}{\gamma^*_L(\vartheta^*_m - \vartheta^*_o)} \qquad (3.1.5.5)$$

Equations (3.1.5.4) and (3.1.5.5) constitute a pair of simultaneous, ordinary differential equations which can be solved for surface temperature and thermal layer thickness variations once the cooling conditions at the outer layer are known.

The analytical integration of the two equations is performed in appendix (2).

This mode terminates:

when a) $\vartheta^*_o = \vartheta^*_L$ while $t^*_L < D^*$ in which case it is followed by mode 1 or:

when b) $t^*_L = D^*$ while $\vartheta^*_o > \vartheta^*_L$ in which case it is followed by mode 2S.

Which of the above is acheived first depends on cooling conditions, alloy characteristics and degree of superheat.

3.1.5.2 Mode 1 - Semi infinite partial solidification

This mode represents semi infinite solidification taking place between the liquidus and solidus temperatures of the alloy. It will only start after mode 1S has finished if condition (3.1.5.4) applies.

The substitution of equation (3.1.3.6) into this condition gives:

$$\vartheta^*_L > \left(\vartheta^*_m - \frac{D^* q^*_o}{2K^*_L}\right) \qquad (3.1.5.6)$$

If condition (3.1.5.6) is satisfied some of the liquid close to the insulated surface will not have been cooled by the time that the temperature of the cooled surface has reached the liquidus.

The partial layer will then expand together with the thermal layer and the following conditions exist:

$$\theta^*_{(p,o)} = \theta^*_o \ ;$$

$$\theta^*_{(p,t)} = \theta^*_{(L,o)} = \theta^*_L = \text{constant}$$

$$\theta^*_{(L,t)} = \theta^*_d = \theta^*_m > \theta^*_L = \text{constant}$$

$$q^*_{(p,o)} = q^*_o \ ; \quad q^*_{(p,t)} = q^*_{(L,o)} = q^*_L \ ; \quad q^*_{(L,t)} = 0$$

$$(\alpha^* ; \gamma^* ; E^* ; K^*)_{p,t} = (\alpha^* ; \gamma^* ; E^* ; K^*)_L = \text{constant}$$

$$(\alpha^* ; \gamma^* ; E^* ; K^*)_{p,o} = (\alpha^* ; \gamma^* ; E^* ; K^*)_o \neq \text{constant}$$

From the equation (3.1.2.22):

$$q^*_o = \frac{2(E^*_L - E^*_o)\alpha^*_o}{t^*_p} - q^*_L \frac{\alpha^*_o}{\alpha^*_L} \qquad (3.1.5.7)$$

differentiating equation (3.1.5.7):

$$\frac{d\, q^*_o}{d\,\xi} = \left[\frac{2\alpha'^*}{t^*_p}\,(E^*_L - E^*_o) + \frac{2\alpha^*_o E'^*_o}{t^*_p} - \frac{q^*_L}{\alpha^*_L}\alpha'^*_o\right] \frac{d\,\theta^*_o}{d\,\xi} -$$

$$\frac{2(E^*_L - E^*_o)}{t^{*2}_p}\alpha^*_o \frac{dt^*_p}{d\xi} - \frac{d\, q^*_L}{d\,\xi} \cdot \frac{\alpha^*_o}{\alpha^*_L} \qquad (3.1.5.8)$$

(For the derivatives of the effective - thermal properties ($\alpha^{*\prime}$, $E^{*\prime}$ etc.) see section 3.3).

From equation (3.1.2.21) we get:

$$q^*_o - q^*_L = \tfrac{1}{3}\,(E^*_L - E^*_o + \frac{q^*_L}{\alpha^*_L} t^*_p)\frac{dt^*_p}{d\,\xi} - \tfrac{1}{3}\, t^*_p\, E^{*\prime}_o \frac{d\,\theta^*_o}{d\,\xi} +$$

$$\frac{1}{6}\frac{t^{*2}_p}{\alpha^*_L}\frac{d\, q^*_L}{d\,\xi} \qquad (3.1.5.9)$$

q^*_L is a function of either partial layer thickness or of time, or of both. i.e. $q^*_L = (t^*_p : \Xi)$

hence:

$$\frac{dq^*_L}{d\Xi} = \frac{\partial q^*_L}{\partial t^*_p} \cdot \frac{dt^*_p}{d\Xi} + \frac{\partial q^*_L}{d\Xi} = g'_t \frac{dt^*_p}{d\Xi} + g'_\xi \qquad (3.1.5.10)$$

Substituting for $\frac{d\,q^*_L}{d\Xi}$ from (3.1.5.10) into (3.1.5.8) and (3.1.5.9) and rearranging yields:

$$\frac{d\,\theta^*}{d\Xi} = -\frac{q^*_L + (q^*_L + g'_t\, t^*_p)\frac{\lambda^*_o}{\lambda^*_L}\frac{dt^*_p}{d\Xi} + (f'_\xi + g'_\xi \frac{\lambda^*_o}{\lambda^*_L})t^*_p}{t^*_p(f'_\theta - q^*_o\frac{\lambda^{*\prime}_o}{\lambda^*_o}) + 2k^*_o} \qquad (3.1.5.11)$$

and

$$\frac{dt^*_p}{d\Xi} = -\frac{\left[t^*_p(f'_\theta - q^*_o\frac{\lambda^{*\prime}_o}{\lambda^*_o} + 2K^*_o\right]\left[g'_\xi\frac{t^{*2}_p}{2\lambda^*_L} - 3(q^*_o - q^*_L)\right] + (f'_\xi + g'_\xi\frac{\lambda^*_o}{\lambda^*_L})\gamma^*_o\, t^{*2}_p}{\left[t^*_p(f'_\theta - q^*_o\frac{\lambda^{*\prime}_o}{\lambda^*_o} + 2K^*_o\right]\left[E^*_L - E^*_o + q^*_L\frac{t^*_p}{\lambda^*_L} + g'_t\frac{t^{*2}_p}{2\lambda^*_L}\right] + \left[q^*_o + (q^*_L + g'_t\, t^*_p)\frac{\lambda^*_o}{\lambda^*_L}\right]\gamma^*_o t^*_p} \qquad (3.1.5.12)$$

rearranging equation (3.1.3.5) gives

$$\frac{dt^*_L}{d\Xi} = 3\left[\frac{q^*_o}{\gamma^*_L(\theta^*_m - \theta^*_L)} - \left(\frac{dt^*_\delta}{d\Xi} + \frac{dt^*_\beta}{d\Xi}\right)\right] \qquad (3.1.5.13)$$

Equations (3.1.5.11), (3.1.5.12) and (3.1.5.13) are ordinary differential equations for the variations of the surface temperature and the partial and thermal layer thicknesses during this mode. They can be solved numerically once the value of the surface heat flux is known.

The partial differentials of the heat flux entering the partial layer from the liquid can be evaluated by comparing coefficients as

described in appendix (3).

In this mode, limiting values have to be established for the differential equations at zero time when the equations become indeterminate.

Those equations which are used during the numberical integration at the start of this mode are derived in appendix (1).

This mode terminates:

when a) $\theta^*_o = 1$ while $t^*_p + t^*_L < D^*$ when it is followed by mode 3.

or:

when b) $t^*_p + t^*_L = D^*$ while $\theta^*_o > 1$ when it is followed by mode 2.

Which of these conditions is achieved first will depend on cooling conditions, alloy characteristics and degree of superheat.

3.1.5.3 Mode 2S - Finite cooling of the thermal layer

This finite cooling mode follows the semi infinite cooling mode 1S in preference to mode 1, if:

$$\theta^*_L < \left(\theta^*_m - \frac{D^* q^*_o}{2 K^*_L}\right) \qquad (3.1.5.14)$$

Relationship (3.1.5.14) is evaluated from equation (3.1.3.6) when substituted into the condition (3.1.5.2)b.

The following are the boundary conditions

$$\theta^*(L,o) = \theta^*_o \geq \theta^*_L \; ; \quad \theta^*(L,t) = \theta^*_d$$

$$q^*(L,o) = q^*_o \; ; \quad q^*(L,t) = 0 \; ; \quad t^*_L = D^*$$

From equation (3.1.3.5):

$$q^*_o = -\tfrac{1}{3}\gamma^*_L D^* \left(2\frac{d\theta^*_d}{d\xi} + \frac{d\theta^*_o}{d\xi}\right) \qquad (3.1.5.15)$$

and from equation (3.1.3.6):

$$\theta^*_d = \frac{q^*_o D^*}{2 K^*_L} + \theta^*_o \qquad (3.1.5.16)$$

Differentiation of equation (3.1.5.16) yields:

$$\frac{d\vartheta^*_d}{d\xi} = \left(\frac{D^*}{2K^*_L}\,\Gamma'_\theta + 1\right)\frac{d\vartheta^*_o}{d\xi} + \frac{D^*}{2K^*_L}\,\Gamma'_\varepsilon \qquad (3.1.5.17)$$

Using equation (3.1.5.17) to eliminate $\frac{d\vartheta^*_d}{d\xi}$ from equation (3.1.5.15): thus

$$\frac{d\vartheta_o}{d\xi} = -\frac{3\,q^*_o K^*_L + \Upsilon^*_L D^{*2}\Gamma'_\varepsilon}{\Upsilon^*_L D^*(3K^*_L + D^*\Gamma'_\theta)} \qquad (3.1.5.18)$$

Equations (3.1.5.17) and (3.1.5.18) are two simultaneous differential equations to be solved for the variations of the two extreme temperatures in this mode.

The analytical integration of those equations is given in appendix (2).

This mode terminates when the cooled surface temperature reaches the liquidus, and it is followed by mode 2.

3.1.5.4 Mode 2 - Expansion and contraction of the partial and thermal layers respectively

In this mode, the entire metal region is cooling, the partial layer expands and the thermal layer contracts in front of it.

The following conditions exist:

$$\theta^*_{(L,o)} = \Theta^*_{(p,t)} = \Theta^*_L = \text{constant}$$

$$\vartheta^*_{(L,t)} = \theta^*_d \quad ; \quad \theta^*_m \cong \vartheta^*_d \cong \theta^*_L$$

$$\theta^*_{(p,o)} = \Theta^*_o \quad ; \quad \vartheta^*_L \geq \vartheta^*_o \geq 1$$

$$t^*_p + t^*_L = D^*$$

$$\left(\alpha^*, \Upsilon^*, E^*, K^*\right)_{p,t} = \left(\alpha^*, \Upsilon^*, E^*, K^*\right)_L = \text{constant}$$

$$\left.\phi(\alpha^*, \gamma^*, E^*, K^*)\right|_{p,o} = \left.\phi(\alpha^*, \gamma^*, E^*, K^*)\right|_{o} \neq \text{constant}$$

From equation (3.1.3.5):

$$\frac{d\theta^*_d}{d\xi} = \frac{(\vartheta^*_d - \vartheta^*_L)\left(\frac{dt^*_s}{d\xi} + \frac{dt^*_p}{d\xi}\right) - \frac{3}{2}\frac{a^*_L}{\gamma^*_L}}{D^* - t^*_s - t^*_p} \qquad (3.1.5.19)$$

Equation (3.1.5.19) is an ordinary differential equation for the variations of the remote boundary temperature in this mode. It is to be solved simultaneously with equations (3.1.5.11) and (3.1.5.12) from mode 1 for the variations of the surface temperature and partial layer thickness respectively.

The partial differentials of the heat flux into the partial layer from the thermal layer are derived in appendix (3).

The limiting equations for the start of numerical integration in this mode are derived in appendix (1).

This mode terminates

when (a) $\vartheta^*_o = 1$ while $t^*_L > 0$ when it is followed by mode 4 or

when (b) $t^*_L = 0$ while $\vartheta^*_o > 1$ when it is followed by mode 5.

The condition which occurs first will depend on alloy characteristics and cooling conditions.

3.1.5.5. Mode 5 - The finite cooling of the partial layer

In this mode which follows mode 2, the partial layer cools as a finite body occupying the whole ingot length.

Both boundary temperatures drop. The existing conditions are:

$$\theta^*_{(p,o)} = \vartheta^*_o \quad ; \quad \vartheta^*_{(p,t)} = \vartheta^*_d$$

$$q^*_{(p,o)} = q^*_o \quad ; \quad q^*_{(p,t)} = 0; \; t^*_p = D^*$$

$$\left.\phi(\alpha^*, \gamma^*, K^*, E^*)\right|_{(p,o)} = \left.\phi(\alpha^*, \gamma^*, K^*, E^*)\right|_{o} \neq \text{constant}$$

$$\left.\phi(\alpha^*, \gamma^*, K^*, E^*)\right|_{(p,t)} = \left.\phi(\alpha^*, \gamma^*, K^*, E^*)\right|_{d} \neq \text{constant}$$

From equation (3.1.2.22):

$$q^*_o = \frac{2\alpha^*_o\,(E^*_d - E^*_o)}{D^*} \qquad (3.1.5.20)$$

Differentiating equation (3.1.5.20) and rearranging:

$$\frac{d\vartheta^*_d}{d\Xi} = \frac{\left(\frac{D^*}{2}\,\gamma'_\theta - \alpha^*_o\,(E^*_d - E^*_o) + K^*_o\right)\frac{d\vartheta^*_o}{d\Xi} + \frac{D^*}{2}\,\gamma'_\xi}{\alpha^*_o\,\gamma^*_d} \qquad (3.1.5.21)$$

From equation (3.1.2.21):

$$q^*_o = -\frac{D^*}{3}\left[2\gamma^*_d\,d\,\frac{d\vartheta^*_d}{d\Xi} + \gamma^*_o\,\frac{d\vartheta^*_o}{d\Xi}\right] \qquad (3.1.5.22)$$

Using equation (3.1.5.21) to eliminate $\frac{d\vartheta^*_d}{d\Xi}$ from equation (3.1.5.22) and rearranging:

$$\frac{d\vartheta^*_o}{d\Xi} = -\frac{3\,q^*_o\,\alpha^*\,D^* + D^*\,\gamma'_\xi}{D^*\,\gamma'_\theta - 2\alpha^*_o\,(E^*_d - E^*_o) + 3K^*_o} \qquad (3.1.5.23)$$

Equations (3.1.5.21) and (3.1.5.23) are two differential equations to be solved simultaneously for the two remote boundary temperatures in this mode.

Mode 5 terminates when $\theta^*_o = \theta^*_S$ and it is followed by mode 6.

3.1.5.6 Mode 3 - The growth of all three layers

In this mode, the thermal, partial and solid layers are all expanding one in front of the other while there is some uncooled liquid still left near the insulated end.

The mode follows mode 1, and the following conditions exist:

$$\vartheta^*(s,t) = 1 \;;\; \vartheta^*(s,o) = \vartheta^*_o \;\; 1 \;;\; \vartheta^*(p,o) = \vartheta^*(s,t) = 1$$

$$\theta^*(p,t) = \vartheta^*(L,o) = \theta^*_L \;;\; \vartheta^*(L,t) = \vartheta^*_d = \vartheta^*_m$$

$$q^*(s,o) = q^*_o \;;\; = q^*(s,t) = q^*(p,o) = q^*_S \;;\; q^*(p,t) = q^*(L,o) = q^*_L$$

$$q^*(L,t) = 0 \quad ; \quad t^*_s + t^*_p + t^*_L \geq D^*$$

The rate of change of the solid, partial and thermal layer thickness are given respectively by equations (2.1.1.20) (3.1.5.12) and (3.1.5.13).

The cooled surface temperature is given by equation (2.1.1.19).

The partial differentials of the heat flux into the partial layer are evaluated in appendix (3). Mode 3 terminates when the thermal layer reaches the remote boundary, i.e. $t^*_s + t^*_p + t^*_L = D^*$ and it is followed by mode 4.

3.1.5.7 Mode 4 - Contraction of the thermal layer

In this mode, which follows either mode 3 or mode 2, both solid and partial layers expand while the thermal layer shrinks.

The following conditions exist.

$$\vartheta^*(s,o) = \vartheta^*_o \quad ; \quad \vartheta^*(s,t) = \vartheta^*(p,o) = 1 \quad ; \vartheta^*(p,t) = \vartheta^*(L,o) = \vartheta^*_L$$

$$\vartheta^*(L,t) = \vartheta^*_d \quad ; \quad q^*(s,o) = q^*_o \quad ; \quad q^*(s,t) = q^*(P,o) = q^*_s$$

$$q^*(p,t) = q^*(L,o) = q^*_L \quad ; \quad q^*(L,t) = 0$$

$$t^*_s + t''_p + t^*_L = D^*$$

The solid layer thickness and the temperature of the cooled surface are given by equations (2.1.1.20) and (2.1.1.19) respectively.

The partial layer thickness and the temperature of the remote boundary are given respectively by equations (3.1.5.12) and (3.1.5.17).

The thermal layer thickness is found by difference. The partial differentials of the heat flux to the partial layer are determined in Appendix (3). This mode terminates when $t^*_p + t^*_s = D^*$ and it is followed by mode 6.

3.1.5.8 Mode 6 - The final solidification mode

This is the final solidification mode in which the solid layer expands to occupy the whole of the ingot and the partial layer contracting in front of it. Equations (2.1.1.20) and (2.1.1.19) are used for the solid layer thickness and the surface temperature variations respectively, and equation (3.1.5.17) is used for the remote boundary temperature.

The partial layer thickness is obtained by difference.

3.1.6 Convenient forms for solutions in the case of zero superheat

Zero superheat can be treated as a special case although no new equations are developed for it. The principle differences lie in the starting modes. When superheat is involved, there is a thermal layer moving in front of the partial, providing the heat flux into it. Under conditions of zero superheat, this thermal layer is absent. Instead, a liquid layer, maintained at the liquidus temperature is shrinking in front of the expanding partial layer. The boundary between the partial layer and this liquid is both adiabatic and isothermal. Once this boundary reaches the insulated top of the ingot, solidification is identical to that occurring in mode 5 and in mode 6 when the thermal layer has been consumed. The start of solidification will be described by means of modes 7 and 8.

3.1.6.1 Mode 7 - Growth of the partial layer into uncooled liquid

In the absence of superheat, partial solidification starts in this mode. The starting boundary conditions are:

$$\vartheta^*_{(p,o)} = \vartheta^*_o \; : \; \vartheta^*_{(p,t)} = \vartheta^*_L = \text{constant} \; : \; 1 \leq \theta^*_o \leq \theta^*_L$$

$$q^*_{(p,o)} = q^*_o \; : \; q^*_{(p,t)} = 0 \; : \; 0 \leq t^*_p \leq D^*$$

The growth of the partial layer and the variations of the cooled surface temperature are given by the corresponding equations in mode 2. No heat enters this layer from the liquid, hence:

$q^*_L = 0$ and $g'_\zeta = g'_\xi = 0$

This mode terminates when:

$t^*_p = D^*$ while $\vartheta^*_o > 1$ to be followed by mode 5 or,

when:

$\vartheta^*_o = 1$ while $t^*_p < D^*$ to be followed by mode 8 which ever occurs first.

3.1.6.2 Mode 8 - The partial layer is growing into uncooled liquid in front of an expanding solid layer

The equations describing the growth of the partial and solid layers in this mode and that for the variation of surface temperature are identical to the respective equations in mode 3.

Since there is no thermal layer, we have:

$q^*_L = 0$ and $g'_\zeta = g'_\xi = 0$

The starting conditions are:

$$\vartheta^*_{(s,o)} = \vartheta^*_o \; : \; \vartheta^*_{(s,t)} = 1 = \vartheta^*_{(p,o)} \; : \; \vartheta^*_{(p,t)} = \vartheta^*_L$$

$$q^*_{(s,o)} = q^*_o \; : \; q^*_{(s,t)} = q^*_s = q^*_{(p,o)} \; : \; q^*_{(p,t)} = 0$$

$$t^*_s + t^*_p \leq D^*$$

This mode ends when $t^*_s + t^*_p = D^*$ to be followed by mode 6.

3.1.7 Unidirectional solidification and Newtons' Law of cooling

The equations described in this chapter are general and hold for any cooling conditions to which the cooled surface may be subjected.

When the cooling conditions conform with Newtons' Law of cooling we have:

$$q^*_o = \vartheta^*_o$$

and

$$\frac{\partial \vartheta^*}{\partial \tau} = 1 : \frac{\partial \vartheta^*}{\partial \xi} = 0.$$

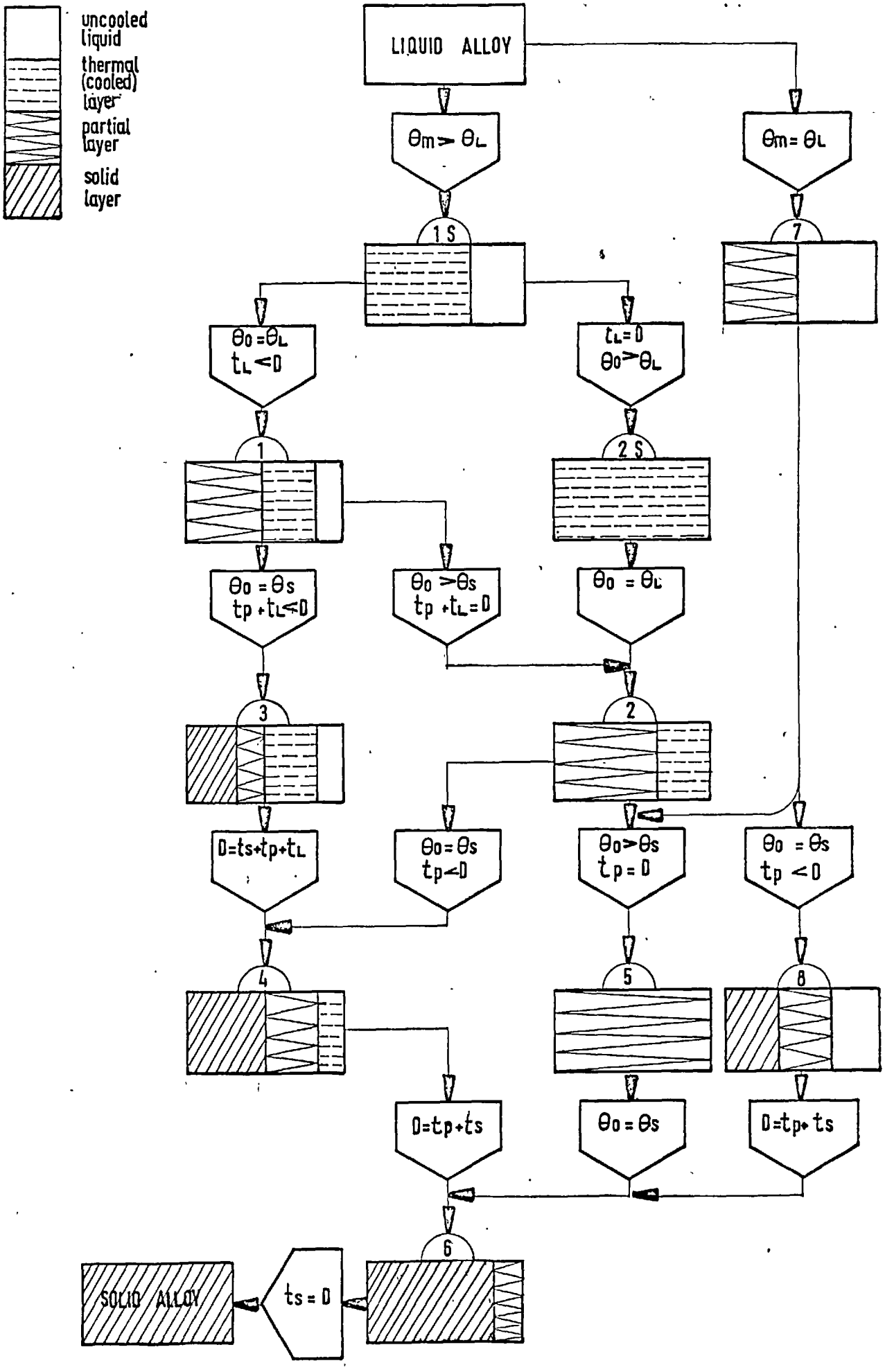

Fig 3.3 : SOLIDIFICATION ALGORITHM FOR BINARY ALLOYS

3.2 Physical and Thermal Properties

This section presents the way in which the thermal and physical properties are assumed to vary between the various layers, and in particular, their variations with position in the partial layer. This latter relationship is a function of the fraction solid in the partial layer.

3.2.1. Fraction solid in the partial layer

The volumetric fraction of solid in the partial layer is given byScheil's equation:

$$F_s = 1 - \left(\frac{\vartheta^*_F - \vartheta^*}{\vartheta^*_F - \vartheta^*_L} \right)^{\frac{1}{k-1}} \qquad (3.2.1.1)$$

Where ϑ^*_F is the dimensionless melting point of the pure solvent metal and k is the equilibrium partition coefficient.

This equation assumes a) constant partition coefficient; b) constant liquidus slope, c) complete diffusion in the liquid, d) no diffusion in the solid.

At the non equilibrium solidus temperature for the alloy, the fraction solid is constant and is given by:

$$Fsu = 1 - \left(\frac{\vartheta^*_F - 1}{\vartheta^*_F - \vartheta^*_L} \right)^{\frac{1}{k-1}} \qquad (3.1.2.2)$$

The following relationship exists:

$$\frac{dFs}{d\xi} = \frac{dFs}{d\vartheta} \cdot \frac{d\vartheta}{d\xi} = Fs' \frac{d\vartheta}{d\xi} \qquad (3.1.2.1.3)$$

3.2.2. Thermal Conductivity

The thermal conductivities of the solid and liquid layers are treated as constants, K_S and K_L respectively, and as such are the

average values for the thermal conductivity of the phases over the temperature range of interest.

The thermal conductivity of the partial layer where solid and liquid phases co-exist, varies with position. This variation is assessed by assuming that the average conductivity of the solid dendrites in this layer is K_S and that of the interdendritic liquid is K_L.

The actual conductivity at any given position in the partial zone can be described approximately by a linear function:

$$K_p = K_S F_S + K_L (1 - F_S) \qquad (3.2.2.1)$$

This equation assumes that the solid and liquid thermal conductivities are summed up in direct proportion to the volume fractions of the respective phases in the partial layer.

In dimensionless terms equation (3.2.2.1) becomes:

$$K^*_p = F_S + K^*_L (1 - F_S) \qquad (3.2.2.2)$$

3.2.3. Specific Heat

The specific heat values at constant pressure of both solid and liquid layers are treated in the same way as the thermal conductivity i.e. average values, C_S and C_L respectively are used.

The specific heat is similar to the thermal conductivity in that it is a temperature dependent property, but it is less sensitive to changes in physical state, volume or surface area.

Thus, the specific heat in the partial layer is assumed to be the same as C_L, the specific heat in the liquid. However, the value of C_L is determined by extrapolating the specific heat in the liquid down to the solidus temperature.

3.2.4. Density

The density is assumed to be divided as follows:

ρ = average density of the entire alloy in the liquid, partial or solid layers.

ρ_{eu} = Density of the liquid in the partial layer at the eutectic temperature.

ρ_p = Density of the solid alloy in the partial layer at the eutectic temperature.

A simple mass balance at the eutectic surface shows that:

$$\rho_p = \frac{\rho - (1 - F_{su})\rho_{eu}}{F_{su}} \qquad (3.2.4.1)$$

3.2.5. Latent Heat

The total amount of latent heat liberated on the solidifcation of an alloy is divided into the following partial heat quantities.

H_p = The quantity of latent heat liberated between the liquidus and the solidus in the partial zone.

H_{eu} = The quantity of latent heat released by the liquid solidifying at the solidus i.e. the latent heat of the eutectic alloy in the binary system, under consideration.

A simple heat balance shows that

$$H_p = \frac{\rho H - \rho_{eu} H_{eu}(1 - F_s)}{\rho_p F_{su}} \qquad (3.2.5.1)$$

Where H is the total latent heat of solidification of the alloy.

3.2.6. Dimensionless partial layer properties and their differentials

The dimensionless values of the thermal properties in the partial layer are defined as follows:

$$\alpha^*_p = \frac{\alpha_p}{\alpha_s} = \frac{\alpha_p}{k_s/C_s\rho_s} = \frac{k^*_p}{\gamma^*_p} \qquad (3.2.6.1)$$

$$\gamma^*_p = \frac{\gamma_p}{\gamma_s} = \frac{\rho_p C_L - \rho_p H_p \frac{dF_s}{d\vartheta}}{} = C^* - H^*_p F'_s \qquad (3.2.6.2)$$

$$K^*_p = \frac{K_p}{K_s} = \frac{K_s F_s + K_L(1-F_s)}{K_s} = F_s + K^*_L (1-F_s) \qquad (3.2.6.3)$$

$$E^* = \frac{E}{\rho_s C_s \vartheta_s} = \frac{\rho_p C_L \vartheta - \rho_p H_p F_s}{\rho_s C_s \vartheta_s} = C^* \Theta^* - H^*_p F_s \qquad (3.2.6.4)$$

$$H^*_p = \frac{\rho_p H_p}{\rho_s C_s \vartheta_s} = \frac{\rho H - \rho_{eu} H_{eu}(1-F_s)}{\rho_s F_{su} C_s \vartheta_s} \qquad (3.2.6.5)$$

$$H^*_s = \frac{\rho_{eu} H_{eu}(1-F_{su})}{\rho_s C_s \vartheta_s} \qquad (3.2.6.6)$$

Since all the functions above are temperature dependent only, either directly or via Fs their differentials, will obey the total differentiation rule i.e.

$$\frac{d}{d\vartheta}(\alpha^*_p; \gamma^*_p; K^*_p; E^*_p; F_s) = \frac{d}{d\vartheta}(\gamma^*_p; \alpha^*_p; K^*_p; E^*_p F_s) \frac{d\vartheta^*}{d\vartheta}$$

$$= (\gamma^*_p; \alpha^*_p; K^*_p; E^*_p; F_s)' \qquad (3.2.6.7)$$

and

$$E^{*\prime} = \gamma^* \qquad (3.2.6.8)$$

3.3 The Variations with Time of Heat Transfer Coefficient for the Solidification Front to move at a Constant Rate

If the heat transfer coefficient at the cooled surface is to vary, then under Newtonian cooling conditions

$$q^*_o = h^* \theta^*_o \qquad (3.3.1)$$

where $h^* = h/h(\text{start})$, $h(\text{start})$ being the value of the heat transfer coefficient at zero time.

Differentiating equation (3.3.1):

$$\frac{d\, q^*_o}{d\, \xi_o} = h^* \frac{d\, \theta^*}{d\, \xi} + \theta^*_o \frac{d\, h^*}{d\, \xi_o} \qquad (3.3.2)$$

Comparing coefficients between equation (3.3.2) and the following equation

$$\frac{d\, q^*_o}{d\, \xi_o} = f'_\theta \frac{d\, \theta^*}{d\, \xi} + f'_\xi$$

yields

$$h^* = f'_\theta \; ; \quad \theta^* \frac{dh^*}{d\xi} = f'_\xi \qquad (3.3.3)$$

at $\xi = o$ we have $h^* = \theta^* = q^* = 1$ and $t^*_s = 0$.

Using the above values at zero time and equation (2.1.1.7) we get:

$$\lim_{t^*_s \to o} \left| \frac{dt^*_s}{d\, \xi} \right| = \frac{1}{H^*} \qquad (3.3.4)$$

When a eutectic front moves at a constant rate, the dimensionless growth rate is equal to the reciprocal of the dimensionless latent heat.

If the eutectic is to grow at a constant rate, this will be $\frac{1}{H^*}$ at all values of t^*_s.

Thus from (3.3.4)

$$t^*_s = \xi H^* \qquad (3.3.5)$$

Substituting from the above into equations (2.1.1.7) and (2.1.1.16)

of the integral profile solution:

$$\frac{d\theta^*_o}{d\Xi} = \frac{6H^*(1 - t^*h^*) + 4(1 - \theta^*_o) - t^*_s(2\theta^*_o h^* - 1)}{3H^* t^*_s} \qquad (3.3.6)$$

and

$$\frac{dh^*}{d\Xi} = \frac{1 + H^*(1 - t^*h^*)\frac{d\theta^*_o}{d\Xi}}{H^* t^*_s \theta^*} \qquad (3.3.7)$$

Equation (3.3.5), (3.3.6) and (3.3.7) are three equations to be solved simultaneously for variations of solid thickness, cooled surface temperature and heat transfer coefficient with time when the eutectic is required to grow at a constant rate.

The starting value of the heat transfer coefficient will depend on the required growth rate and can be calculated as follows:

$$\frac{dt^*_s}{d\tau} = \frac{d(\frac{h}{K}t)}{d(\frac{h^2\tau}{PcX})} = \frac{c}{h}\frac{dt}{dT} = \frac{1}{H^*} = \frac{C\theta_s}{H} \qquad (3.3.8)$$

hence

$$h(\text{start}) = \frac{\rho H}{\theta_s}\frac{dt}{dT} \qquad (3.3.9)$$

Plots of dimensionless heat transfer coefficients and surface temperature variation with dimensionless time, for various values of dimensionless latent heats, as obtained from the numerical integration of equation (3.3.6) and (3.3.7) are given respectively in Figs. (3.4) and (3.5). The limiting values of $\frac{d\theta^*_o}{d\tau}$ and $\frac{dh^*}{d\tau}$ at zero time are evaluated in Appendix (5).

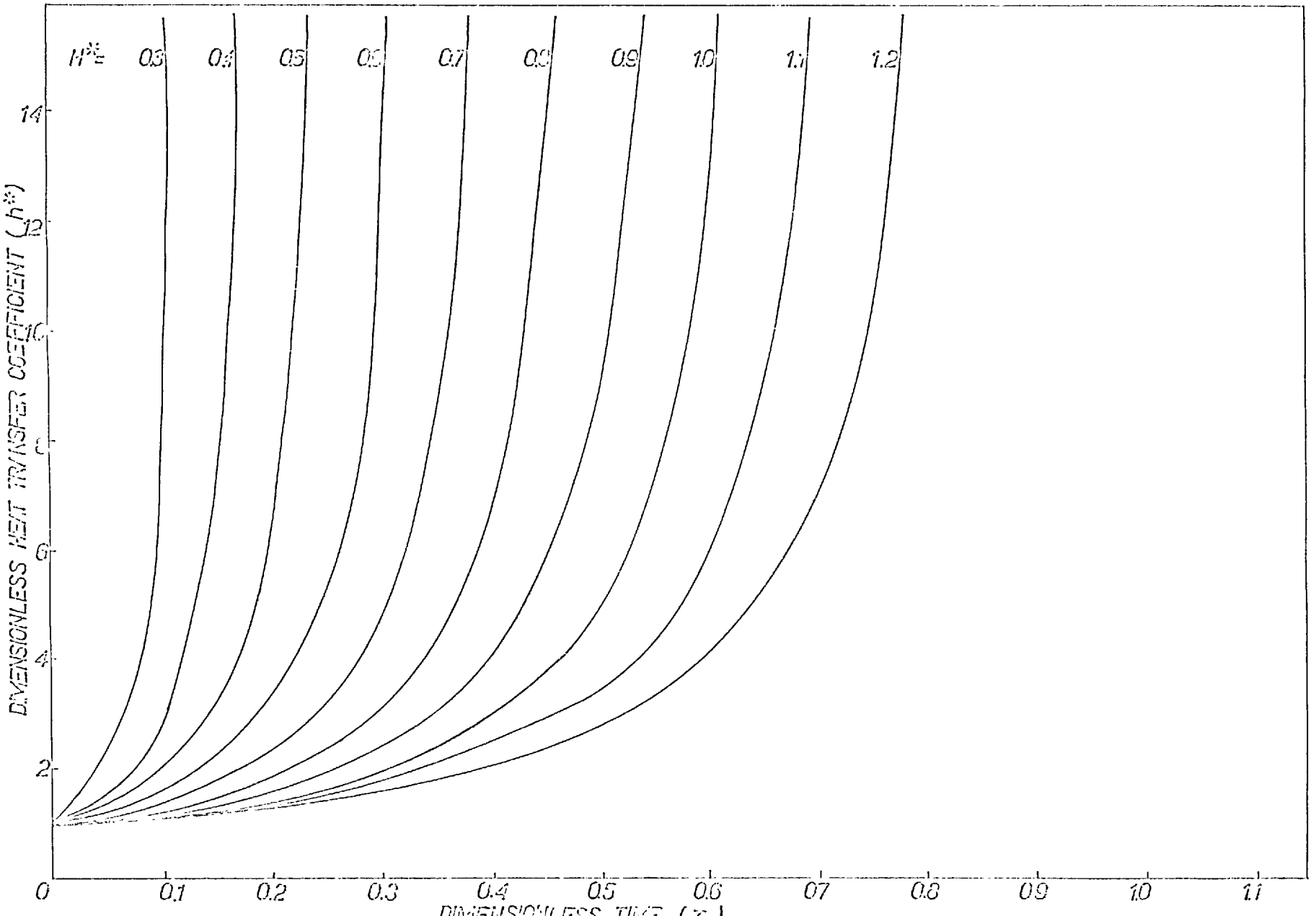

Fig 3.4 THEORETICAL PLOTS OF DIMENSIONLESS HEAT TRANSFER COEFFICIENT VERSUS DIMENSIONLESS TIME, FOR SOLIDIFICATION WITH CONSTANT GROWTH RATES, AND DIFFERENT VALUES OF DIMENSIONLESS LATENT HEAT (H^*)

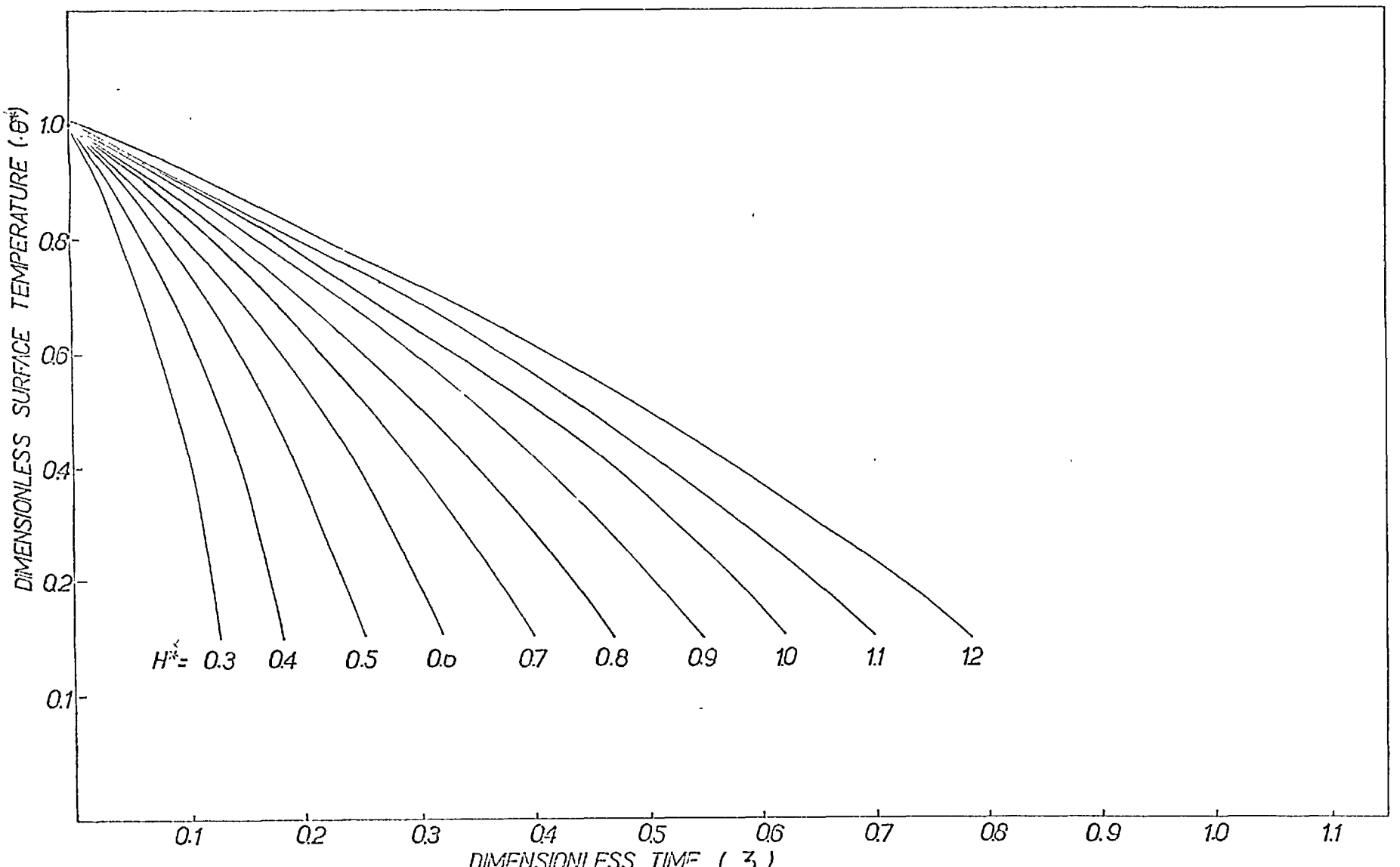

Fig 3.5 THEORETICAL VARIATIONS IN DIMENSIONLESS SURFACE TEMPERATURE VERSOUS DIMENSIONLESS TIME, FOR DIFFERENT VALUES OF DIMENSIONLESS H^{**} . SOLIDIFICATION WITH CONSTANT GROWTH RATE.

3.4 Numerical Methods of Solution and Computer Programme

The differential equations developed in this Chapter can be solved numerically using a Runge-Kutta method of integration.

A special computer programme has been written which follows the various solidification modes for a particular case. It consists of a main programme and three subroutines written in Fortran IV language.

The flow charts for the main programme and for subroutine Difrel are presented in Fig. (3.6) and (3.7). The two other subroutines, Rukut 4 and Step 4 were developed by Hills (17).

The main programme converts the data to dimensionless terms and calculates the values of the thermal constants. It then determines in what mode the partial solidification will start and the corresponding time from start of cooling.

All the claculated values for the start of integration are then written and subroutine Rukut 4 is called. This subroutine then calls subroutine step 4, the subroutine in which the numerical integrations are carried out. Rukut 4 controls the integration by varying the step length used in Step 4. The original step length and print intervals are read from the main programme to which the values of the parameters are returned after integration and written at more or less constant print intervals. Subroutine step 4 calls subroutine Difrel in which the actual values of the differentials are calculated.

The following checks are performed:
In the main programme, to which control is transferred from Rukut 4, check calculations are performed to prevent mode 'overshooting'. If an end condition of the current mode has been exceeded, Rukut 4 is recalled with the previous values of the parameters but with a reduced step length.

This procedure is repeated until the end conditions for the mode can be assumed to have been reached. The accuracy required is set in the check. The integration is recommenced in the following mode using

the end parameters of the previous mode as starting values.

In Difrel, checks are maintained to prevent the differentials from becoming indeterminant. The values of the variables that change with temperature are calculated in Difrel and substituted in the expressions for the differentials. Checks are also maintained to prevent the expressions for the heat fluxes from becoming negative.

The relevant equations for a given mode are distinguished from that of other modes by means of an integer Mode 1. stored in common.

The integer Mode 2 is used for setting up the starting conditions for integrations in the various modes.

The integer Mode 3 is used for introducing parameters into the differential expressions during the time intervals in which Rukut 4 has control.

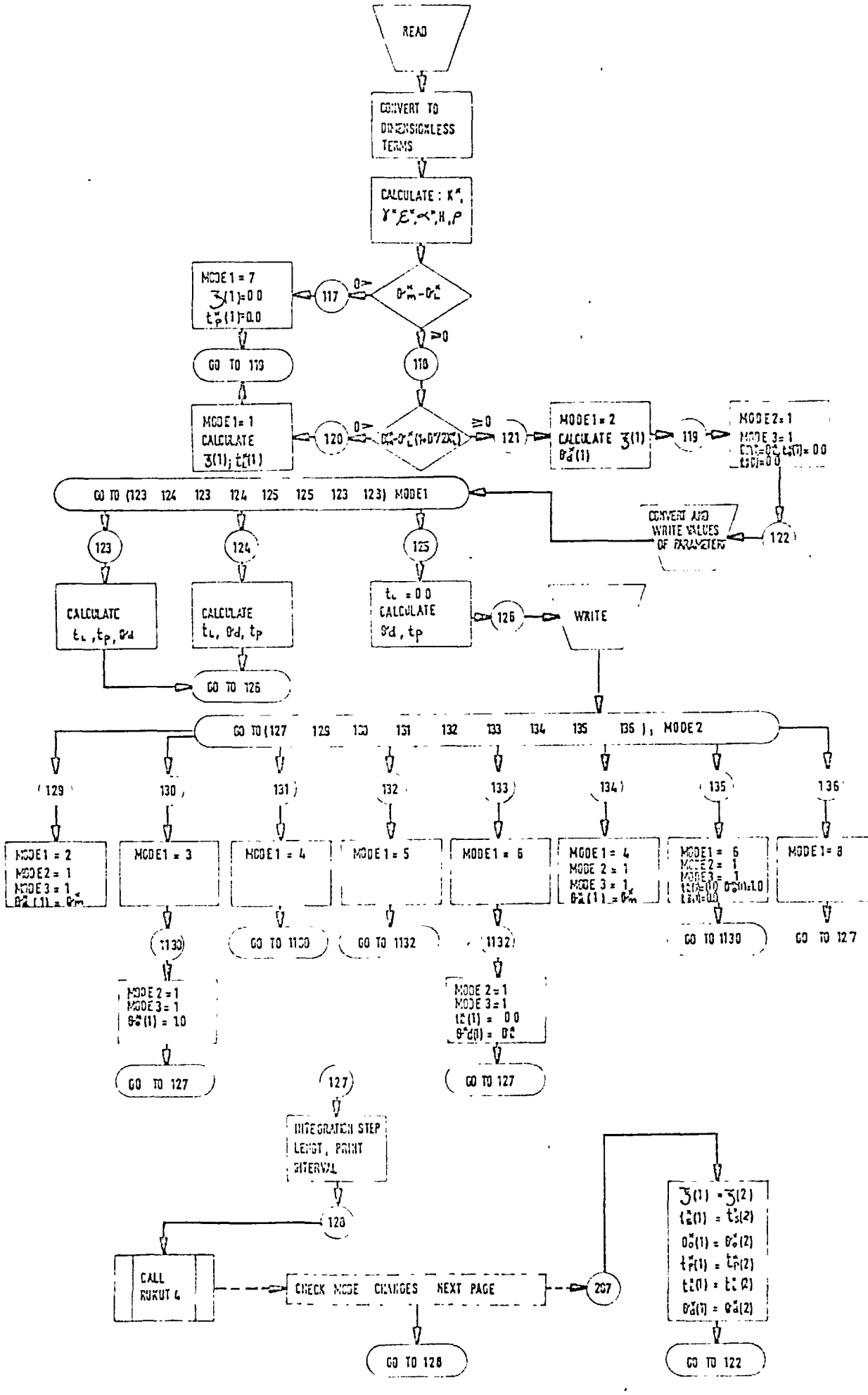

Fig 3.6 FLOW DIAGRAM FOR THE MAIN COMPUTOR PROGRAMME

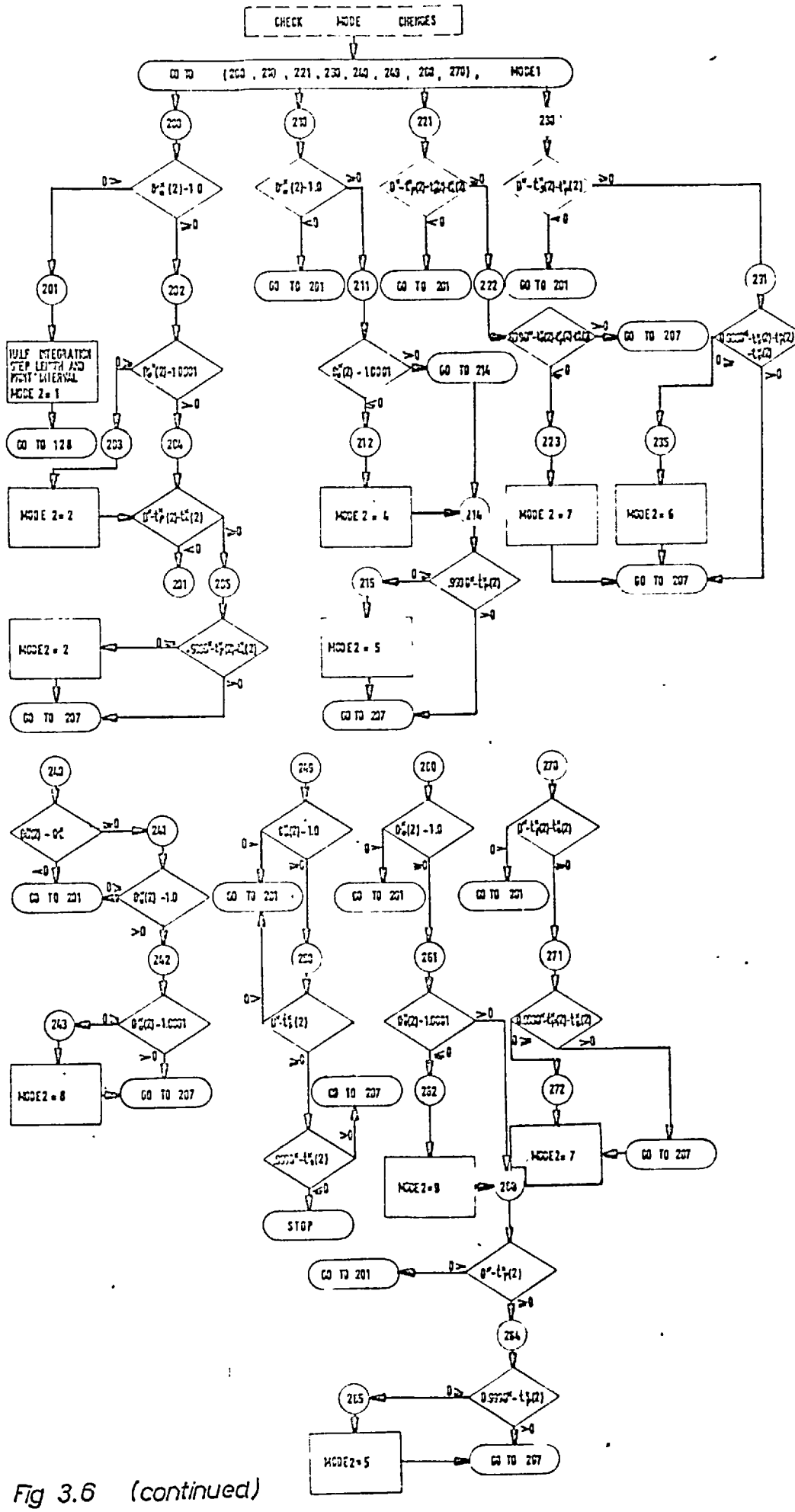

Fig 3.6 (continued)

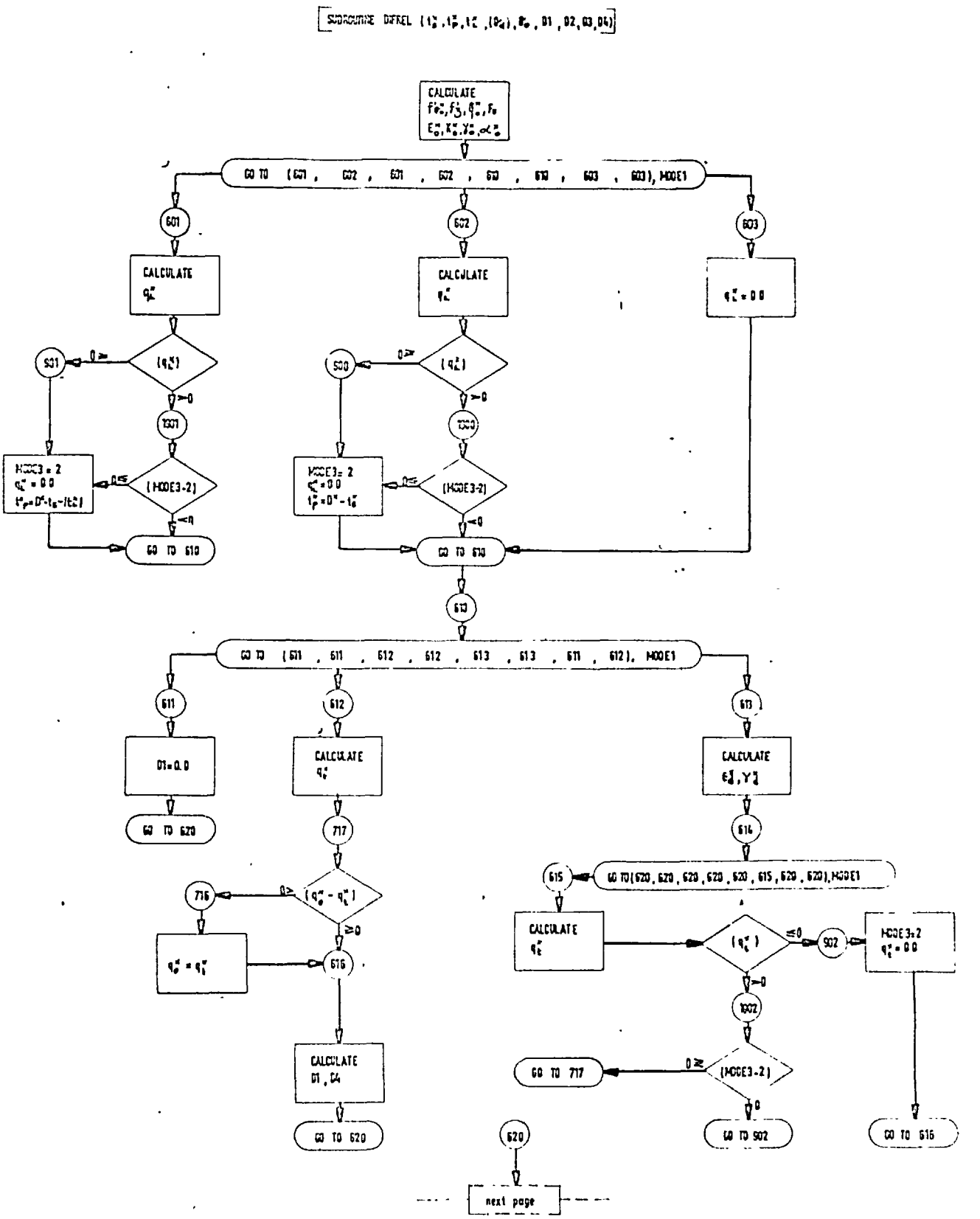

Fig 3.7 FLOW DIAGRAM FOR THE SUBROUTINE DIFREL

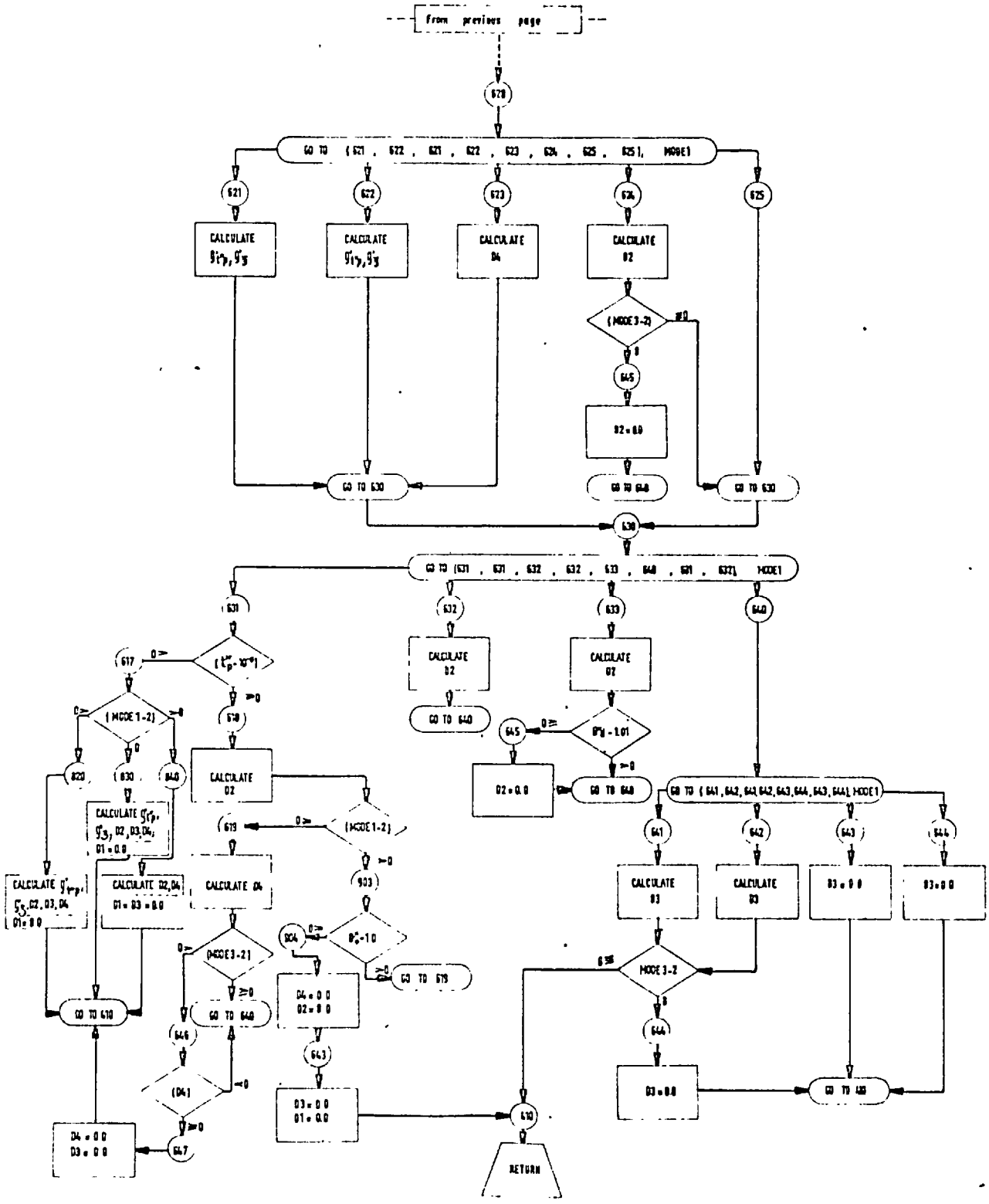

Fig 3.7 (continued)

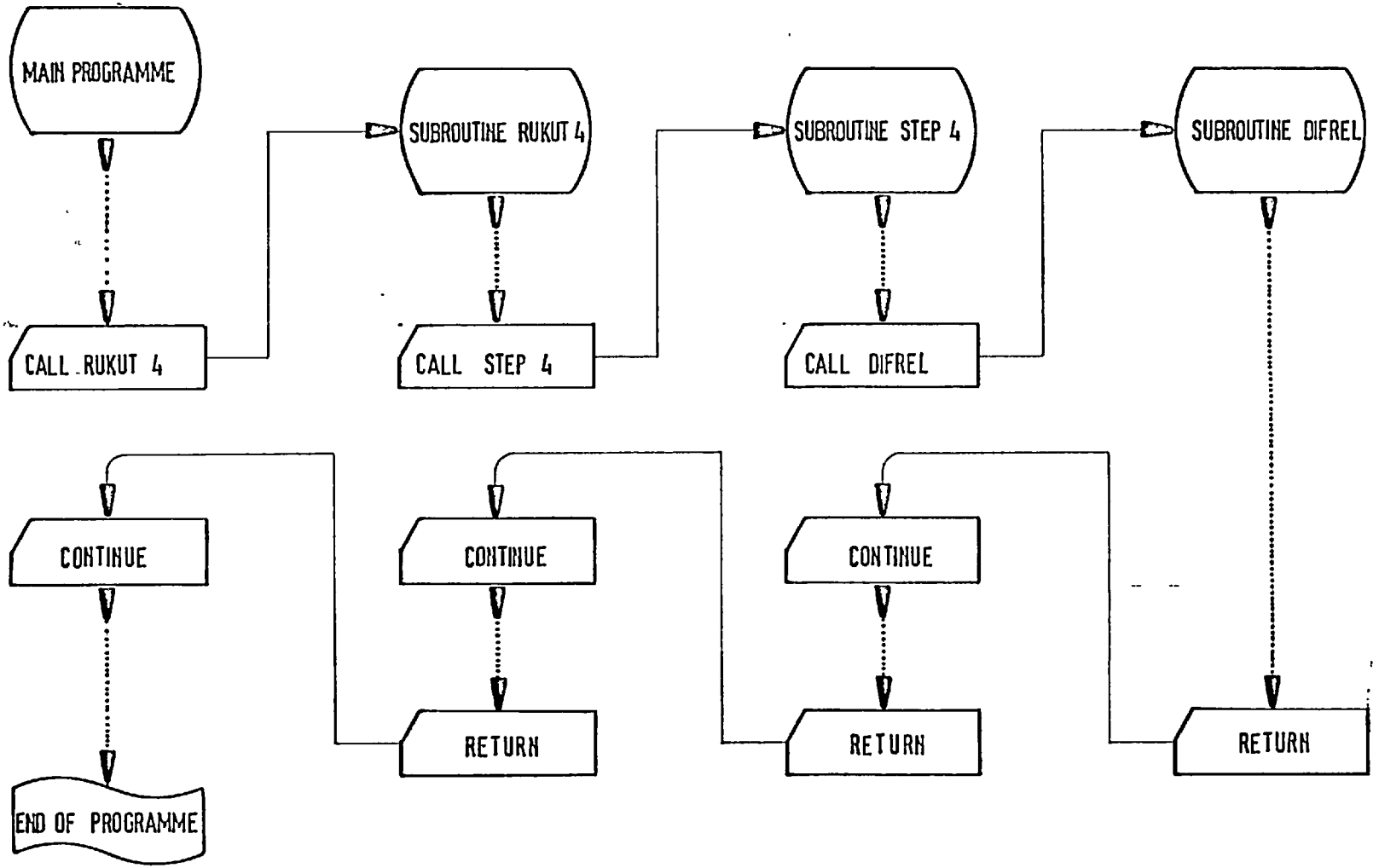

Fig 3.8 THE RELATIONSHIP BETWEEN THE MAIN PROGRAMME AND THE SUBROUTINES

CHAPTER 4

EXPERIMENTAL APPARATUS AND PROCEDURE

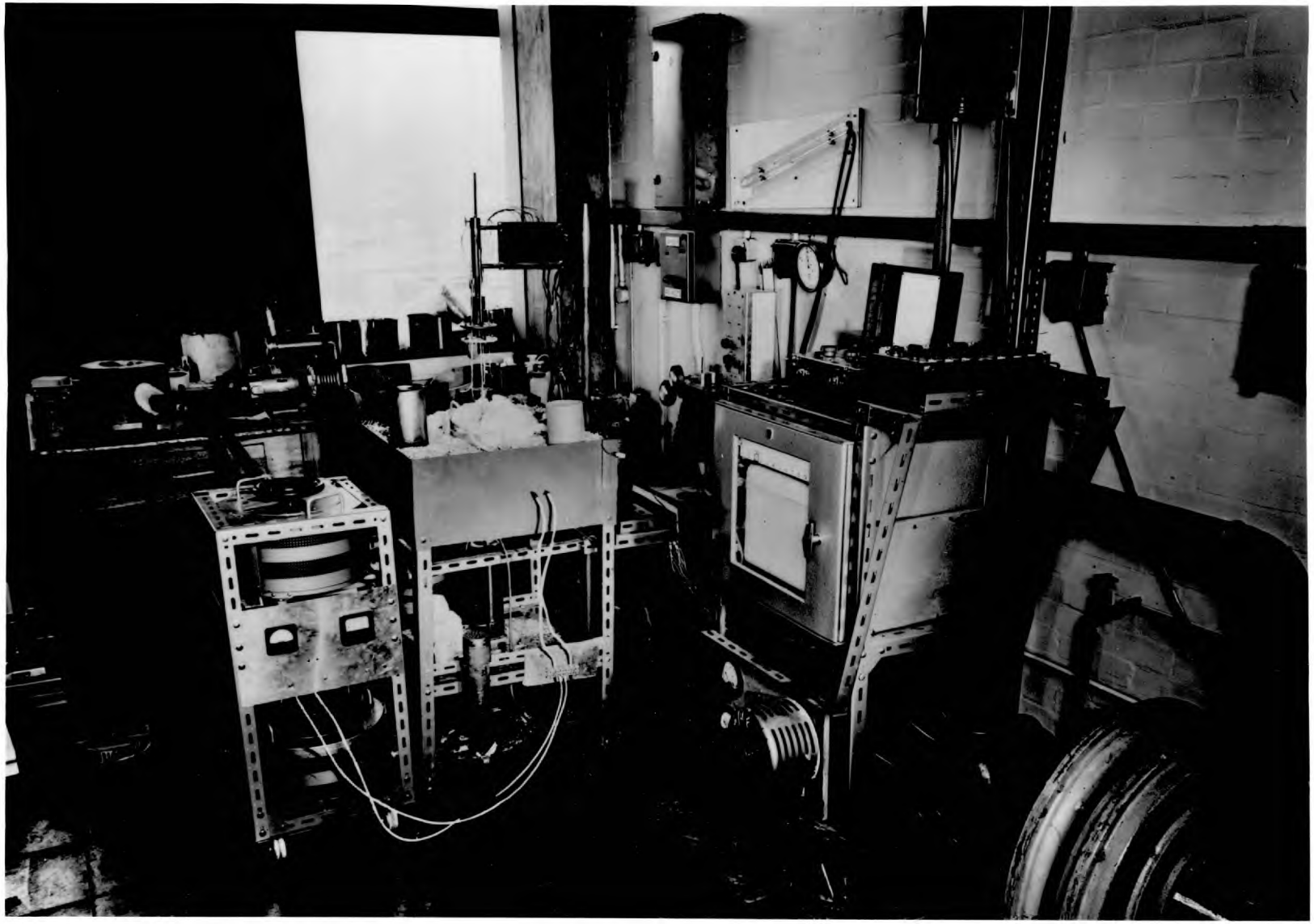

PLATE 1 EXPERIMENTAL UNIT

CHAPTER 4
EXPERIMENTAL APPARATUS AND PROCEDURE

4.1. Apparatus

The experimental apparatus (plate 1 and fig. 4.1) was designed to study the solidification process under controlled unidirectional heat flow conditions. It consisted of the following system units.

a. Melting and casting unit

b. Temperature measuring assembly

c. Cooling system.

4.1.1. Melting and Casting Unit

This unit, shown in Fig. 4.2, consisted of the following components.

I The crucible

II Heating device

III Thermal insulation

4.1.1.1 The Crucible

The crucible serves both as a melting pot and an ingot mould, thus eliminating splashing, turbulence and any other phenomena associated with the pouring of molten metal that may disturb the position of the thermocouples.

The two types of moulds used are shown in plate 2 and their relevant properties are set out in table (4.1).

To prevent the formation of an air gap when the 18/8 stainless steel crucibles were used, the crucibles were subjected to a stress relief operation involving annealing at 850°C for 8 hours prior to use.

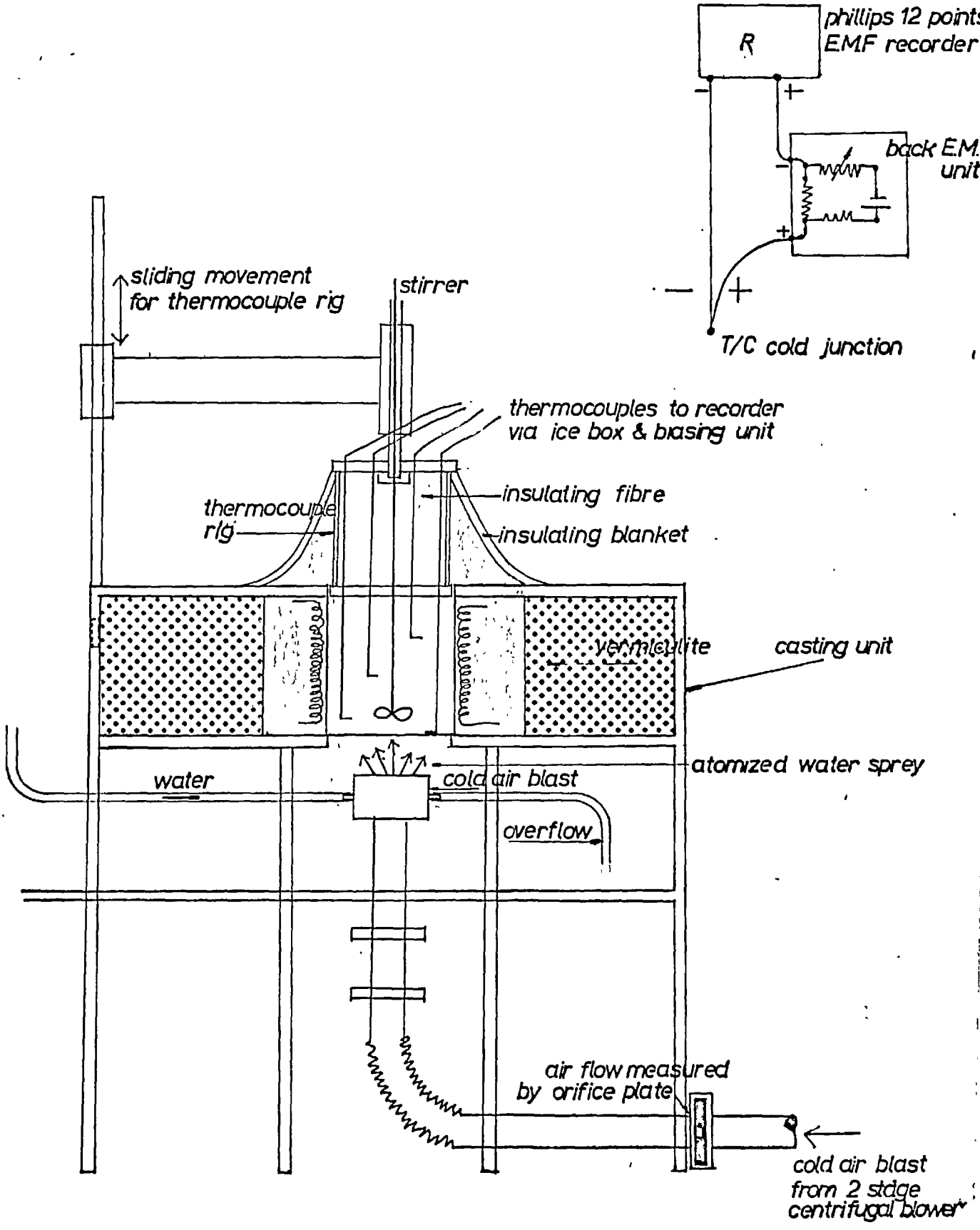

Fig 4.1 : DIAGRAM OF APPARATUS

A refractory wash 'Koron 510' was also applied on the inside walls of both types of crucibles before use.

Metal system	Non Ferrous Metals	Ferrous Metal
Mould material	18/8 stainless steel	25/12 stainless steel
Fabrication method	Deep drawing	Casting
Inside Diameter	100 mm	90 mm
Depth	170 mm	130 mm
Wall thickness	1.15 mm	5 mm
Maximum operating temperature	750°C	1000°C
Thermal history prior to use	Annealed	As cast
Coating material	Koron 510	Koron 510

TABLE 4.1 Details of Ingot Moulds

4.1.1.2 Heating Devices

Two types of furnace arrangement were used. For the non-ferrous experiments a heating cable was wound around the 18/8 stainless steel crucible.

For the ferrous experiment, a flexible heating blanket was wrapped around the 25/12 stainless steel crucible.

Both arrangements are shown in plate 2. Each system was connected to the power suppy via a variac so that the power input could be controlled.

Details of the two systems are set out in Table 4.2

PLATE 2 *MOULDS AND FURNACE HEATERS*

1000 W armoured heater coiled round a 1250 ml deep drawn stainless steel crucible : (800 °c max) [LEFT]

80V , 40A flexible furnace (1050°c max) [CENTRE]

Cast stainless steel mould [RIGHT]

	Cable Heater	Flexible 'blanket heater
Method of construction around pot	Coiled	Wrapped
Maximum temperature	800°C	1050°C
Maximum power	1000 W	3280 W
Maximum current	4 A	40 A*
Maximum voltage	250 V	82 V
Resistance heating wire	Nickel chrome	Kanthal
Heater insulation and thickness	Ceramic beads (6 mm)	Ceramic blocks (9 mm)
Heater's form	Cable enclosed in braided nickel alloy sheet.	Mat formed by the interlocking of blocks.
Overall dimensions	3050 mm, long 8 mm o.d.	125 mm x 3200 mm x 9 mm.
Used in conjunction with	18/8 stainless steel crucibles	25/12 stainless steel crucibles.
Metal system melted	Non-ferrous	Ferrous

TABLE 4.2 Furnace Heaters

* Two 20 amp variacs were connected in parallel across a shunt to provide the required current.

4.1.1.3 Thermal Insulation

Two types of insulating material were used. The hot face around the crucible was packed with 45% alumina 52% silica ceramic fibres in the form of wool, to the depth of 200 mm.

The reaminder of the 560x560x180mm box surrounding the crucible was filled with loose file vermiculite.

The base of the box containing the crucible and the insulating material was made of 8 mm syndanyo plate with a 100 mm hole in its

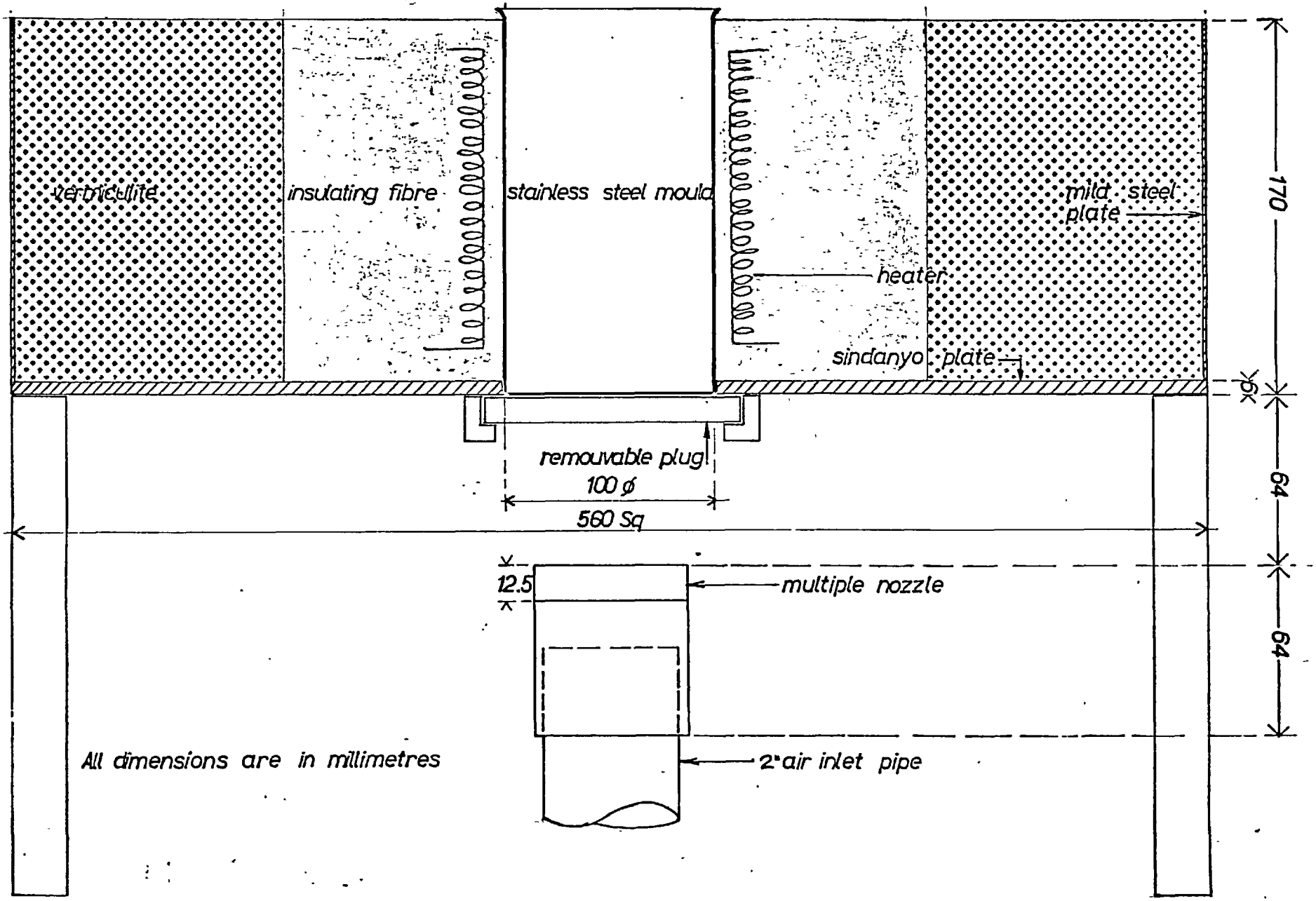

Fig 4.2 : CASTING UNIT

centre exposing the crucible base to the cooling air.

4.1.2 Temperature Measuring Assembly

The progress of the solidification process was studied by thermal analysis, temperatures measured inside the mould being recorded continuously.

4.1.2.1. Thermocouples and supporting rig

The thermocouples were suspended vertically inside the mould at various heights from the base, the ends being bent so that the last 15 mm were horizontal.

The level of the rig holding the thermocouples could be adjusted vertically to facilitate the positioning of the thermocouples.

An 8 mm thick, 100 mm diameter syndanyo plate was fitted to the top of the crucible to act as an insulating lid. It was joined by studs to a metal disc which in turn was screwed to a central shaft (the stirrer was introduced through a hole in this shaft).

The thermocouples were suspended by being passed through holes drilled in both plates and secured by locking nuts.

The space between the two discs was packed with ceramic insulating wool. Details of the thermocouples are set out in Table 4.3.

Experimental metal system	Non-ferrous alloys	Ferrous alloys
Thermcouple type	Chromel-alumel	Chromel-alumel
Sheath material	18/8 stainless steel	Inconnel
Insulation	Magnesite powder	Magnesite powder
Type of hot function	Bonded to sheath	Bonded to sheath
Overall diameter	2.3 mm	3.2 mm
Overall length	300 mm	300 mm
Tail length	300 mm	300 mm
Average response time	1 second	2 seconds
Maximum operating temperature	870°C	1150°C
Accuracy	$\pm \frac{3}{4}\%$	$\pm$ 1%

TABLE 4.3 Details of Thermocouples

4.1.2.2. E.M.F. Biasing Unit

Each thermocouple was connected to a biasing unit as shown schematically in Fig. 4.1 and the balance E.M.F. fed to one channel of the recorder. Each unit provided a known but variable biasing potential.

4.1.2.3. The Recorder

The thermocouple readings were recorded continuously on the chart of a Phillips 12 point millivolt recorder. The recorder has scale ranges of 1-10, 1-20, 1-50 and 1-100 m.v. The chart speed used was 600 mm/hr. (24 seconds per channel).

4.1.3 The Cooling System

The controlled cooling conditions were achieved by directing a stream of air, or of an air-water mixture onto the base of the crucible.

4.1.3.1. Air supply

The cold air blast was provided by a 5 Hp two stage centrifugal blower, and delivered through a 2 inch diamter pipe to the nozzle.

Air flow measurements were made using an orifice plate, $1\frac{1}{2}$ inch diamter. The pressure drop across the orifice was measured by a one in four inclined water manometer. The orifice plate and pressure tappings were constructed in accordance with B.S. 1043: 1943 Flow Measurements.

4.1.3.2. Air flow control

The air flow rate was regulated by a gate valve in the piping system.

For solidifying eutectics with continuous variations in the air flow rate, the device shown in Fig. 4.5 was used. A rubber friction wheel drove the valve control wheel at the required rate. The rubber wheel itself was driven by a reversible D.C. motor working through reduction gears. A variable resistance and a reversing switch were used to control the speed and direction of the motor.

4.1.3.3 The multiple air nozzle

The multiple nozzle shown in Fig. 4.3 was designed (15) to give a uniform distribution of high velocity cooling air over the moulds base when situated at a distance of 64 mm from it.

A second design shown in section in Fig. 4.3 enabled water to be introduced into the nozzle and to be atomised in the air stream.

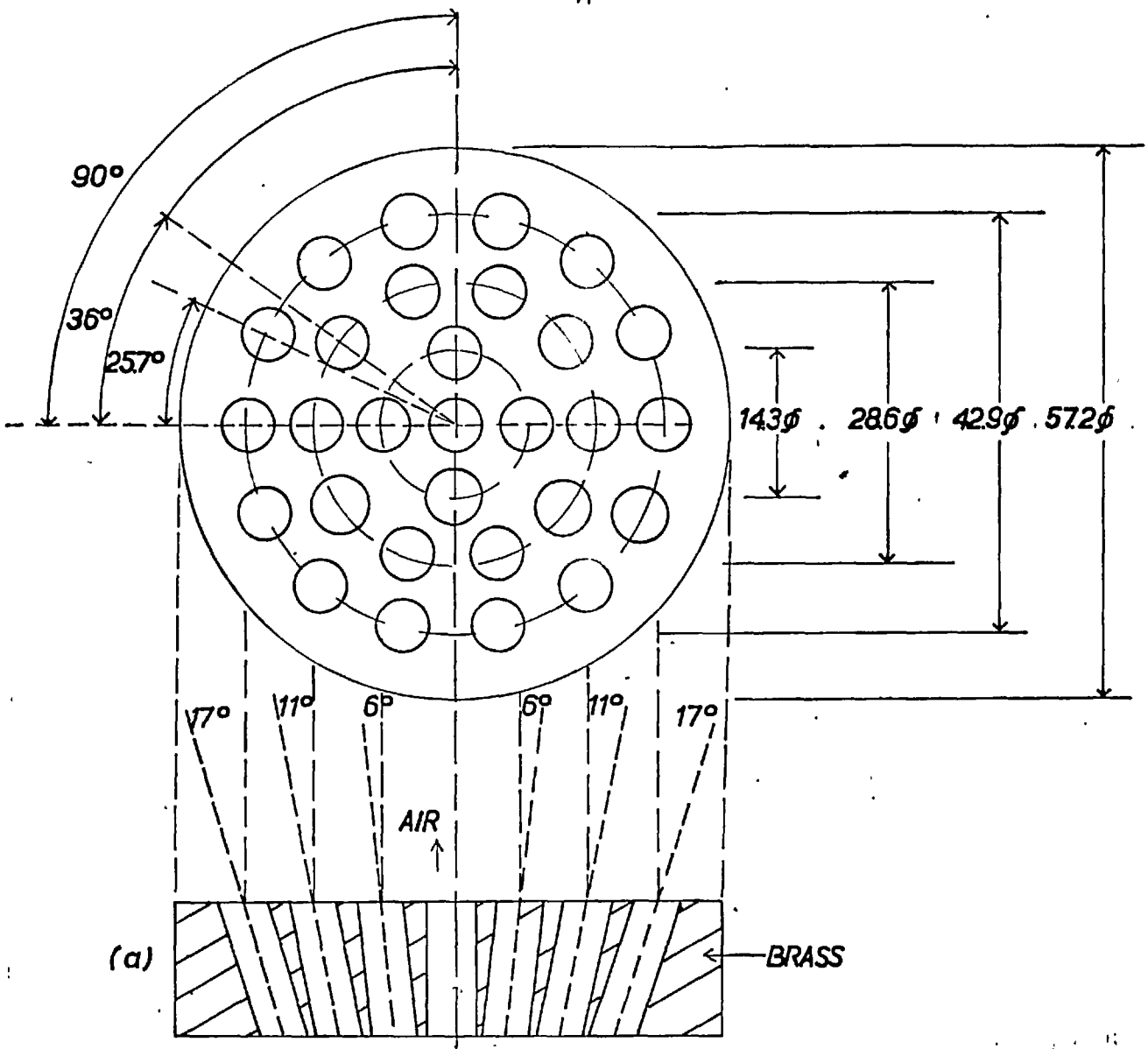

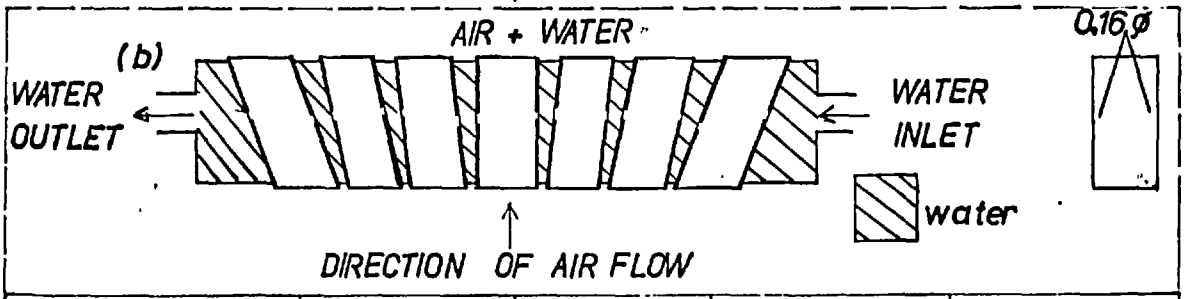

RADIUS FROM CENTRE OF NOZZLE PLATE	FRACTIONAL RADIUS R=28.5	NO. OF 4.8 DIA. HOLES	ANGULAR SPACING OF 4.8 DIA HOLES	INCLINATION OF HOLES TO VERTICAL
0	CENTRE	1		0°
7.1	R/4	4	90°	6°
14.3	R/2	10	36°	11°
21.4	3R/4	14	25.7°	17°

Fig 4.3 : MULTIPLE NOZZLE
(a) AIR NOZZLE
(b) AIR WATER NOZZLE

4.1.3.4 The cooling water arrangement

A constant head water tank of 7.5 litre capacity was suspended on a cable passing over a pulley, and counter balanced so that it's level could be altered.

Water was fed from the tank to the nozzle through flexible pipes, the overflow from the nozzle being collected in a tray beneath the casting unit.

4.1.4 Immersed Heater

A heater was immersed in the metal so that the heat transfer coefficients from the ingots base to the cooling medium could be determined. The position of this heater varied from system to system. In the aluminium system it was at a distance of 80 mm from the base. In the ferrous system the distance varied from 40 mm to 90 mm.

For the aluminium system a 1 m. long heater of 2.5 Kw capacity enclosed in a stainless steel sheath and insulated from it by a refractory powder was coiled up to form a flat heater.

For the ferrous sytem two separate 750 w heaters in Inconnel sheaths were coiled up as shown in Fig. 4.4 and were connected in parallel with the flat surfaces of the coils placed against one another.

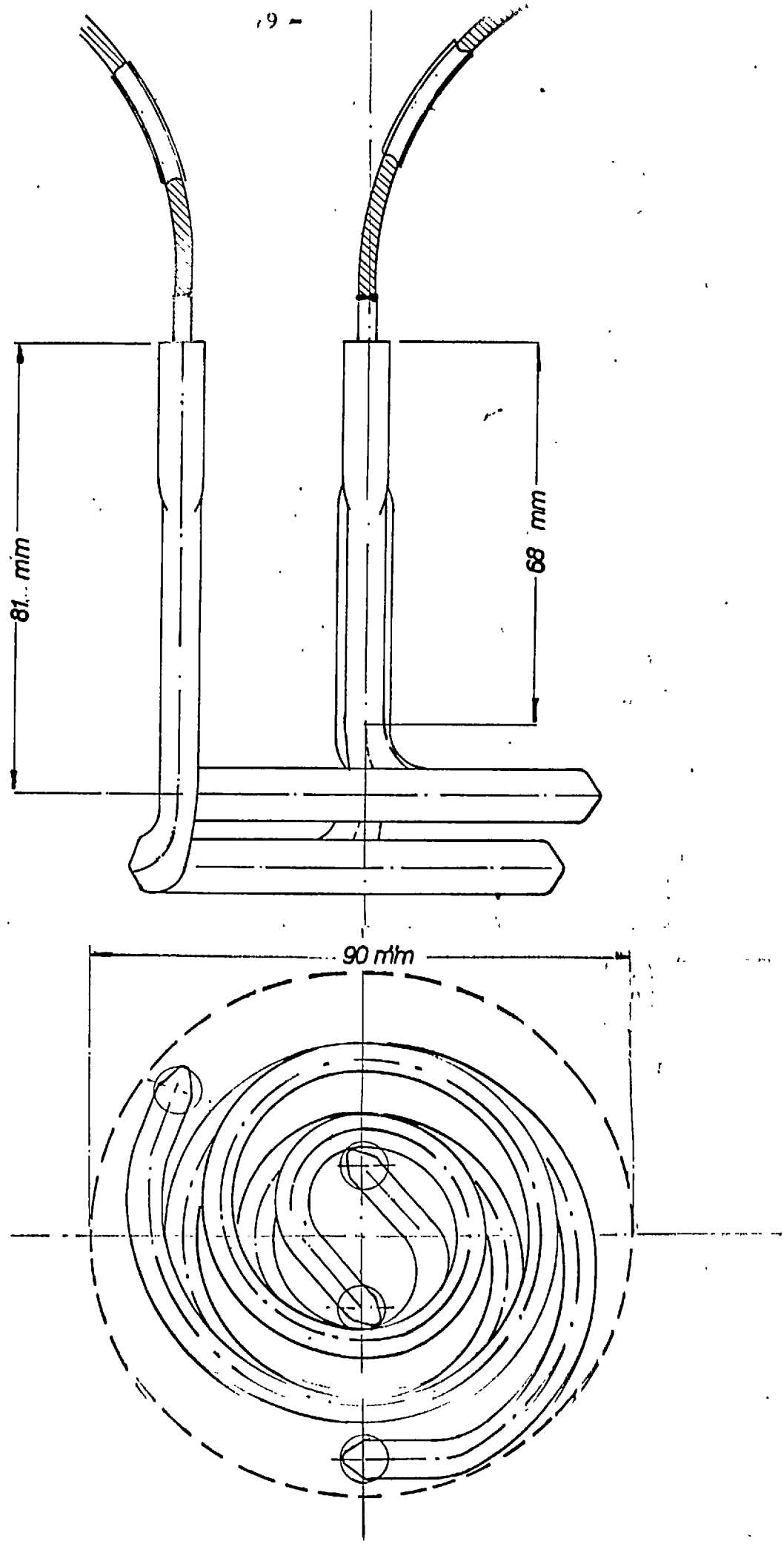

Fig 4.4 : 2 -750W IMMERSED HEATERS ARRANGEMENT

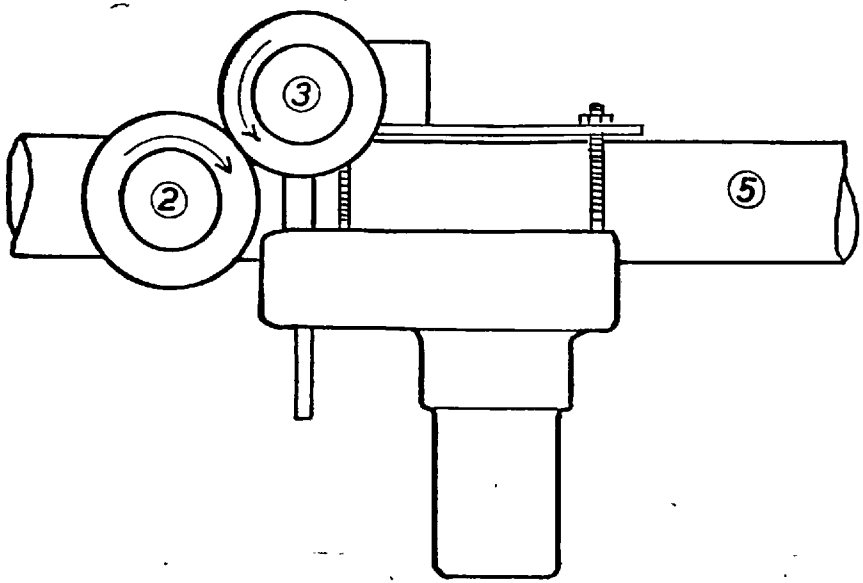

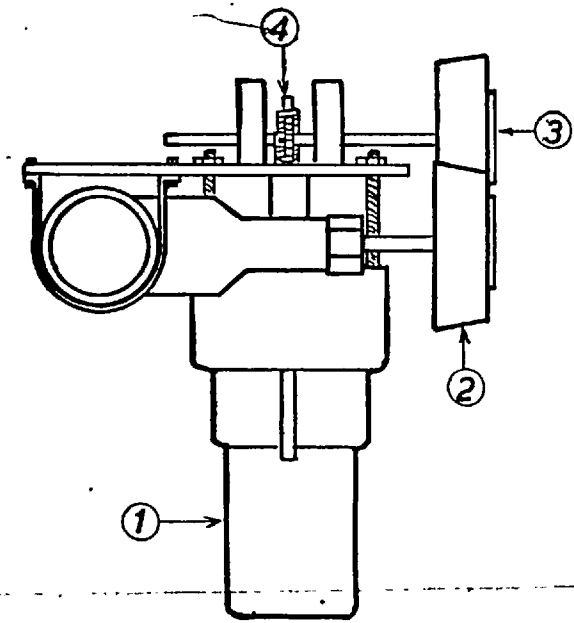

① Reversible D.C motor

② Gate valve control wheel

③ Valve driving wheele

④ Gear arrangement

⑤ 2" Air pipe from blower

6 Motor support bracket

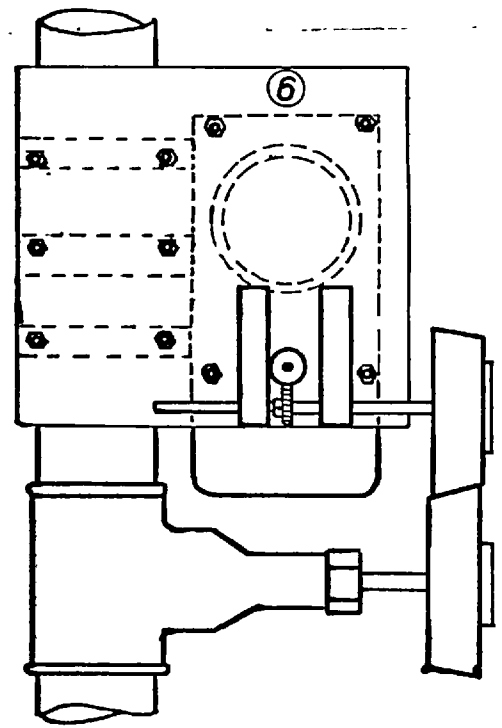

Fig 4.5 : MOTORISED VALVE ARRANGEMENT *SCALE 1:4*

4.2. Procedures

4.2.1. Measurement of Heat Transfer Coefficient

The special heater was immersed in the molten metal and the thermocouples positioned at various heights inside the melt. Additional thermocouples were in the following positions: a) inside the air stream just below the nozzle and, b) welded to the outside of the base of the crucible.

The height of the heater above the base varied with the system investigated.

After solidifying around the heater, the metal in the crucible was heated by the external heater to a steady temperature below its melting point. The internal heater and the air blower were then switched on, both being ajusted until steady state conditions were achieved, with the base temperature as close as possible to its original value.

The manometer reading, the temperatures and power input to the immersed heater were then recorded.

4.2.2. Determination of the Progress of Solidification

The alloy to be investigated was melted in situ and the thermocouple assembly introduced and secured in the required position. The metal was then heated to a temperature just above the desired value, the heater switched off and the melt stirred continuously with a stainless steel rod to even out any temperature or composition gradients. When the desired temperature was reached the butterfly valve in the air line was opened, the gate valve having been preadjusted to give the desired flow rate of cooling air. The temperatures were recorded continuously

All the required results were then obtained from the cooling curves.

Before each series of experiments the crucible thermocouples and stirrer were coated with Koron 510. This involved diluting the refractory paste with water in the ratio of 5:2. and swabbing the resulting solution onto the surface to be coated, these surfaces having been preheated to 100°C. The coating was then flame dried.

Each batch of thermocouples was calibrated before use, the melting point of pure aluminium being taken as the reference.

The biasing units were adjusted each day to give the required biasing potentials, and checked against a potentiometer.

4.2.3 The Controlled Growth of Eutectics

The metal was held at its melting point and stirred. The air valve was then opened to give the required initial air flow rate (see sections 3.3 and 5.3).

With the heater switched off the metal was solidified, the air valve being continuously adjusted at the rate determined as described in section 5.3.

Thermocouples were placed in the melt to verify that the solid-liquid interfaces moved at the constant rate.

The experiments were repeated without the thermocouples for structural and mechanical properties studies.

CHAPTER 5

RESULTS

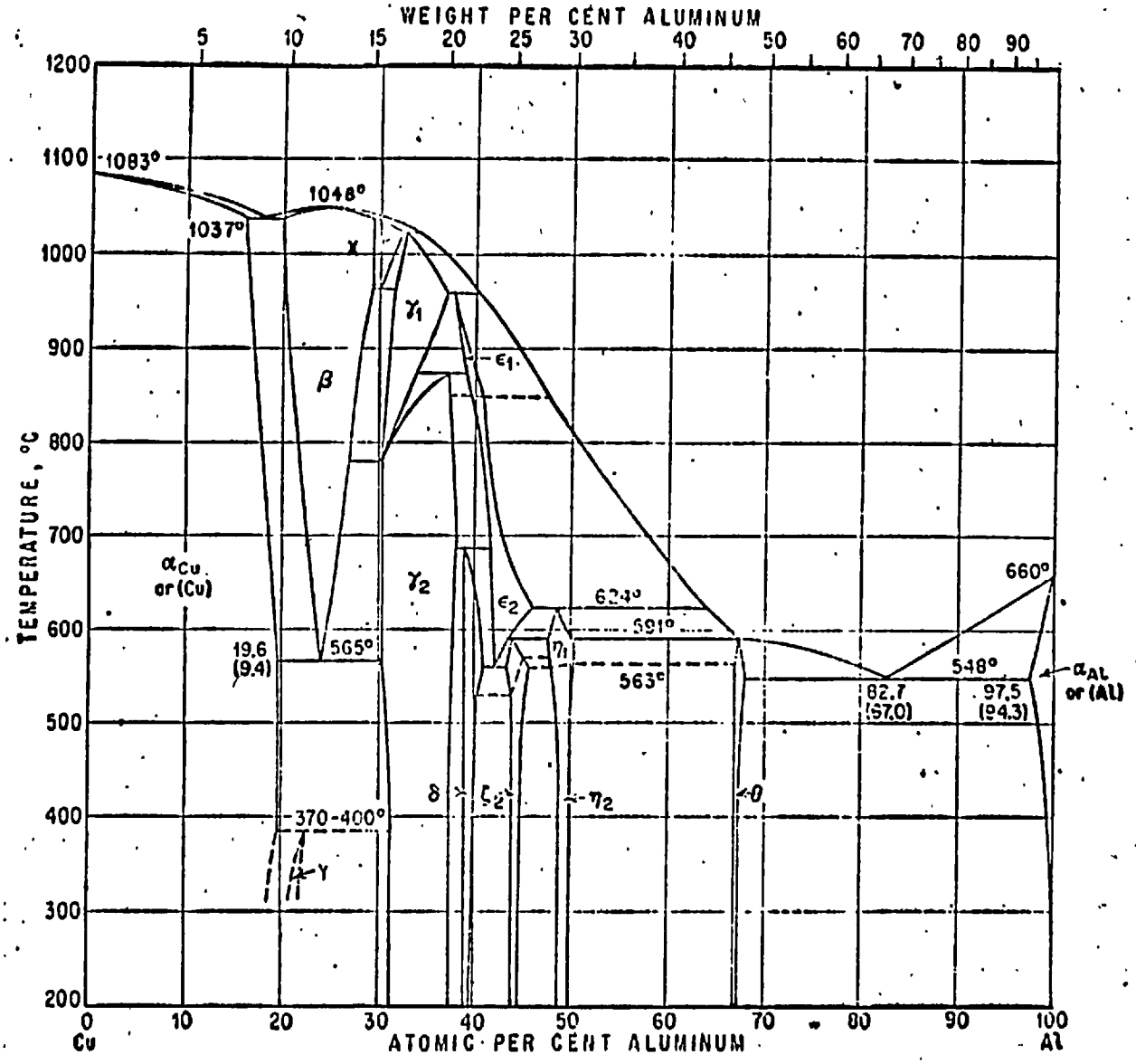

Fig 5.1 ALUMINIUM -COPPER PHASE DIAGRAM

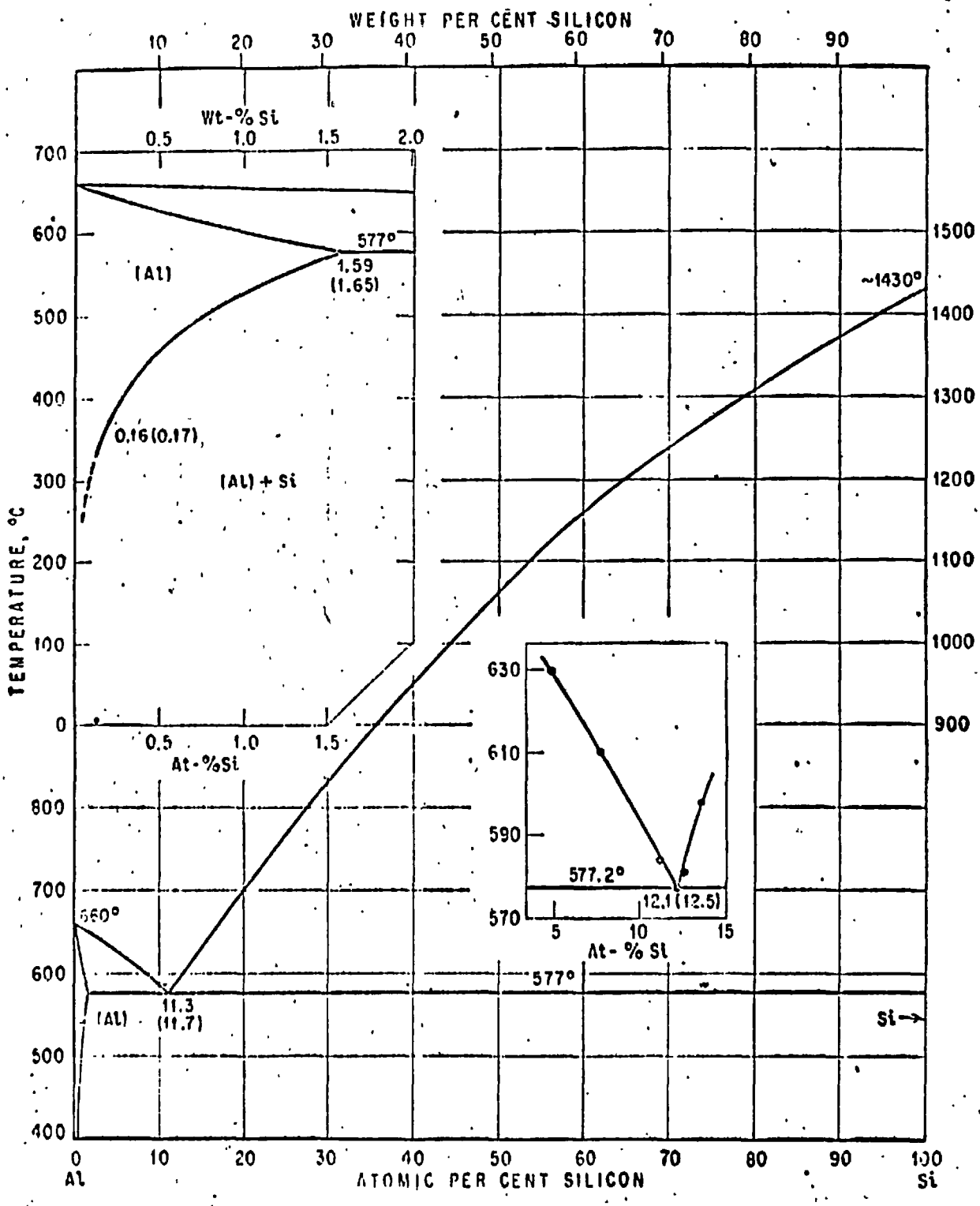

Fig 5.2 ALUMINIUM - SILICON PHASE DIAGRAM

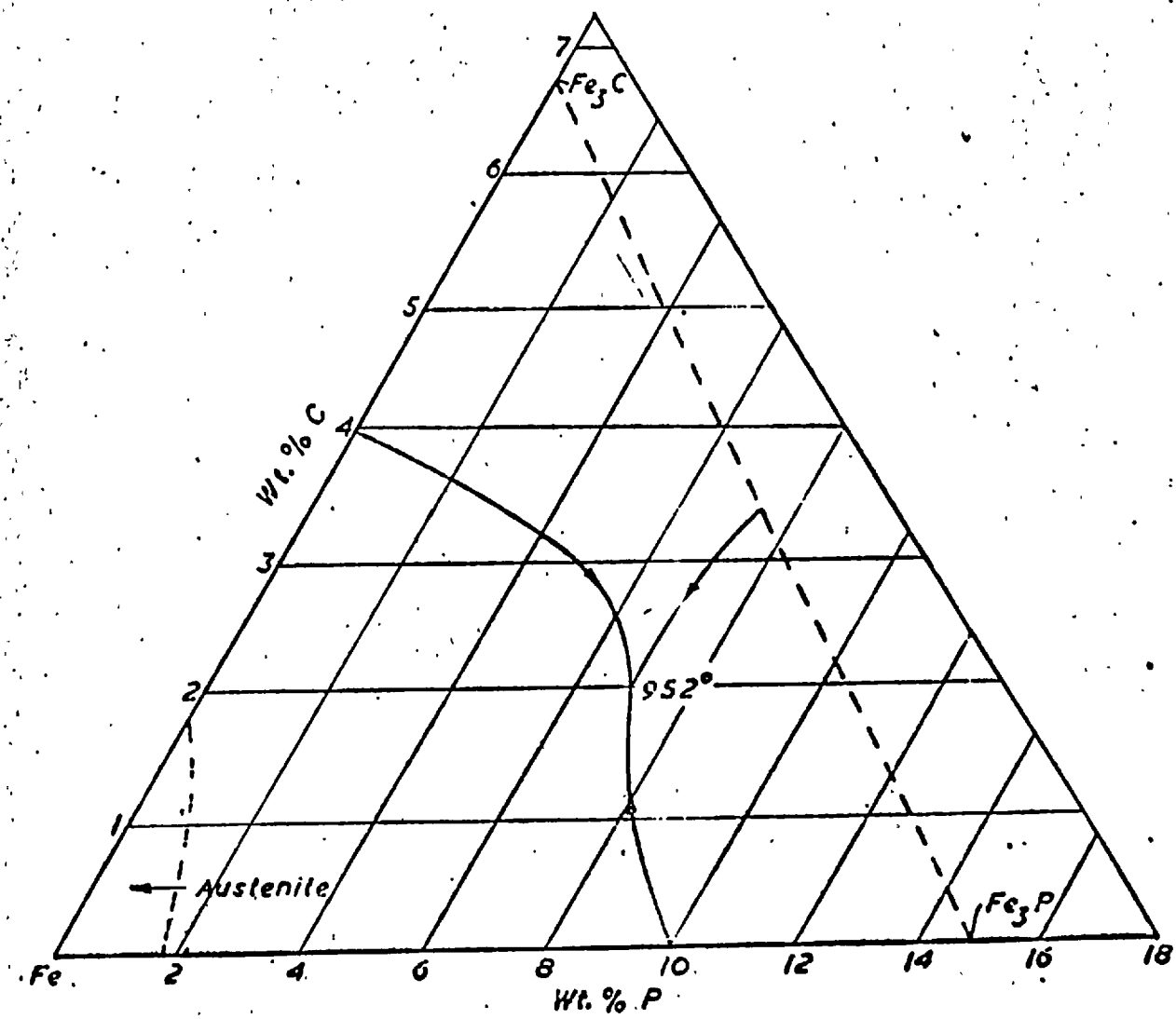

Fig 5.3 C–Fe–P Liquidus

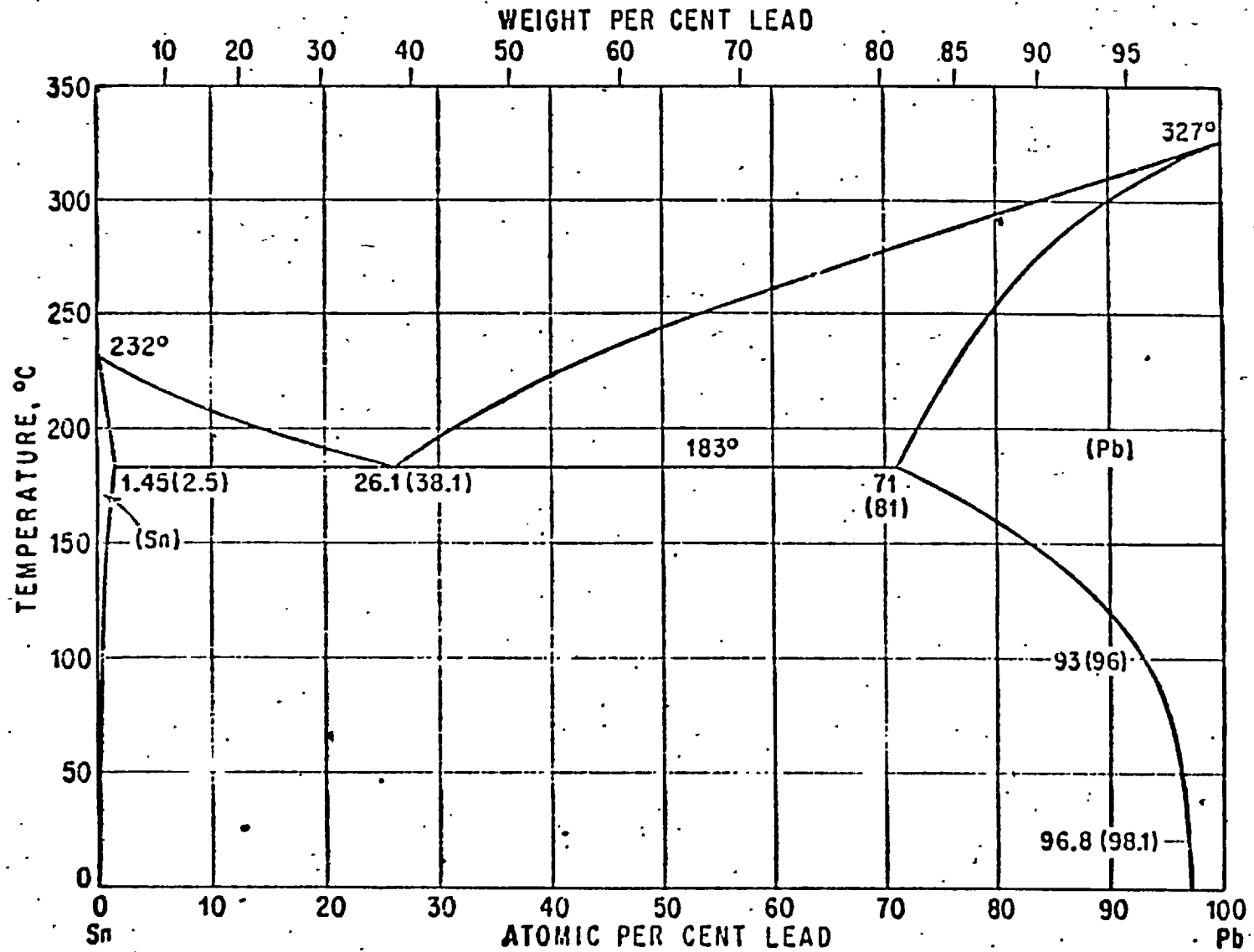

Fig 5.4 LEAD-TIN PHASE DIAGRAM

CHAPTER 5

RESULTS

The experimental work involved the following:

1) Determination of heat transfer coefficients.
2) Study of the progress of solidification and of temperature variations during solidification for a) pure metals and eutectic alloys and b) binary alloys of compositions intermediate between the pure solvent and the eutectic.
3) Investigation into controlling cooling conditions so as to solidify eutectics at a constant rate.
4) Study of the structure and mechanical properties of the eutectics solidified under controlled cooling conditions.

The experimental results are given in the following sections and compared with theoretical predictions as described in Chapter 3.

The phase diagrams of the systems investigated are given in Figs. 5.1, 5.2, 5.3 and 5.4

5.1 Heat Transfer Coefficients

5.1.1 Determination of Heat Transfer Coefficient

Assuming cooling conditions obeying Newton's Law of cooling we have

$$\dot{q}''_o = -h(\theta_o - \theta_{air}) \qquad (5.1.1.)$$

where

$\dot{q}''_o$ = heat flux leaving cooled surface of an ingot cooled from one side only.

h = heat transfer coefficient between the cooled surface and the cooling air.

$\theta_o - \theta_{air}$ = temperature difference between the cooled and cooling media.

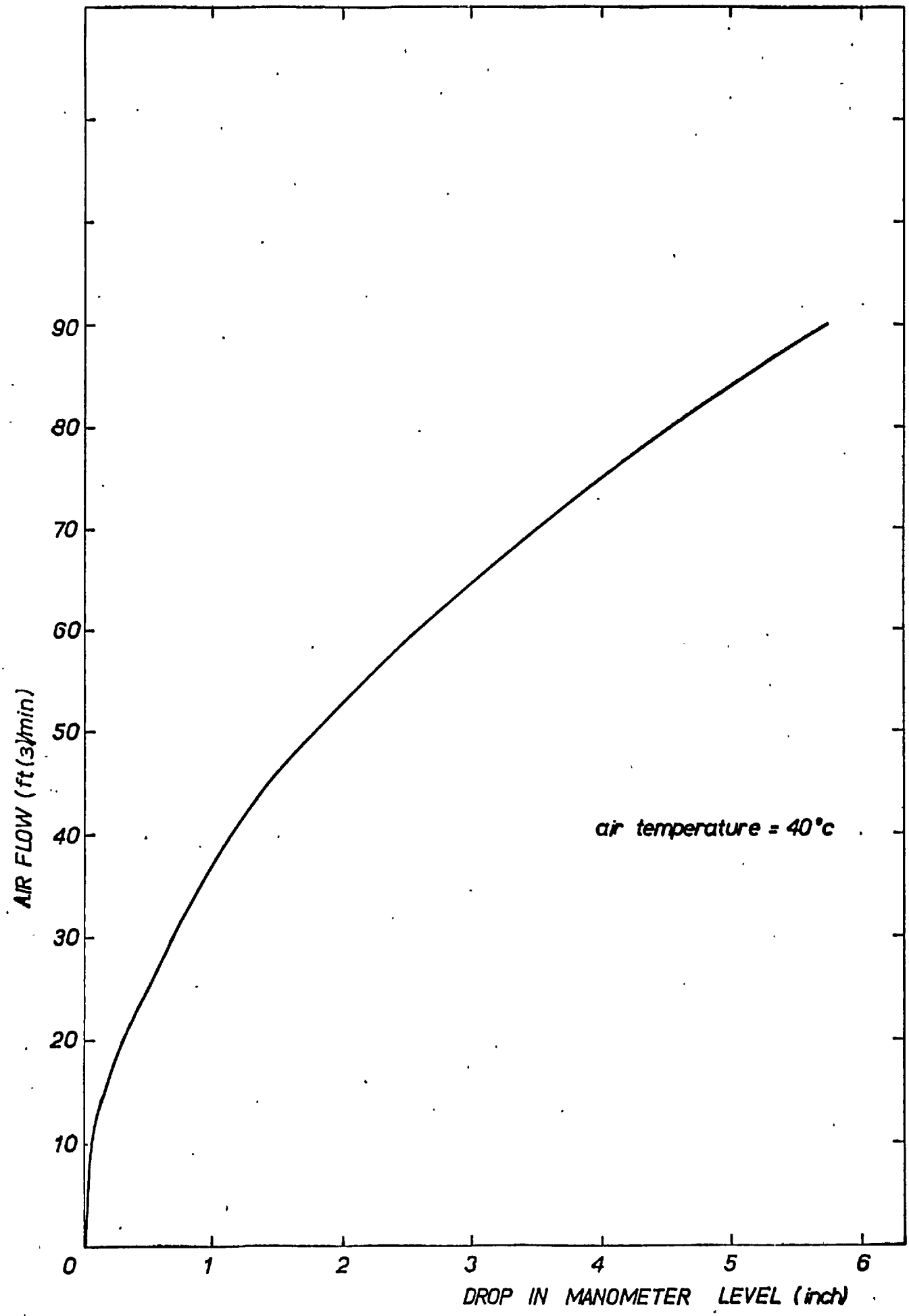

Fig 5.5 CALIBRATION CURVE FOR AIR FLOW DETERMINATIONS

If heat is conducted inside the metal, then under steady state conditions the heat flux involved is given by:

$$\dot{q}''_o = - K \frac{d\theta}{dx} \qquad (5.1.2)$$

where

K is the thermal conductivity of the material and $\frac{d\theta}{dx}$ the temperature gradient established.

Since all the heat conducted through the metal is removed by the cooling medium, we have:

$$h = \frac{K \frac{d\theta}{dx}}{(\theta_o - \theta_{air})} \qquad (5.1.3)$$

5.1.2 The Heat Transfer Coefficient between Metal and Air

The blower was capable of passing about 90 c.f.m. of air through the piping system and nozzle.

Values of heat transfer coefficients corresponding to different air flow rates were determined using the procedure described in section 4.2.1 above and equation (5.1.3).

The air flow rate correxponding to a given manometer reading was calculated from a standard formula given in British Standard B.S. 1043, and this formula has been used in plotting the calibration curve for the manometer (Fig.5.5).

The experiments were conducted at three different temperatures using aluminium as the ingot material in the 18/8 stainless steel crucible and repeated at a fourth temperature using the cast iron eutectic in the cast 25/12 stainless steel mould.

Specimen calculation tables, and plots of temperature gradients are given respectively in table 5.1.1 and Fig. 5.6 Relationships

Air Flow Ft(3)/Min	Steady State Ingot's base temperature (°C)	Approximate power to immersed heater cal/sec.	Temperature gradient (best fit lines) °C/cm.	Heat conducted through metal cal/sec.	Heat transfer coefficient $\frac{K}{\Delta\theta} \cdot \frac{d\theta}{dK}$ cal/cm(2).S.°C x 10^4
85.0	590	290	7.4	294	68.0
85.0	540	260	6.6	262	67.0
85.0	500	240	6.1	242	66.3
85.0 + water	200	398	10.2	405	270
57.5	590	240	5.9	234	54.0
57.5	540	220	5.3	210	53.0
57.5	500	200	4.9	195	52.5
57.5 + water	200	325	8.4	332	220
35.5	590	160	4.5	179	41.0
35.5	540	140	4.0	159	40.5
35.5	500	150	3.6	143	39.8
35.5 + water	200	230	6.1	240	160

K = 0.505 cal/cm.S.°C Average air temperature = 40°C Ingot's base area = 78.7 cms.

Average air - water mixture temperature = 8°C

TABLE 5.1.1 DETERMINATION OF HEAT TRANSFER COEFFICIENT (Aluminium with air and air water mixtures)

Air flow Ft(3)/min	Steady State Ingot's base temperature (°C)	Approximate power to immersed heater Cal/sec	Temperature gradient (best fit lines) °C/cm	Heat conducted through metal cal/sec	Heat transfer coefficient $\frac{K}{\Delta\Theta} \cdot \frac{d\Theta}{dK}$ cal/cm(2).S.°C x10^4
74.5	710	298	76	308	79
66.7	725	285	74	300	75
52.7	730	235	63	258	64
40.8	745	230	56	227	55
33.3	750	203	50	210	49
52.7 + water	300	300	79	320	190
40.8 + water	300	260	66	270	160
33.3 + water	300	245	62	250	150

K = 0.07 cal/cm.S.°C Average cooling air temperature = 35°C Ingot's base area = 58 cm^3

Average air-water mixture's temperature = 10°C

TABLE 5.1.2. DETERMINATION OF HEAT TRANSFER COEFFICIENT (Fe-C-p eutectic, with air and air-water mixtures)

between the air flow rates and the heat transfer coefficients are shown in Fig. 5.7 for different temperatures of the crucible base.

5.1.3 The Heat Transfer Coefficient between Metal and Air-Water Mixtures.

Two series of experiments were carried out to determine the heat transfer coefficients obtained using an air-water mixture.

a) constant flow rate of water into the nozzle.

b) variable flow rate of water into the nozzle.

5.1.3.1 Constant flow rate of water.

A constant water head of 4 meters above the air-water nozzle was maintained in the experiments involving aluminium and of 2.5 meters in those involving the iron eutectic.

The water flowing into the nozzle was atomised by air passing through the nozzle at different flow rates. Except for the use of water and the air-water nozzle, the procedure was identical to that described for air alone and the results are reported in the same manner in Fig. 5.7 and Table 5.1.2.

The temperature of the mixture was obtained by a thermal balance calculation.

5.1.3.2 Variable flow rates of water

The rates of flow of water as a function of water head above the nozzle were determined by collecting measured volumes of the water over timed intervals.

The measurements were taken at various flow rates of atomising air.

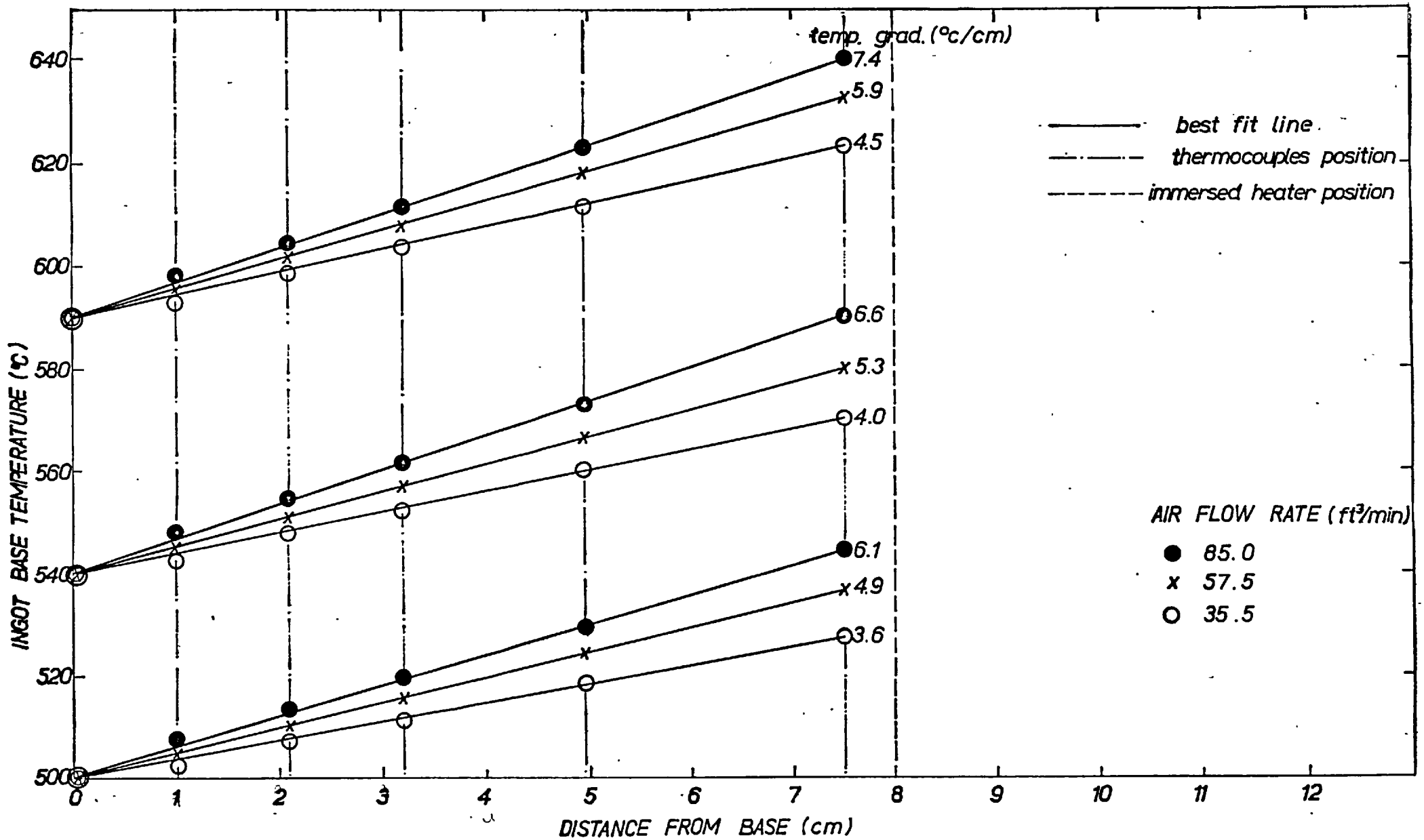

Fig 5.6 AVERAGE TEMPERATURE PROFILES IN SOLID ALUMINUM AT STEADY STATE EXPERIMENTS

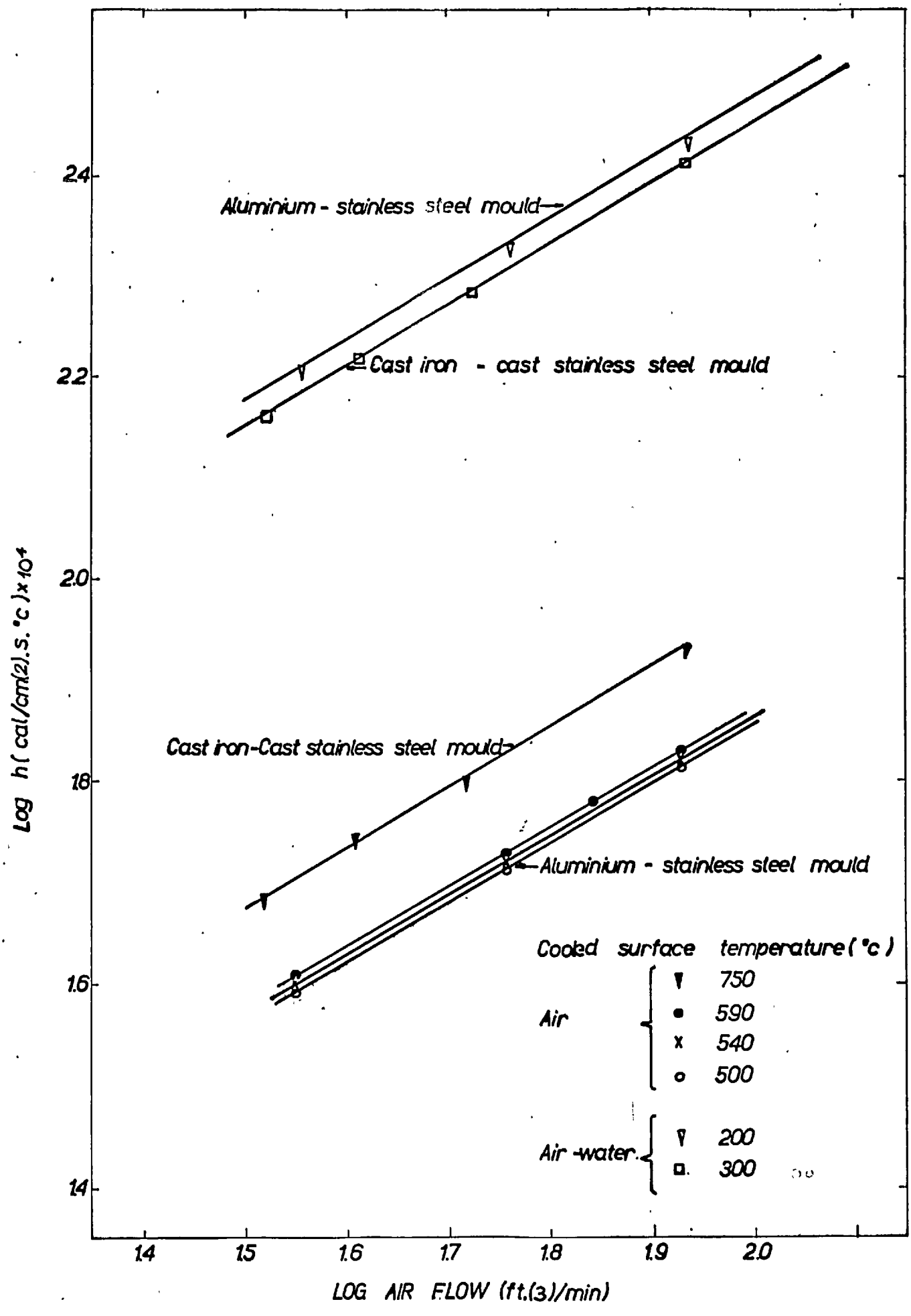

Fig 5.7 STEADY STATE HEAT TRANSFER COEFFICIENT DETERMINATION

Water head above nozzle (m)	1.0	1.5	2.2	2.5	Air flow rate ft(3)/min.
Water entering nozzle (cc/sec)	33	41	46.5	49	
Water overflowing from nozzle (cc/sec) for different air flow rates	6.6	9.2	9.8	10.8	75
	6.3	9.0	9.9	10.9	53
	6.2	8.9	10.0	11.0	36
Average overflow (cc/sec)	6.3	9.3	9.9	10.9	
Net flow through nozzle (cc/sec)	26.7	31.7	36.6	38.1	

TABLE 5.1.3 THE FLOW OF WATER FOR VARIOUS WATER HEADS.

Water head (m)	No water	1.0	1.5	2.2	2.5	Air flow rate (ft(3)/min)
Heat transfer coefficient cal/cm(2).S.°C and mixture temperature °C.	0.0064 (35°C)	0.017 (11.3°C)	0.017 (10.5°C)	0.018 (10°C)	0.0190 (9.4°C)	52.7
	0.0055 (35°C)	0.015 (9.4°C)	0.016 (8.7°C)	0.016 (8.5°C)	0.0160 (8.3°C)	40.8
	0.0050 (35°C)	0.015 (8°C)	0.014 (7.7°C)	0.014 (7.7°C)	0.0150 (7.7°C)	33.3

TABLE 5.1.4 HEAT TRANSFER COEFFICIENTS FOR VARIOUS AIR WATER MIXTURES

Steady state experiments were then conducted to determine the heat transfer coefficient as a function of the atomised water flow rates, using the ternary iron carbon phosphorous eutectic metal experimental system.

Typical average results are reported in Tables 5.1.3 and 5.1.4.

5.2 The Progress of Solidification under Unidirectional Heat Flow Conditions

The following systems were investigated:

I Aluminium (99.99%)

II Aluminium copper alloys

a) AL - $CUAl_2$ eutectic (33% Cu)

b) AL - 4% Cu

c) AL - 8% Cu

d) AL - 30% Cu

III Aluminium - silicon eutectic (12.7% Si)

IV Fe - 6.6% P - 2.1% C eutectic

For any one system, experimental runs were carried out from various temperatures above the melting point (liquidus) and from the melting point itself (i.e. with or without superheat) under varying cooling conditions.

The temperatures inside the metal, at various heights above the cooled surface were recorded continuously. From the cooling curves the following information was obtained.

a) The temperature profiles inside the ingot at any time during the solidification process.

b) The temperature of the cooled surface as a function of cooling time.

c) The position of the interfaces between solid and liquid in pure metals and the position of the solidus and liquidus in the binary alloys.

At least three experimental runs were carried out for each set of conditions.

5.2.1 Pure Metals and Eutectic Alloys

The alloys were prepared to specification by the Fulmer Research Institute.

The experimental results were compared with theorectical predictions obtained using Hills' integral profile method (1).

5.2.1.1 Aluminium

Super purity aluminium was used. The arrest was observed at 660°C. Experiments were conducted at zero super heat and with 30°C and 50°C super heat, and under cooling conditions corresponding to three different heat transfer coefficients.

The rates of solidifications and surface temperature variations are compared with the theoretical predictions in Fig. 5.7 to Fig. 5.13. Thermal balances were drawn up on typical experiments as shown in Tables 5.3 and 5.4.

5.2.1.2. Al - $CuAL_2$ eutectic

The eutectic at 33% Cu between aluminium ~~reach~~ rich solid solution and the intermetallic compound $CuAl_2$ (θ' phase) was found to melt at 548°C in accordance with the phase diagram Fig. 5.1. Experiments were conducted at the melting point., and at three different cooling rates. The comparison between theoretical predictions for the rate of solidification and temperature variations and the experimental results are given in Figs. 5.14 to 5.19. Thermal balances are set out in Tables 5.5 and 5.6

Initial temperature = 660°C

Solidification temperature = 660°C

Height of metal = 11.4 cm

Cooling air temperature = 40°C

Heat transfer coefficient (cal/cm(2).S.°C) x 10^4	68.0		54.0		41.0	
Casting time (sec)	300	600	300	600	300	600
Solid layer (cm)	4.5	8.5	3.8	7.2	3.0	5.8
Latent heat liberated at the melting point (Kcal)	86.5	163	73	137.5	57.5	111
Temperature in metal (°C)						
0.0 cm.	626	599	636	618	646	638
0.3 cm	628	601	638	620	647	639
2.1 cm	641	614	651	630	656	648
4.3 cm	658	630	660	643	660	658
6.3 cm	660	644		555	660	660
9.0 cm	660	660		660	660	660
Sensible heat liberated in solid layer (Kcal)	5.08	17	4.6	17	1.4	4.25
Total heat liberated in metal	91.5	180	77.6	154.5	59	115.25
Base temperature at mid time (°C)	640	626	647	636	652	646
Heat removed by cooling air	96.5	188	77.6	152.5	59.5	117.5
Excess heat losses (Kcal)	-	-	-	2	-	-
Excess heat gains (Kcal)	5	8	-	-	0.5	2.35

TABLE 5.3 THERMAL BALANCE FOR THE SOLIDIFICATION OF ALUMINIUM AT ZERO SUPERHEAT.

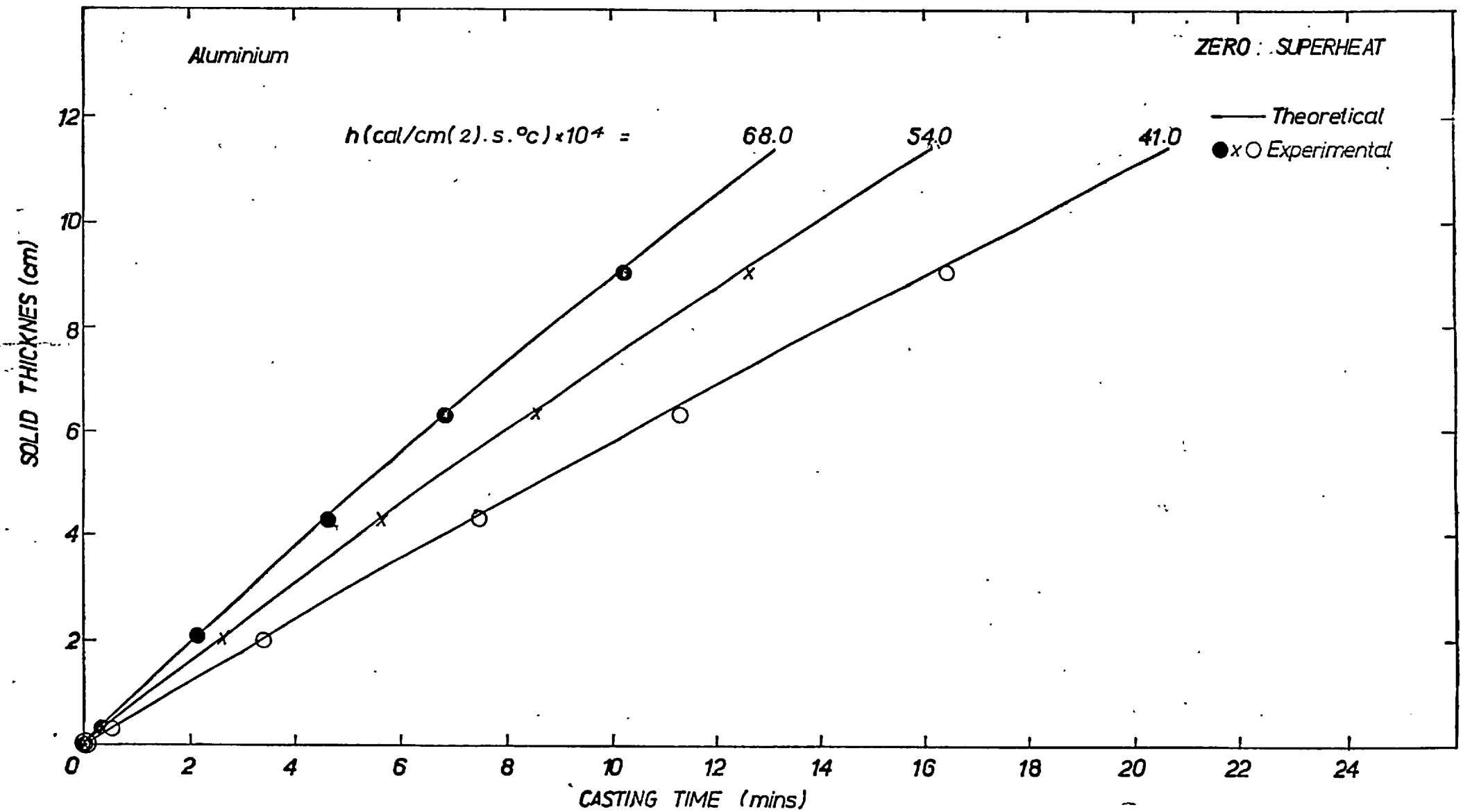

Fig 5.8 SOLIDIFICATION OF ALUMINIUM AT ZERO SUPERHEAT
comparison of theoretical and experimental results

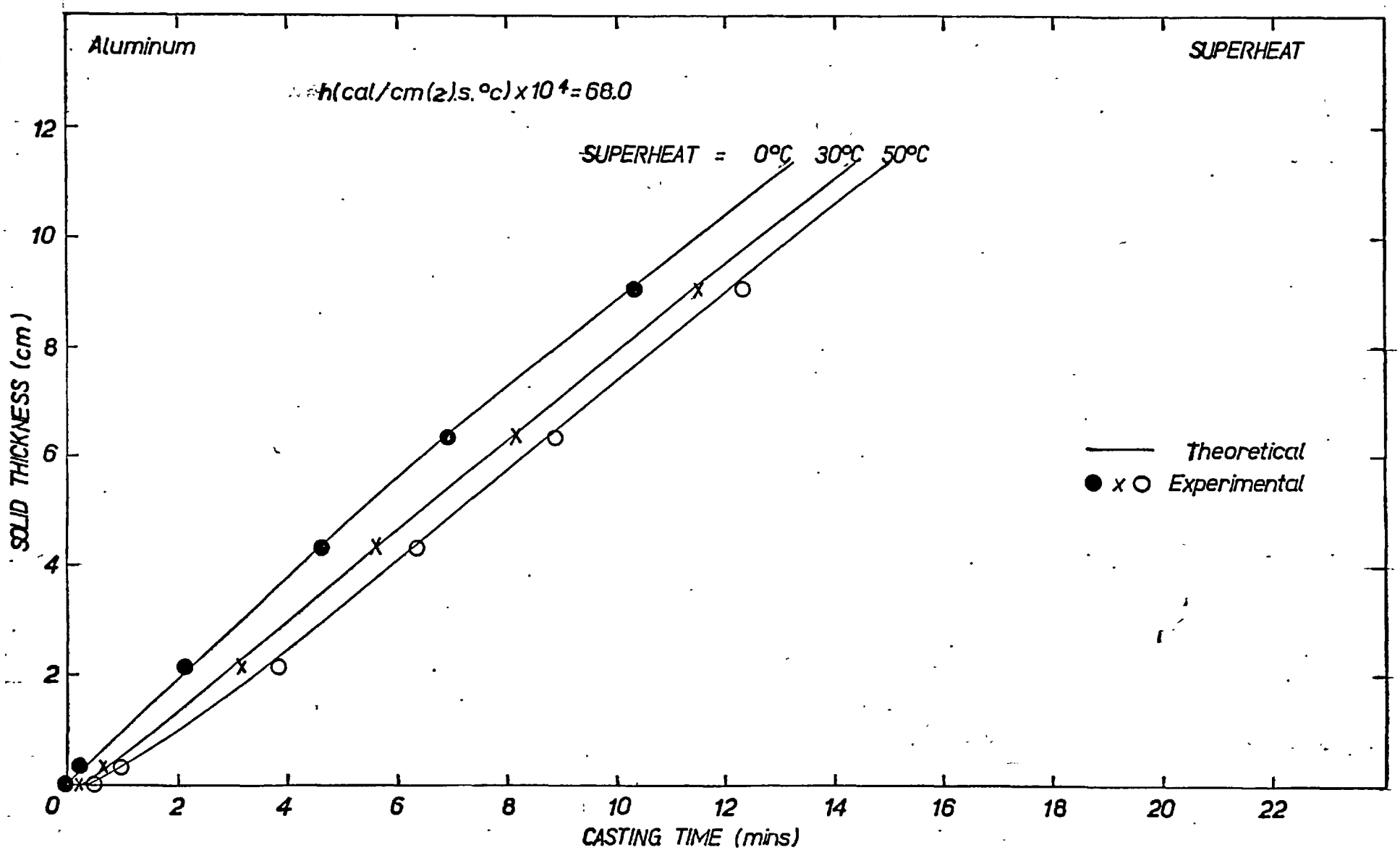

Fig 5.9 SOLIDIFICATION OF ALUMINUM AT POSITIVE SUPERHEAT
comparison of theoretical and experimental results

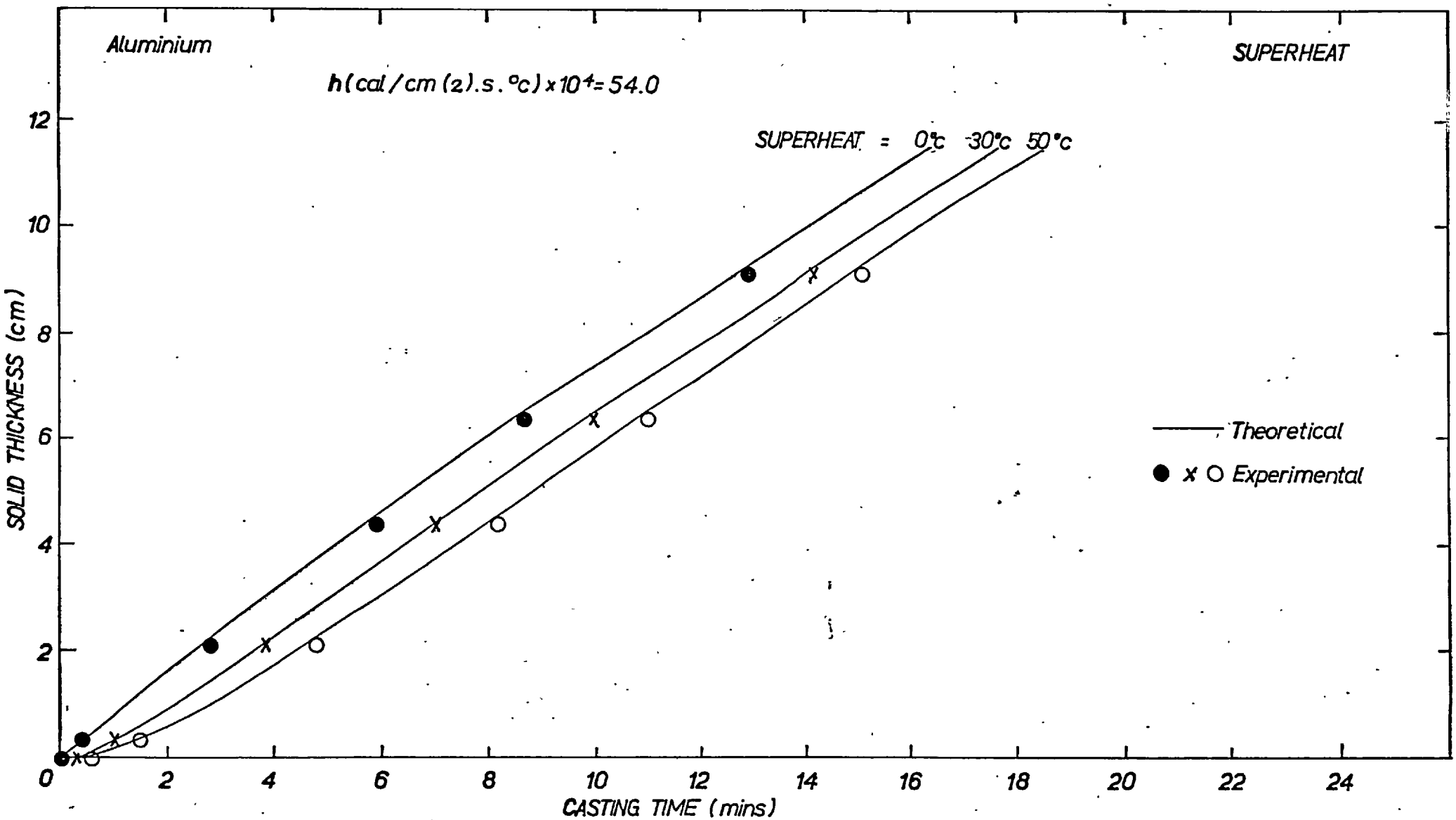

Fig 5.10 SOLIDIFICATION OF ALUMINUM AT POSITIVE SUPERHEAT
comparison of theoretical and experimental results

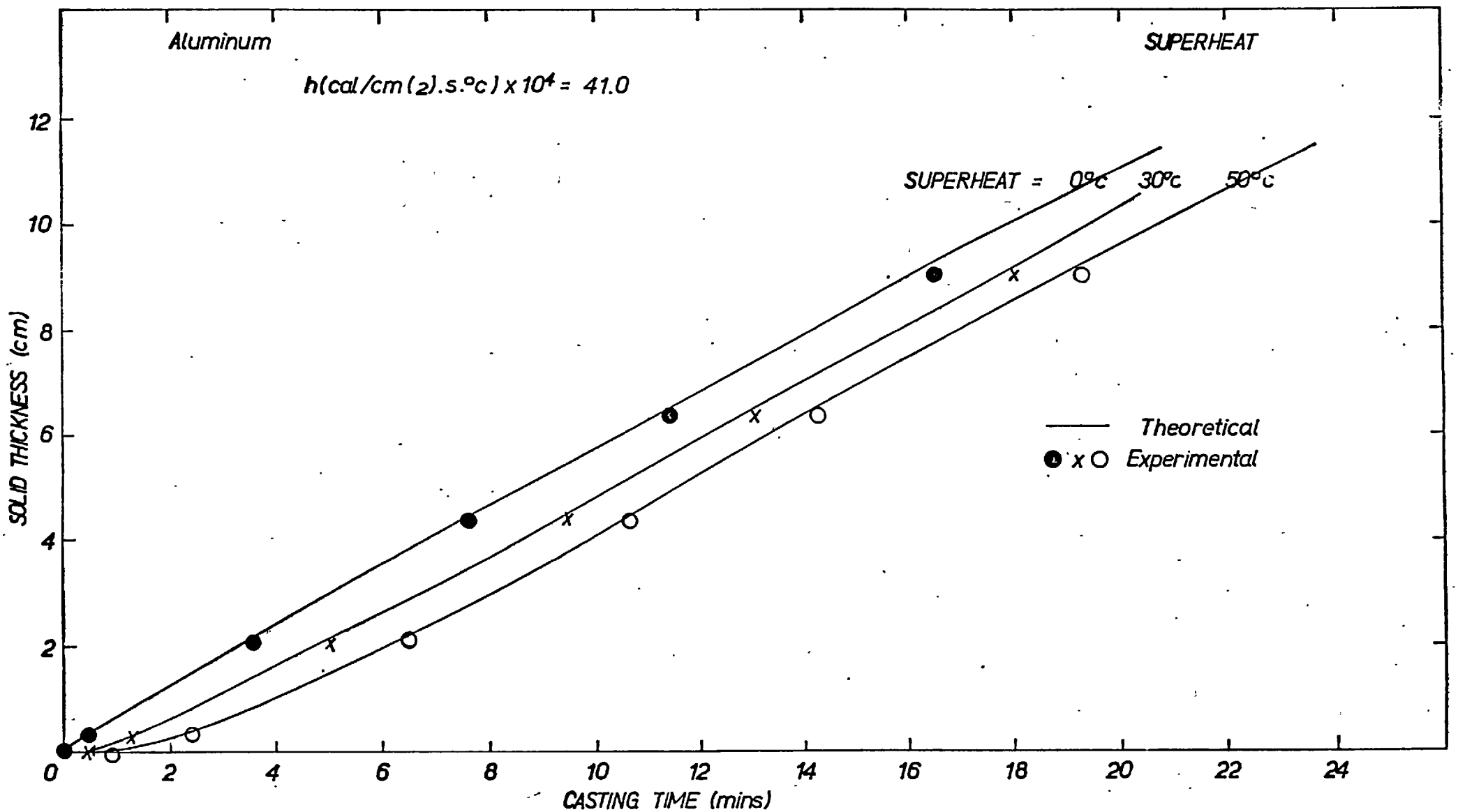

Fig 5.11 SOLIDIFICATION OF ALUMINUM AT POSITIVE SUPERHEAT comparison of theoretical and experimental results

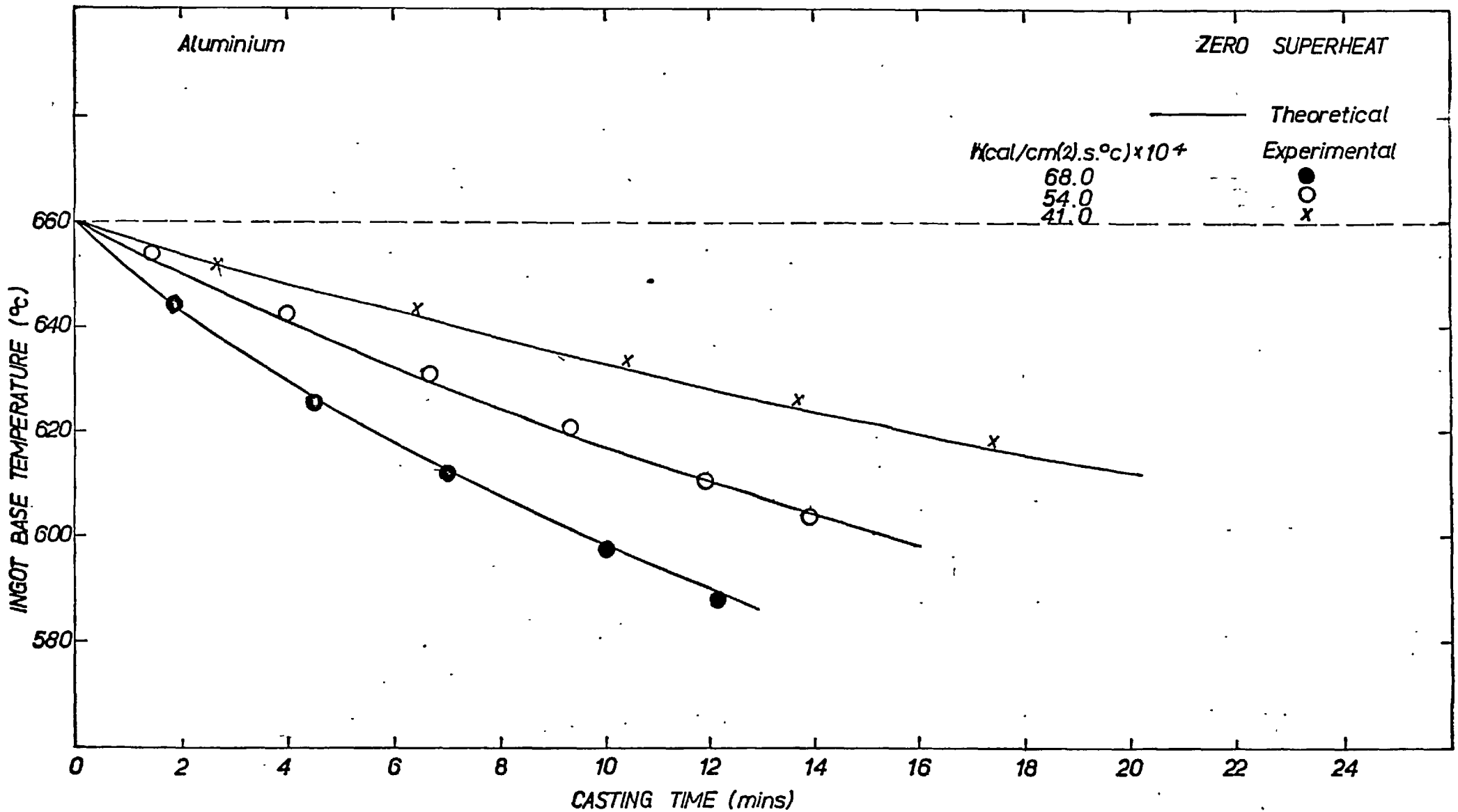

Fig 5.12 SOLIDIFICATION OF ALUMINIUM AT ZERO SUPERHEAT. comparison of theoretical and experimental results

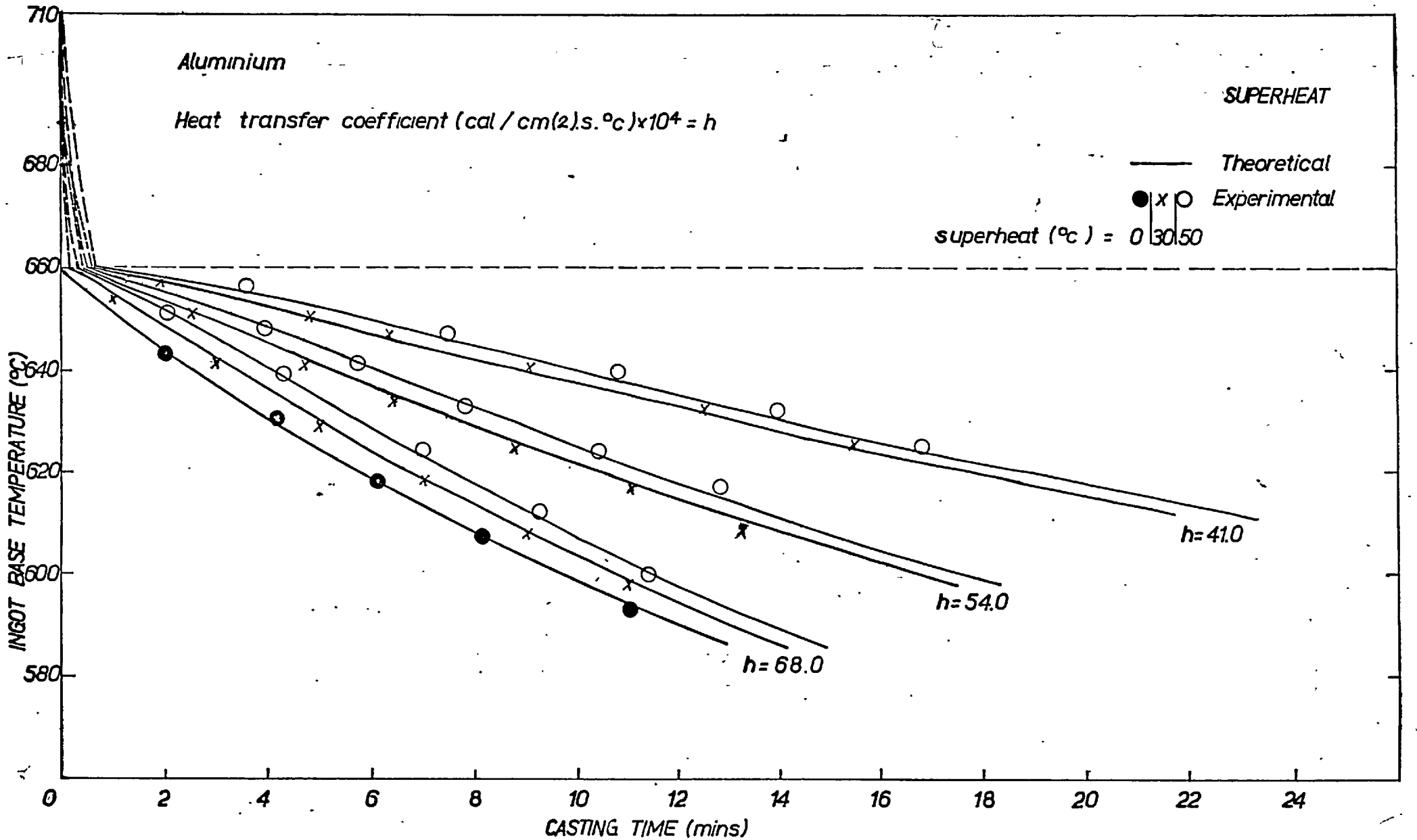

Fig 5.13 SOLIDIFICATION OF ALUMINIUM AT POSITIVE SUPERHEAT
comparison of theoretical and experimental results

Initial temperature = 710°C

Solidification temperature = 660°C

Height of metal = 11.4 cm.

Cooling air temperature = 40°C

Heat transfer coefficient (cal/cm(2).S.°C) x 10^4	68.0		54.0		41.0	
Casting time (min)	5	10	5	10	5	10
Sold layer(cm)	3.2	7.5	2.4	5.9	1.5	4.1
Thermal layer (cm)	8.2	3.9	9.0	5.5	9.9	7.3
Heat liberated on removal of superheat from solid layer (Kcal)	9.65	22.6	7.24	17.8	4.5	12.3
from thermal layer (Kcal)	16.00	4.5	18.3	9.35	19.4	14.8
Latent heat released (Kcal)	61.42	144.0	46.1	113.25	28.8	78.7
Temperature in metal (°C)						
at 0.0 cm	635	606	645	623	652	641
0.3 cm	637	619	647	625	654	643
2.1 cm	651	622	658	637	660	651
4.35 cm	661	640	661	648	662	660
6.3 cm	662	653	662	660	664	660
9.0 cm	664	660	664	660	667	660
Sensible heat liberated in cooling of solid layer (Kcal)	2.64	13.4	1.2	7.25	0.4	2.58
in cooling of thermal layer (Kcal)	5.88	3.6	3.7	3.61	3.6	3.61
Total heat liberated (Kcal)	95.59	188.1	76.54	151.26	56.7	112
Base temperature mid time (°C)	650	635	654	645	655	652
Heat removed by cooling air (Kcal)	97.93	191.0	78.28	154.3	59.53	118
Heat lost to system (Kcal)						
Heat gained from system (Kcal)	2.34	2.9	1.74	3.04	2.83	6

TABLE 5.4 THERMAL BALANCE FOR THE SOLIDIFICATION OF ALUMINIUM WITH 50°C OF SUPERHEAT.

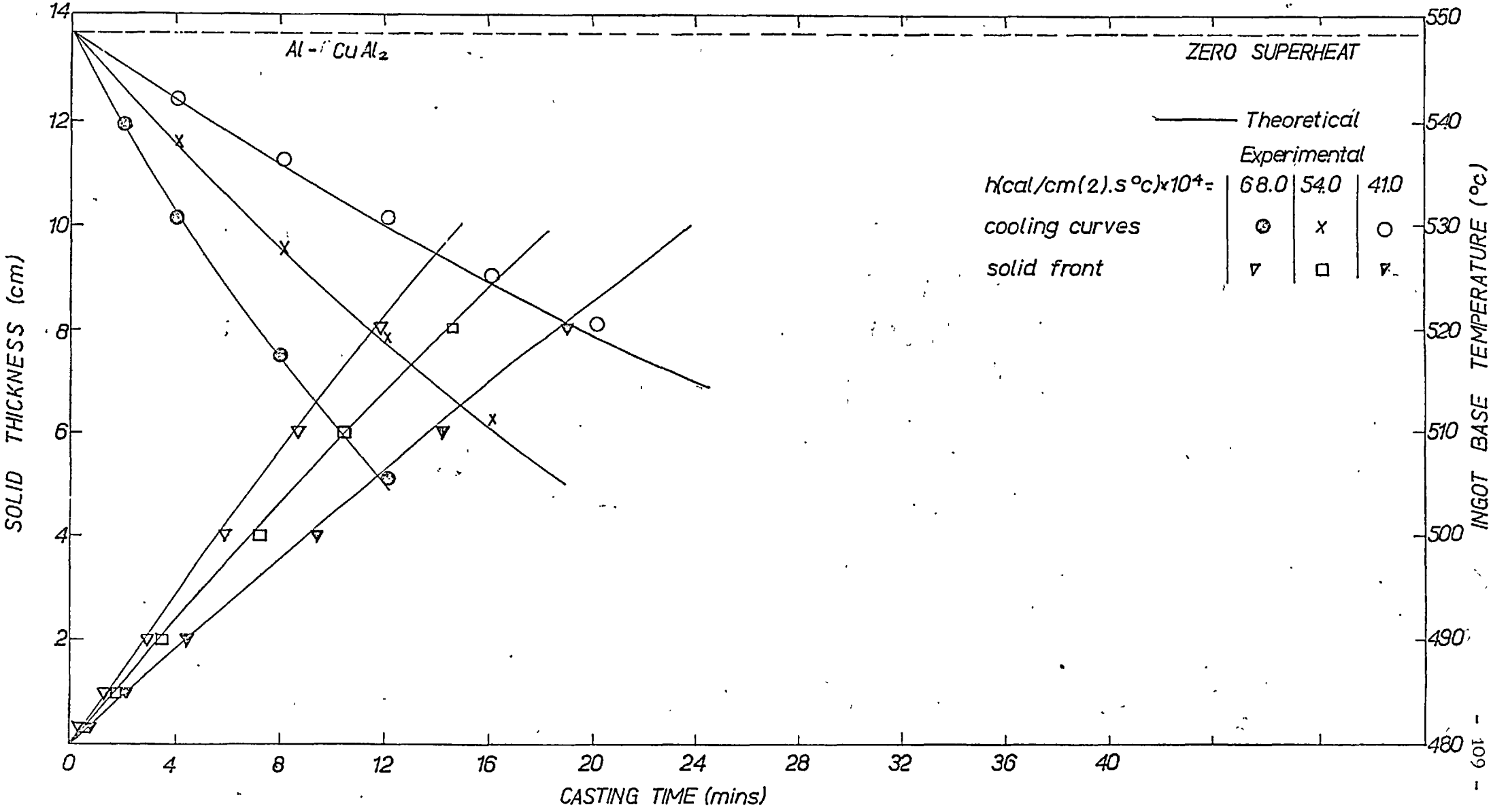

Fig 5.14 SOLIDIFICATION OF ALUMINUM - Cu Al_2 EUTECTIC AT ZERO SUPERHEAT
comparison of theoretical and experimental results

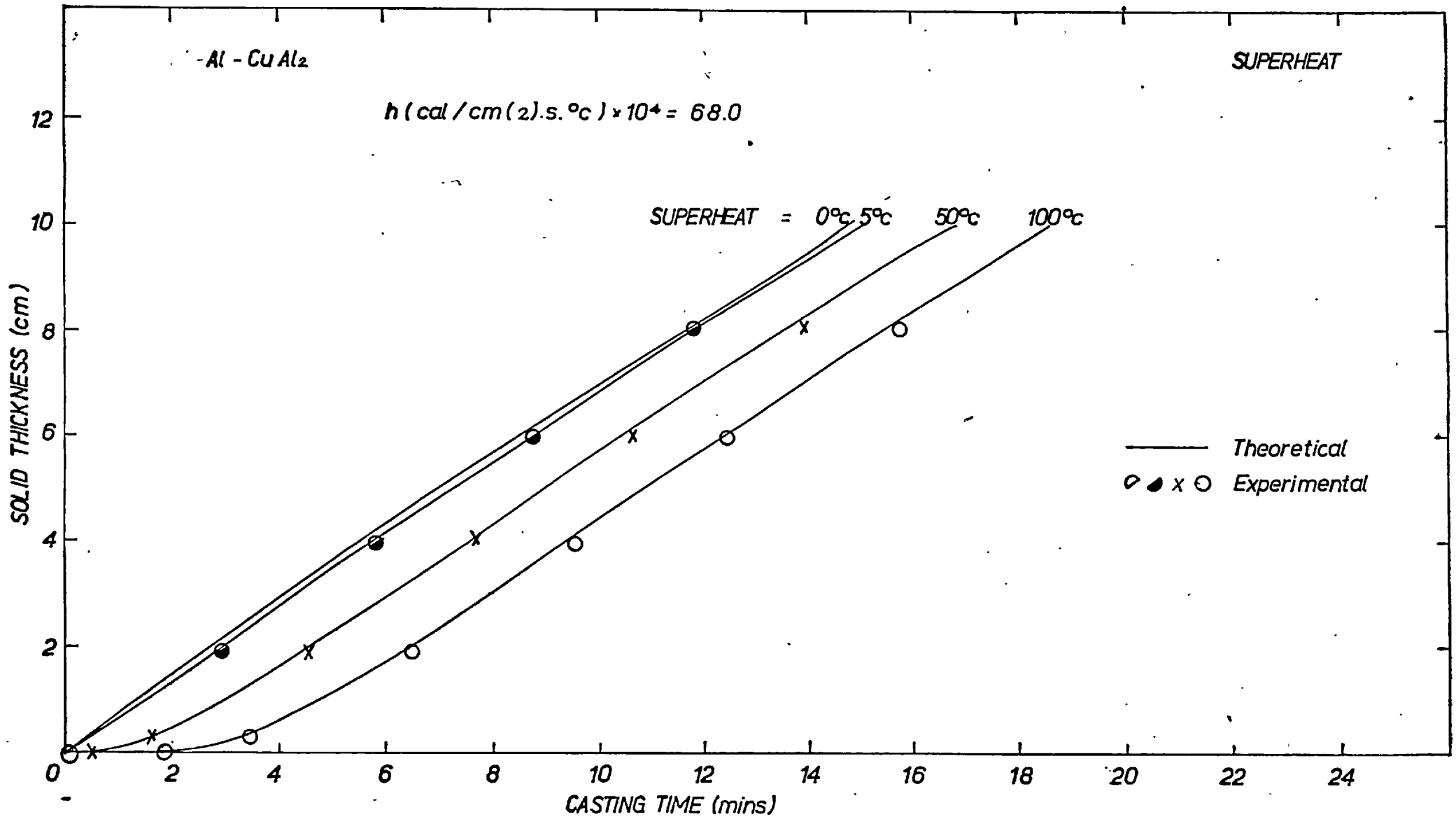

Fig 5.15 SOLIDIFICATION OF ALUMINUM - $CuAl_2$ EUTECTIC AT POSITIVE SUPERHEAT comparison of theoretical and experimental results

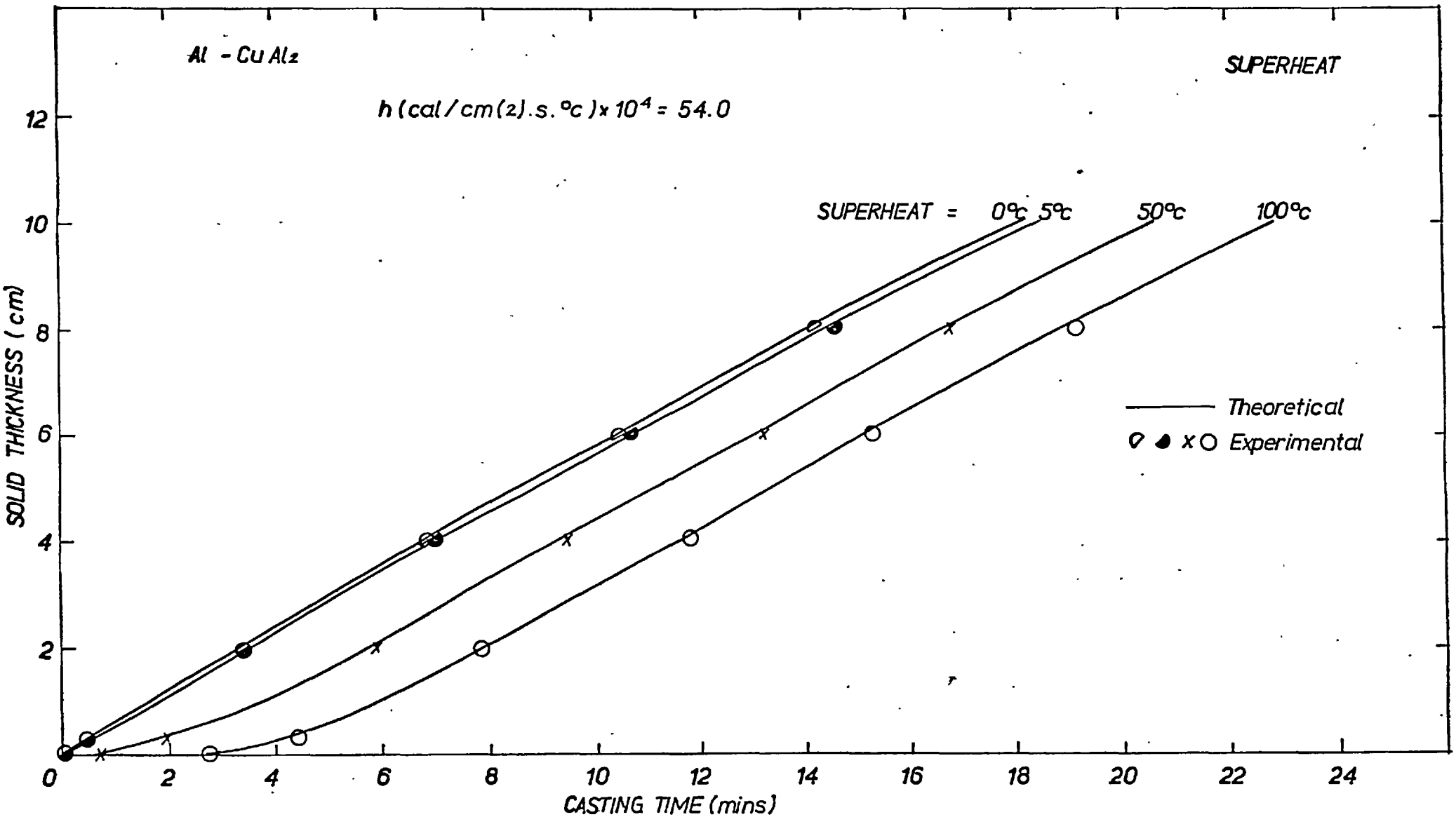

Fig 5.16 SOLIDIFICATION OF ALUMINUM - Cu Al2 EUTECTIC AT POSITIVE SUPERHEAT
comparison of theoretical and experimental results

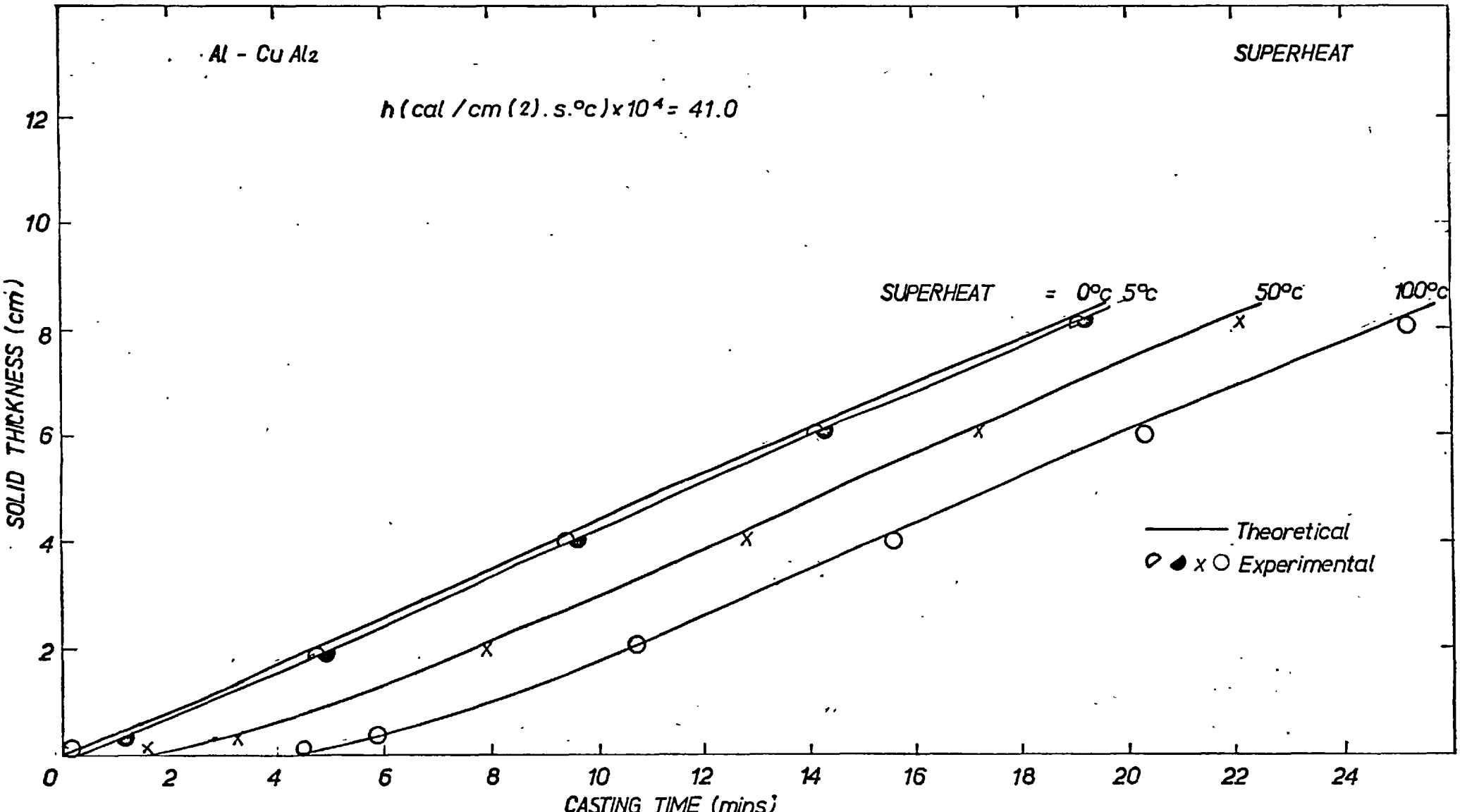

Fig 5.17 SOLIDIFICATION OF ALIMINUM - Cu Al_2 EUTECTIC AT POSITIVE SUPERHEAT comparison of theoretical and experimental results

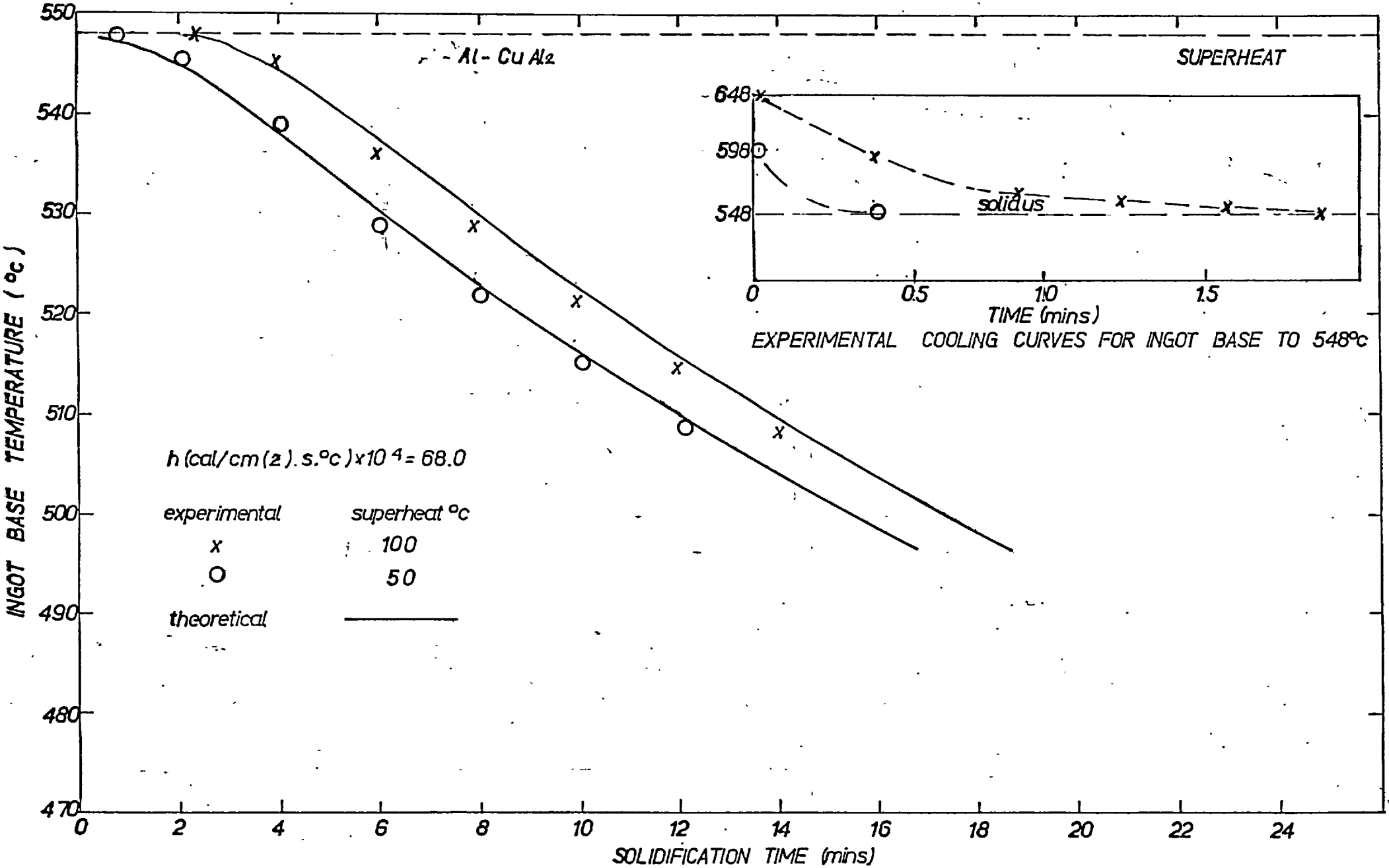

Fig 5.18 SOLIDIFICATION OF Al - CuAl2 EUTECTIC AT POSITIVE SUPERHEAT
comparison of theoretical and experimental results

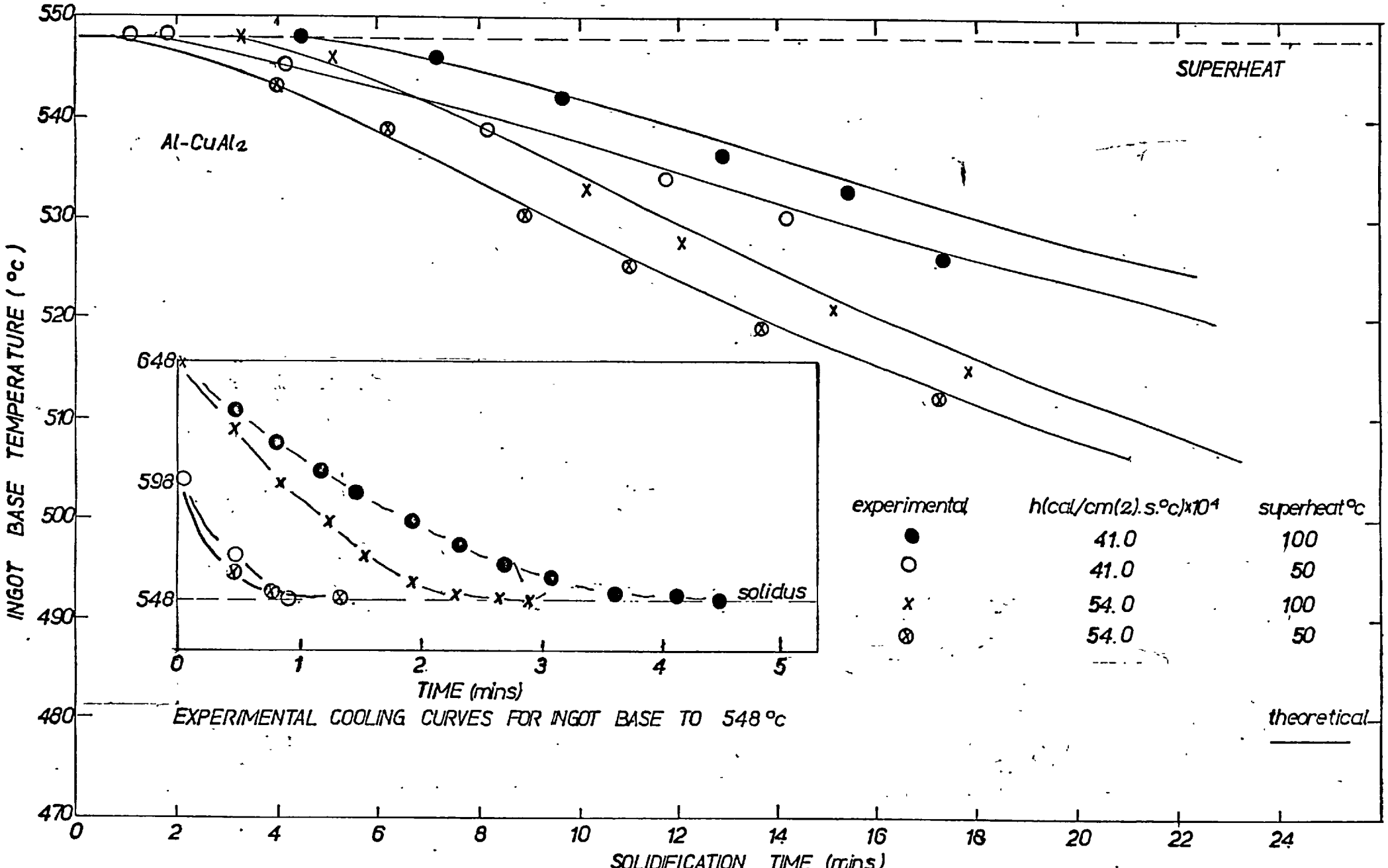

Fig 5.19 SOLIDIFICATION OF Al - $CuAl_2$ EUTECTIC AT POSITIVE SUPERHEAT
comparison of theoretical and experimental results

Initial temperature = 548°C

Solidification temperature = 548°C

Height of metal = 10.0 cm

Cooling air temperature = 40°C

Heat Transfer Coefficient (cal/cm(2).S.°C) x 10^4	68.0		54.0		41.0	
Casting time (min)	5	10	5	10	5	10
Solid layer (cm)	3.7	7.0	3	5.8	2.2	4.5
Latent heat liberated at melting temperature (Kcal)	78.5	148	63.5	123	47	95.5
Temperature in metal (°C)						
0.0 cm	528	510	534	523	540	532
0.30 cm	529	513	535	525	541	534
1.97 cm	539	522	543	531	546	539
4.02 cm	548	534	548	541	548	546
5.98 cm		544		548		548
8.00 cm		548				
Sensible heat liberated in metal (Kcal)	2.25	8.1	1.28	4.4	0.54	2.2
Total heat liberated in metal (Kcal)	80.75	156.1	64.78	127.4	47.54	97.7
Base temperature at mid time (°C)	537	528	541	534	543	540
Heat removed by cooling air (Kcal)	80.0	157	64	126	48.7	97
Excess heat losses (Kcal)	0.75	-	0.78	1.4		0.7
Excess heat gains (Kcal)	-	0.9	-	-	1.2	-

TABLE 5.5 THERMAL BALANCE FOR THE SOLIDIFICATION OF Al-$CuAl_2$ EUTECTIC AT ZERO SUPERHEAT.

Initial. temperature = 648°C Height of metal = 10 cm.

Solidification temperature = 548°C Cooling air temperature = 40°C

Heat transfer coefficient (cal/cm(2)/x10^4	68.0		54.0		41.0	
Casting time (min)	5	10	5	10	5	10
Solid layer (cm)	1.2	4.5	0.5	3	0.3	1.5
Heat liberated during superheat removal (Kcal)	44.1	50.7	44.6	50.7	40.5	50.7
Latent heat liberated (Kcal)	25	94.5	10.5	63	6.3	31.4
Temperature in metal (°C) at						
0.0 cm	540	522	546	535	548	540
0.3 cm	543	523	547	537	548	542
2.0 cm	554	533	556	545	558	548
4.0 cm	558	546	560	548	570	548
6.0 cm	561	548	560	548	580	548
8.0 cm	561	548	560	548	580	548
Sensible heat liberated in solid layer (Kcal)	0.3	3.7	0.03	1.25	-	0.35
Sensible heat liberated in thermal layer (Kcal)	6.1	6.35	6.2	6.35	6.25	6.35
Total heat liberated (Kcal)	75.5	154.75	61.33	121.3	-	88.8
Base temperature mid time (°C)	548	540	550	546	560	548
Heat removed by cooling air (Kcal)	81.7	161	65	129	50.3	98
Excess heat losses (Kcal)	-	-	-	-	3.2	-
Excess heat gains (Kcal)	6.2	6	3.67	7.7	-	9.2

TABLE 5.6 THERMAL BALANCE FOR THE SOLIDIFICATION OF Al-$CuAl_2$ EUTECTIC WITH 100°C OF SUPERHEAT.

5.2.1.3. AL - Si Eutectic

The alloy containing 12.7% silicon and exhibiting an arrest at 577°C was taken to be the eutectic alloy.

Experiments were conducted at three different cooling rates, at zero super heat and with 50°C and 100°C of super heat. Comparisons between theoretical and experimental results are shown in Figs. 5.20 to 5.24 and thermal balances are presented in Table 5.7.

5.2.1.4 Iron - phosphorus - carbon ternary eutectic

This relatively low melting point alloy in the ferrous system (Fig. 5.3) with 6.6% p and about 2.1% C melts at 952°C. ± 2°C.

The results of solidification experiments conducted at 950°C and at 1000°C are reported in Figs. 5.25 - 5.28 and compared with the theorectical predictions.

Heat balances are summarised in Table 5.8.

5.2.2 Binary Alloys Freezing over a Range of Temperatures.

The theory presented in this work (Chapter 3) was compared with the experimental results for three alloys in the aluminium copper system. All three freeze over a range of temperatures and have a eutectic in their non-equilibrium system.

The 4% and 30% copper alloys were prepared by the Fulmer Research Institute.

Initial temperature = 627°C

Solidification temperature = 577°C

Heat transfer coefficient = 0.0054 cal/cu(2).S.°C

Cooling air temperature = 40°C

Height of metal = 11 cm.

Cooling time (min)	5	15
Solid thickness(cm)	2	7.5
Latent heat liberated (Kcal)	45	170
Temperature in metal °C at height (cm)		
0	564	532
1	566	540
2	577	546
3	578	552
6	580	570
9	581	577
Sensible heat liberated (Kcal)	25	37
Total heat liberated (Kcal)	70	207
Base temperature (°C) at mid time	573	556
Heat removed by cooling air (Kcal)	68	197
Excess heat liberated in metal (Kcal)	2	10
Excess heat removed by cooling air (Kcal)	-	-

TABLE 5.7 THERMAL BALANCE FOR THE SOLIDIFICATION OF ALUMINIUM - SILICON EUTECTIC ALLOY WITH 50°C OF SUPERHEAT.

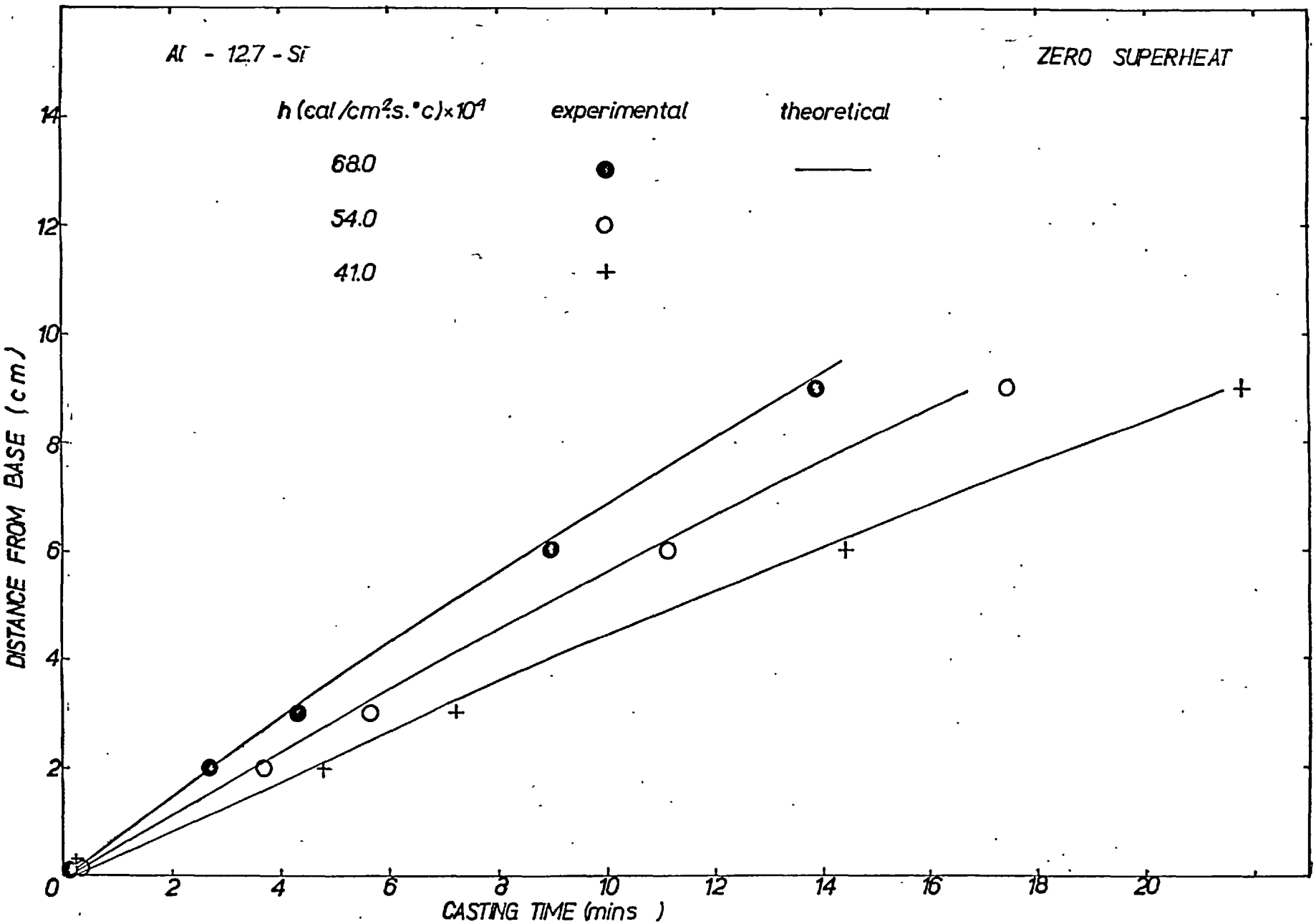

Fig 5.20 SOLIDIFICATION OF 12.7% Si, Al - Si EUTECTIC AT ZERO SUPERHEAT
comparison of theoretical and experimental results

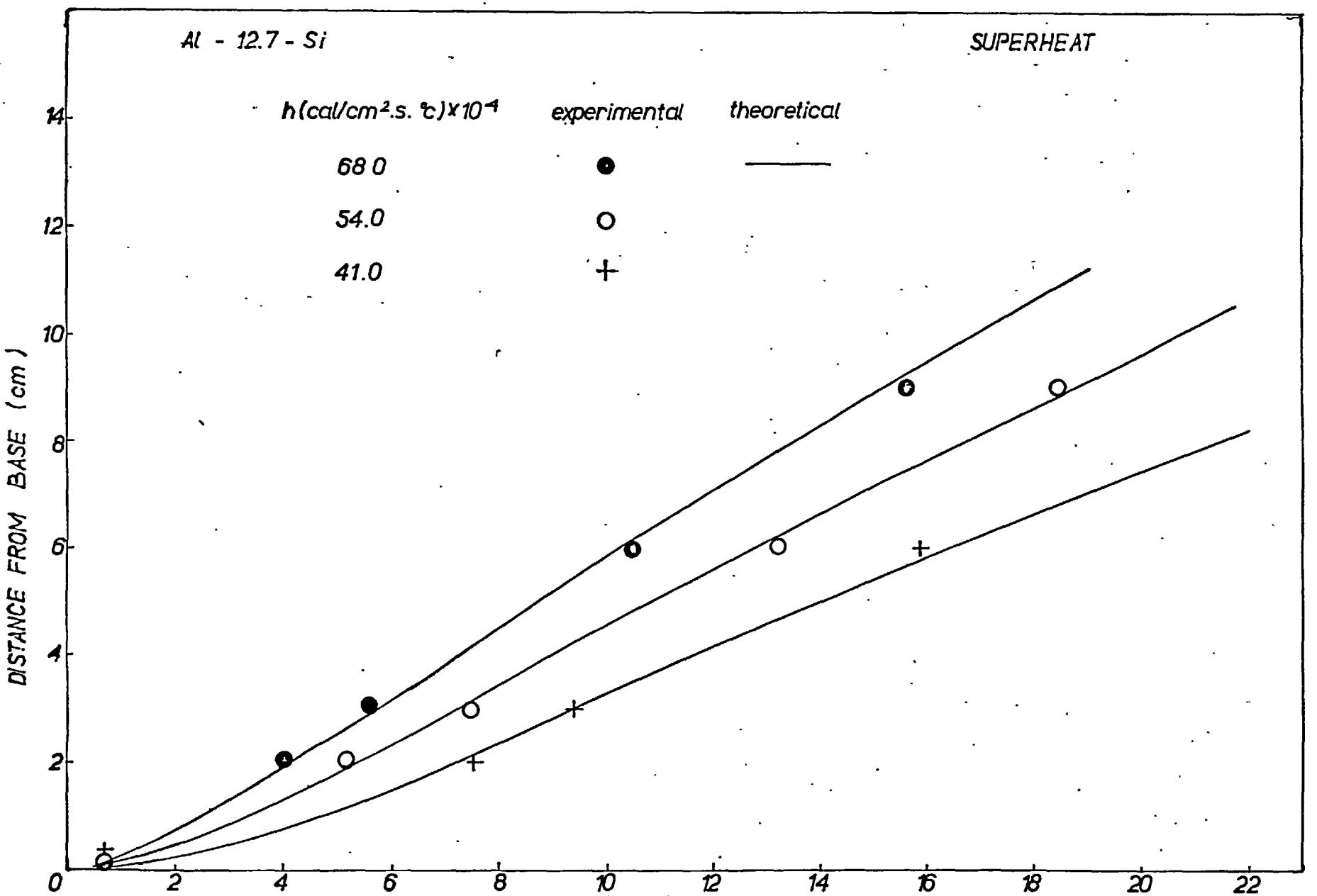

Fig 5.21 SOLIDIFICATION OF 12.7 % Si Al-Si EUTECTIC WITH 50 °c SUPERHEAT
comparison of theoretical and experimental results

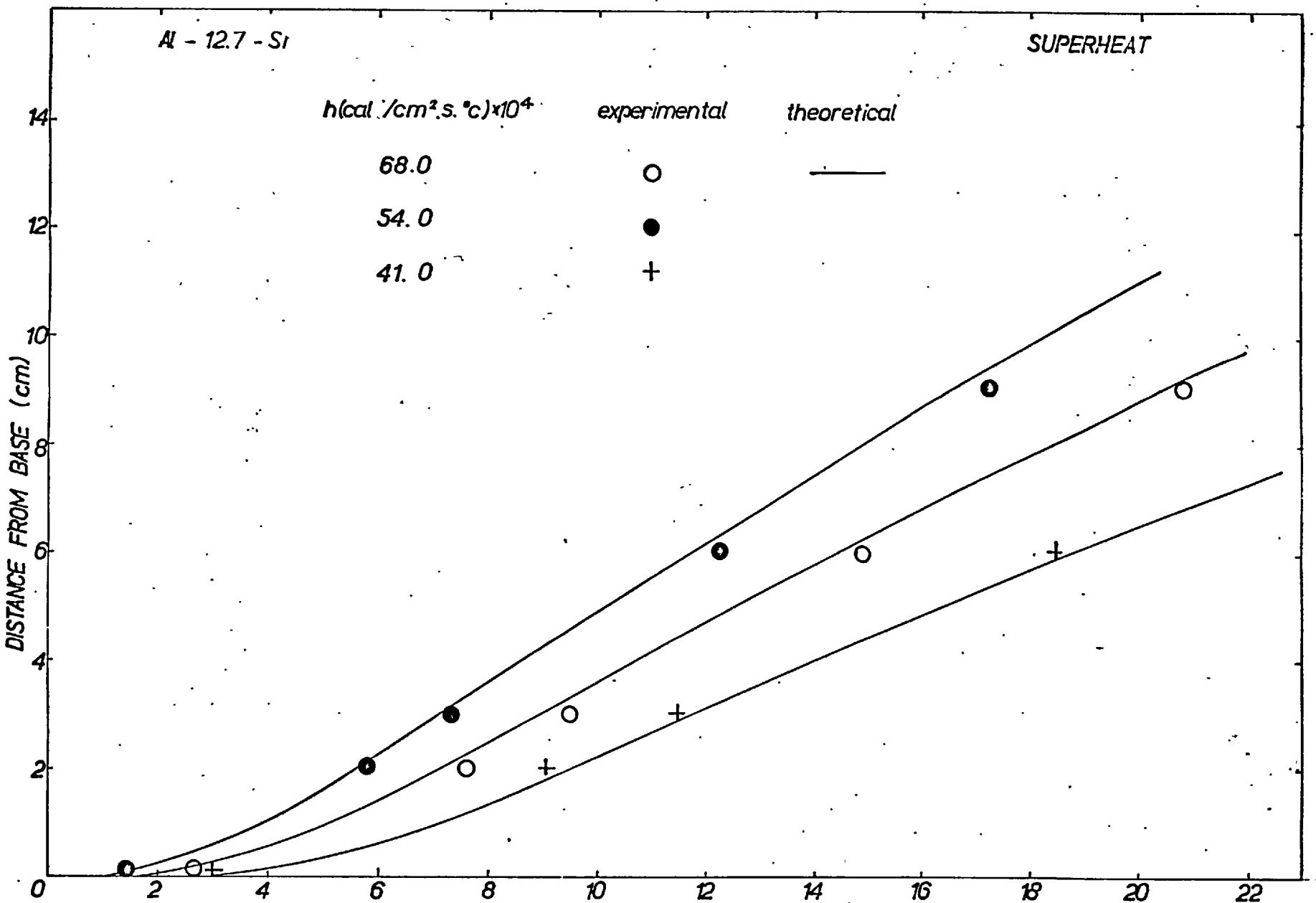

Fig 5.22 SOLIDIFICATION OF 12.7% Si, Al-Si EUTECTIC WITH 100°c SUPERHEAT
comparison of theoretical and experimental results

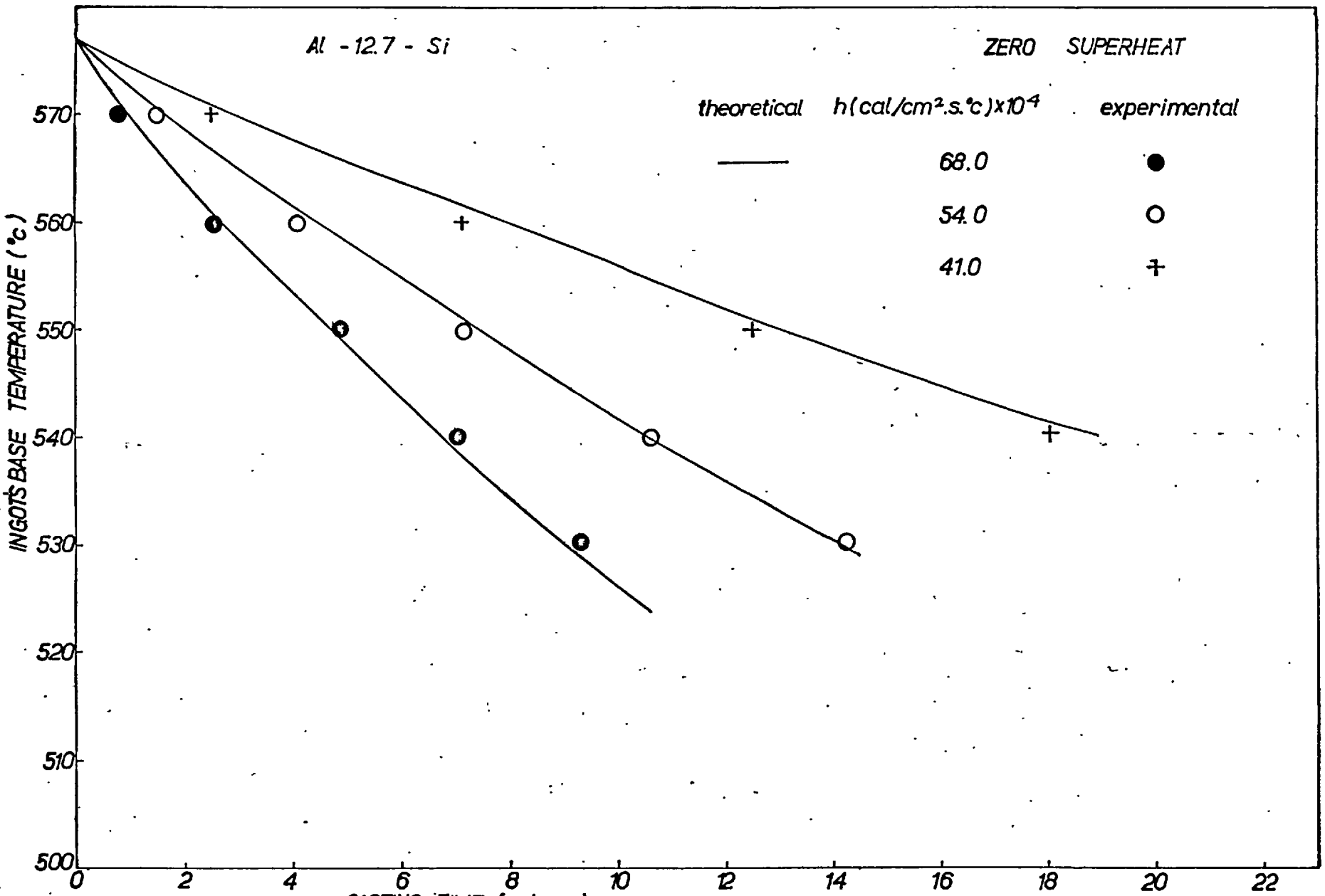

Fig 5.23 SOLIDIFICATION OF 12.7% Si, Al - Si EUTECTIC AT ZERO SUPERHEAT
comparison of experimental and theoretical results

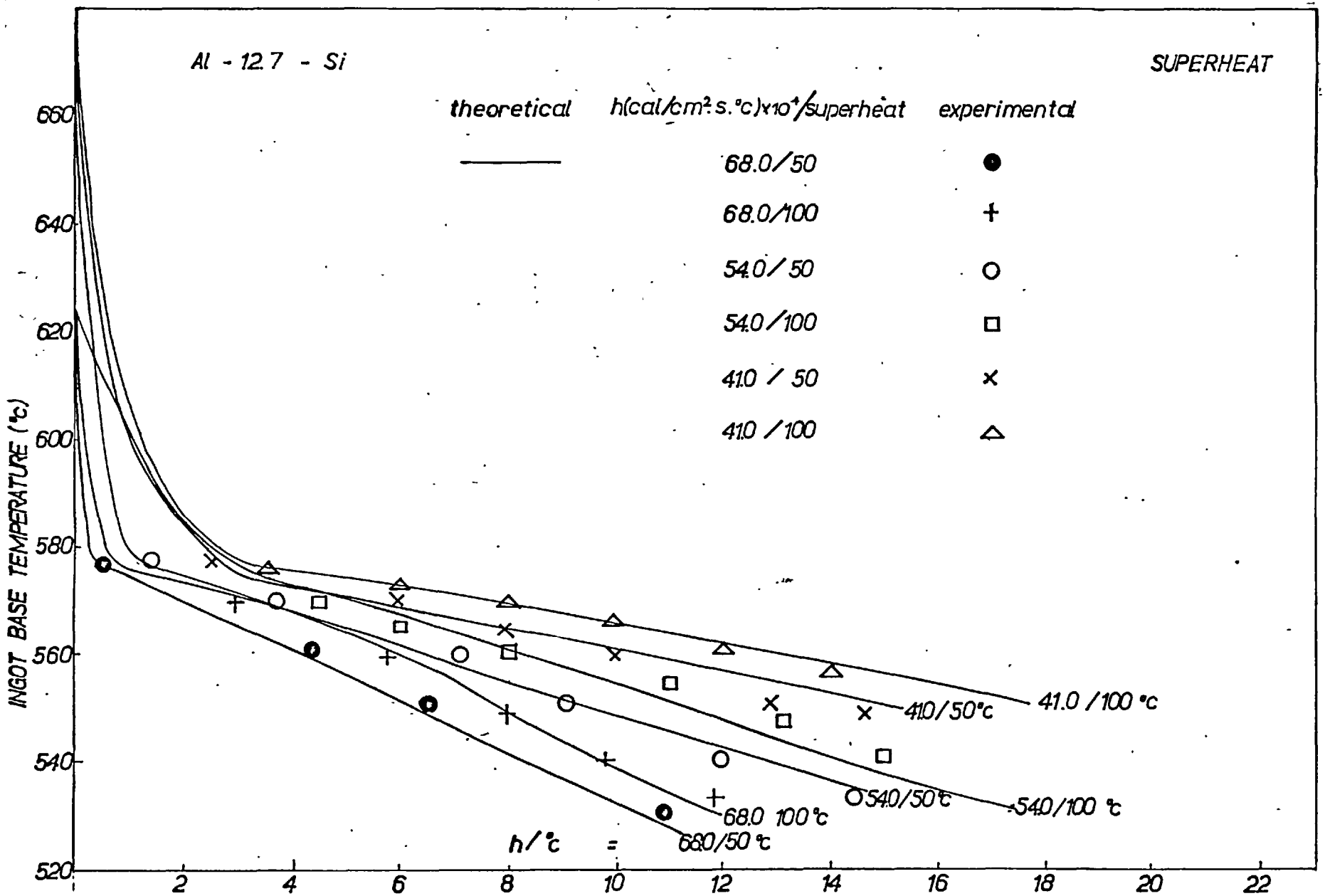

Fig 5.24 SOLIDIFICATION OF 12.7% Si, Al - Si EUTECTIC AT POSITIVE SUPERHEAT
comparison of experimental and theoretical results

Initial temperature = 1000°C

Solidification temperature = 950°C

Heat transfer coefficient = 0.007 cal/cm(2).S.°C

Cooling air temperature = 40°C

Height of metal = 12 cm.

Ingot surface area = 58 cm(2)

Area of moulds' base = 78.5 cm(2)

Cooling time (min)	6	12
Solid thickness (cm)	3.2	5.6
Latent heat liberated (Kcal)	81	141
Temperature in metal at distances (cm)		
0	765	680
2	894	797
3	945	847
5	994	930
7	999	985
10	1000	988
Sensible heat in cast metal (Kcal)	42	81
Sensible heat in mould (Kcal)	37	61
Base temperature at mid time (°C)	832	765
Heat removed by cooling air (Kcal)	156	290
Excess heat liberated in metal (Kcal)	4	-
Excess heat removed by cooling air (Kcal)	-	7

TABLE 5.8 THERMAL BALANCE FOR THE SOLIDIFICATION OF Fe-C-P EUTECTIC WITH 50°C OF SUPERHEAT.

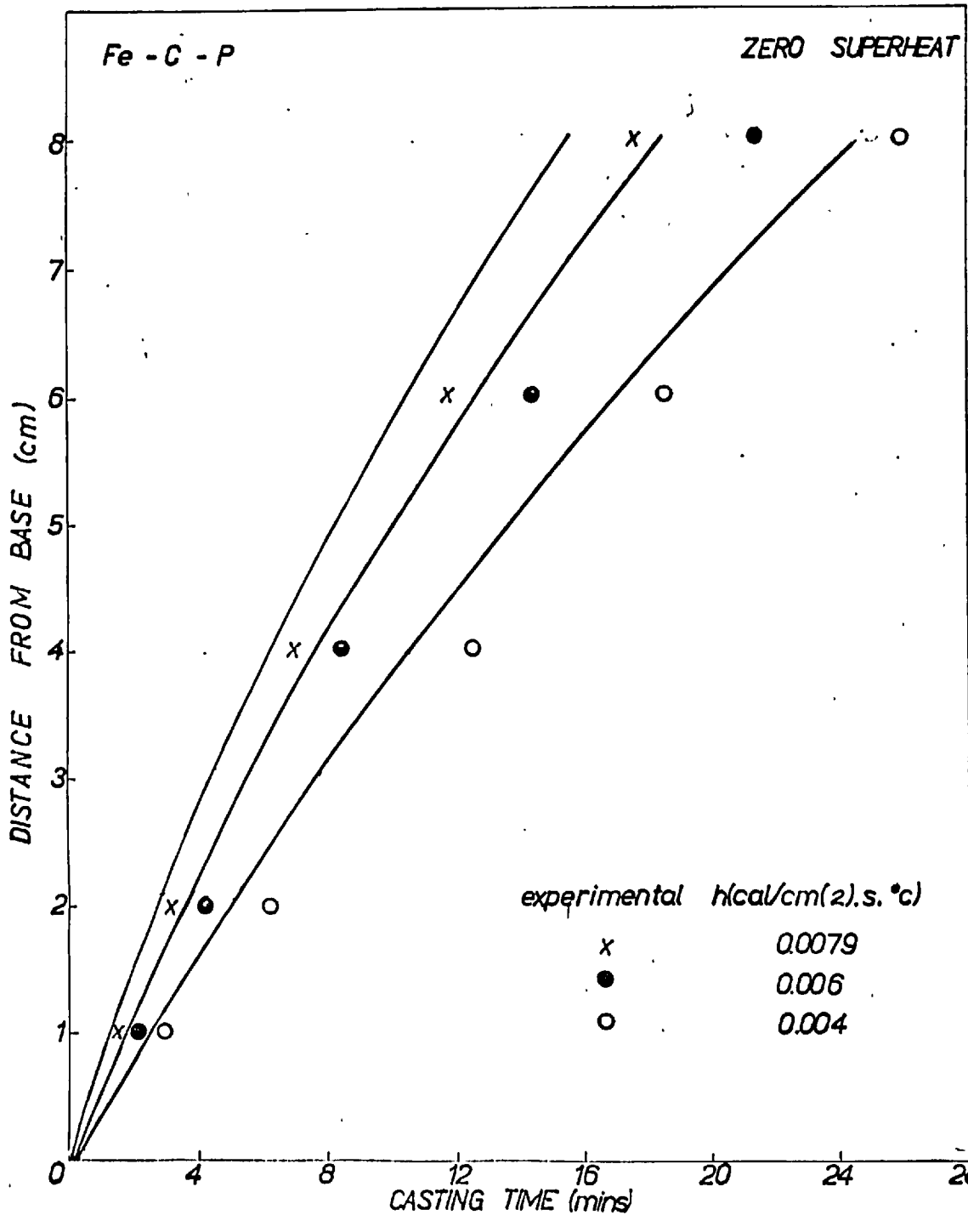

Fig 5.25 SOLIDIFICATION OF Fe -C - P TERNARY EUTECTIC ALLOY
comparison of theoretical and experimental results

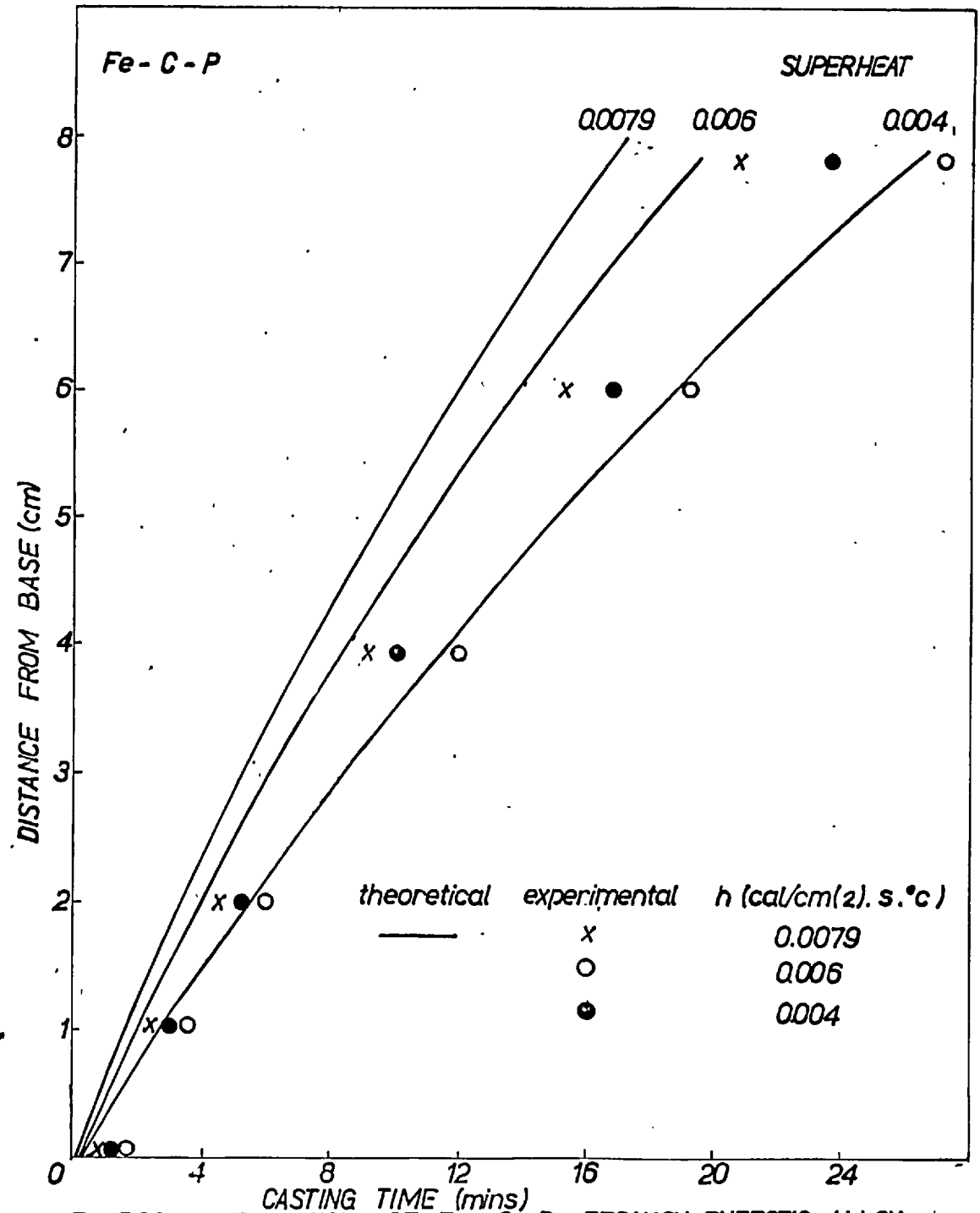

Fig 5.26 SOLIDIFICATION OF Fe - C -P TERNARY EUTECTIC ALLOY WITH 50 °c SUPERHEAT
comparison of theoretical and experimental results.

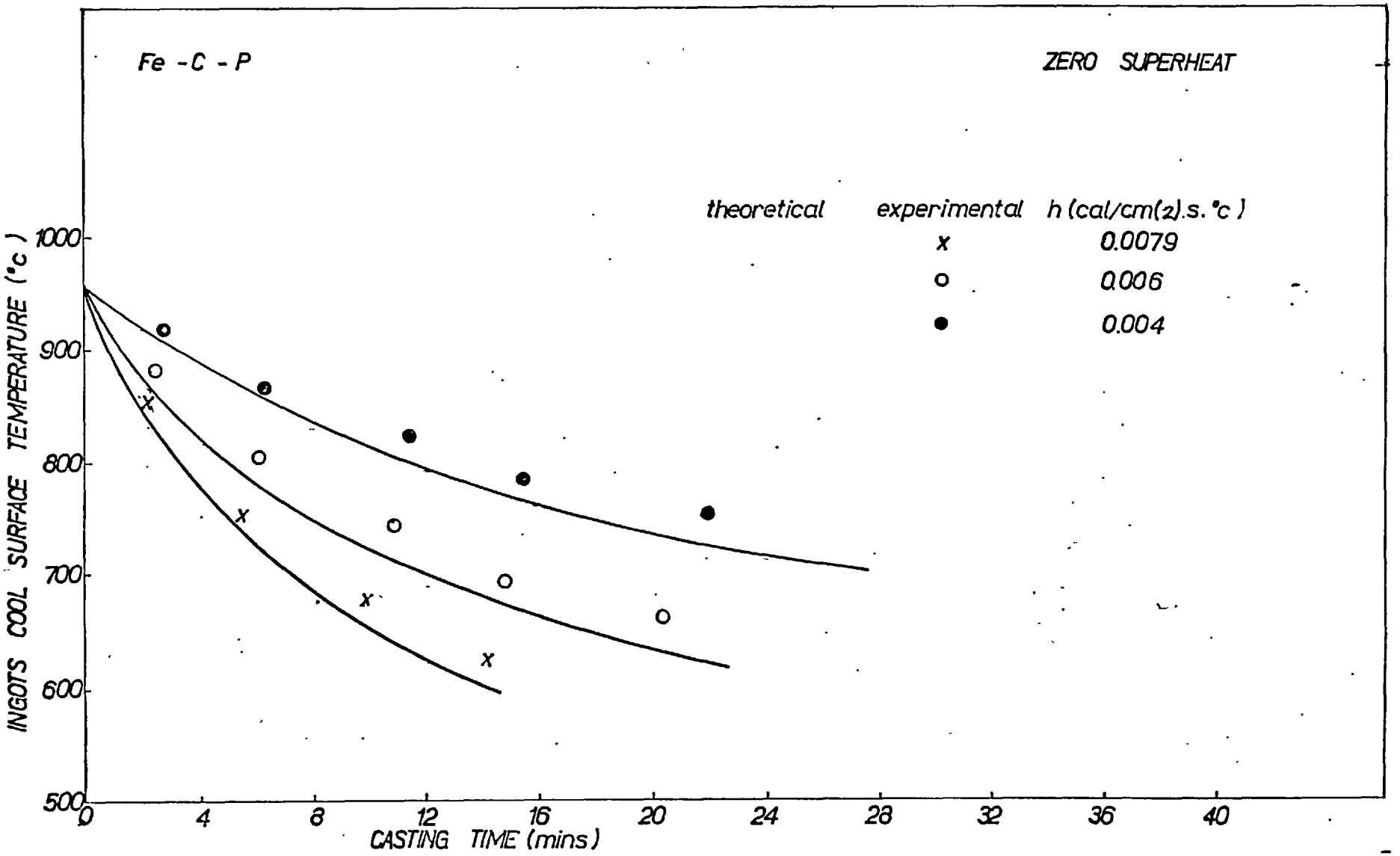

Fig 5.27 SOLIDIFICATION OF Fe-C-P TERNARY EUTECTIC ALLOY AT ZERO SUPERHEAT
comparison of experimental and theoretical results

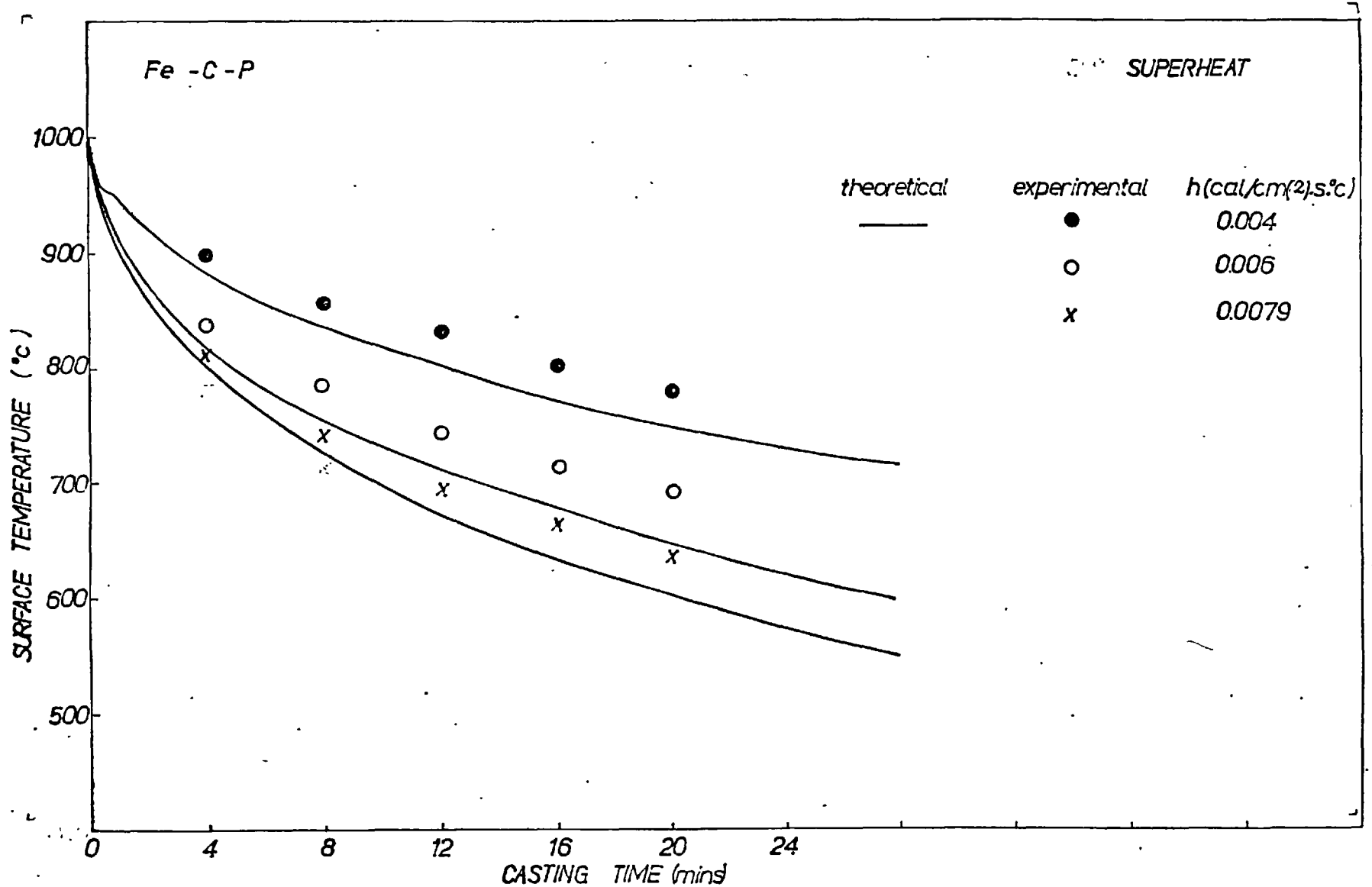

Fig 5.28 THE SOLIDIFICATION OF Fe-C-P TERNARY EUTECTIC ALLOY WITH 50° SUPERHET comparison of theoretical and experimental results.

5.2.2.1 4% Copper in Aluminium

This alloy has a liquidus temperature of 650°C and under the experimental cooling conditions still contained some liquid on reaching 548°C, the eutectic temperature. This was therefore taken as the non-equilibrium solidus temperature.

The cooling was performed with air and air-water mixtures at zero super heat and with 30°C and 50°C of superheat.

Positions of both the solidus and liquidus fronts, at different times, as determined from the thermocouple readings and measured values of the surface temperature, are plotted in Figs. 5.29 to 5.34 and compared to the predictions of the theory.

Typical thermal balances are given in Table 5.4

5.2.2.2 8% Copper in Aluminium

The alloy was prepared in situ by adding pure aluminium to the aluminium - $CuAL_2$ eutectic.

Solidification experiments were conducted with various cooling rates and at different degrees of super heat. The liquidus and solidus arrests were observed at 635°C and 548°C respectively.

The thermal balances for this alloy are given in Table 5.10 and the theorectical and experimental results are compared in Figs. 5.35 to 5.40

5.2.2.3 30% Copper in Aluminium

The near eutectic composition of 30% copper has a freezing range of 12°C.

Experiments were conducted with various degrees of super heat and cooling rates, and the theoretical and experimental results are compared in Figs. 5.41 to 5.46a.

Thermal balances are given in Tables 5.11 and 5.12

PLATE 3 MACRO STRUCTURE OF Al 4% Cu

Vertical section through centre of ingot

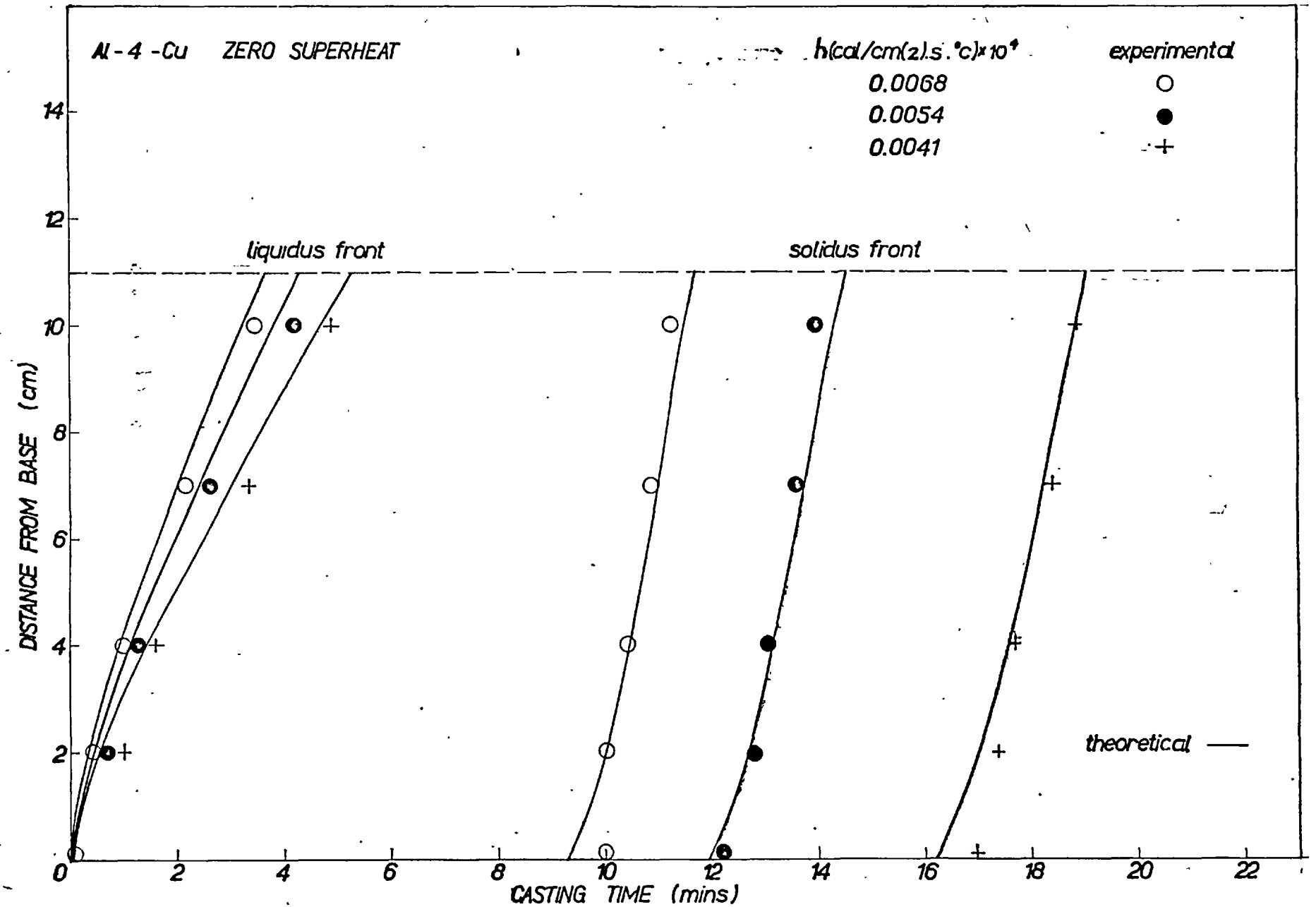

Fig 5.29 SOLIDIFICATION OF Al - 4% Cu AT ZERO SUPERHEAT
comparison of theoretical and experimental results

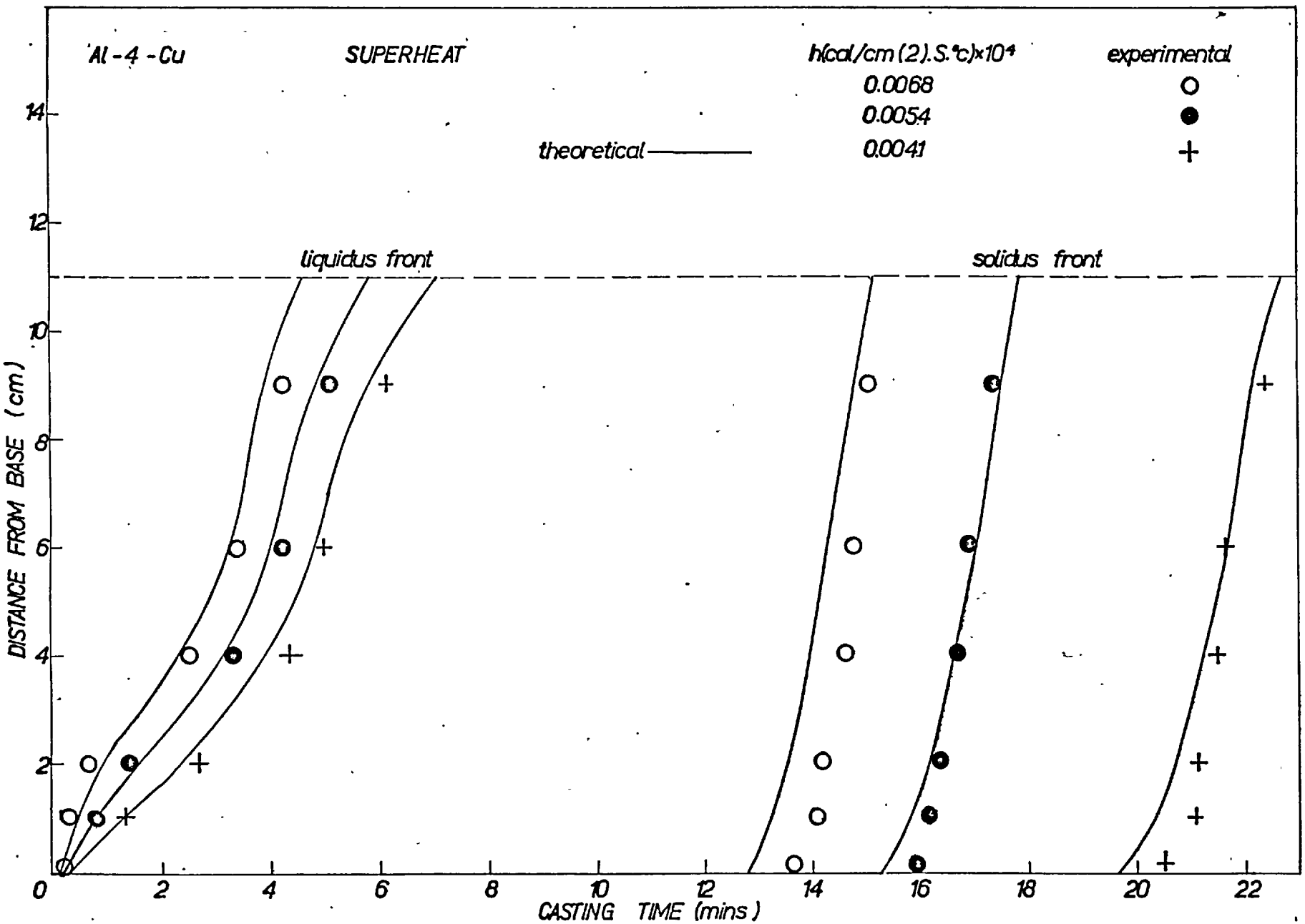

Fig 5.30 SOLIDIFICATION OF Al - 4% Cu ALLOY WITH 30°c SUPERHEAT
comparison of theoretical and experimental results

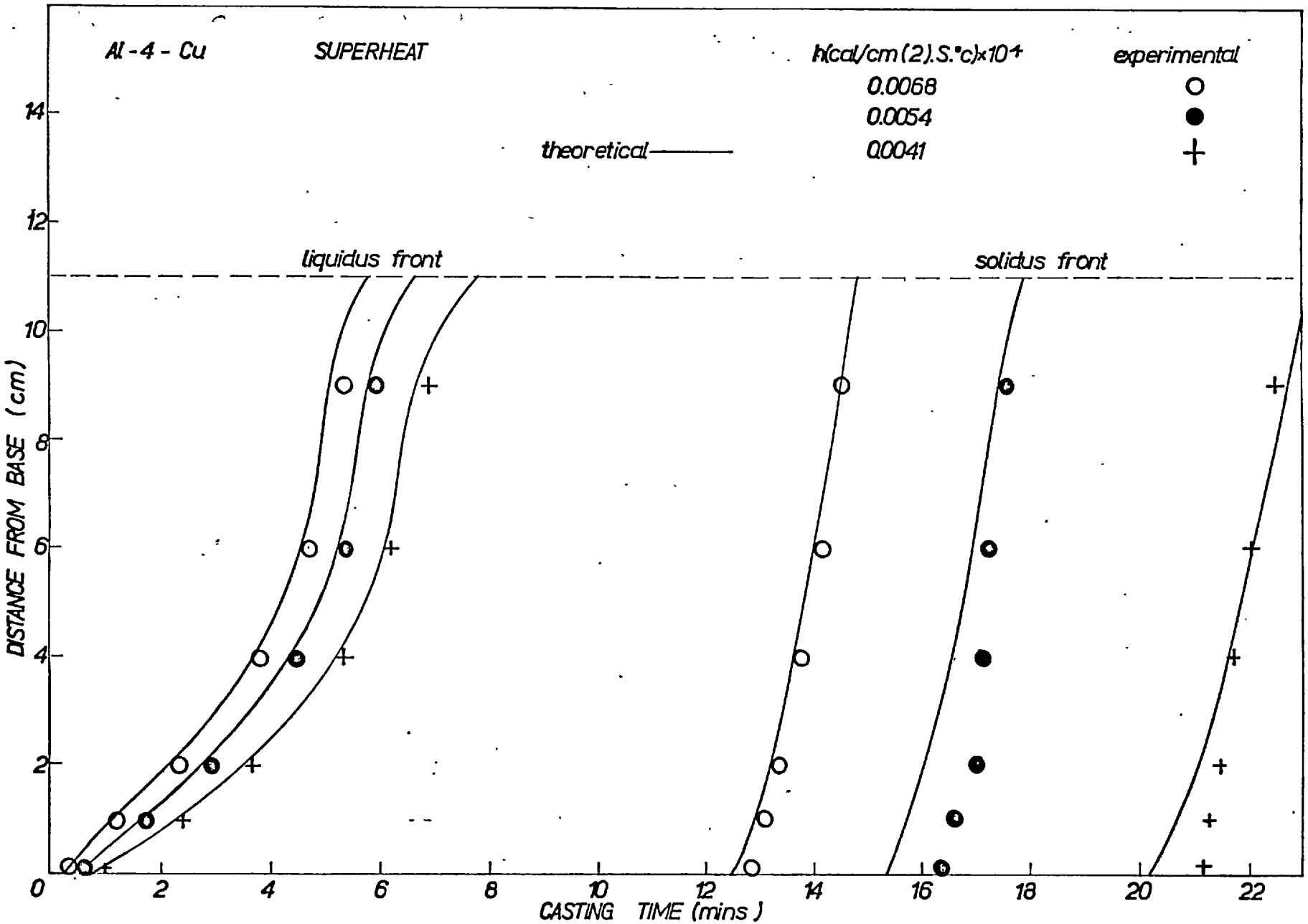

Fig 5.31 SOLIDIFICATION OF Al - 4% Cu ALLOY WITH 50°c SUPERHEAT
comparison of theoretical and experimental results

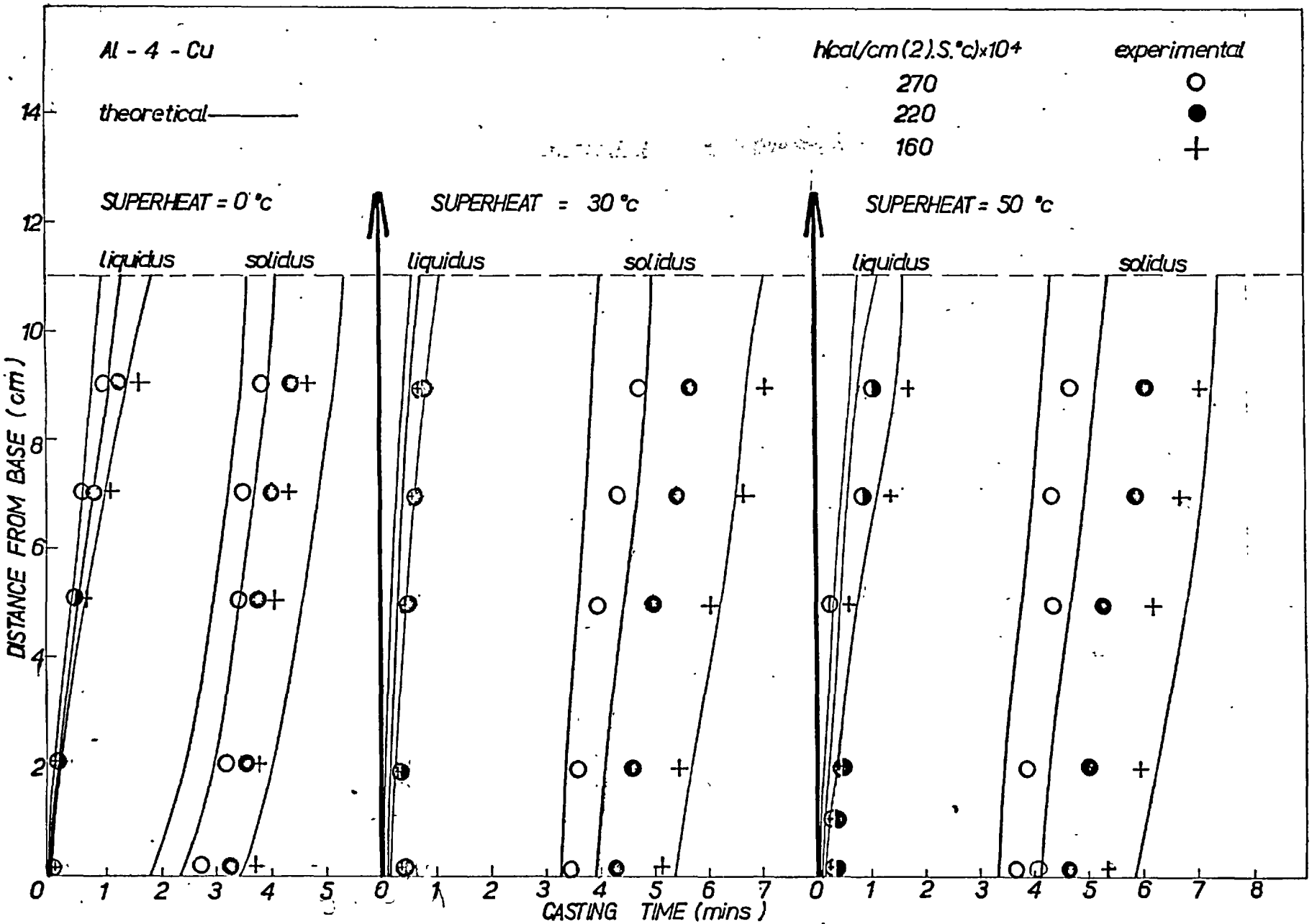

Fig 5.32 SOLIDIFICATION OF Al - 4% Cu ALLOY HEAT REMOVED BY AIR - WATER MIXTURE
comparison of theoretical and experimental results

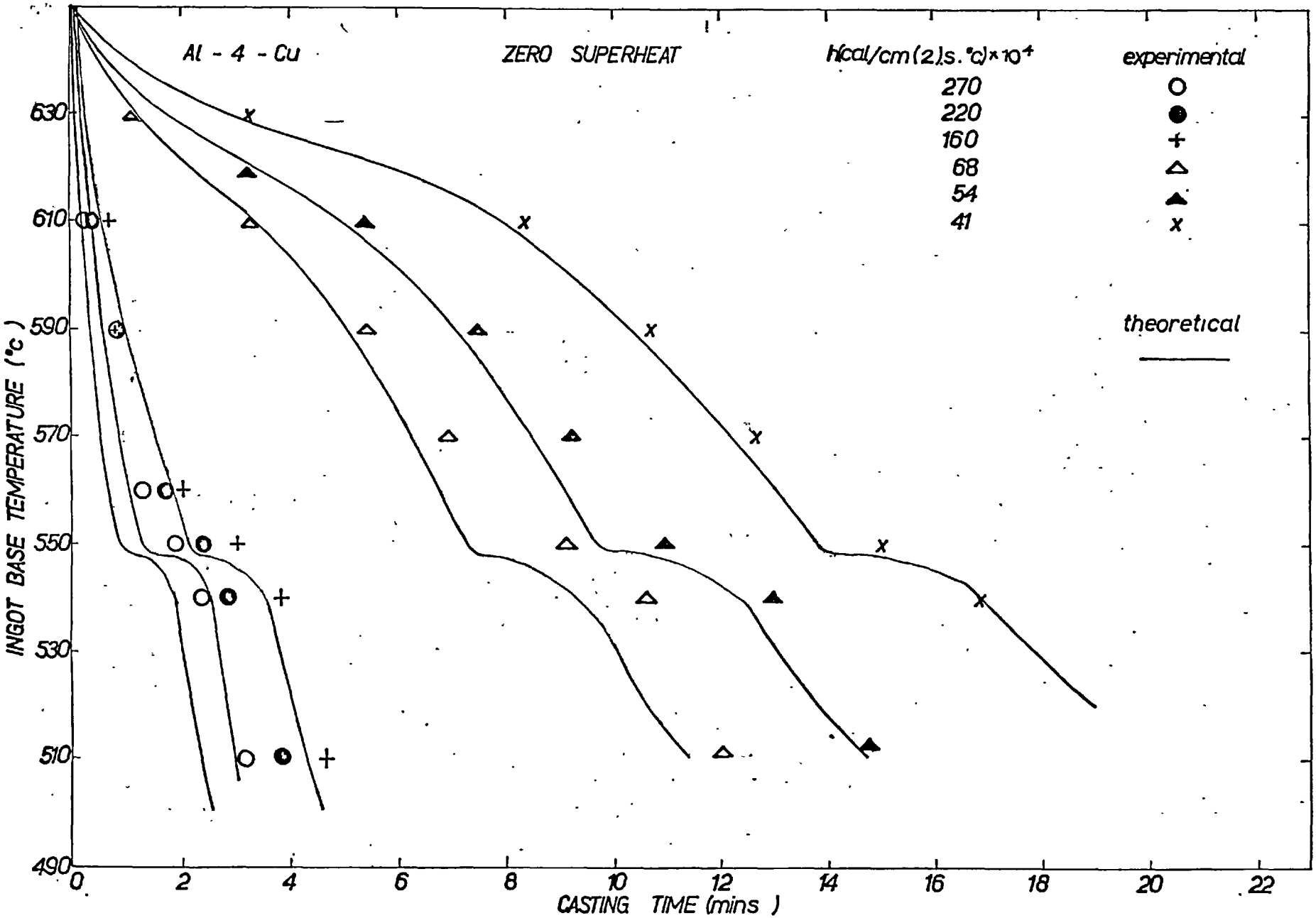

Fig 5.33 SOLIDIFICATION OF Al - 4% Cu ALLOY AT ZERO SUPERHEAT
comparison of theoretical and experimental results

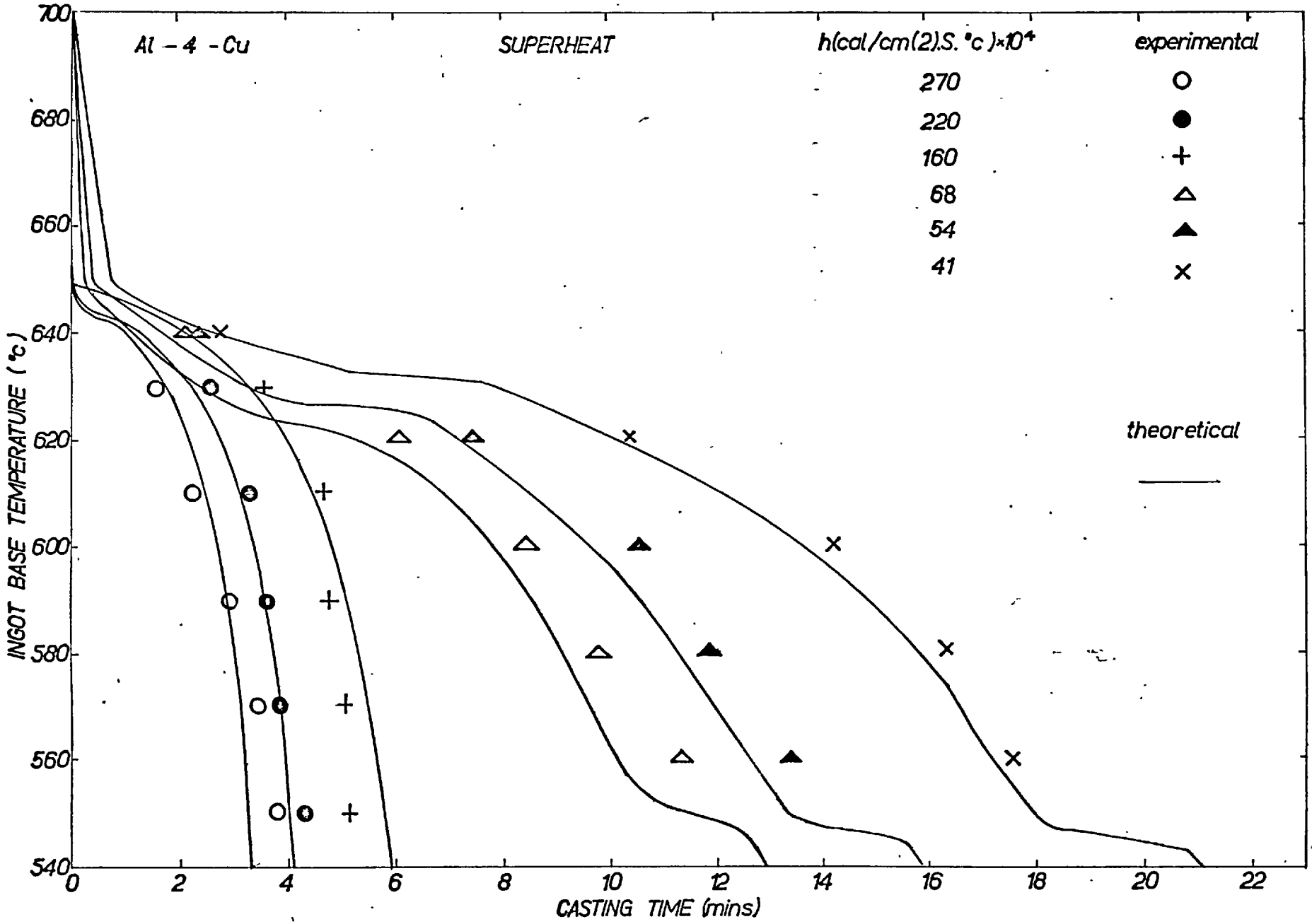

Fig 5.34 SOLIDIFICATION OF Al- 4% Cu ALLOY WITH 50°c SUPERHEAT
comparison of theoretical and experimental results

Initial temperature = 700°C

Liquidus temperature = 650°C

Solidus temperature = 548°C

Heat transfer coefficient = 0.0054 cal/cm(2).S.°C.

Height of metal = 11 cm

Cooling air temperature = 40°C

Cooling time (min)	5	10	18
Solid layer thickness (cm)	-	-	4
Partial layer thickness (cm)	5.6	11	7
Thermal layer thickness (cm)	5.4	-	-
Latent heat liberated at solidus (Kcal) -	-	-	4.3
Latent heat liberated in partial layer (Kcal)	41	120	180
Temperature in metal °C at distances (cm			
0	630	598	531
2	640	610	536
4	647	620	540
6	650	628	545
8	650	636	551
10	658	647	555
Sensible heat in solid layer (Kcal)	-	-	4.7
Sensible heat in partial layer (Kcal)	19	42	58
Sensible heat in thermal layer (Kcal)	10	-	30
Total heat liberated in metal (Kcal)	70	162	277
Base temperature at mid time (°C)	640	630	606
Heat removed by cooling air (Kcal)	76.3	152	259
Excess heat liberated in metal (Kcal)	-	10	18
Excess heat removed by cooling air (Kcal)	6	-	-

TABLE 5.9 THERMAL BALANCE FOR THE SOLIDIFICATION OF 4%cu, Al-cu ALLOY WITH 50°C SUPERHEAT.

(a)

x 224

(b)

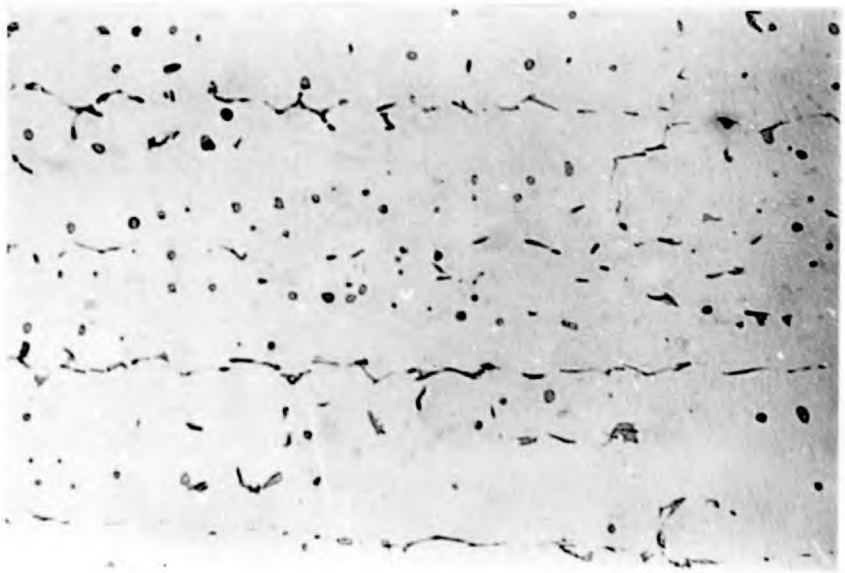

x 112

PLATE 4 Al - 4% Cu

(a) h=0.0068 cal/cm(2).s.°c

(b) h=0.027 cal/cm(2).s.°c

1.5%: 2.5%:1.5% HCl : HNO_3 : HF etch

arrows indicate heat flow direction

(a)

x 224

(b)

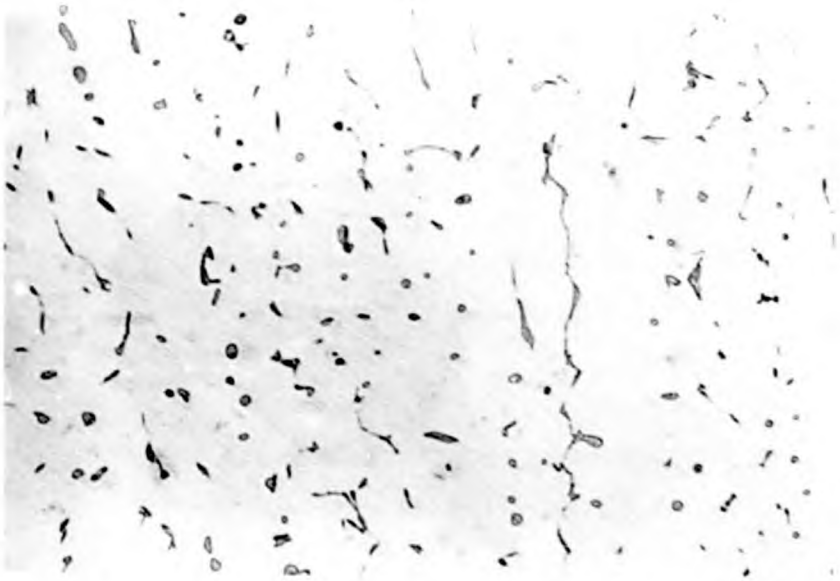

x 112

PLATE 5 Al - 4% Cu

(a) h = 0.0054 cal/cm (2).s. °c

(b) h = 0.022 cal/cm (2).s. °c

15%:25%:15% $HCl : HNO_3 : HF$ etch

arrows indicate heat flow direction

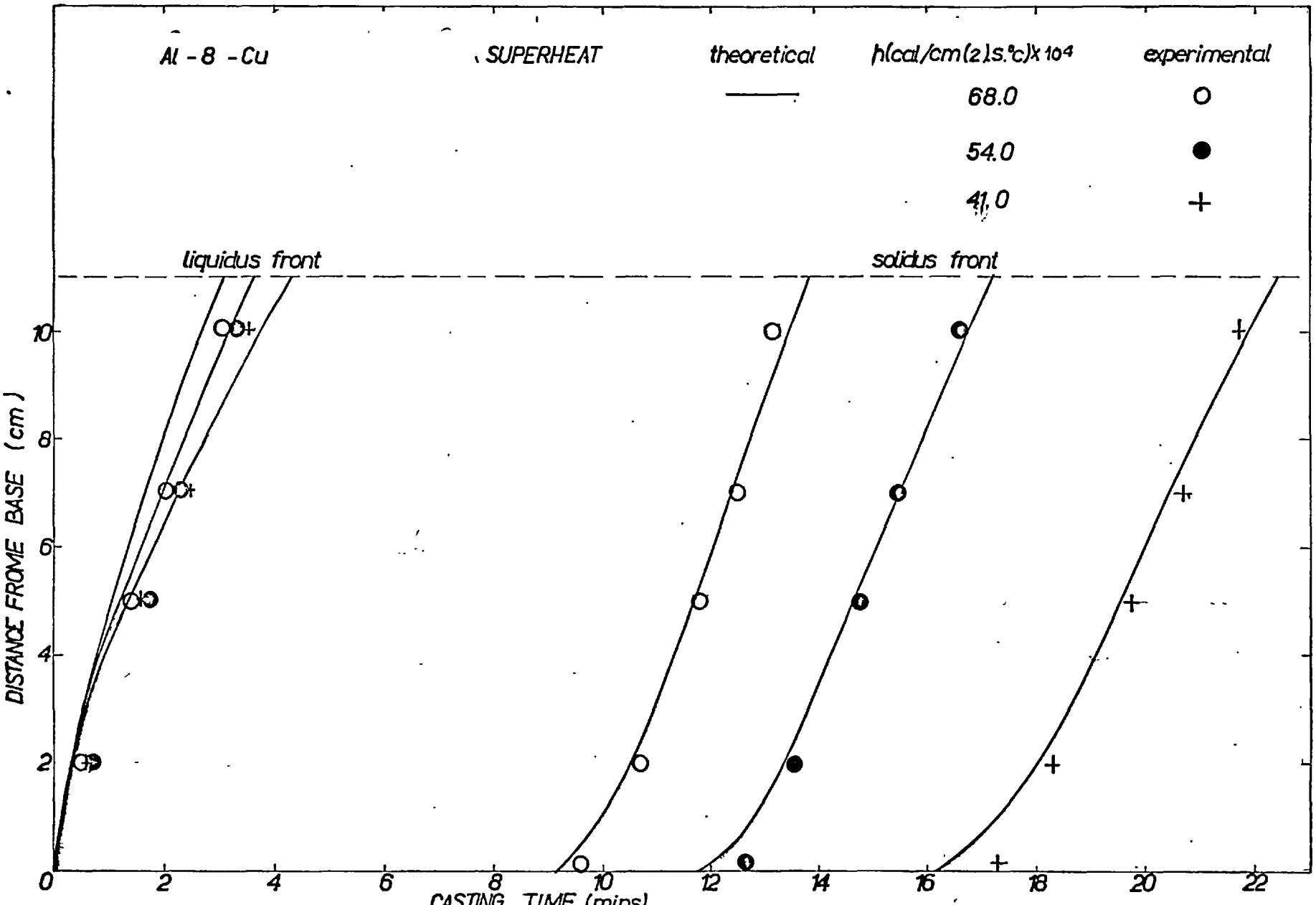

Fig 5.35 SOLIDIFICATION OF Al - 8% Cu ALLOY AT ZERO SUPERHEAT
compairison of theoretical and experimental results

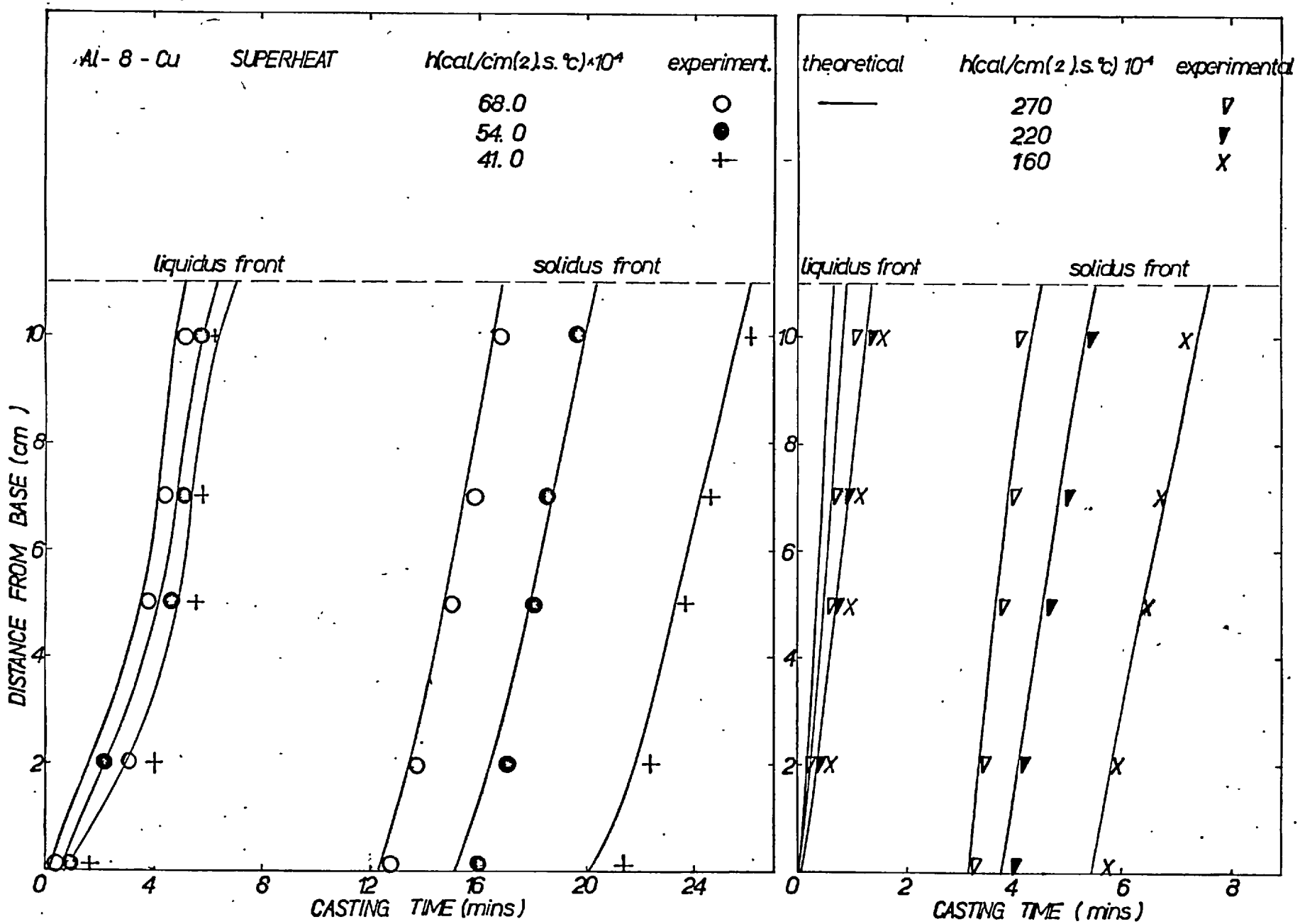

Fig 5.36

SOLIDIFICATION OF Al - 8% Cu ALLOY WITE 50°c SUPERHEAT
comparison of theoretical and experimental results

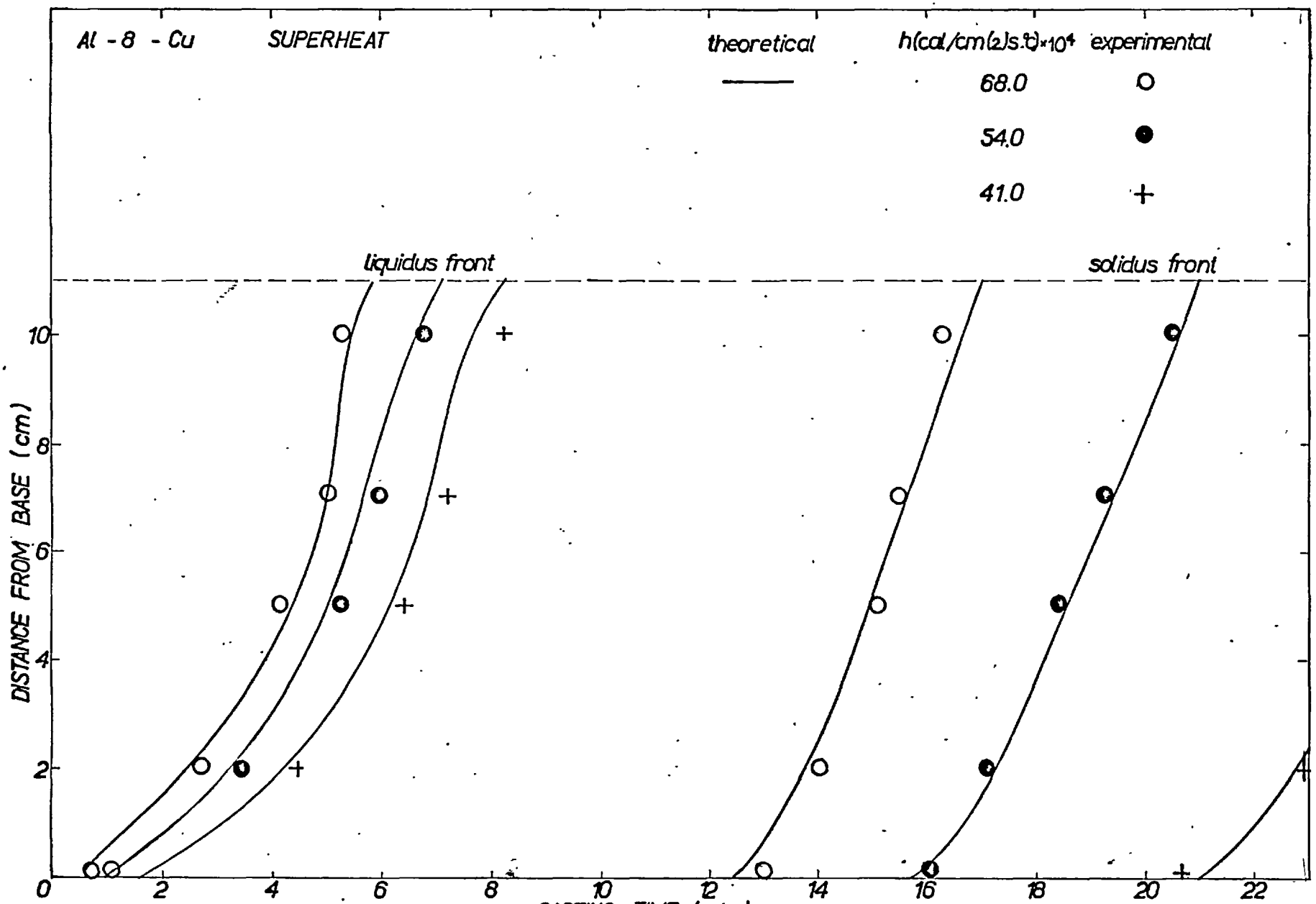

Fig 5.37 SOLIDIFICATION OF Al - 8% Cu ALLOY WITH 70°c SUPERHEAT
comparison of theoretical and experimental results

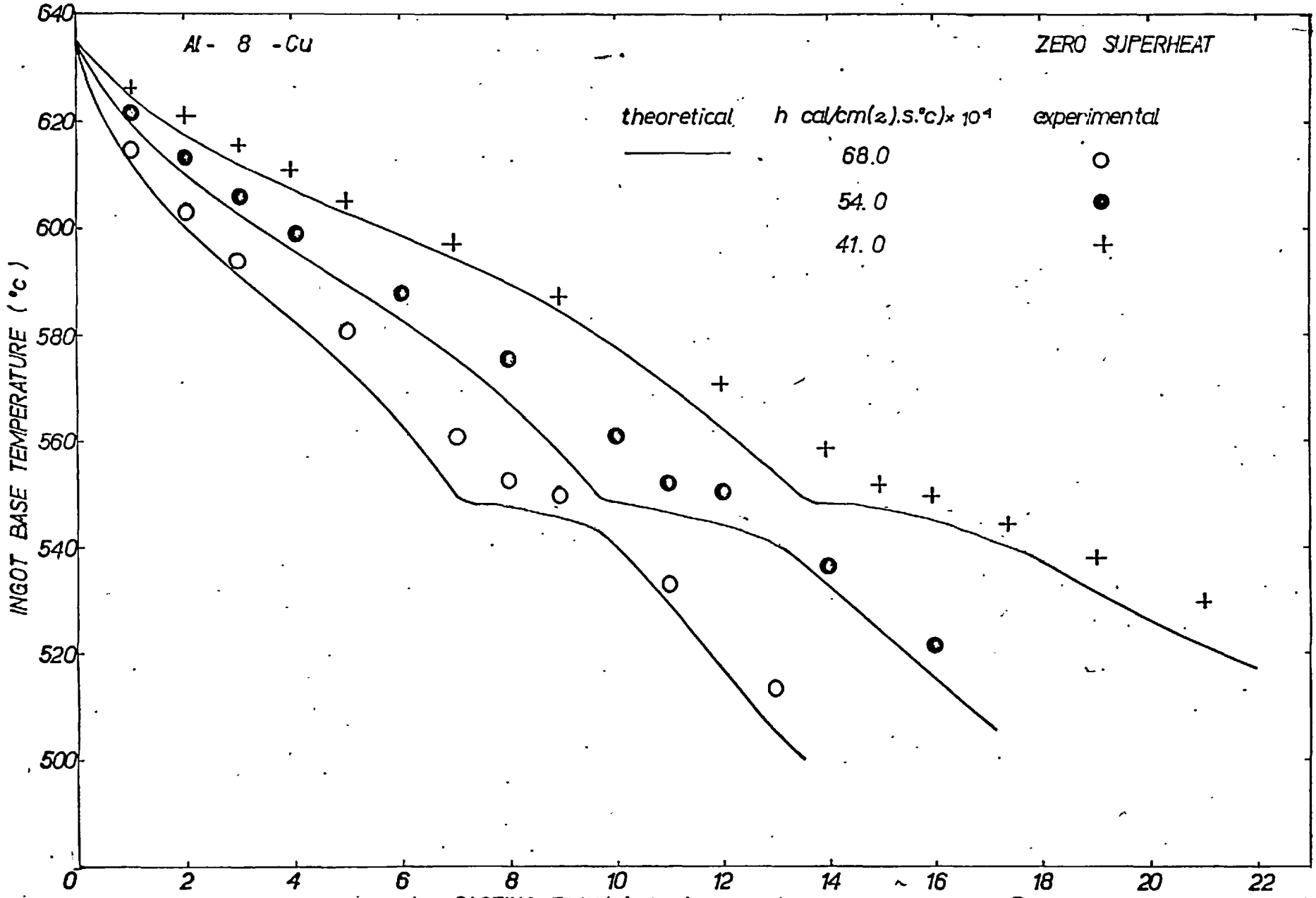

Fig 5.38 SOLIDIFICATION OF Al - 8 %Cu ALLOY AT ZERO SUPERHEAT
comparison of theoretical and experimental results

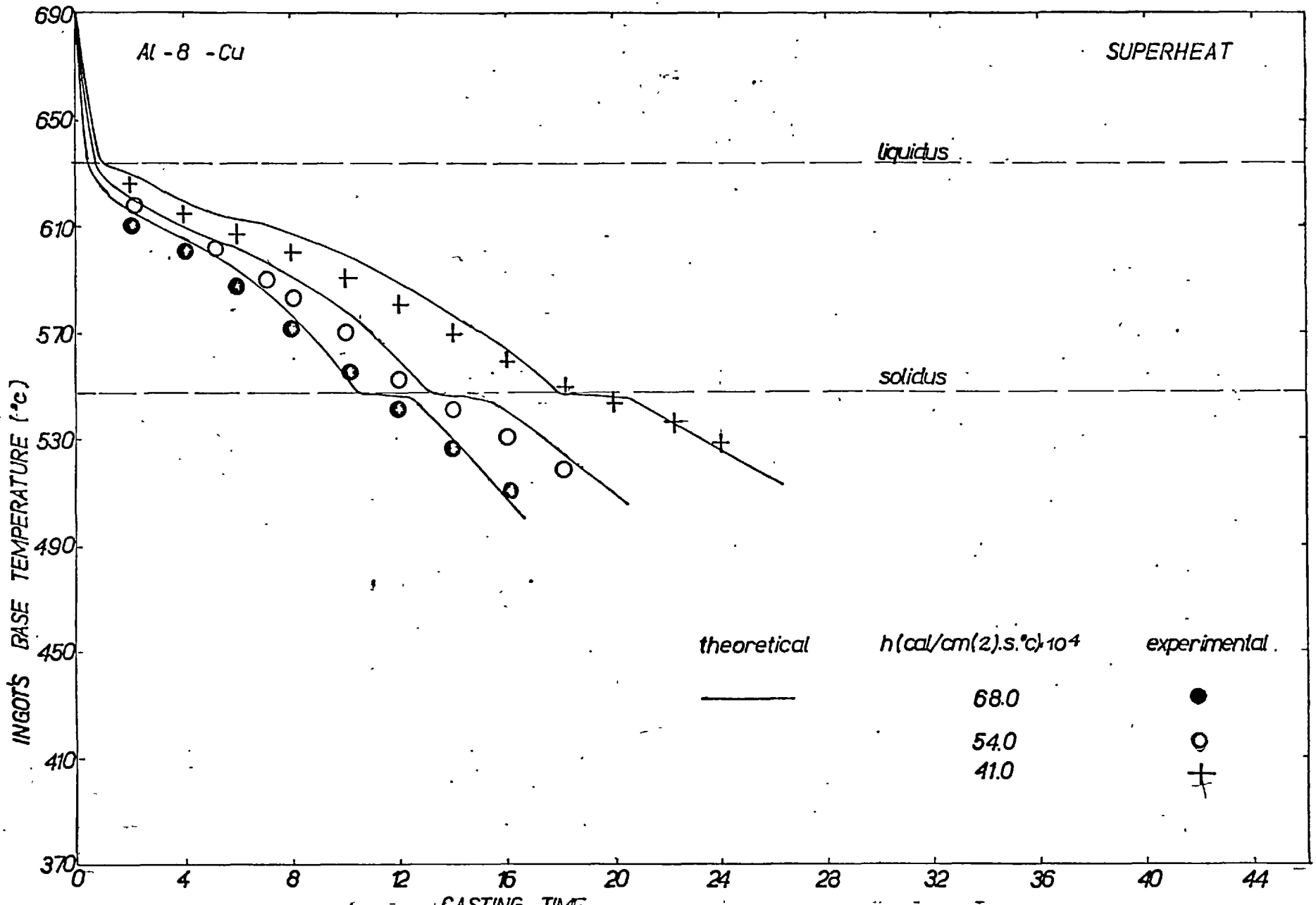

Fig 5.39 SOLIDIFICATION OF Al - 8 % Cu ALLOY WITH 50 °c SUPERHEAT
comparison of theoretical and experimental results

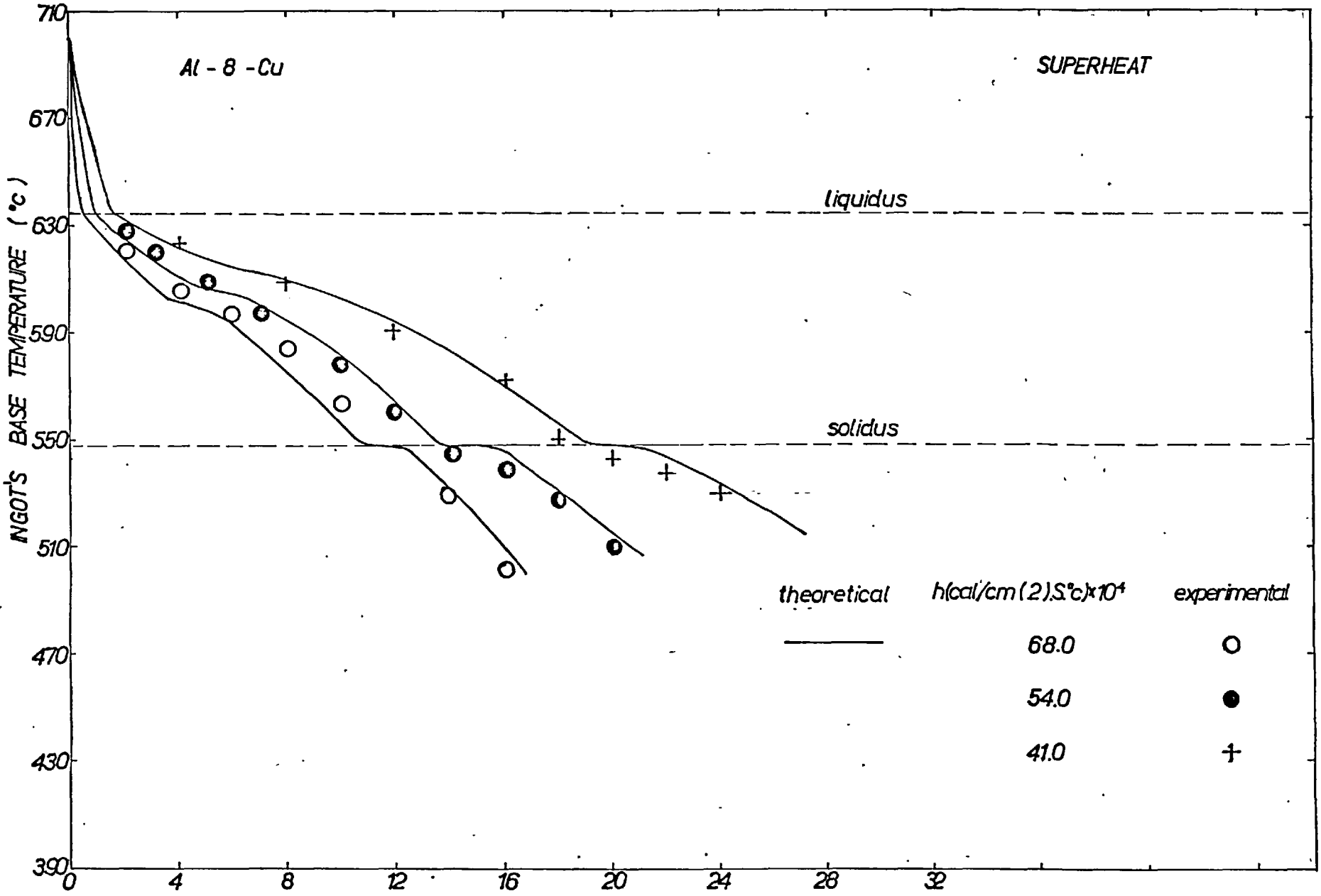

Fig 5.40 SOLIDIFICATION OF Al - 8% Cu ALLOY WITH 70°c SUPERHEAT
comparison of theoretical and experimental results

Initial temperature = 705°C

Liquidus temperature = 635°C

Solidus temperature = 548°C

Heat transfer coefficient = 0.0068 cal/cm(2).S.°C.

Height of metal = 11 cm

Cooling air temperature = 40°C

Cooling time (min)	5	10	15
Solid layer thickness (cm)	-	-	2.6
Partial layer thickness (cm)	8.4	11	8.4
Thermal layer thickness (cm	2.6	-	-
Latent heat liberated at solidus (Kcal)	-	-	8.7
Latent heat liberated in partial layer (Kcal)	52	125	163
Temperature in metal (°C) at distances (cm)			
0	601	563	530
2	609	572	538
4	618	583	548
6	625	595	557
8	632	607	566
10	640	620	571
Sensible heat in solid layer (Kcal)	-	-	1.3
Sensible heat in partial layer (Kcal)	8	16	6
Sensible heat in thermal layer (Kcal)	37	50	82
Total heat liberate in metal (Kcal)	97	191	261
Base temperature at mid time (°C)	612	601	580
Heat removed by cooling air (Kcal)	91.6	180	259
Excess heat liberated in metal (Kcal)			
Excess heat removed by cooling air (Kcal)	5.4	11	2

TABLE 5.10 THERMAL BALANCE FOR THE SOLIDIFICATION OF 8% CU - Al-CU ALLOY WITH 70°C OF SUPERHEAT.

(a)

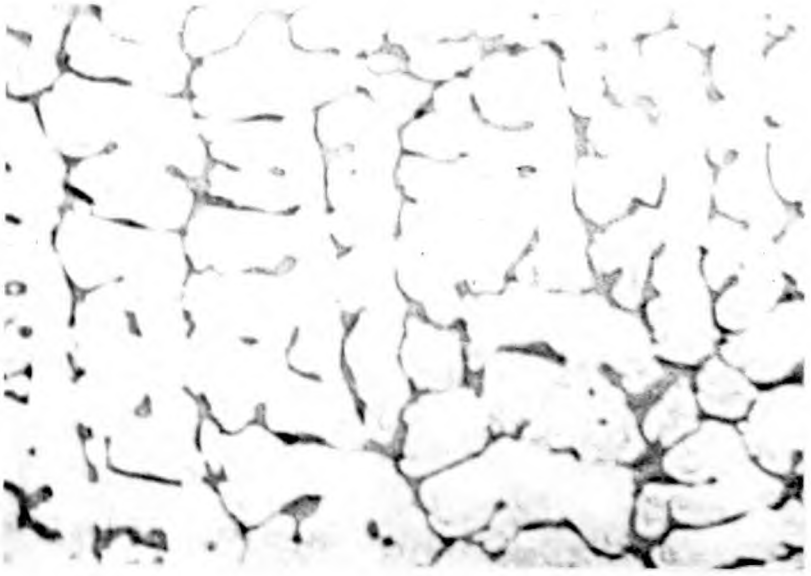

x 112

(b)

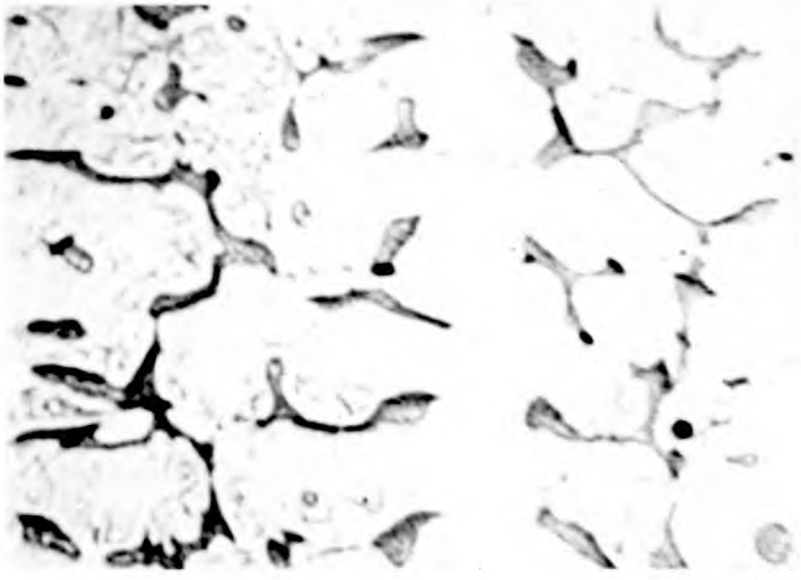

x 224

PLATE 6

Al - 8% Cu

h = 0.0068 cal/cm(2).s. °c

sections normal to cooled surface

15% : 25% : 15% $HCl : HNO_3 : HF$ etch

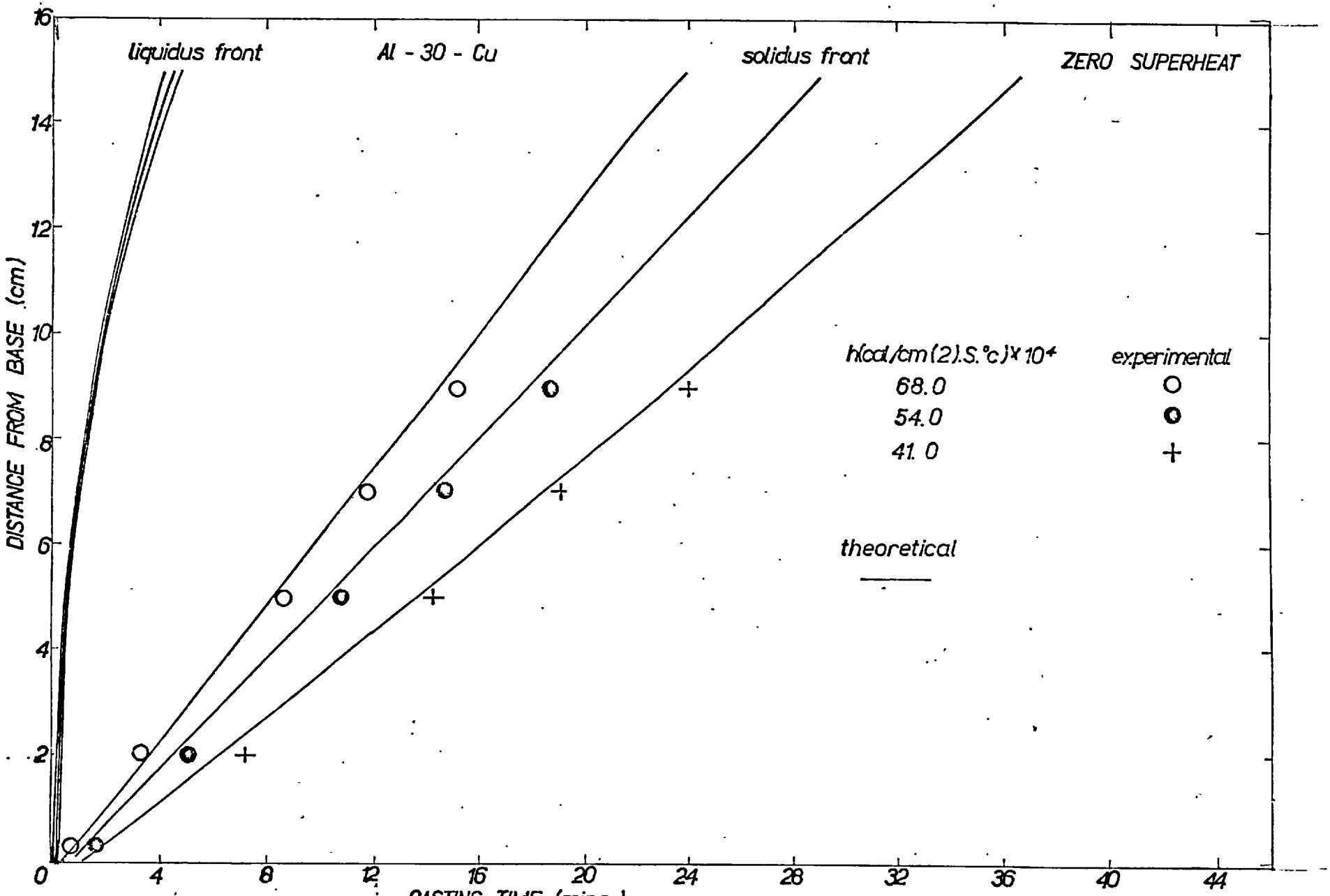

Fig 5.41 SOLIDIFICATION OF Al - 30% Cu ALLOY AT ZERO SUPERHEAT
comparison of theoretical and experimental results

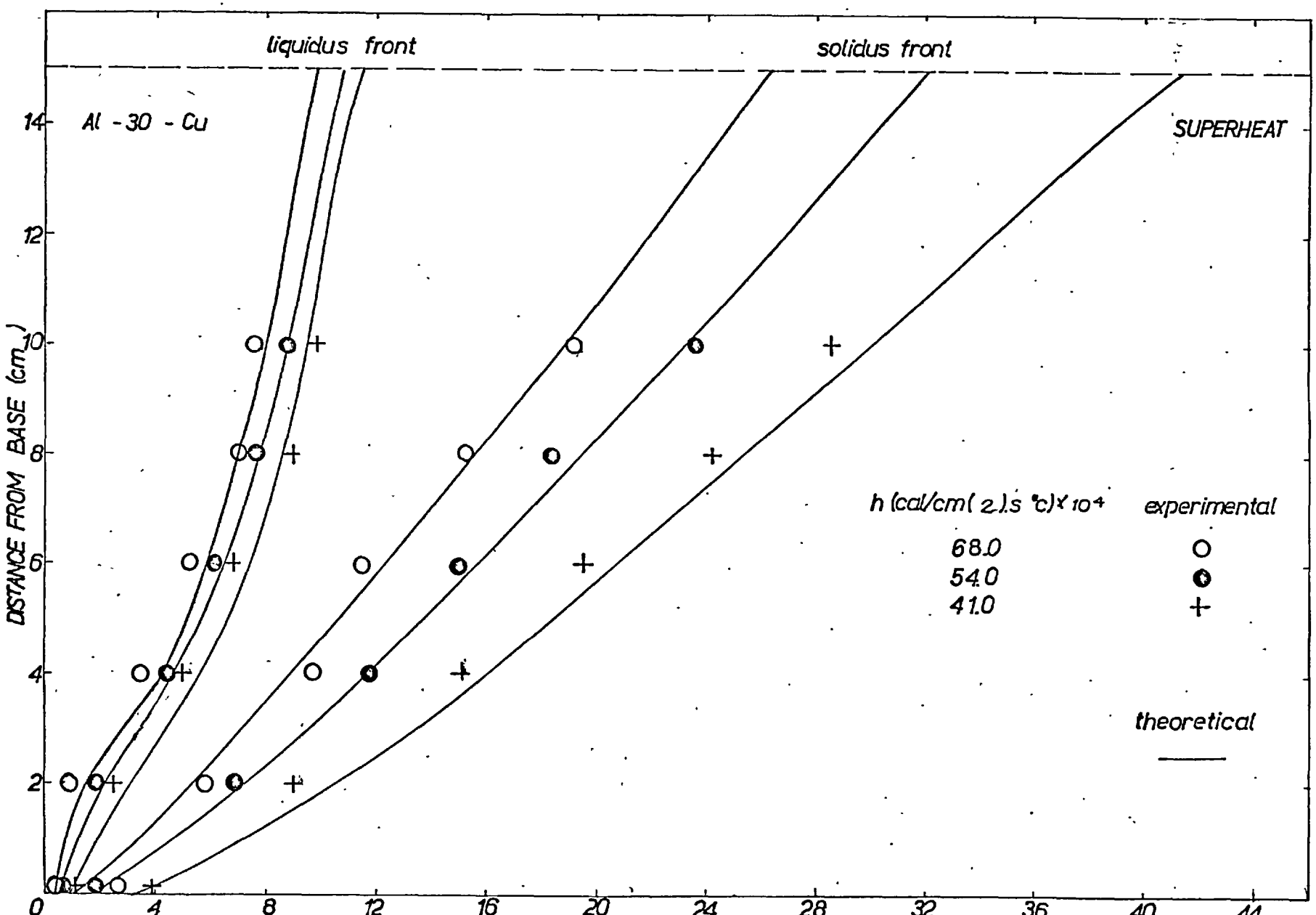

Fig 5.42
SOLIDIFICATION OF Al - 30%Cu ALLOY WITH 50°c SUPERHEAT
comparison of theoretical and experimental results

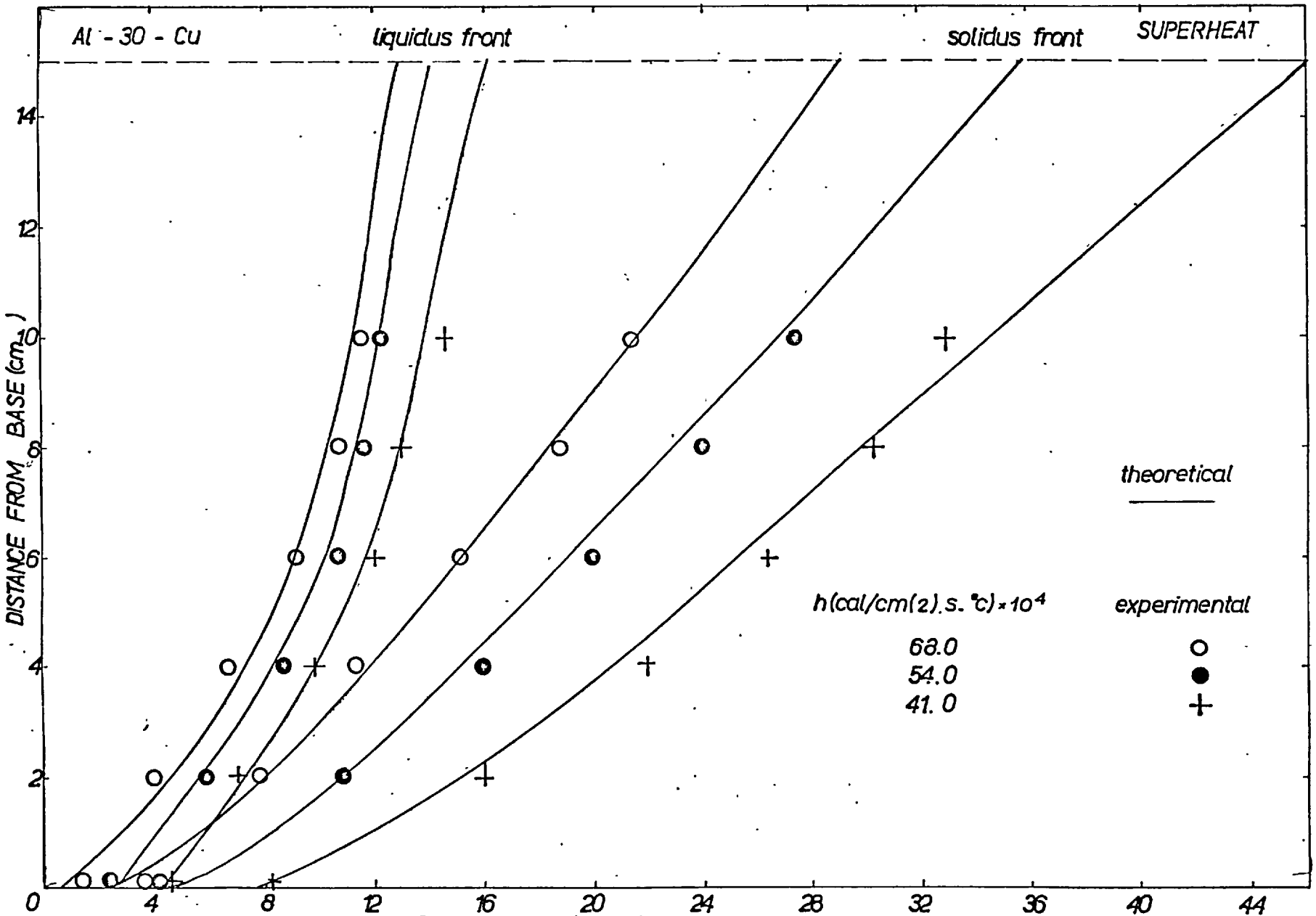

Fig 5.43 SOLIDIFICATION OF Al - 30% Cu ALLOY WITH 100°c SUPERHEAT
comparison of theoretical and experimental results

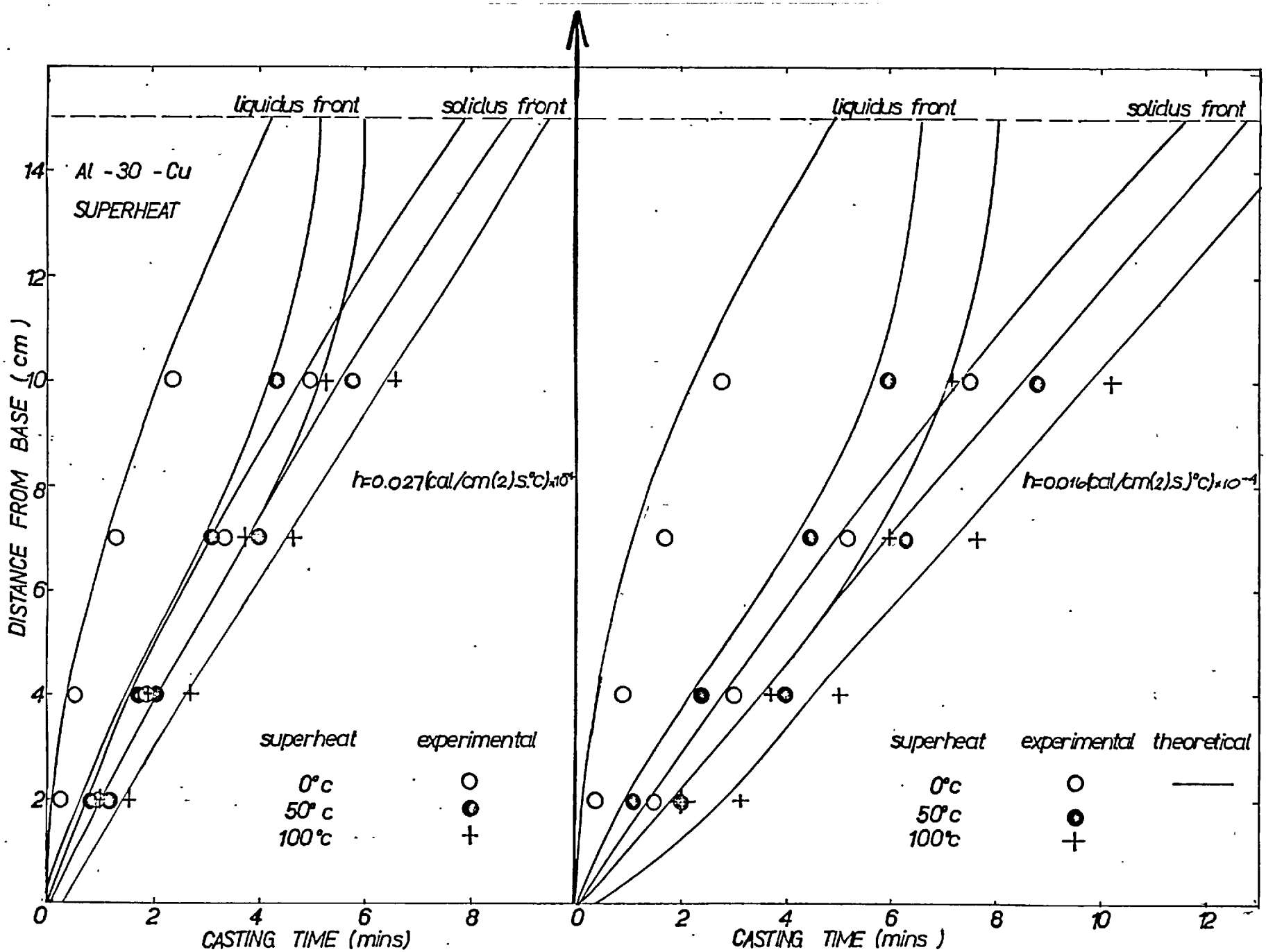

Fig 5.44 SOLIDIFICATION OF Al - 30% Cu ALLOY WITH VARIOUS AMOUNTS OF SUPERHEAT
comparison of theoretical and experimental results

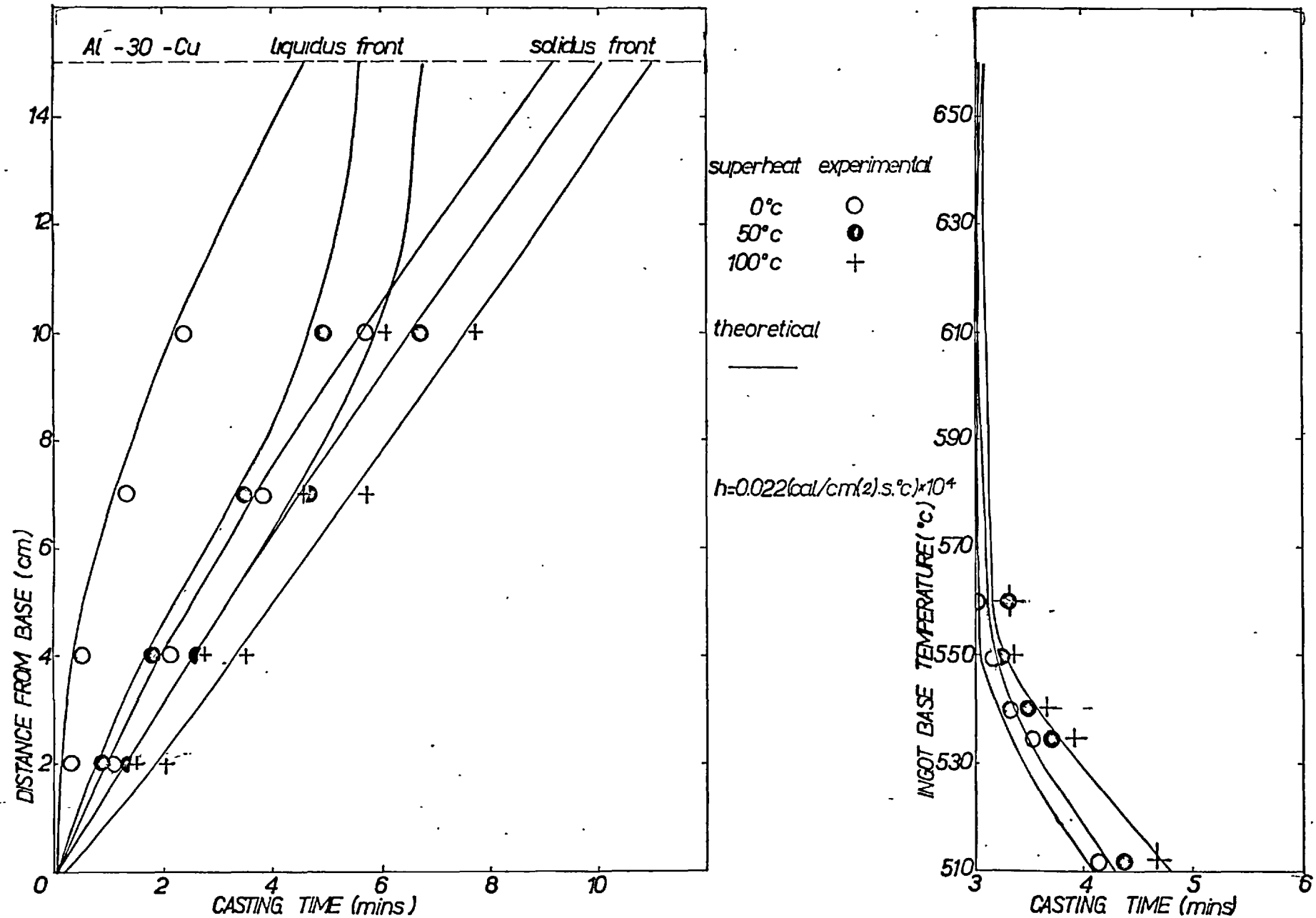

Fig 5.44a

SOLIDIFICATION OF Al - 30% Cu ALLOY WITH VARIOUS AMOUNTS OF SUPERHEAT
comparison of theoretical and experimental results

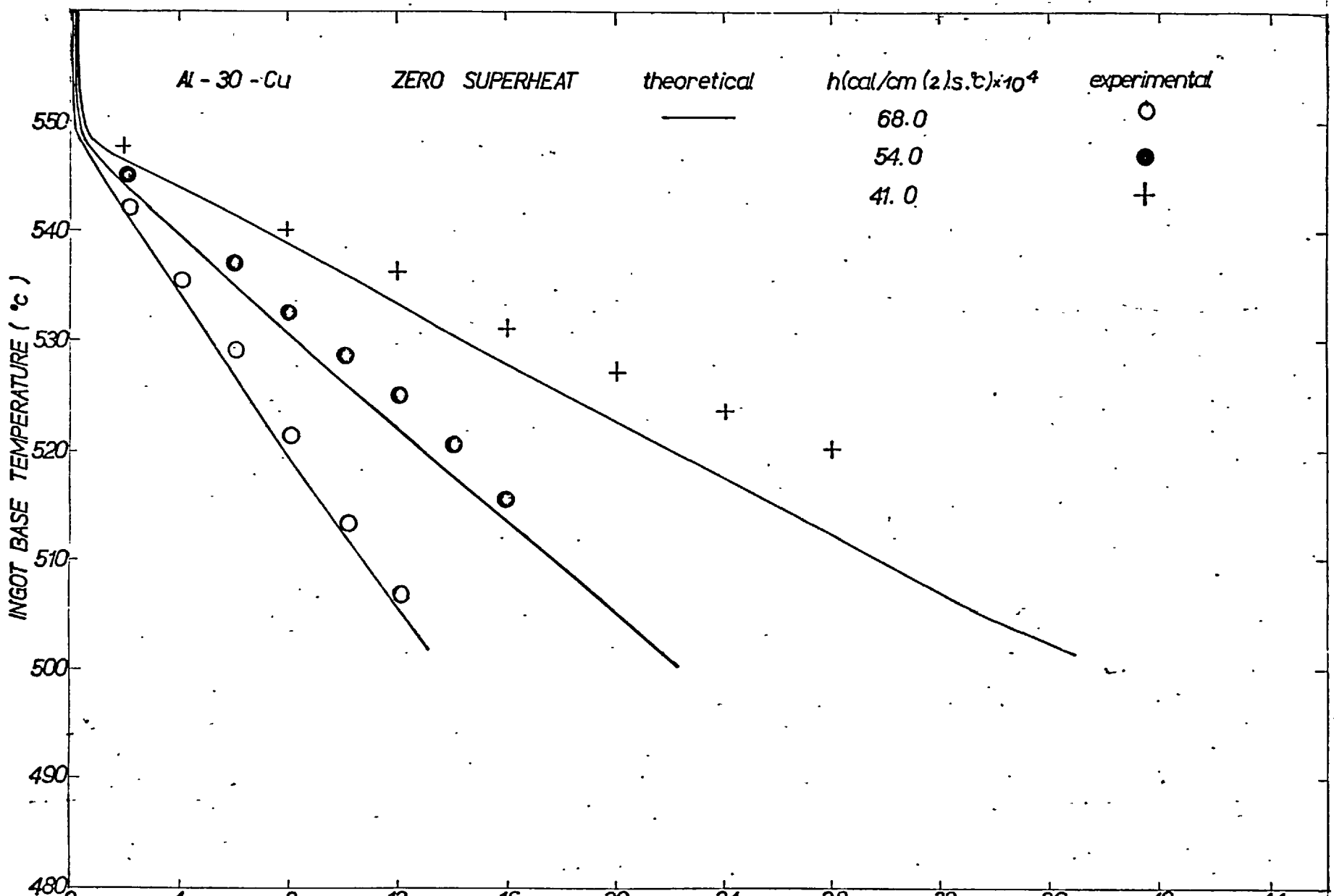

Fig 5.45
SOLIDIFICATION OF Al - 30% Cu ALLOY AT ZERO SUPERHEAT
comparison of theoretical and experimental results

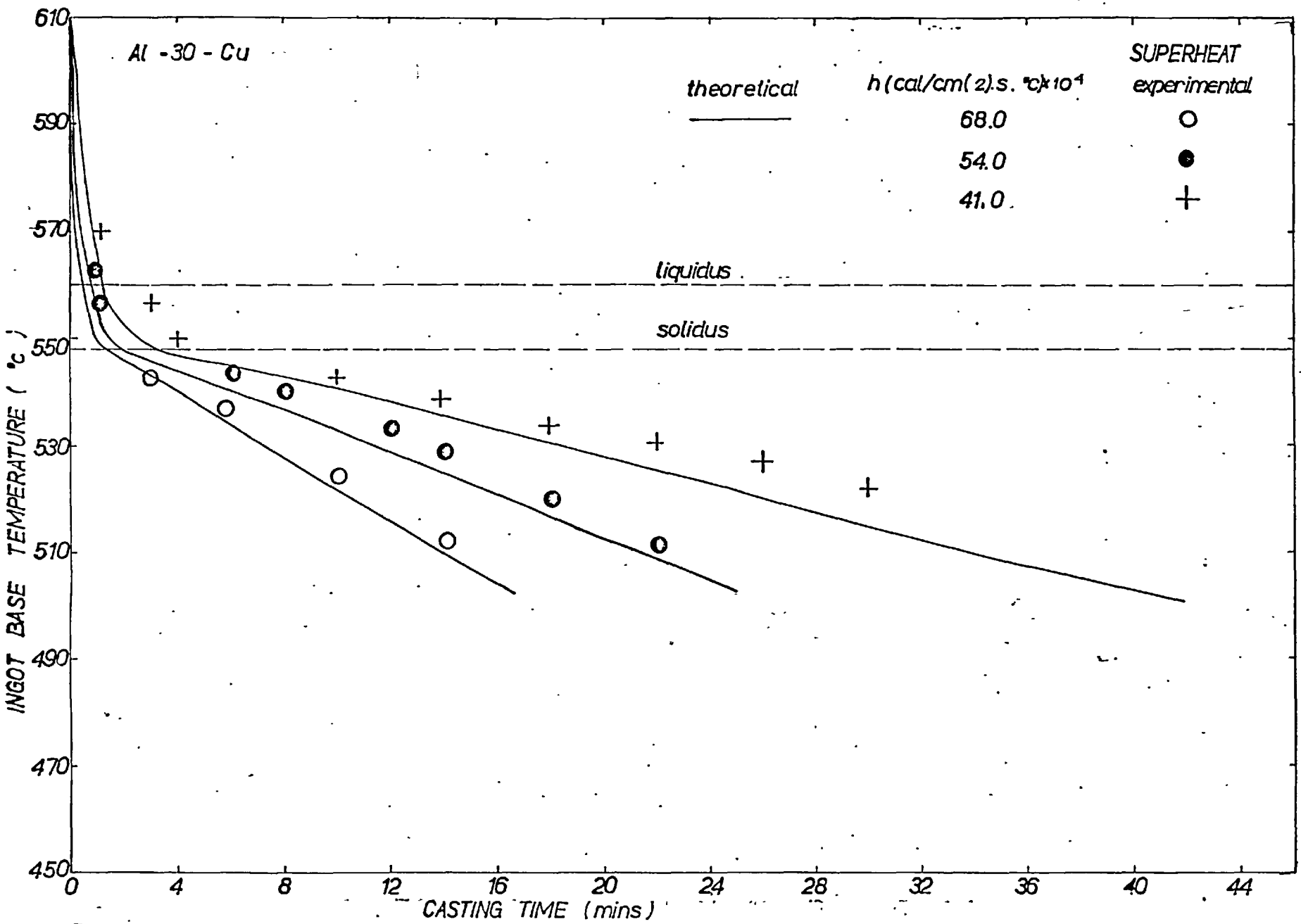

Fig 5.46 SOLIDIFICATION OF Al - 30% Cu ALLOY WITH 50°c SUPERHEAT
comparison of theoretical and experimental results

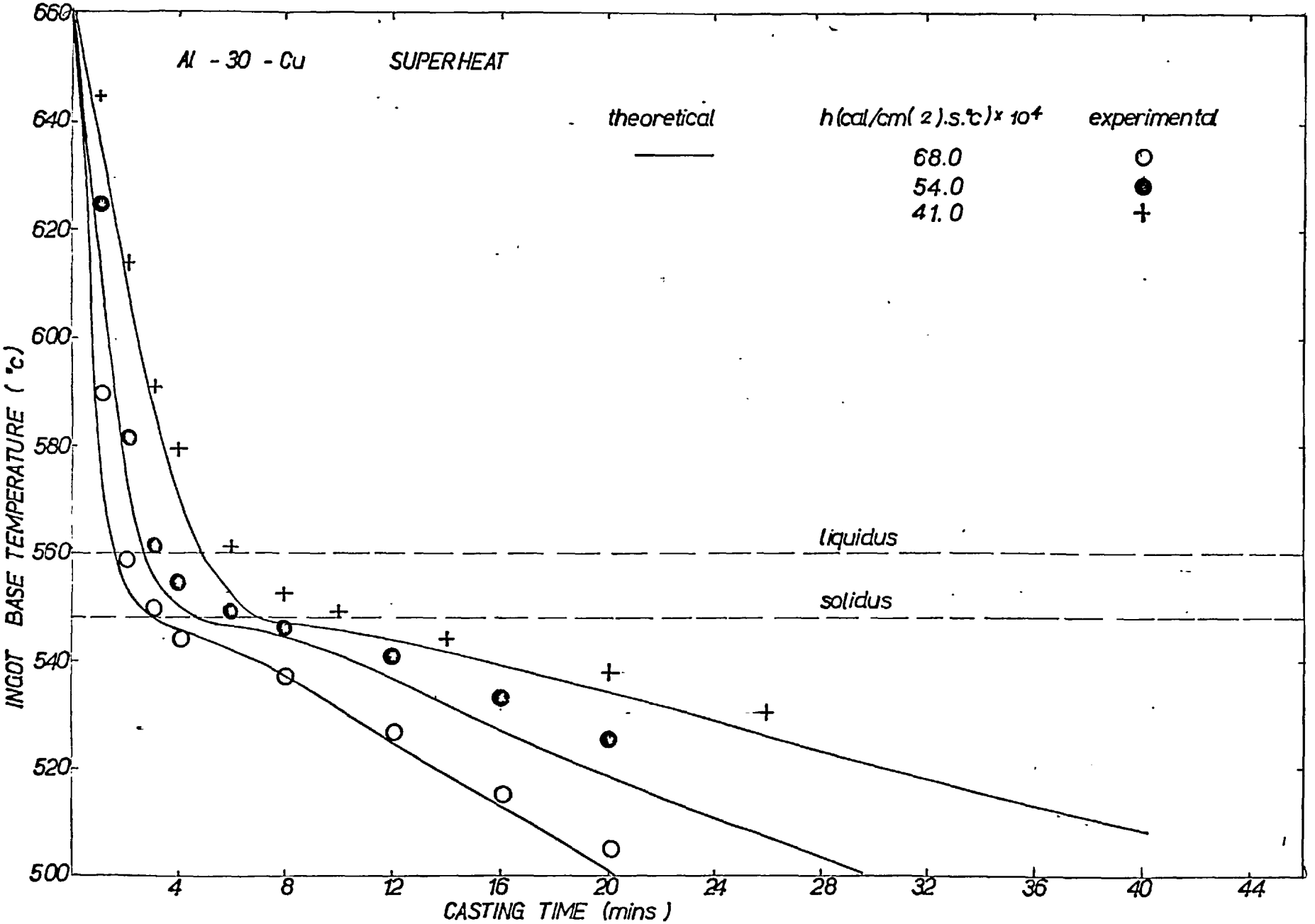

Fig 5.46a SOLIDIFICATION OF Al - 30% Cu ALLOY WITH 100°c SUPERHEAT
comparison of theoretical and experimental results

h = 68.0 (cal/cm(2).S.^{o}C) Solidus temperature = 548^{o}C

Liquidus temperature = 560^{o}C Air temperature = 40^{o}C

Casting time (min)	5	10	15
Solid layer (cm)	3	6.5	9.5
Partial layer (cm)	12	8.5	5.5
Latent heat liberated at solidus temperature (Kcal)	56.5	123	174
Temperature in metal (^{o}C)			
0 cm	530	515	501
2.0 cm	541	527	514
5.0 cm	552	543	530
7.0 cm	554	548	538
9.0 cm	555	548	545
Heat liberated in partial layer (Kcal)	13.5	11.3	7.4
Sensible heat liberated in solid layer (Kcal)	4.3	11.48	20.2
Total heat liberated in metal (Kcal)	74.3	145.8	206.6
Base temperature mid time (^{o}C)	536	530	520
Heat removed by cooling air (Kcal)	80	157	231
Excess heat liberated (Kcal)	-	-	-
Excess heat gained (Kcal)	5.7	11.2	24.4

TABLE 5.11 THERMAL BALANCE FOR THE SOLIDIFICATION OF 30% wt.cu. Al-cu ALLOY AT ZERO SUPERHEAT.

(a)

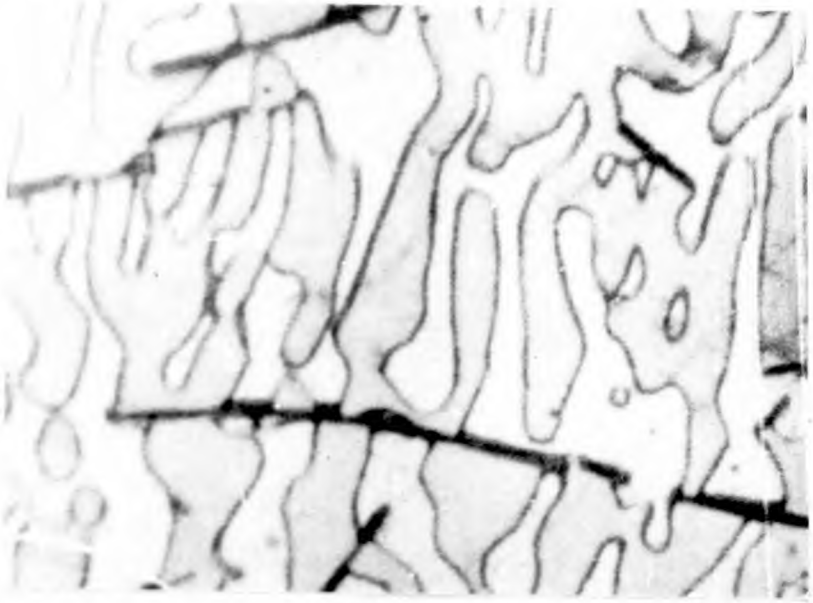

x 560

(b)

x 35

PLATE 7

Al - 30% Cu

h = 0.0054 cal/cm(2).s.°c

sections normal to cooled surface

15%:25%:15% $HCl : HNO_3 : HF$ etch

(a)

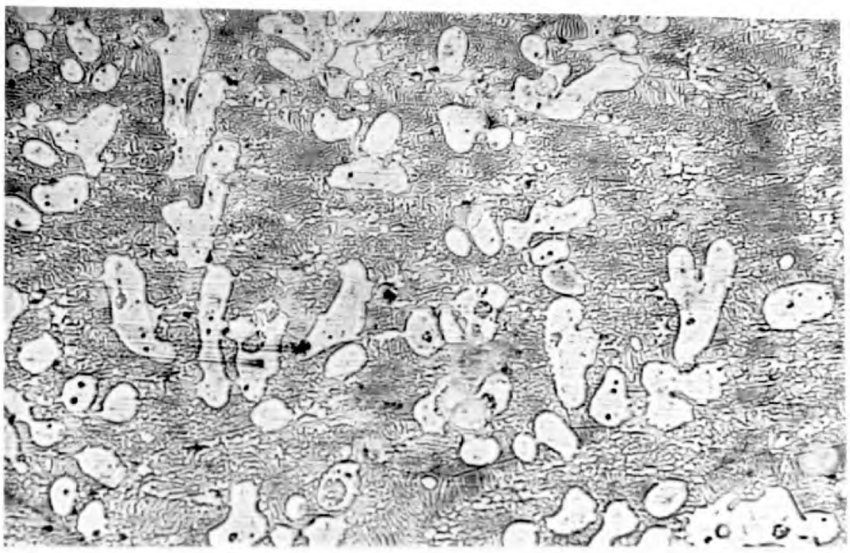

×224

(b)

× 112

PLATE 8 Al - 30% Cu

sections normal to cooled surface.

(a) h= 0.016 cal/cm(2).s. °c

(b) h= 0.022 cal/cm(2).s. °c

15% : 25% : 15% $HCl : HNO_3 : HF$ etch

Initial temperature = 660°C

Liquidus temperature = 560°C

Solidus temperature = 548°C

Heat transfer coefficient = 0.0041 cal/cm(2).S.°C

Height of metal = 15 cm

Cooling air temperature = 40°C.

Castint time (min)	5	15
Solid layer thickness (cm)	-	2
Partial layer thickness (cm)	0.5	10
Thermal layer thickness (cm)	14.5	3
Latent heat liberated at solidus (Kcal)	-	35
Latent heat liberated in partial layer (Kcal)	0.75	14
Temperature in metal (°C) at distances (cm)		
0	555	540
2	563	548
4	571	550
6	579	553
8	584	540
10	600	560
Sensible heat in solid layer (Kcal)	-	13
Sensible heat in partial layer (Kcal)	0.06	58
Sensible heat in thermal layer (Kcal)	53	17
Total heat liberated in metal (Kcal)	53.8	137
Base temperature at mild time (°C)	610	559
Heat removed by cooling air (Kcal)	55	150
Excess heat removed by cooling air (Kcal)	1.2	13
Excess heat liberated in metal (Kcal)	-	-

TABLE 5.12 THERMAL BALANCE FOR THE SOLIDIFICATION OF 30% wt.cu. Al-cu ALLOY WITH 100°C SUPERHEAT.

5.3 Controlled Growth of Eutectics

The experimental work in this study involved solidifying a molten eutectic alloy at its melting point by continuously increasing the rate of air cooling. For the solidification interface to move at a constant rate, the air flow rate had to be varied during each experiment in a prescribed manner. This was calculated from the graphs shown in Fig. 5.7 and from equations (3.3.5) and (3.3.8). The latter equation allows the initial value of the heat transfer coefficient to be fixed for any required solidification rate, and Fig. 5.47 shows how this value must be varied during a typical experiment. The same figure shows also, the required variations of air flow rate as converted from Fig. 5.7.

The following example illustrates the method.

In order to solidify an aluminium-silicon eutectic alloy at a constant rate of 0.5 cm/min., equation 3.3.8 shows that the initial heat transfer coefficient is to be:

$$h(\text{start}) = \frac{\rho H}{\theta s} \frac{dt}{dT} = 0.0045 \text{ cal/cm(2).S.}^{\circ}\text{C.}$$

The rate of change of the heat transfer coefficient is given by equation (3.3.5) which is integrated numerically from the value h(start) given above.

The relationship between heat transfer coefficient and air flow rates is found from Fig. 5.7 to be:

$$\text{Air flow rate} = \text{Exp}\ \ 1.8(\ln h - 1.75)$$

During the computer solution of equation (3.3.5), the value of h determined at each time increment are substituted into this equation showing how the air flow rate has to be varied with thime during the experiment.

Fig. 5.5 shows the relation between air flow rate and manometer

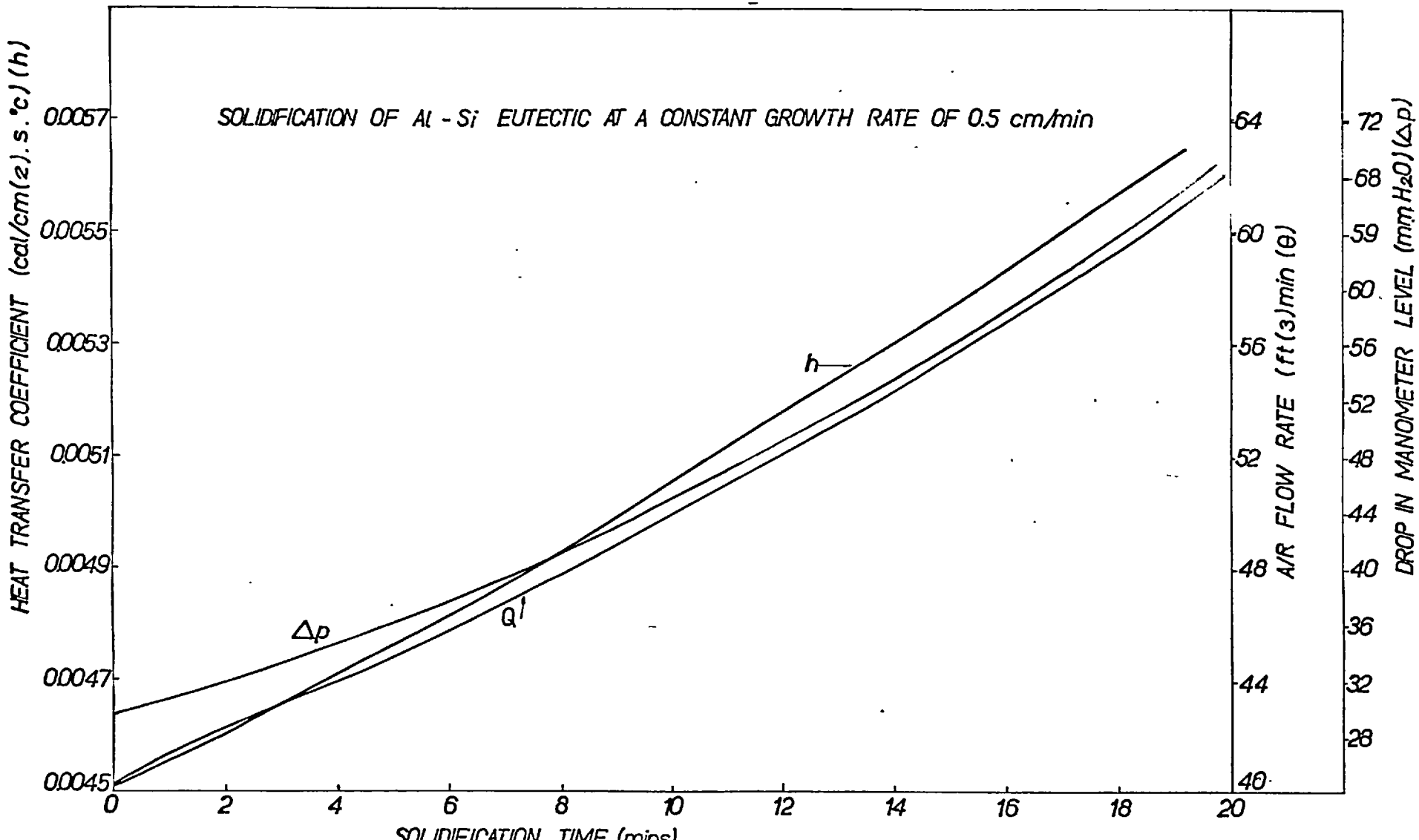

Fig 5.47 CALIBRATION CURVE SHOWING VARIATIONS OF HEAT TRANSFER COEFFICIENT AND THE CORRESPONDING VARIATIONS IN AIR FLOW RATE AND MANOMETER READINGS

readings. The equation for this calibration curve is given by British Standard B.S. 1043 and is of the form:

$$\text{Air flow rate} = \text{constant} \times \sqrt{\Delta p}$$

Where p is the manometer reading. The substitution of the required values of air flow rate into this equation shows how the manometer reading is to vary during an experiment.

Typical calculated relationships are shown in Fig. 5.47, and specimen computed results are given in Appendix (6).

Since the cooling air flow rate was limited to a maximum of about 90 c.f.m., there was a limit to the values of heat transfer coefficients that could be obtained and correspondingly a limit to the length of metal ingot that could be solidified. This length varied with the solidification rate required. Four eutectic systems were investigated. Tensile tests were carried out using a Hounsfield Tensometer.

5.3.1 Lead-Tin Eutectic

The eutectic alloy at 38.1% lead has a low melting point at 183°C. It was prepared by melting in situ, the right proportions of lead and tin. Table 5.13 set out the constant rates at which the alloys were solidified and the height of metal that could be solidified at that speed.

Solidification rate (cm/min)	Length of ingot (mm)
0.2	100
0.3	100
0.4	100
0.5	75
0.6	50

TABLE 5.13 Dimensions of lead-tin eutectic ingots solidified at constant rates.

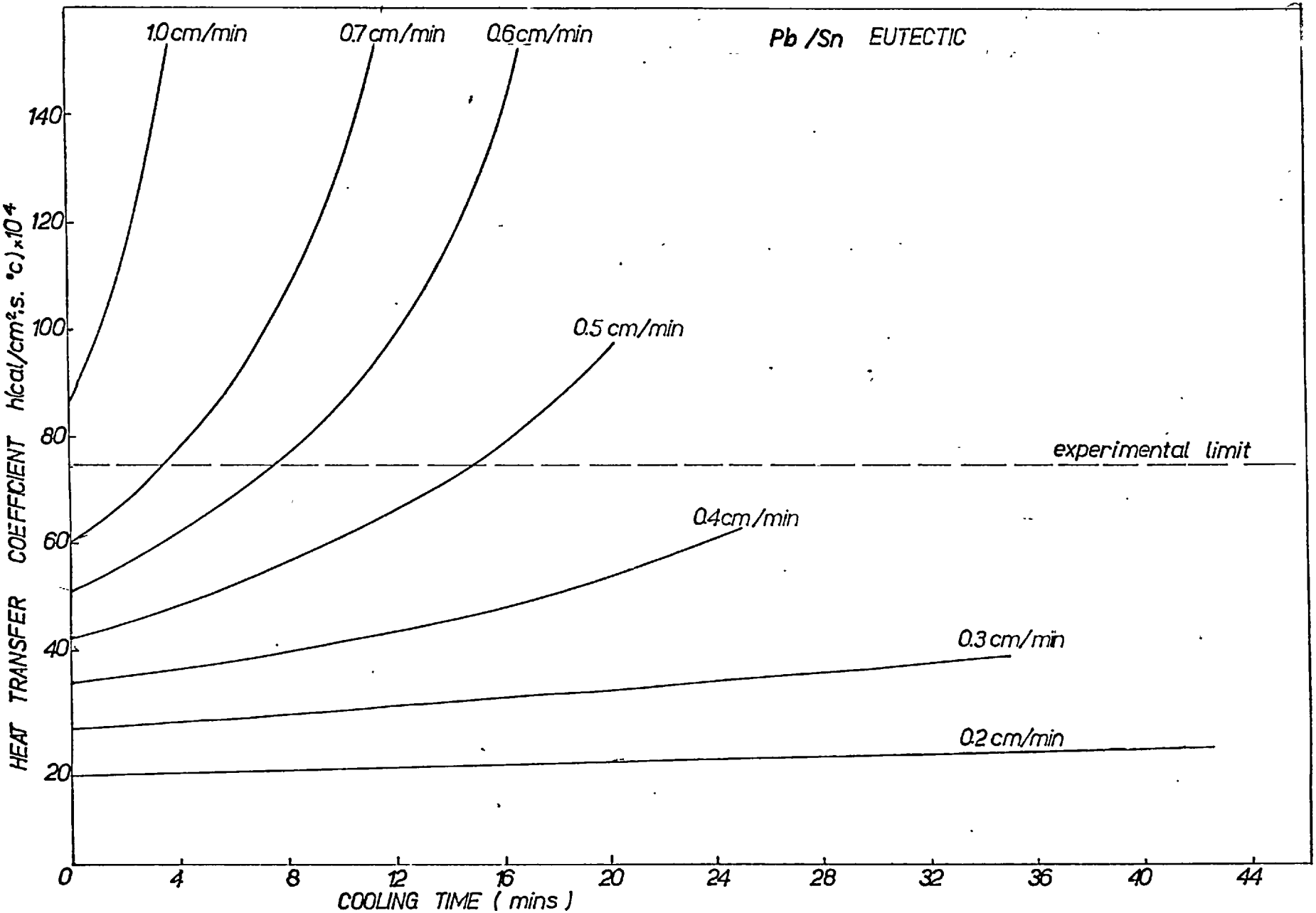

Fig 5.48 CALCULATED RATES OF CHANGE IN OVERALL HEAT TRANSFER COEFFICIENT AT INGOTS OUTER SURFACE TO SOLIDIFY AT CONSTANT GROWTH RATES

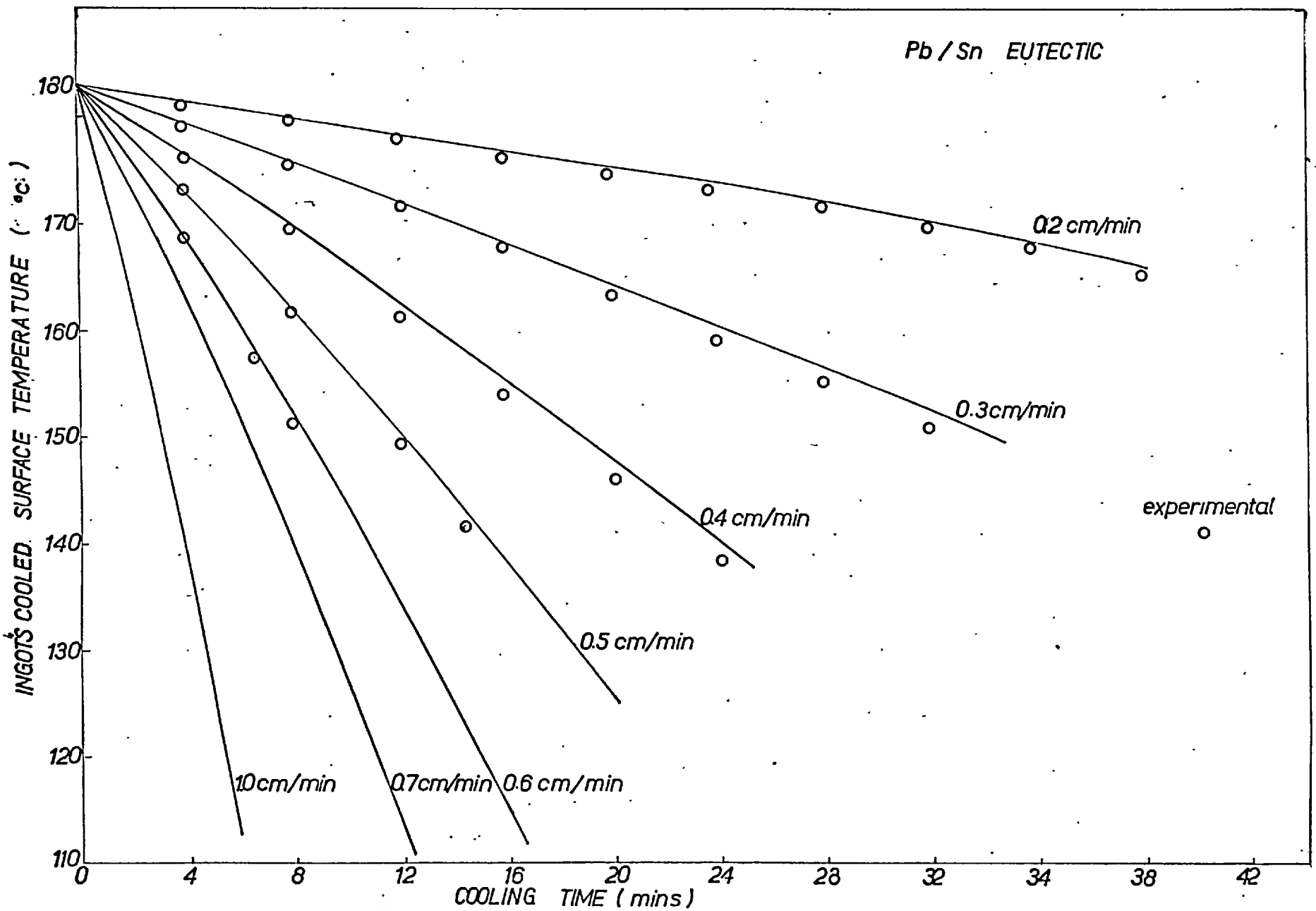

Fig 5.49 THEORETICAL COOLING CURVES FOR EUTECTIC METALS SOLIDIFYNG WITH CONSTANT GROWTH RATE

Direction of Tension	Parallel to heat flow			Normal to heat flow		
Solidification rate cm/min	Load kg	Tensile strength kg/mm.^{2}	Average Tensile Strength kg/mm.^{2}	Load kg	Tensile strength kg/mm.^{2}	Average tensile strength kg/mm.^{2}
	150	4.63		130	4.00	
	160	4.94		125	3.86	
0.25	150	4.63	4.73	135	4.16	4.00
	180	5.55		150	4.63	
	170	5.24		140	4.32	
0.50	160	4.94	5.24	150	4.63	4.52
	180	5.55		150	4.63	
	170	5.24		150	4.63	
	180	5.55		150	4.63	
0.6	170	5.24	5.39			4.63
Test Bar: Hounsfield tensometer specimen No. 14 (32.417 mm(2)).						

TABLE 5.14 TENSILE STRENGTH OF LEAD TIN EUTECTIC SOLIDIFIED AT CONSTANT RATES.

Fig. 5.58 gives the movement of the solid liquid interface with time; experiment compared with theory. Fig. 5.48 gives the calculated variations of the heat transfer coefficient that were followed in the experiment at the various growth rates. Fig. 5.49 gives theoretical curves for the variations of the ingots cooled surface temperature under the various cooling conditions, together with some experimentally measured values.

Tensile tests were carried out on specimens machined from the centre of the ingots, both longitudinally and horizontally and the results are reported in Table 5.14.

Photomicrographs are shown in plates 12, 13 and 14.

5.3.2 Aluminium - $CuAL_2$ Eutectic

The following ingot lengths were solidified at the corresponding constant solidification rates.

Solidification rate (cm/min)	Ingot length (mm)
0.33	100
0.50	100
0.66	50

TABLE 5.15 Dimensions of AL-$CuAL_2$ eutectic ingots solidified at constant growth rates.

The calculated variations in heat transfer coefficients that were followed in the experiments for the various growth rates are given in Fig. 5.50. The calculated variations in surface temperature in those rates together with experimental values are given in Fig. 5.51. Fig. 5.57 gives the movement of the solidification front with time compared

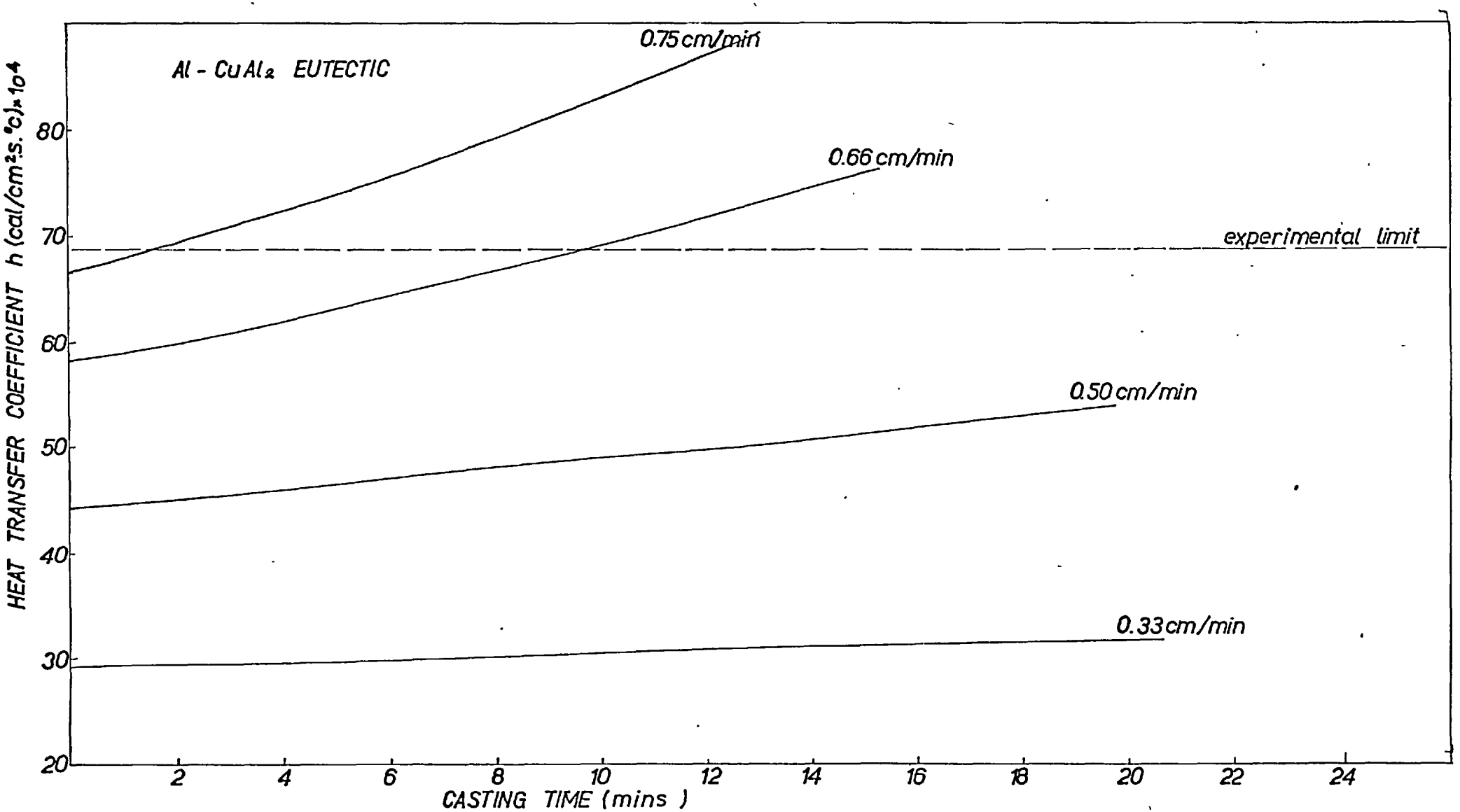

Fig 5.50 CALCULATED RATES OF CHANGE IN OVERALL HEAT TRANSFER COEFFICIENT AT INGOT'S OUTER SURFACE, TO SOLIDIFY AT CONSTANT GROWTH RATES

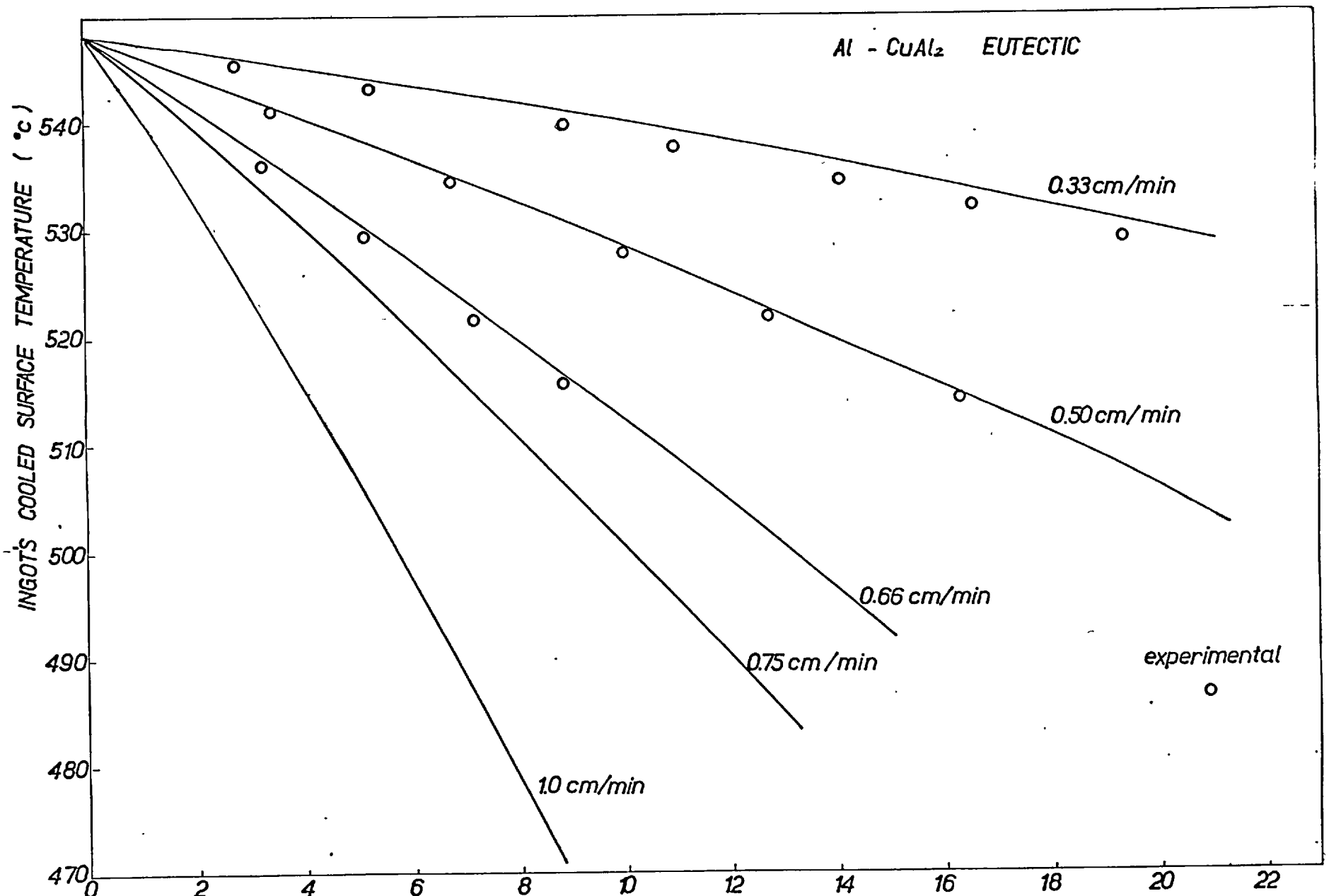

Fig 5.51 THEORETICAL COOLING CURVES FOR EUTECTIC METALS SOLIDIFYING WITH CONSTANT GROWTH RATE

(a)

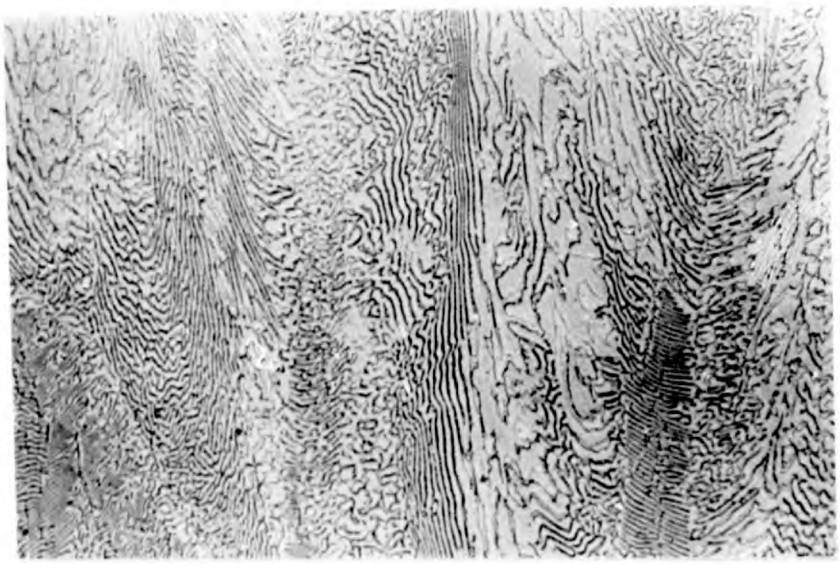

x 56

(b)

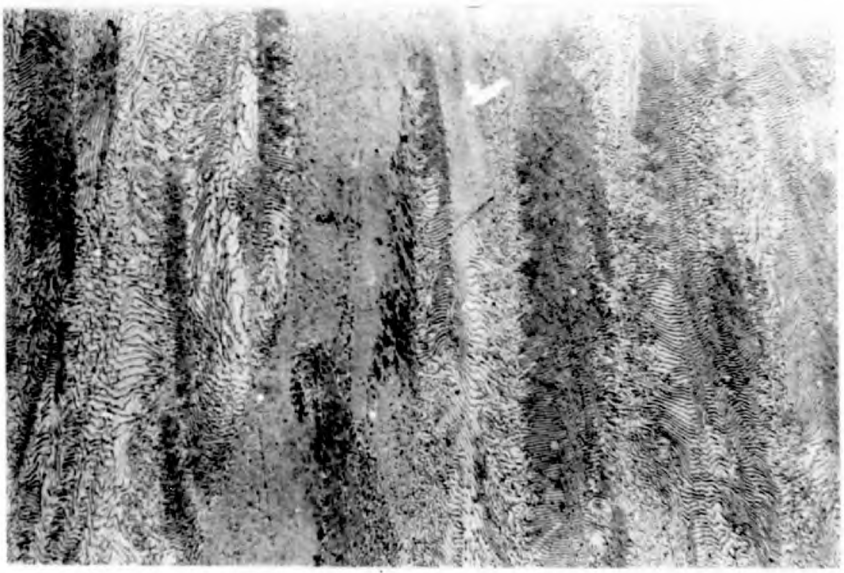

x 56

PLATE 9 Al - $CuAl_2$ EUTECTIC

sections normal to cooled surface.

(a) h = 0.016 cal/cm(2).s. °c

(b) h = 0.027 cal/cm (2).s. °c

10 % NaOH etch

(a) ↑

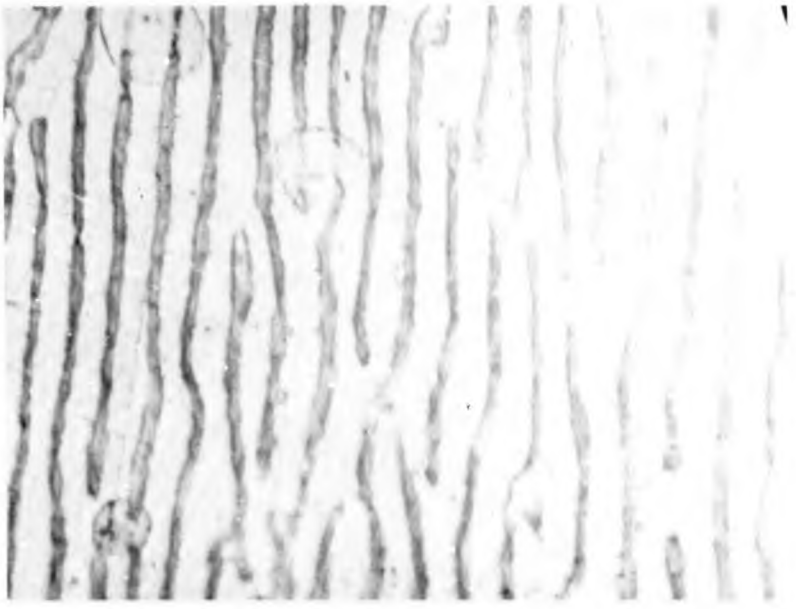

x 560

(b) ↑

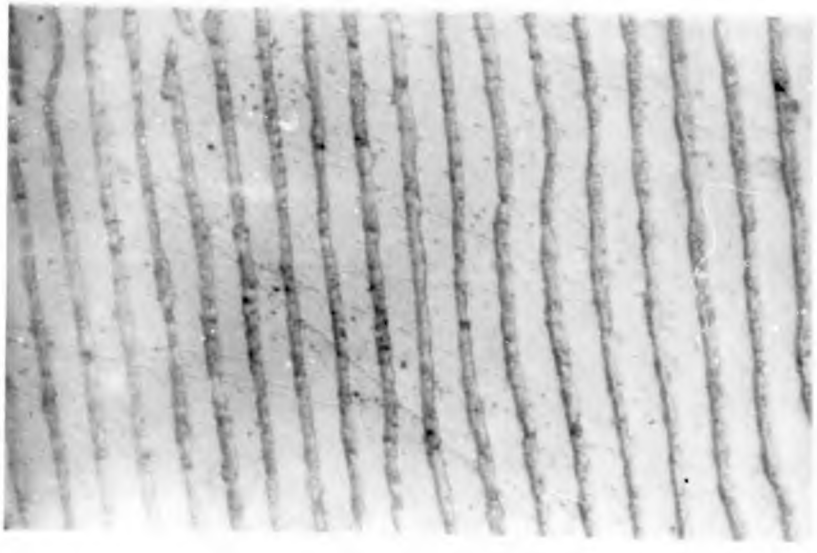

x 560

PLATE 10

Al - $CuAl_2$ EUTECTIC.

CONSTANT GROWTH RATE

(a) G=0.4 cm/min, 5 cm from cooled surface.

(b) G=0.6 cm/min, 2 cm from cooled surface.

10% NaOH etch

arrows indicate heat flow direction

Direction of tension	Parallel to heat flow			Normal to heat flow		
Solidification rate cm/min	Load kg	Tensile strength kg/mm(2)	Average tensile strength kg/mm(2)	Load kg	Tensile strength kg/mm(2)	Average tensile strength kg/mm(2)
	300	9.3		280	8.65	
	310	9.6		270	8.35	
0.33	300	9.3	9.4	280	8.65	8.55
	380	11.7		300	9.3	
	360	11.1		300	9.3	
0.50	370	11.4	11.4	290	8.95	9.2
	440	13.5		320	9.9	
	420	12.9		300	9.3	
0.66	460	14.2	13.5	310	9.6	9.6

Test bar: Hounsfield tensometer specimen No.14 (32.417 mm(2))

TABLE 5.16 TENSILE STRENGTH OF ALUMINIUM - $'CUAL_2$ EUTECTIC SOLIDIFIED AT CONSTANT RATES.

(a)

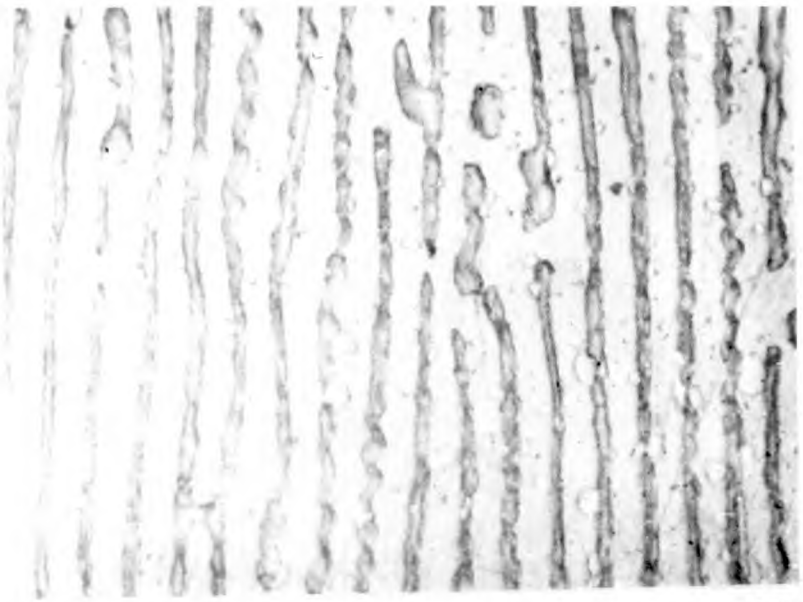

x 560

(b)

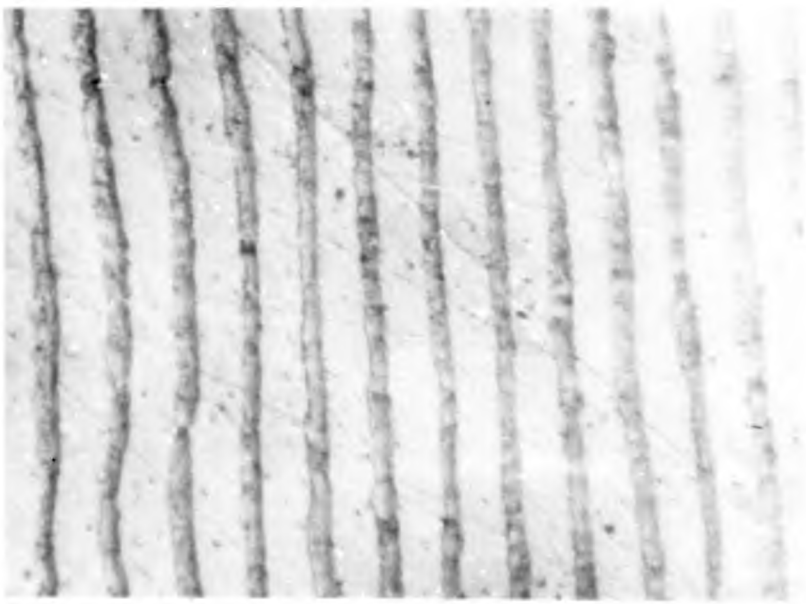

x 560

PLATE 11

Al - $CuAl_2$

CONSTANT GROWTH RATE

(a) G = 0.33 cm/min; 2 cm from cooled surface.

(b) G = 0.5 cm/min ; 2 cm from cooled surface.

10 % Na OH etch

to the theoretical rates. Tensile test results, are reported in Table 5.16 and photomicrographs are shown in plates 10 and 11.

5.3.3 Aluminium - Silicon Eutectic

Table 5.17 gives the length of the aluminium - silicon eutectic ingots solidified at various constant solidification rates.

Constant solidification rate (cm/min)	Ingot length (mm)
0.33	100
0.50	100
0.66	50

TABLE 5.17 Dimensions of Aluminium-Silicon Eutectic ingots solidified at constant rates.

The movement of the solidification front at these rates is compared with the experimental measurements in Fig. 5.56 and the results of tensile tests on speciments cut from the ingots are reported in Table 5.18. The calculated variations in heat transfer coefficient are shown in Fig. 5.52, and Fig. 5.53 which compare calculated values of the ingots' surface temperature with the measured values. Photomicrographs are shown in Plates 16 and 17.

5.3.4 Iron - Carbon - Phosphorus Ternary Eutectic

An ingot length of 65 mm of this eutectic was solidified at a constant rate of 0.33 cm/min while at a rate of 0.5 cm/min, only 30 mm could be solidified. The measured rates are compared to the theoretical lines in Fig. 5.59.

The variations in the heat transfer coefficients predicted for these solidification rates are given in Fig. 5.54 while calculated variations of the ingots cooled surface temperature are compared with measured values in Fig. 5.55.

(a)

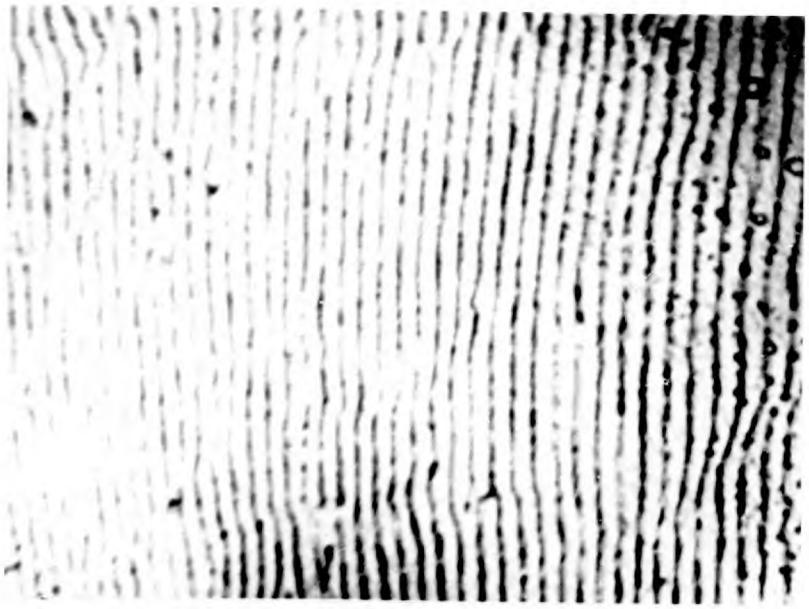

x 112

(b)

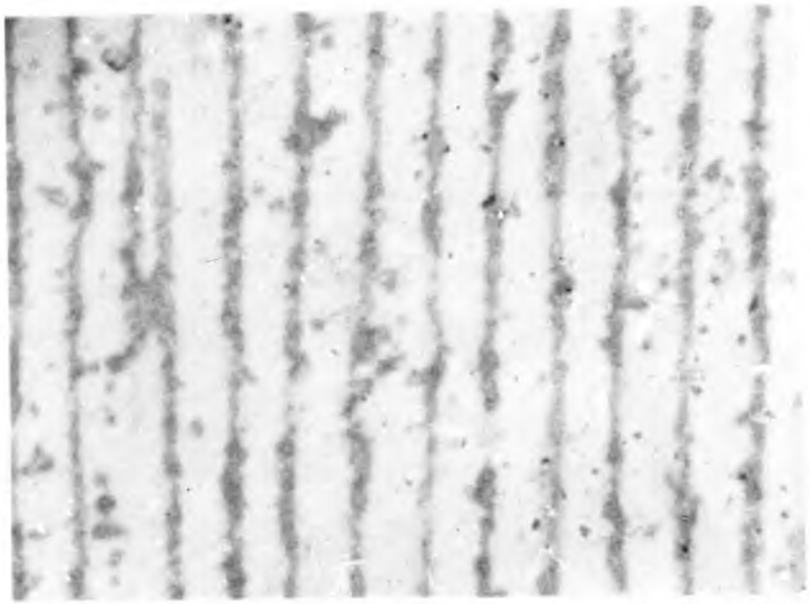

x 560

PLATE 12

LEAD - TIN EUTECTIC

CONSTANT GROWTH RATE

G = 0.33 cm/min

(a) 7 cm from base

(b) 6 cm from base

1:1:4 Acetic acid: Nitric acid : Glycerol etch

(a)

x 560

(b)

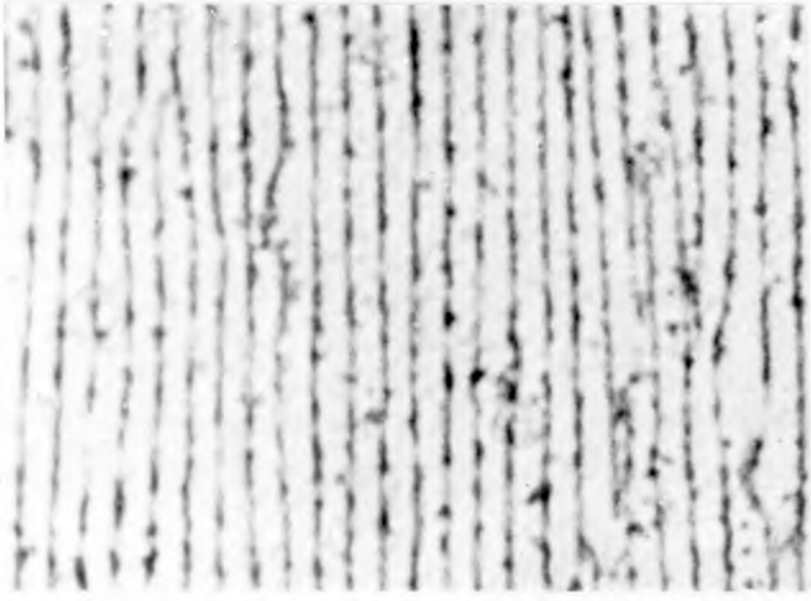

x 560

PLATE 13 Pb-Sn EUTECTIC.

CONSTANT GROWTH RATE

sections normal to cooled surface.

(a) G = 0.5 cm/min; 5 cm from cooled surface

(b) G = 0.66 cm/min; 2 cm from cooled surface.

1:1:4 Nitric acid : Acetic acid : Glycerol etch

arrows indicate heat flow direction

(a) ↑

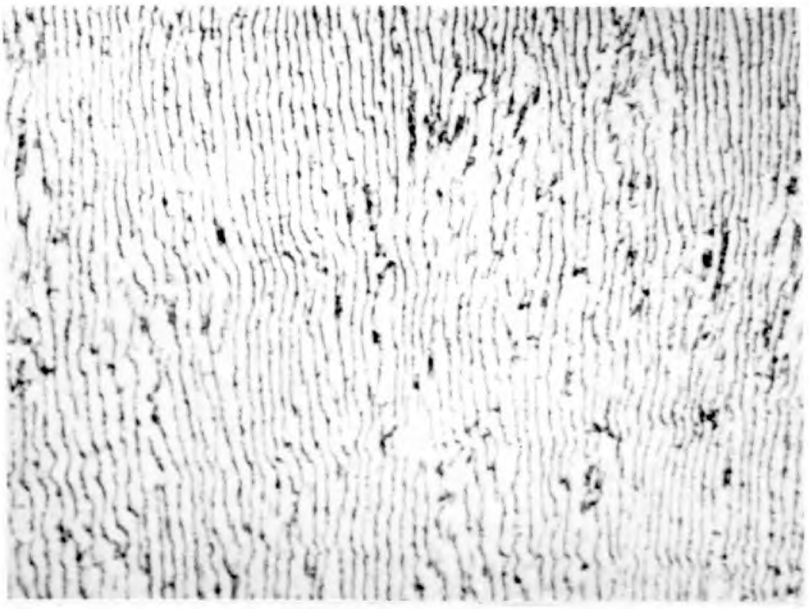

x560

(b) ↑

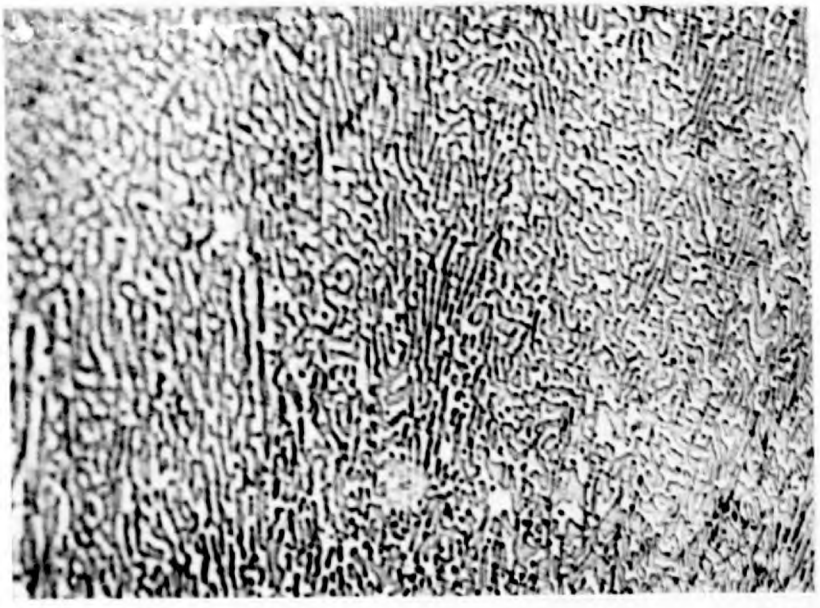

x112

PLATE 14

Pb - Sn EUTECTIC

CONSTANT GROWTH RATE

G = 0.66 cm/min; 1 cm from base

1 : 1 : 4 Acetic acid : Nitric acid : Glycerol etch

arrows indicate heat flow direction

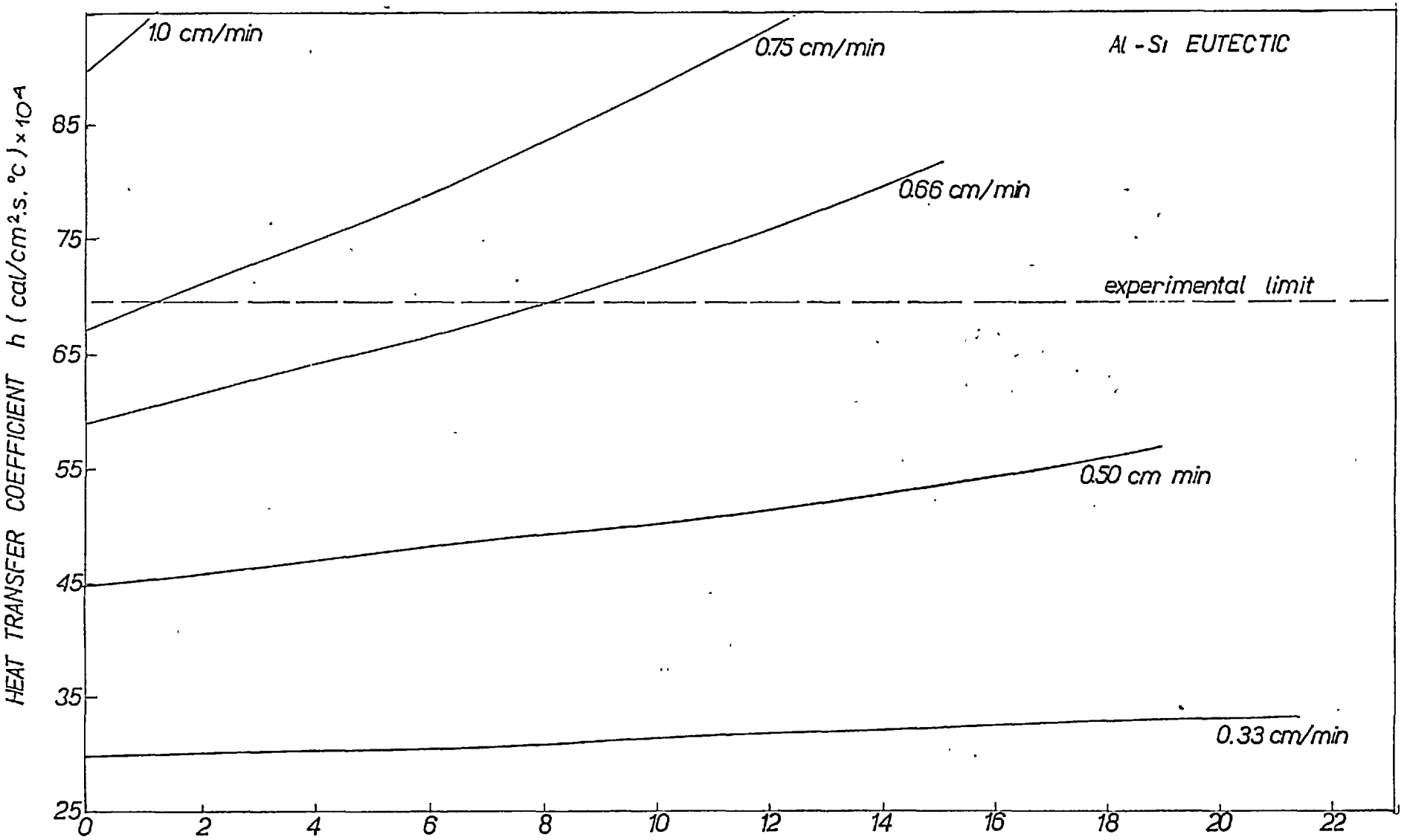

Fig 5.52 CALCULATED RATES OF CHANGE IN OVERALL HEAT TRANSFER COEFFICIENT AT INGOTS OUTER SURFACE, TO SOLIDIFY AT CONSTANT GROWTH RATES

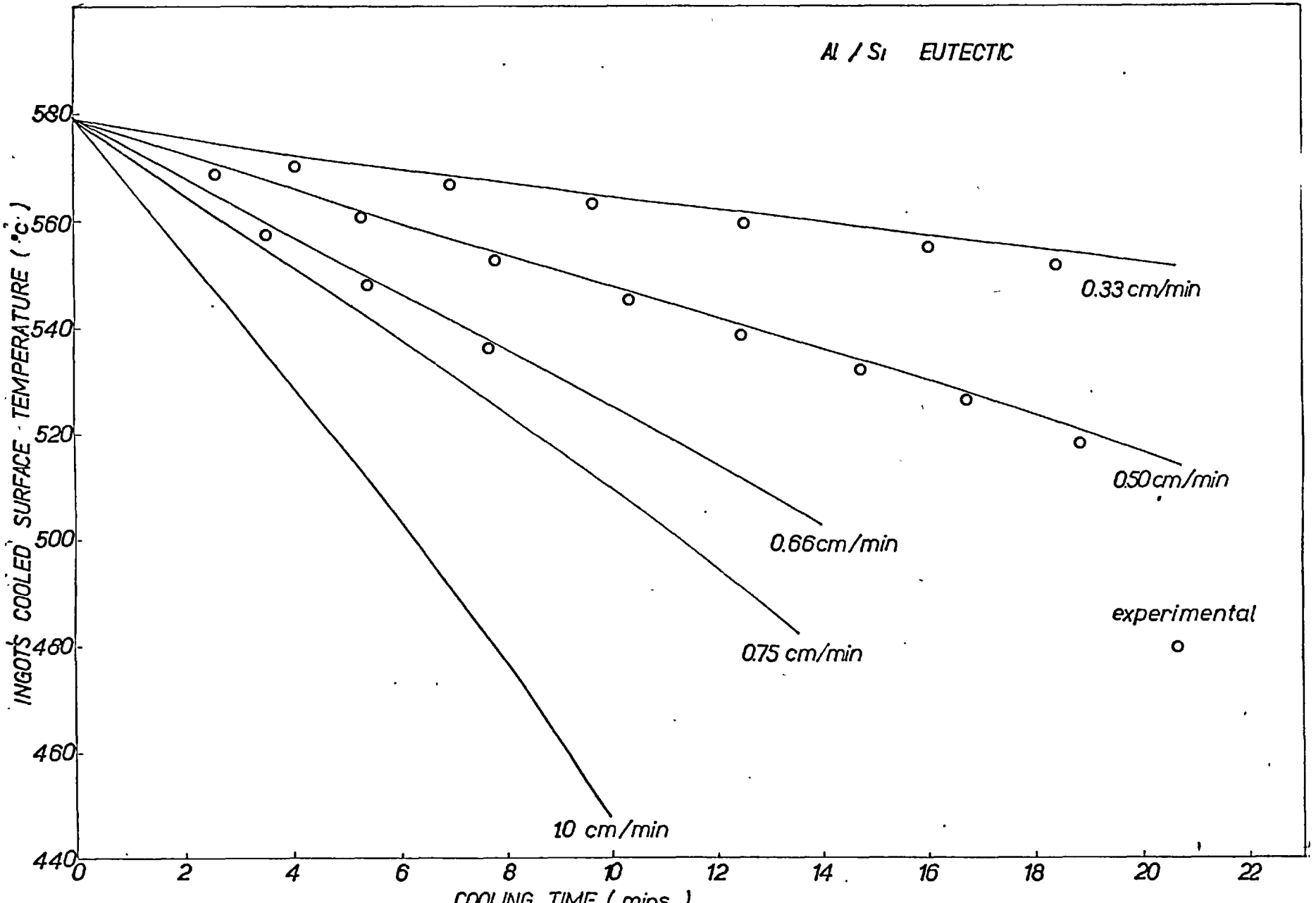

Fig 5.53 THEORETICAL COOLING CURVES FOR EUTECTIC METALS SOLIDIFYNG WITH CONSTANT GROWTH RATE.

Direction of tension	Parallel to heat flow			Normal to heat flow		
Solidification rate cm/min	Load kg	Tensile strength kg/mm^2	Average Tensile strength kg/mm^2	Load kg	Tensile strength kg/mm^2	Average tensile strength kg/mm^2
	450	13.9		340	10.5	
	445	13.7		340	10.5	
0.33	455	14.0	13.9	340	10.5	10.5
	500	15.4		400	12.3	
	550	16.9		380	11.7	
0.50	600	18.5	16.9	400	12.3	12.1
	600	18.5		400	12.3	
	600	18.5		450	13.9	
0.66	625	19.2	18.7	450	13.9	13.3
Test bar: Hounsfield tensometer specimen No. 14 (32.47 mm(2)).						

TABLE 5.18 TENSILE STRENGTH OF ALUMINIUM SILICON EUTECTIC SOLIDIFIED AT CONSTANT RATES.

(a)

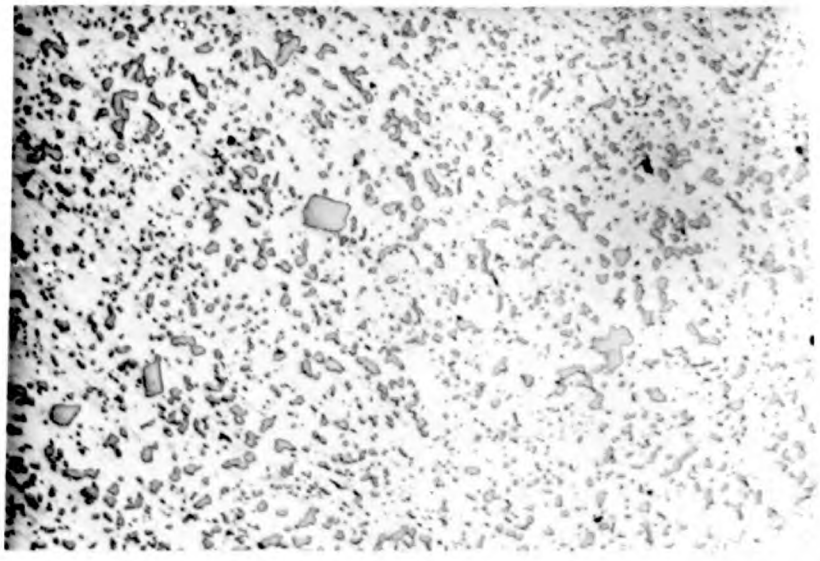

x 110

(b)

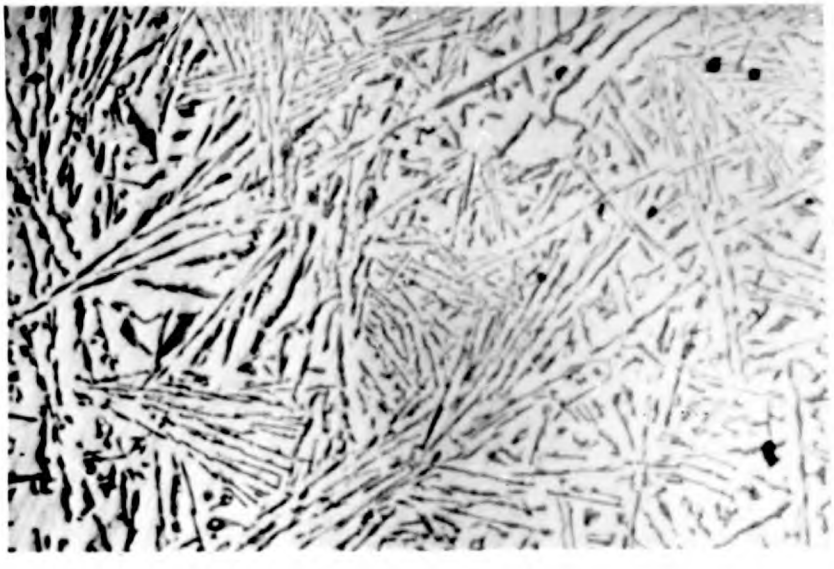

x 110

PLATE 15 Al - Si EUTECTIC

h = 0.0068 cal/cm (2).s. °c

(a) Parallel to cooled surface

(b) Normal to cooled surface.

6 % Nital etch

(a)

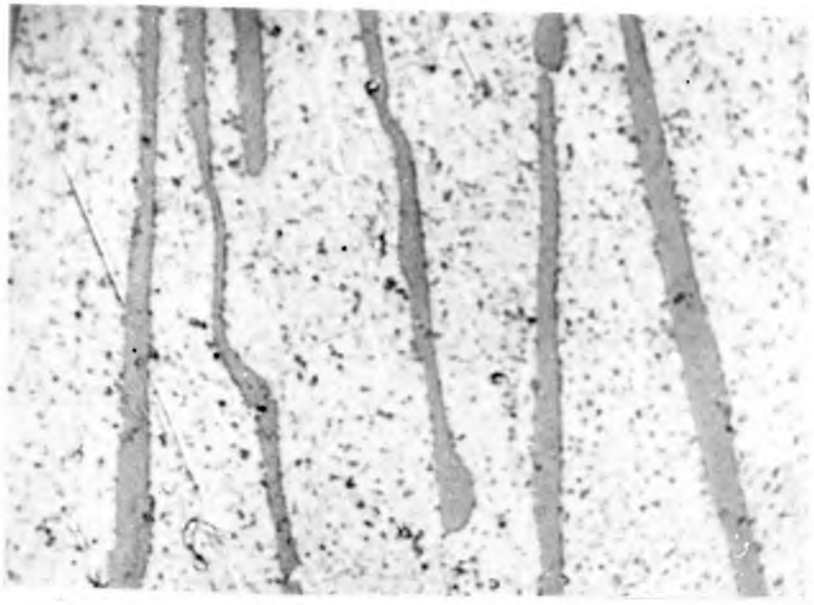

× 224

(b)

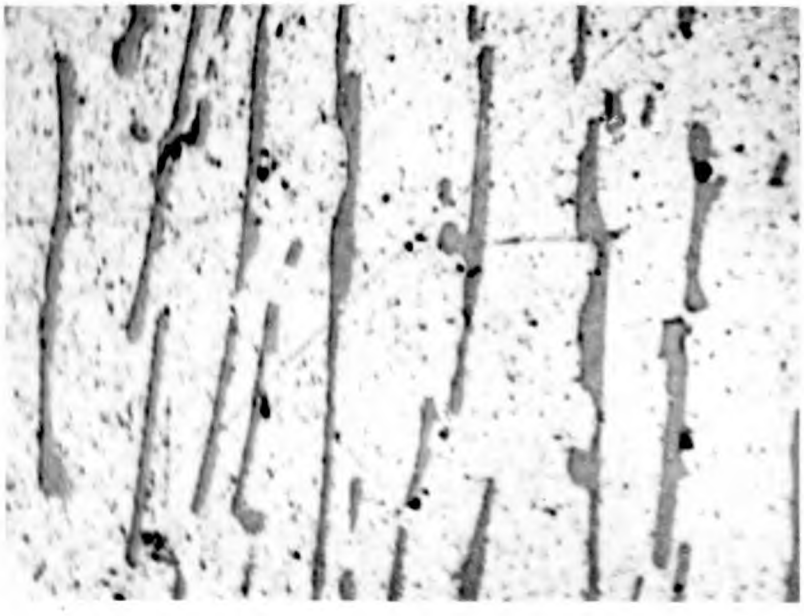

× 224

PLATE 16 Al - Si EUTECTIC.

CONSTANT GROWTH RATE.

sections normal to cooled surface.

(a) G=0.5 cm/min, 5 cm from cooled surface.

(b) G=0.3 cm/min, 7 cm from cooled surface.

6% Nital etch

(a)

x 224

(b)

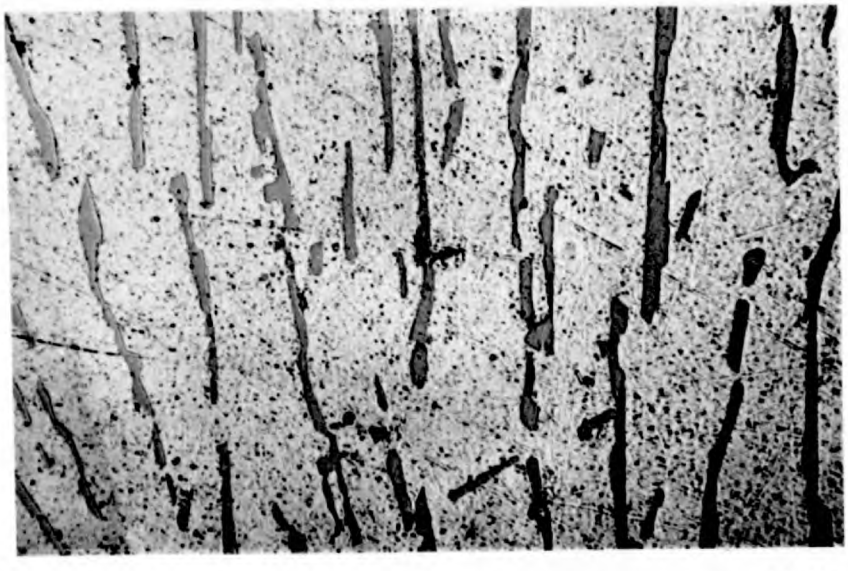

x 224

PLATE 17 Al - Si EUTECTIC.

CONSTANT GROWTH RATE.

sections normal to cooled surface.

(a) G= 0.5 cm/min, 3 cm from cooled surface

(b) G= 0.66 cm/min, 2 cm from cooled surface

6 % Nital etch

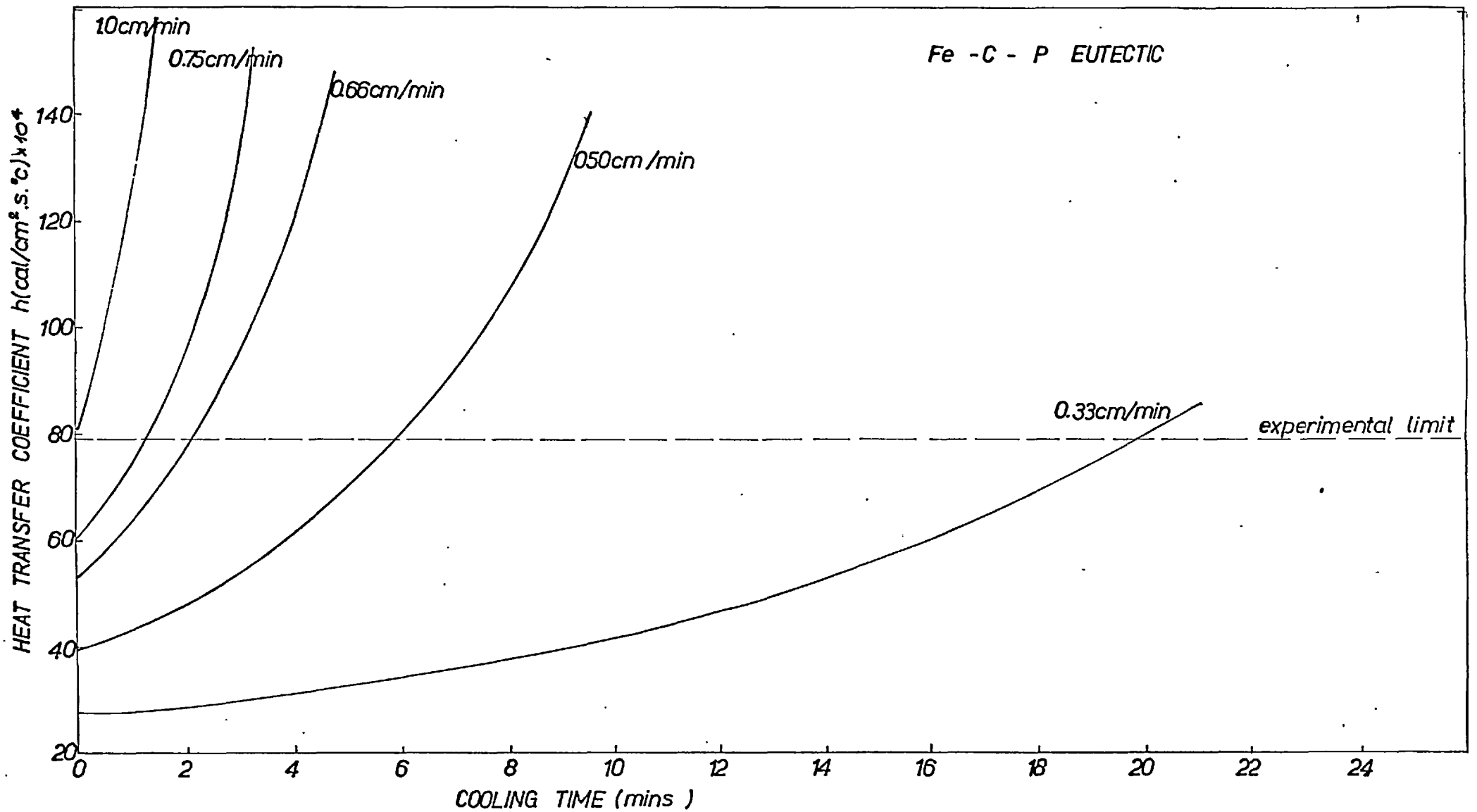

Fig 5.54 CALCULATED RATES OF CHANGE IN OVERALL HEAT TRANSFER COEFFICIENT AT INGOT'S OUTER SURFACE TO SOLIDIFY AT CONSTANT GROWTH RATES

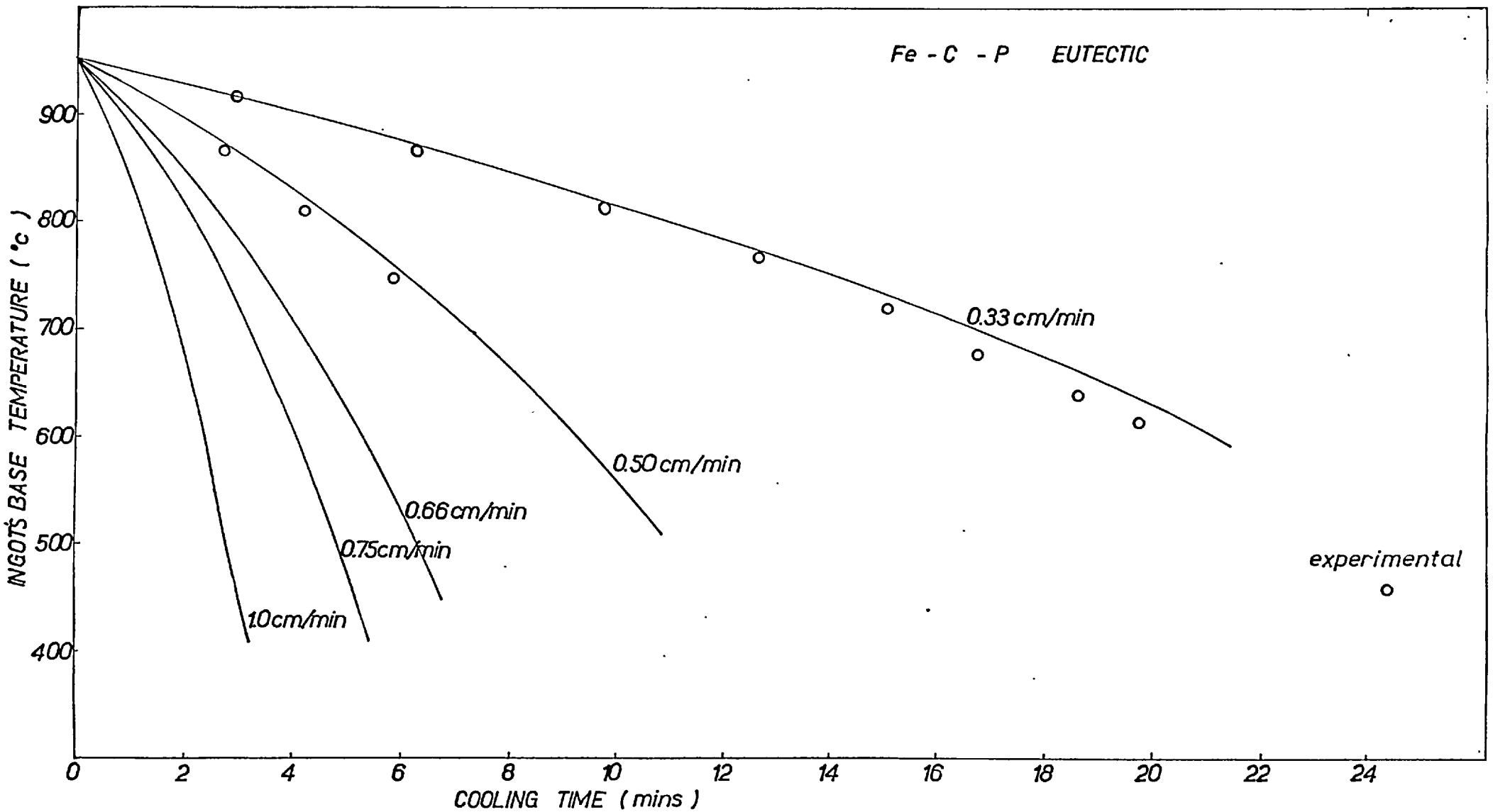

Fig 5.55 THEORETICAL COOLING CURVES FOR EUTECTIC METALS SOLIDIFYING WITH CONSTANT GROWTH RATE

(a)

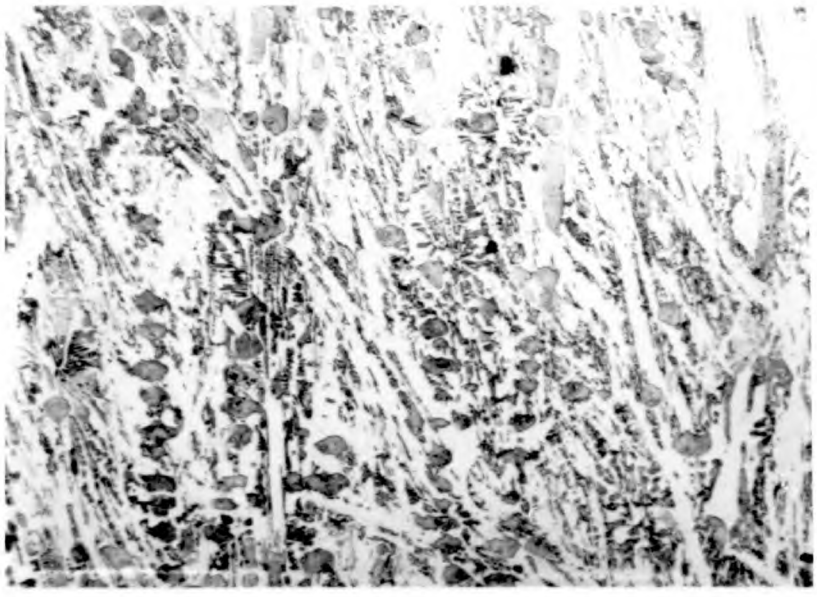

x 112

(b)

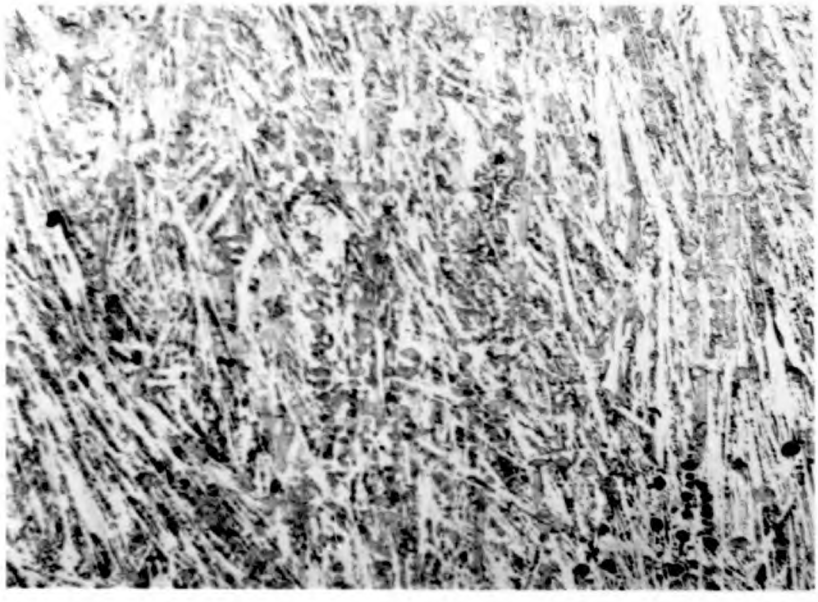

x 112

PLATE 18 Fe - C - P TERNARY EUTECTIC

sections normal to cooled surface

(a) h=0.004 cal/cm(2).s.°c

(b) h=0.006 cal/cm(2).s.°c

5% Nital etch

(a)

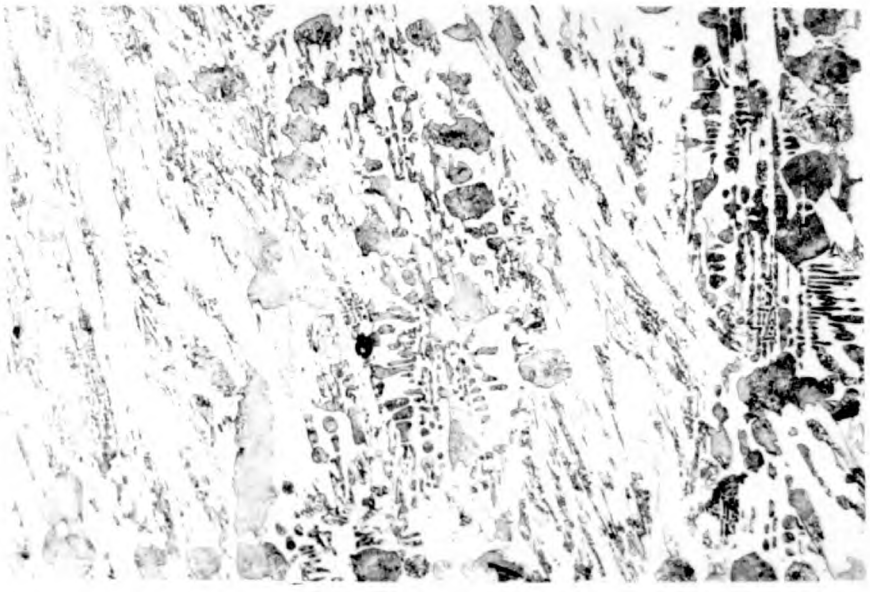

x 112

(b)

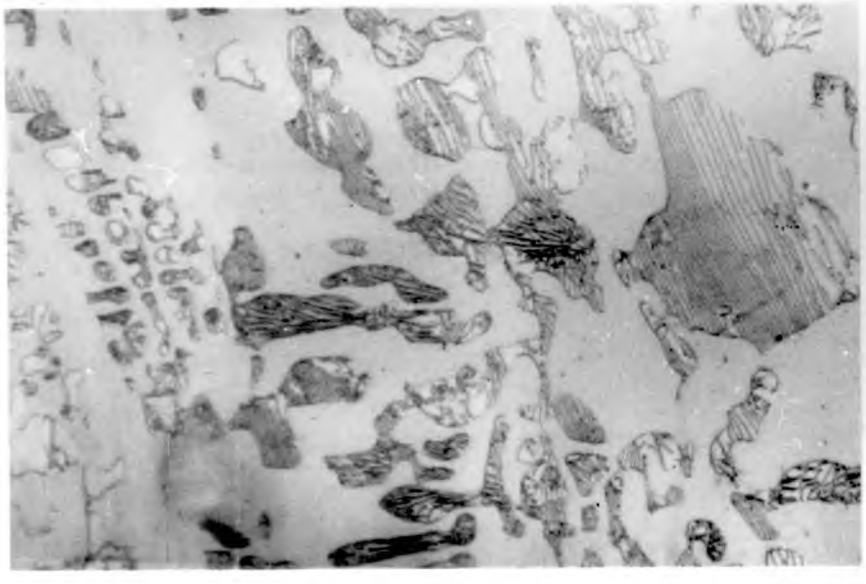

x 560

PLATE 19

Fe-C-P TERNARY EUTECTIC.

CONSTANT GROWTH RATE.

sections normal to cooled surface.

G = 0.3 cm/min ; 3 cm from cooled surface.

5% Nital etch

(a)

× 112

(b)

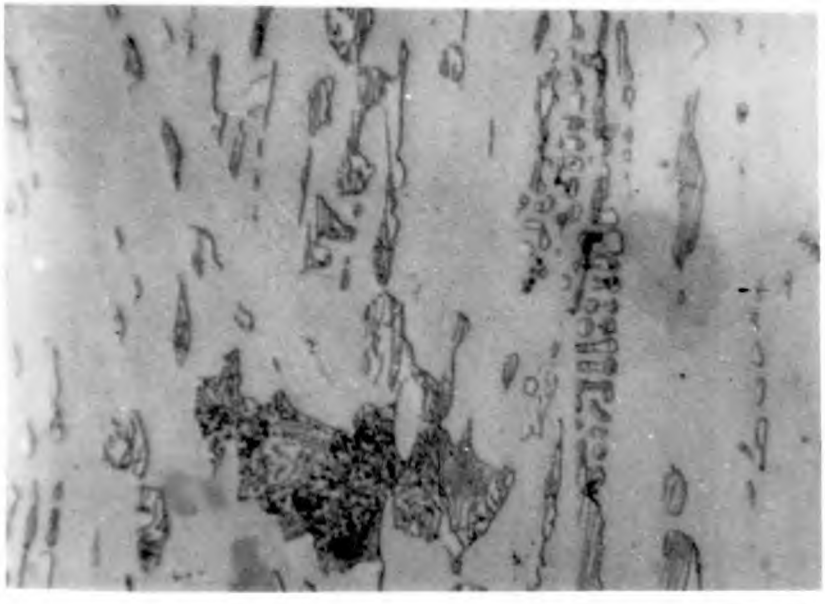

× 560

PLATE 20 Fe - C - P TERNARY EUTECTIC. CONSTANT GROWTH RATE

sections normal to cooled surface.

G = 0.5 cm/min; 2 cm from cooled surface

5 % Nital etch

(a)

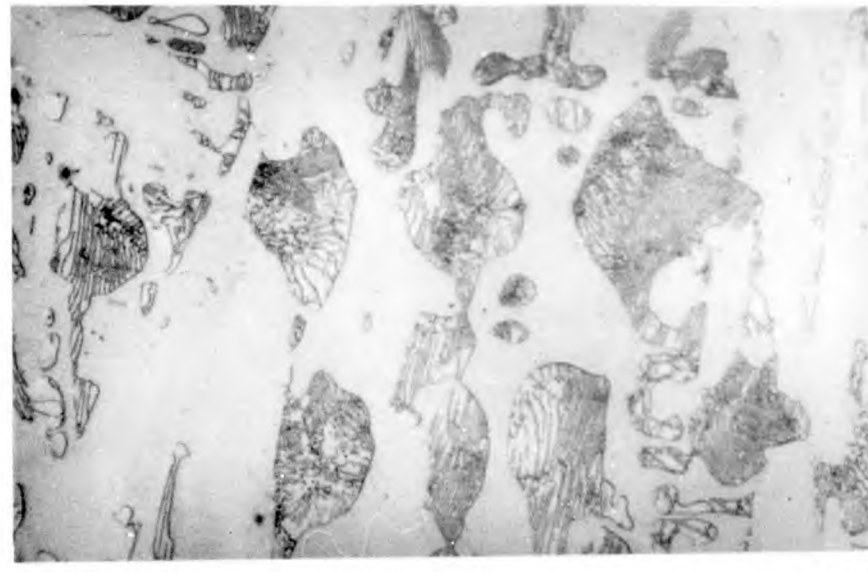

x 560

(b)

x 112

PLATE 21 Fe - C - P TERNARY EUTECTIC . CONSTANT GROWTH RATE.

sections normal to cooled surface

G = 0.66 cm/min ; 1 cm from cooled surface.

5 % Nital etch

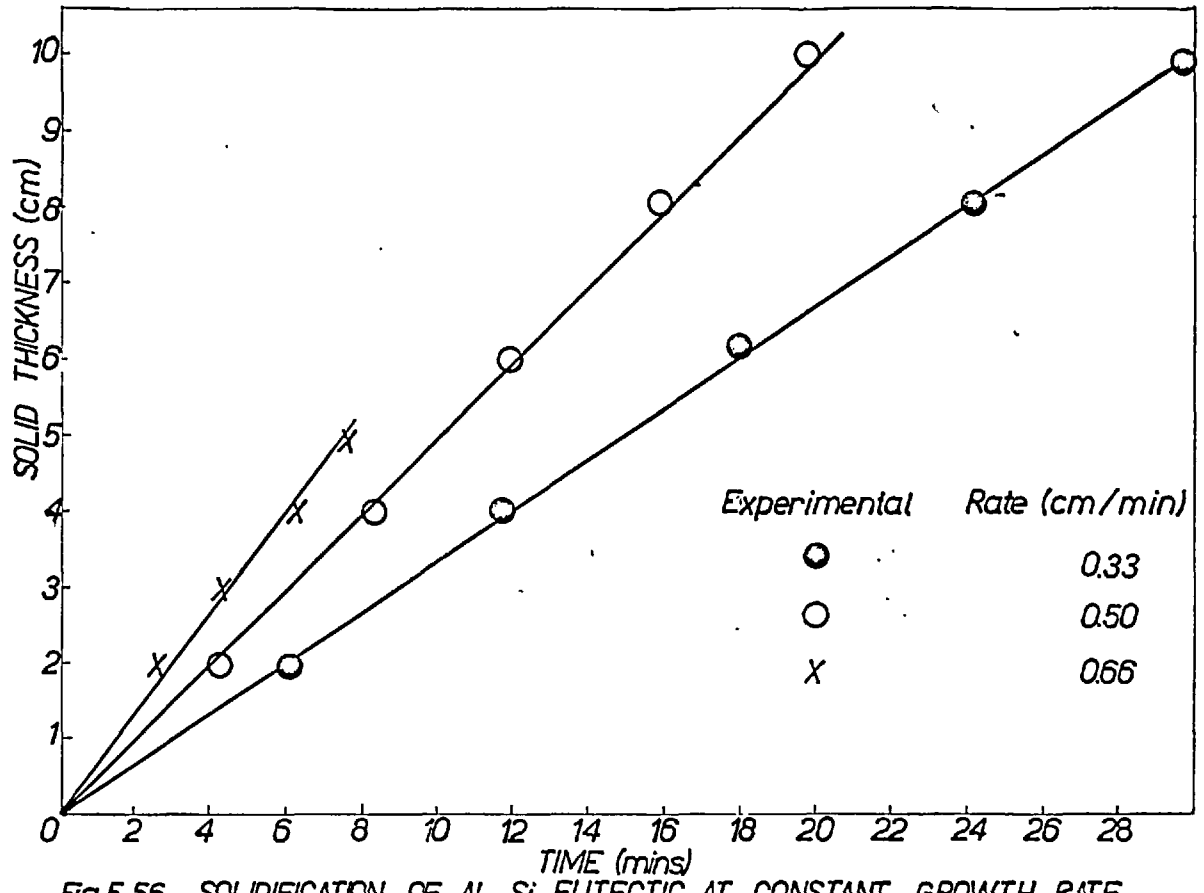

Fig 5.56 SOLIDIFICATION OF Al - Si EUTECTIC AT CONSTANT GROWTH RATE

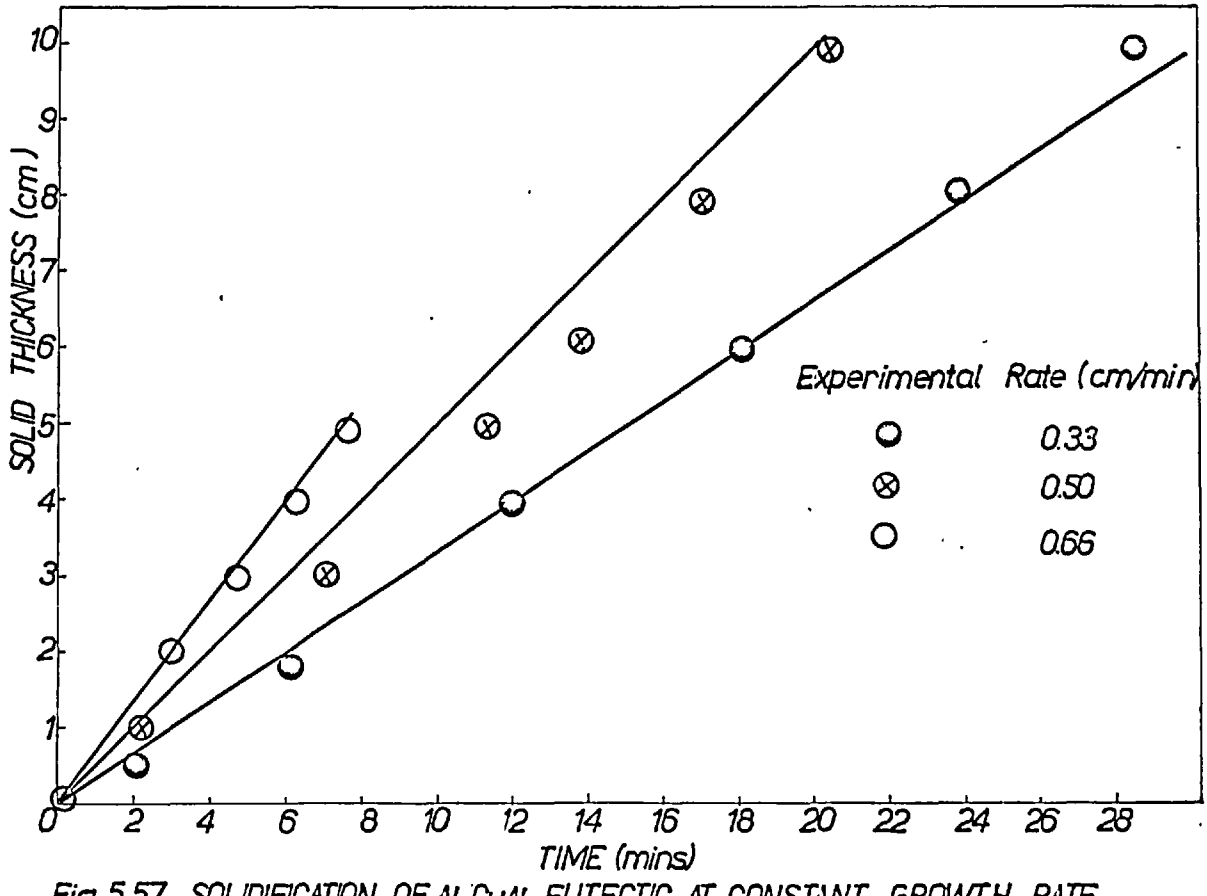

Fig 5.57 SOLIDIFICATION OF Al-$CuAl_2$ EUTECTIC AT CONSTANT GROWTH RATE

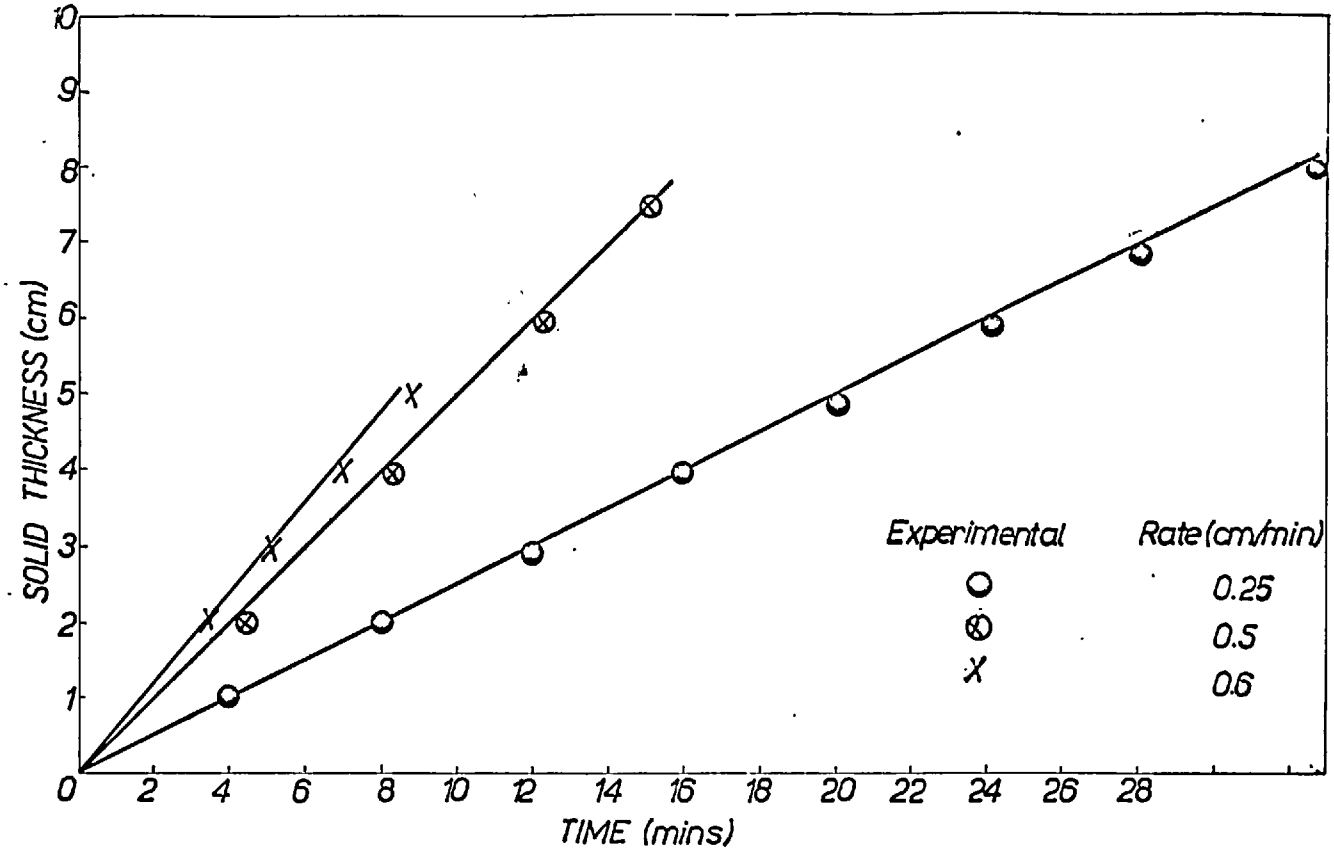

Fig 5.58 SOLIDIFICATION OF Pb-Sn EUTECTIC AT CONSTANT GROWTH RATE

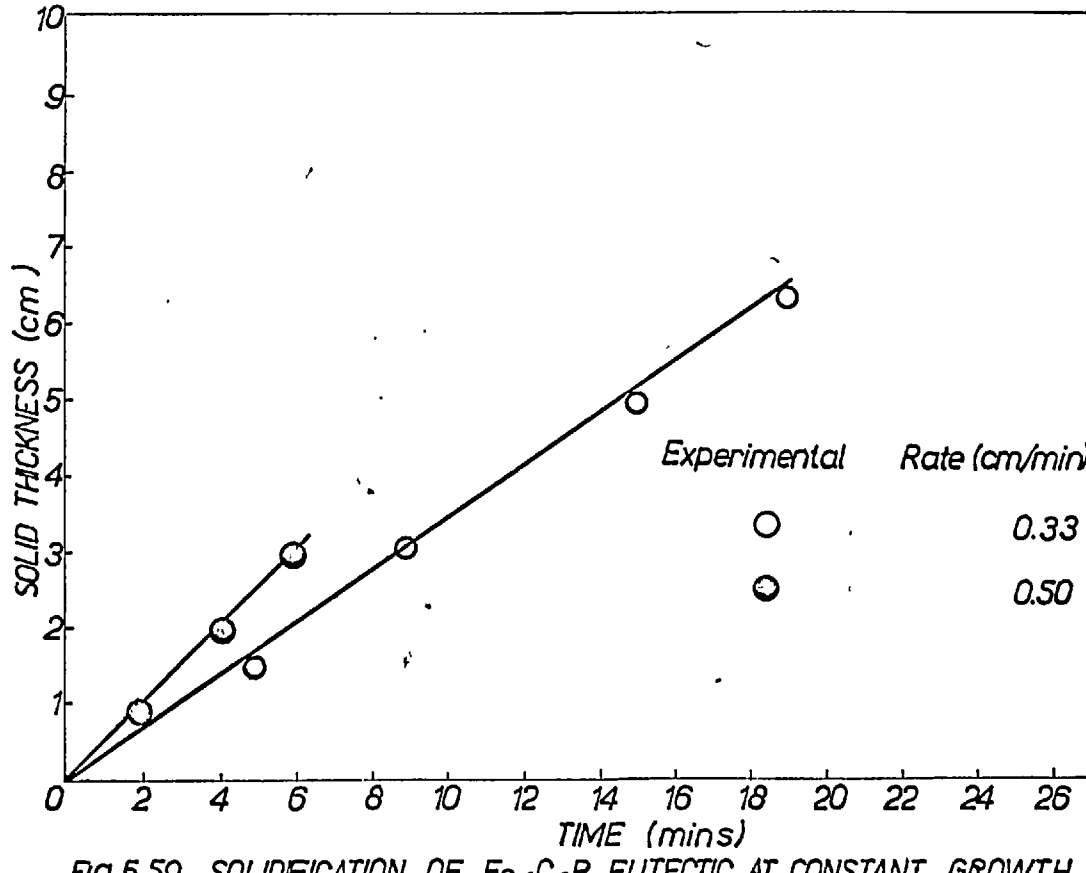

Fig 5.59 SOLIDIFICATION OF Fe-C-P EUTECTIC AT CONSTANT GROWTH RATE

Difficulties associated with a high degree of brittleness and high hardness values (600 HB), did not permit the ready machining of test specimens. In addition, most of the specimens, which were machined, using special tools, contained casting defects (shrinkage cavities) From those specimens which were found to be sound, an average tensile strength of 12 kg/mm(2) was obtained. The specimens were pulled in the heat flow direction out of three ingots solidified at a constant rate of 0.33 cm/min.

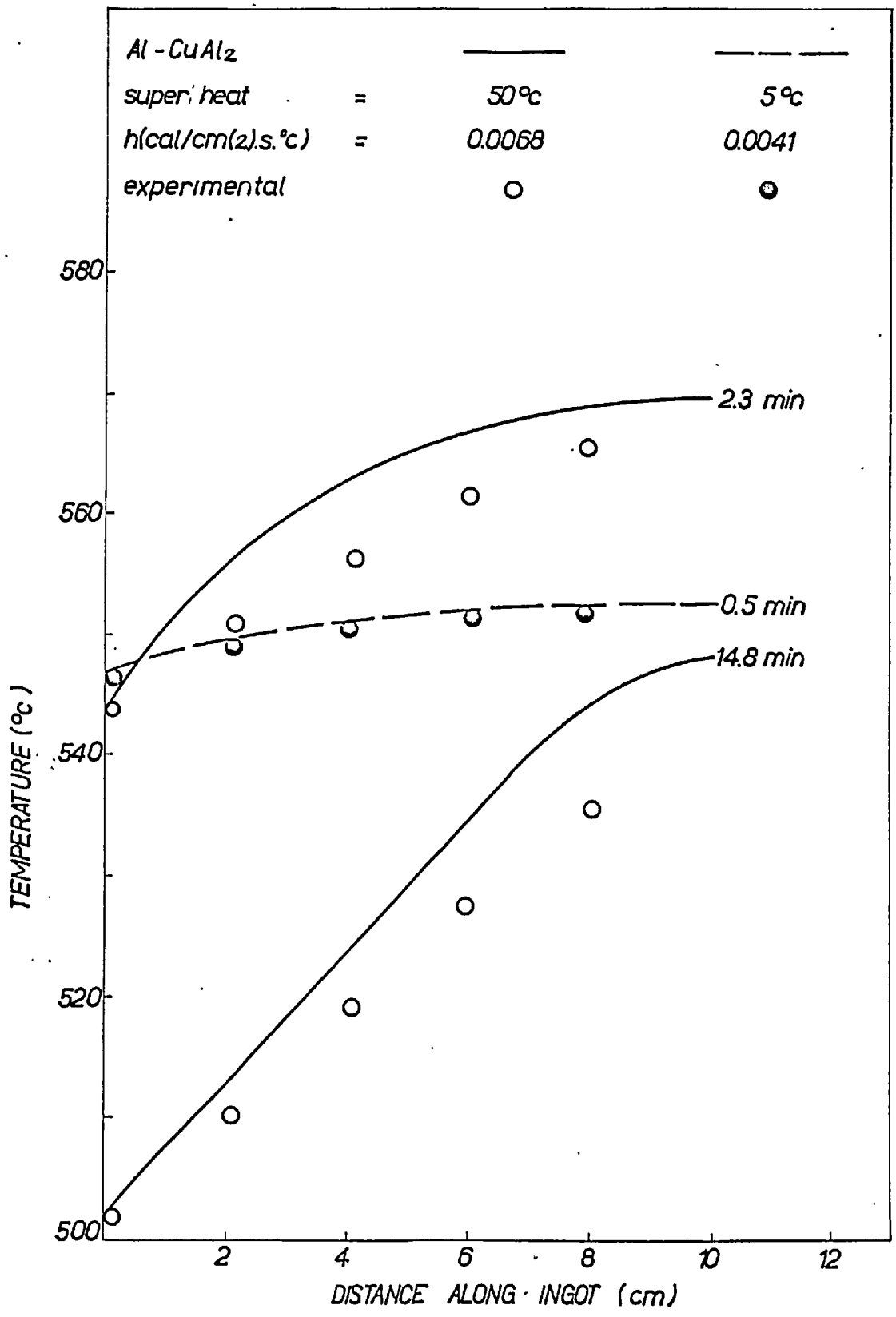

Fig 5.60 PREDICTED TEMPERATURE PROFILES AT VARIOUS TIMES FROM START OF COOLING

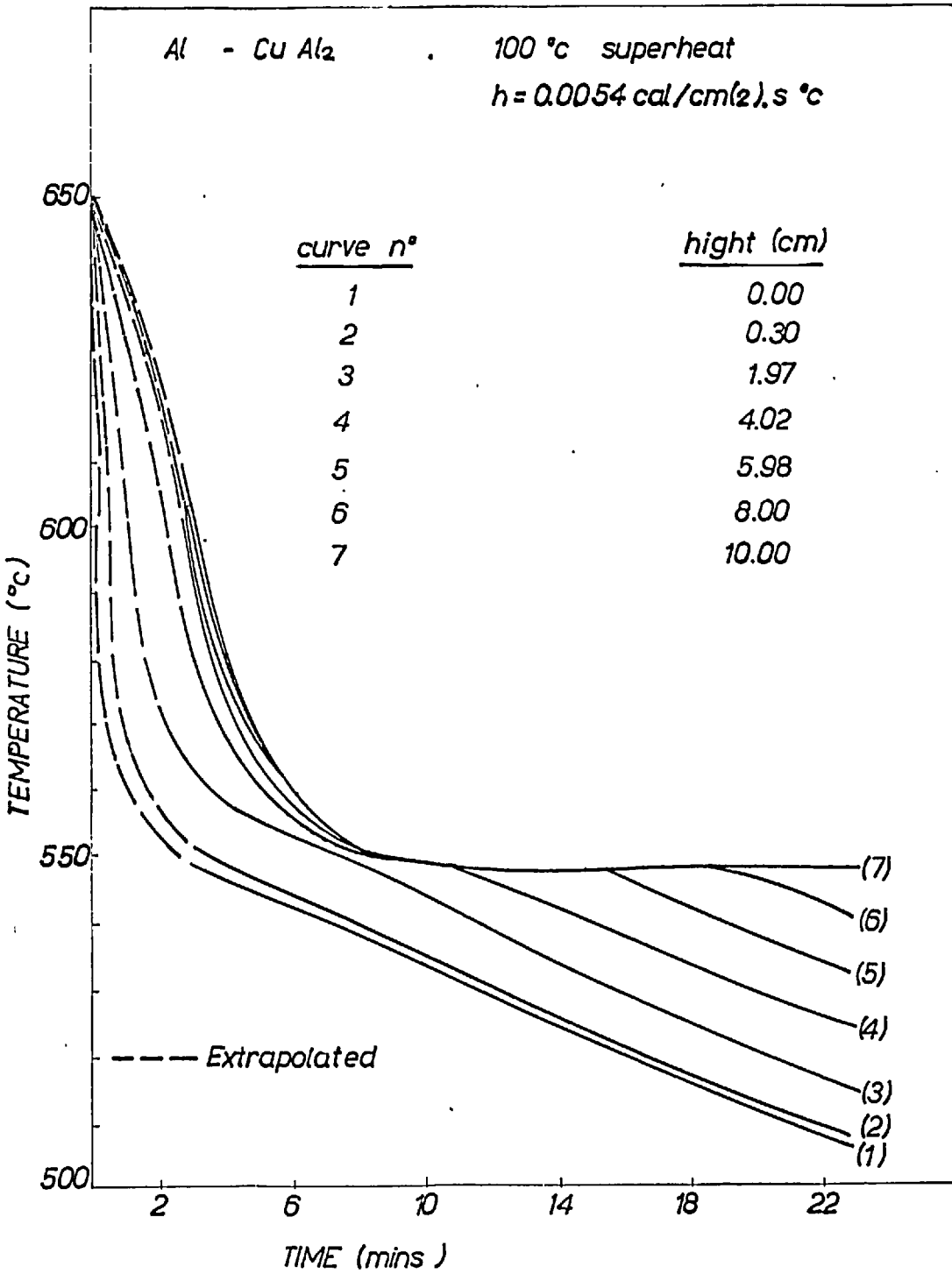

Fig 5.61 PREDICTED COOLING CURVES

CHAPTER 6

DISCUSSION

CHAPTER 6

DISCUSSION

6.1. Experimental Apparatus and Procedures

6.1.1 Unidirectional Heat Flow Conditions and Heat Losses

The design of the experimental apparatus ensured that most of the heat extracted from the ingot flowed in the vertical direction. By varying the thickness of the vermiculite, and replacing part of it with ceramic fibre some degree of matching could be achieved between the heat lost radially through the insulation and the sensible heat liberated by the heater and the walls of the crucible as they cooled down. It was possible to arrange that these two quantities of heat should equal one another in most experiments. For each new set of experiments in a different temperature range, the thicknesses of insulation were adjusted by trial and error until a satisfactory thermal balance was obtained in a trial experiment.

Heat losses from the top of the crucible were reduced by the syndanyo disc of the thermcouples support rig acting as a lid, a ceramic fibre blanket being placed above it.

For solidification experiments without super heat losses from the top had no effect on the solidifying metal as it was being cooled from the bottom of the crucible. When the experiment involved the removal of super heat, it became more difficult to keep the heat flow unidirectional and the solid liquid interface planar, especially at long experimental times and at the slower cooling rates. Even under these conditions, however, the heat balances showed that the magnitude of experimental inaccuracies was of the same order as inaccuracies in the theoretical solution.

6.1.2. The Crucibles

The use of stainless steel crucibles of low thermal mass minimised

the crucibles interferences with the unidirectional cooling processes. When cast stainless steel crucibles of heavier section were used, however, the heat capacity of the crucible had a significant influence on the experimental results, as shown in Table 5.8

Initially break outs were experienced with these crucibles, and it was difficult to strip the ingot without damaging the mould. Both those difficulties were overcome by application of the refractory coat. Several commercial washes were tried and 'Koron 510' a 'Foseco' product was found to be the most satisfactory.

As supplied, the bases of the thin walled crucibles were slightly dished inwards. In previous investigations (15,16) it has been found that after a crucible had been in use for some time, it's base would spring away from the solidifying metal in an uncontrolled fashion, causing an air gap to form.. Once this had occurred, the crucibles were rejected. With the higher temperatures used in this work, however, the base would start to spring away immediately and it was therefore necessary to preheat each crucible.To avoid the formation of an air gap, the crucibles were annealed for 8 hours at 850°C. Frequently, during the annealing process, the bottom would spring out of its own accord, reversing the direction of dishing. If this has not occurred, the crucible was subsequently beaten out by hand.

6.1.3 Thermocouples and Temperature Measurements

The thermocouple beads were bonded to their sheaths thus, ensuring a good response. Bending the ends of the thermocouples through 90° so that the final 15 mm of their length lay along the horizontal isotherms removed any errors due to conduction .

The accuracy with which the thermocouples were portioned was $\pm$ 1 mm

their relative positions being measured with a travelling microscope prior to insertion into the crucible.

By injecting a biasing e.m.f. temperature readings corresponding to 20 m.v. or more were recorded on the 1 - 10 m.v. or 1 - 20 m.v. scales of the recorder, thus increasing the sensitivity of the recording.

6.1.4. The Cooling System

The heat transfer coefficients and the cooling conditions were controlled by adjusting the flow rate of air through the nozzle. With the exceptions stated below the supply of air was sufficient for the cooling rates required in the experiments.

Difficultues were experienced in controlling the flow rate of water to the atomising system so that in turn it was difficult to reproduce any given set of cooling conditions when this system was used. Thus, a larger number of runs had to be carried out and the results for any particular experimental variable were much more scattered than when air was used as the sole cooling medium. Unfortunately, attempts to control the heat transfer coefficient produced with the atomising system, by controlling the height of the water head were not successful. Since the cooling rates were limited by the supply of air when using air only, there was a limit to the length of eutectic ingot that could be produced at any given constant growth rate.

6.2 Heat Transfer Coefficient - Nature and Accuracy

The transfer of heat during the solidification experiments involved its conduction and radiation from the cooled surface of the ingot to the inner surface of the crucible base, its subsequent conduction through the crucible base and its transfer by convection and radiation to the cooling air.

If the thermal resistance to these three steps are R_c, R_m, and $\frac{1}{ha}$ respectively then:

$$\frac{1}{h} = \frac{1}{ha} + R_c + R_m$$

h = overall heat transfer coefficient

ha = heat transfer coefficient from the outer surface of the mould to the cooling air.

In a steady state experiment in which the overall heat transfer coefficient was found to be 0.0068 cal/cm(2) S.°C, the temperatures of the ingots cooled surface, of the cooling air and of the outside surface of the mould were respecitvely

$$\theta_o = 590^oC; \quad \theta_a = 40^oC; \quad \theta_b = 578^oC$$

Thus:

$$\frac{\theta_o - \theta_a}{1/h} = \frac{\theta_o - \theta_b}{R_c + R_m}$$

and

$$R_c + R_m = 3.2 \ (Cal/cm.(2).S.^oC)^{-1}$$

The value of R_m for a stainless steel crucible with a wall thickness of 1 mm is approximately 0.5 $(cal/cm.(2).S.^oC)^{-1}$.

rising to 2.5 $(cal/cm(2).S.^oC)^{-1}$ when the moulds wall is 5 mm thick. These values correspond respectively to $\frac{1}{3}$% and $1\frac{2}{3}$% of the total thermal resistance between the ingot surface and the cooling air. i.e. the value of the contact resistance R_c is about 2% of the total resistance for

the thin crucible and 3% for the cast crucibles (at 800°C).

The radiative contribution h_r and the convective contribution h_c make up the heat transferred from the outer surface of the mould, the former being sensitive to temperature variations.

i.e. $h_a = h_r + h_c$

and $h_r = \sigma\varepsilon(\theta_b + \theta_a)(\theta^2_b + \theta^2_a)$

where σ = Emmissivity of stainless steel

ε = Stephan-Boltzman constant

and θ_a and θ_b are measured on Kelvins scale.

If ϑ_b varies in the range $500^oC < \theta_b < 700^oC$, the radiative contribution will vary from 9% to 16% of the total heat transfer coefficient between the base and the cooling air. Thus the magnitude of the errors produced in the theoretical predictions by using a constant overall heat transfer coefficient value determined in the steady state experiment is relatively small. Certainly the use of a value that corresponds to the cooled surface mid way through the experiment produces sufficient accuracy.

An identical conclusion was reached in a previous investigation (15) in which, in addition the nozzle was tested in a series of analagous mass transfer experiments to ensure uniform distribution of the heat transfer coefficient over the base of the crucible.

6.3 Comparison between experimental results and the predictions of the Integral Profile Method.

6.3.1 The Solidification of Pure Metals and Eutectic Alloys

Predictions made using the integral profile method have already been compared with experiments for the solidification of pure metals or metals of eutectic composition (15,16). These experiments were conducted using lead, tin and lead tin eutectic and good agreement between experiments and theory was achieved. However, these alloys have low melting points low thermal conductivities and low latent heats of solidification and are of little industrial importance.

Thus it was decided to carry out further work at higher temperatures and on alloy systems closer to those of industrial importance.

6.3.1.1 Aluminium

The experiments involving solidification of pure aluminium (99.99%) indicate complete agreement with the theoretical predictions. Thermal balances show a maximum of $\pm$ 5% deviations (Tables 5.3 and 5.4).

6.3.1.2 Aluminium - $CuAL_2$ Eutectic.

This eutectice at 33% copper is formed between the solid solution of copper in aluminium and the intermetallic compound $CuAL_2$. No differences could be found between the theoretical and experimental results. The predominance of unidirectional heat flow is clearly demonstrated in the photomicrograph of plate (9) and in the neat balances (Tables 5.5 and 5.6).

6.3.1.3 Aluminium-Silicon-eutectic

This eutectic is discussed in details in the section dealing with the controlled growth experiments. The experimental results were found to agree well with the theory (to $\pm$ 5%). The micrographs (plate 15) and the thermal balances (table 5.7) show that unidirectional heat flow conditions were adequately maintained.

6.3.1.4 Iron-Phosphorus-Carbon eutectic

This alloy was investigated in order to gain experience with unidirectional heat flow experiments at high temperatures. Without such experiments it will not be possible to work at the even higher temperatures necessary to investigate the solidification of steels or commercial cast irons under unidirectional heat flow conditions in existing experiments system.

As a result of the modification to the casting and melting unit in the work with this eutectic, the thermal capacities of the crucible and the heating furnace were much higher than in the lead and aluminium experiment. Since the theory cannot allow for the heat released by the mould and the furnace on cooling, large differences were found between the experimental and predicted result. However, as shown in the thermal balances (Table 5.8), the differences can be accounted for.

6.3.2 Predicted temperature profiles

The polynomials describing the temperature distribution in the metal in both solid and thermal layers were incorporated in the computer programme which predicted the progress of solidification of pure metals

and eutectics. Temperatures were calculated at various heights above the base (appendix 7, tables A7.11 - A7.13) and were compared with thermocouple readings (Fig. 5.60 and 5.61). Since the quadratic polynomials described the temperature distribution approximately, some disagreement between theory and experiments was to be expected. However, the effects of these errors on the accuracy of the integral profile solution were small, since the approximate functions were further integrated and the integral was more accurate than the function.

6.4 The Solidification of Alloys that Freeze over a Range of Temperatures

A theory was developed in Chapter 3 to predict solidification rates of alloys that freeze over a range of temperatures. The solutions are approximate and form an extension to the generalised integral profile solution given in Chapter 2.

The aluminium - copper, a system of some technological importance, was used to check the validity of the theory.

Three alloys in this system were investigated. 4% cu alloy, its solute content is less than the solubility limit of copper in aluminium. 8% cu, an intermediate composition and 30% cu near eutectic composition; in order to examine the various assumptions of the theory under extreme conditions.

6.4.1 The Theoretical Assumptions

6.4.1.1 No undercooling

It is assumed that solidification starts at the equilibrium liquidus temperature of the alloy and that the alloy is completely solidified when its temperature falls below that of the eutectic in the binary system involved. It is obvious from the variations of the cooled surface temperautre that kinetic effects causing undercooling were absent even in those experiments involving the higher cooling rates. Any undercooling associated with delayed nucleation must therefore be of such a small magnitude that it was not detected by the thermocouple (i.e. $\pm$ 2 - 3^{o}C).

The arrests associated with the start of freezing at the liquidus

and the start of eutectic transformation at the solidus were observed by the thermocouples not immediately touching the cooled surface. The thermocouples at the cooled surface showed only a slight arrest but noticeable changes in the rate of cooling and in the curvature at those points were detected. All these arrests occurred at the same temperature for any one alloy, the temperature being independent of the cooling rate.

6.4.1.2 Complete Mixing in the Liquid and No Diffusion in the Solid

Segregation studies (7,8) have shown that it is valid to assume that no large composition gradients exist in the liquid across distances of the order of the dendritic arm spacing.

Diffusion takes place in the solid, however, and the assumption that it does not must produce some error. This error being mainly important in predicting the fraction of the liquid that solidifies as eutectic. The extent of diffusion is determined by a parameter (7) proprtional to the diffusion coefficient and to the 'local solidification time' and inversely proportional to the square of the half dendritic arm spacing. The dendritic arm spacing varies approximately with the square root of the solidification time, so that this parameter does not vary very much with solidification rate. For slow cooling rates and for large freezing ranges, Fleming et. al. (2) have shown that for an AL-4.5%cu alloy, the volume of eutectic liquid calculated by ignoring solid state diffusion vaires by no more than 2% from that calculated assuming diffusion to occur. Thus, little error will be produced in the theoretical predictions by assuming that diffusion does not occur in the solid.

6.4.1.3 Absence of bulk mass flow

Convective motion of liquid, gravitational feeding of shrinkage,

and the sinking or floating of solid dendrits are not exspected to take place.

The experiments were conducted with an unstirred liquid. Natural convection current could not develop because the liquid was cooled from below and because it was the denser metal that was rejected during solidification. Diffusion in the liquid could not produce any macro-segregation within the crucible so that the liquidus temperature would remain constant during an experiment, as has been reported.

6.4.1.4 The relation between the solid fraction and the temperature

Thermal effects in the partial layer are determined by the relationship between the temperatures at any point and the fraction of solid metal there. In previous solutions, a linear relationship was assumed between solid fraction and temperature (16), introducing errors which are particularly significant when the freezing range of the alloy is large (Fig. 6.1).

In the current treatment, Scheil's equation for classical non eqilibrium solidification is used i.e.

$$F_S = 1 \left(\frac{\vartheta_F - \Theta}{\vartheta_F - \vartheta_L} \right) \frac{1}{k-1}$$

This equation describes the variations of the solid fraction with temperatures for systems in which the liquidus and solidus lines on the phase diagram are straight. In addition it does not account for diffusion after solidification and it assumes complete mixing in the liquid, and absence of convective currents.

6.4.2 Experimental Results

The three compositions studied and reported were 4% cu, 8% cu, and 30% cu.

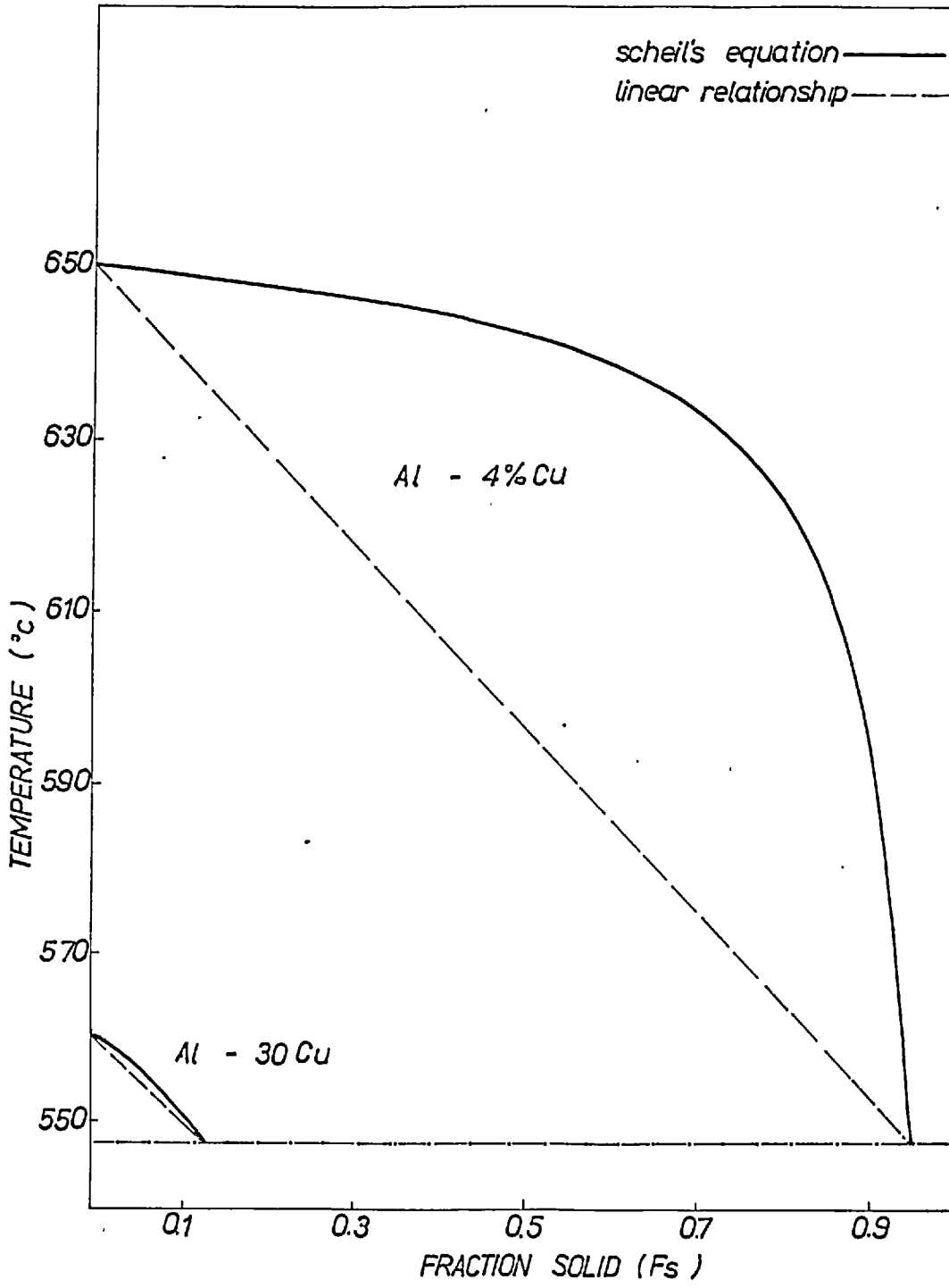

Fig 6.1 VARIATION OF FRACTION SOLID. SCHEIL'S EQUATION COMPARED WITH LINEAR RELATIONSHIP.

6.4.2.1 The solidification of Al - 4% cu alloy

The liquidus temperature was observed at 650°C and the solidus at 548°C. Since this alloy is below the maximum solubility limit (at 5.6% cu), solidification as indicated by the equilibrium diagram should be complete at about 580°C. Although, in certain runs a slight change in gradient of the cooling curve was obsérved at about 600°C there was always some solidification taking place at 548°C, the eutectice temperature. This was consistant with Scheil's equation which predicts that the fraction to solidify as eutectic in this alloy will be 0.05.

Structures of vertical sections which lie in the heat flow direction taken at various heights from ingots cooled at various rates, can be seen in plates 3, 4, and 5. Plate 3, represents a macrostructural photo.showing clearly the directionality associated with the cooling process. A plate like dendritic morphology is revealed by the segregation of impurities in the interdendritic regions.

Plates 4 and 5 show that the amount of eutectic is only slightly dependent on the rate of cooling and is about 5%. as predicted by Scheil's equation. An accurate determination of this fraction is difficult, however, as it is not possible to quench speciments from the eutectic temperature for metallographic examinations. The computed results agree well with measured values over a wide range of cooling rates for both rate of solidification and surface temperature variations.

The only discernable difference is that the solidus moves initially more slowly than predicted by the theory. The thermal balances show deviations that are never more than 8%.

6.4.2.2 The solidification of Al - 8% cu alloy

This alloy represents a composition and freezing rate that was

intermediate amongst the aluminium copper alloys studied. Its' composition was between that of the eutectic and the maximum solid solubility of copper in aluminium so that the eutectic temperature (548°C) corresponded to the equilibrium solidus temperautre. The liquidus was observed at 635°C. The volume fraction of the liquid solidifying with eutectic composition is given by Scheil's equation as 16% which agrees favourably with the structure shown in Plate 6. The rates of solidification and surface temperature variations obtained experimentally, agree with the theory almost completely and the deviations in the thermal balances are of the order of 5%.

6.4.2.3 The solidification of Al - 30% cu alloy

The results obtained with this alloy further confirmed that the agreement obtained between theoretical and experimental results improved as the eutectic composition was approached. The temperature difference between the solidus and liquidus is 12°C (548°C and 560°C respectively). Scheil's equation indicates that the fraction solidifying as eutectic is 87% and this appears to be confirmed by the photomicrograph shown in Plates 7 and 8.

6.5 The Solidification of Eutectics at Constant Growth Rates

6.5.1 Control of growth rates

Eutectics alloys were solidified at constant growth rates in the apparatus discussed above, the growth rate being controlled as described in Chapter 4.

Figs. 5.56, 5.57, 5.58 and 5.59 show that this method of control was adequate, the growth rates achieved in practice agreeing almost precisely with the planned growth rates.

The range of growth rates was restricted by themaximum rate at which cooling air could be supplied. Since it was desired to grow eutectic ingots of at least 100 mm in height, the growth rates used did not exceed 1 cm/min. In addition since the experiments were performed with no superheat, it was necessary to keep the total time involved as short as possible in order to avoid radial and top heat losses becoming predominant. This imposed a lower limit on the growth rates that could be used of $\frac{1}{3}$ cm/min., thus leaving only a narrow range of rates to be employed.

6.5.2 An excact solution for the required variations in heat tranfer coefficient

The experimental runs were controlled using heat transfer coefficient variations predicted by the equations derived in Section 3.3. These equations having been derived using the integral profile methods. After the experimental work had been completed however, it was discovered that an exact solution derived by Stefan could be modified to make the necessary predictions.

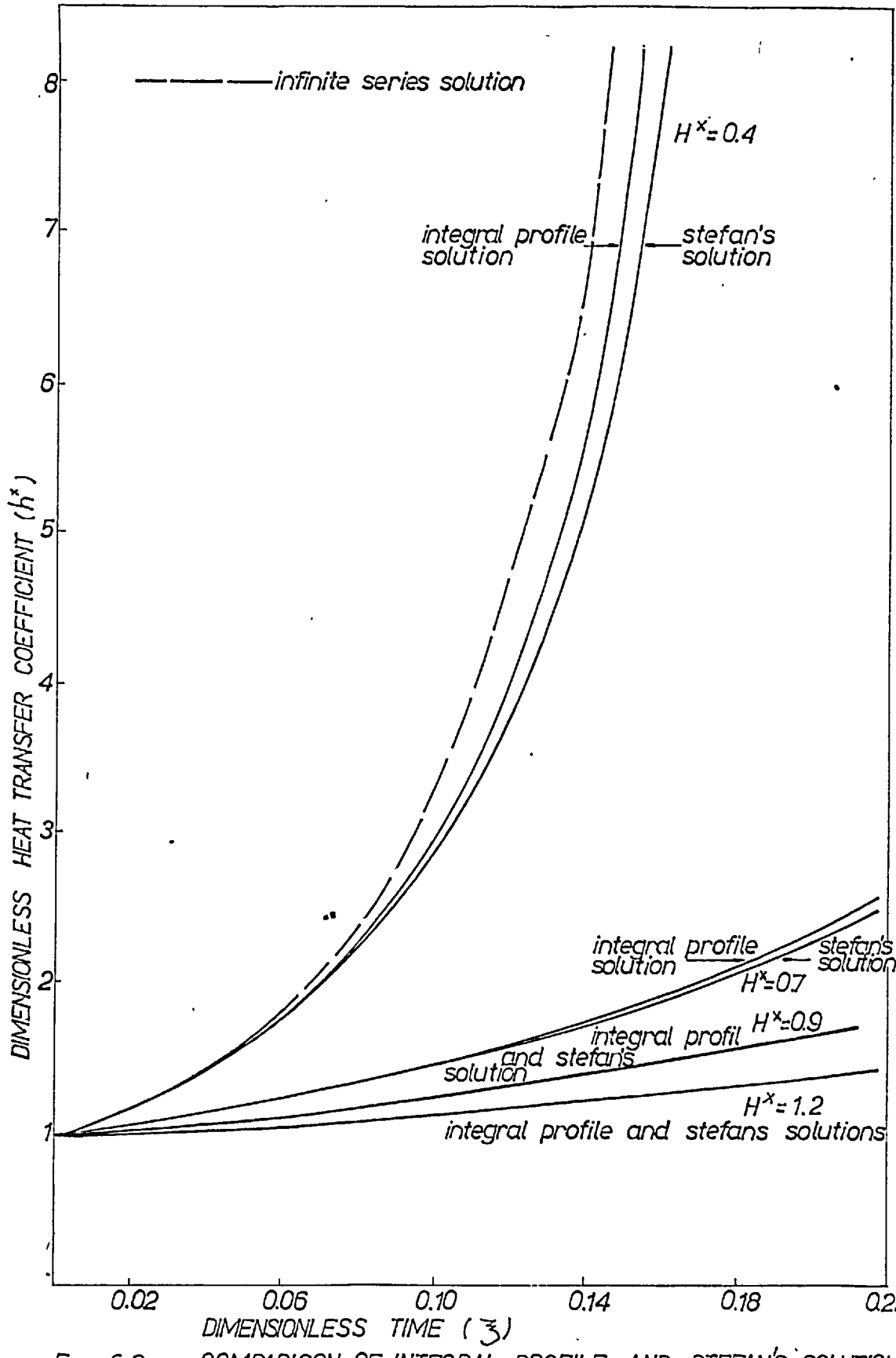

Fig 6.2 COMPARISON OF INTEGRAL PROFILE AND STEFAN'S SOLUTIONS: h^x Vs τ FOR VARIOUS H^x VALUES

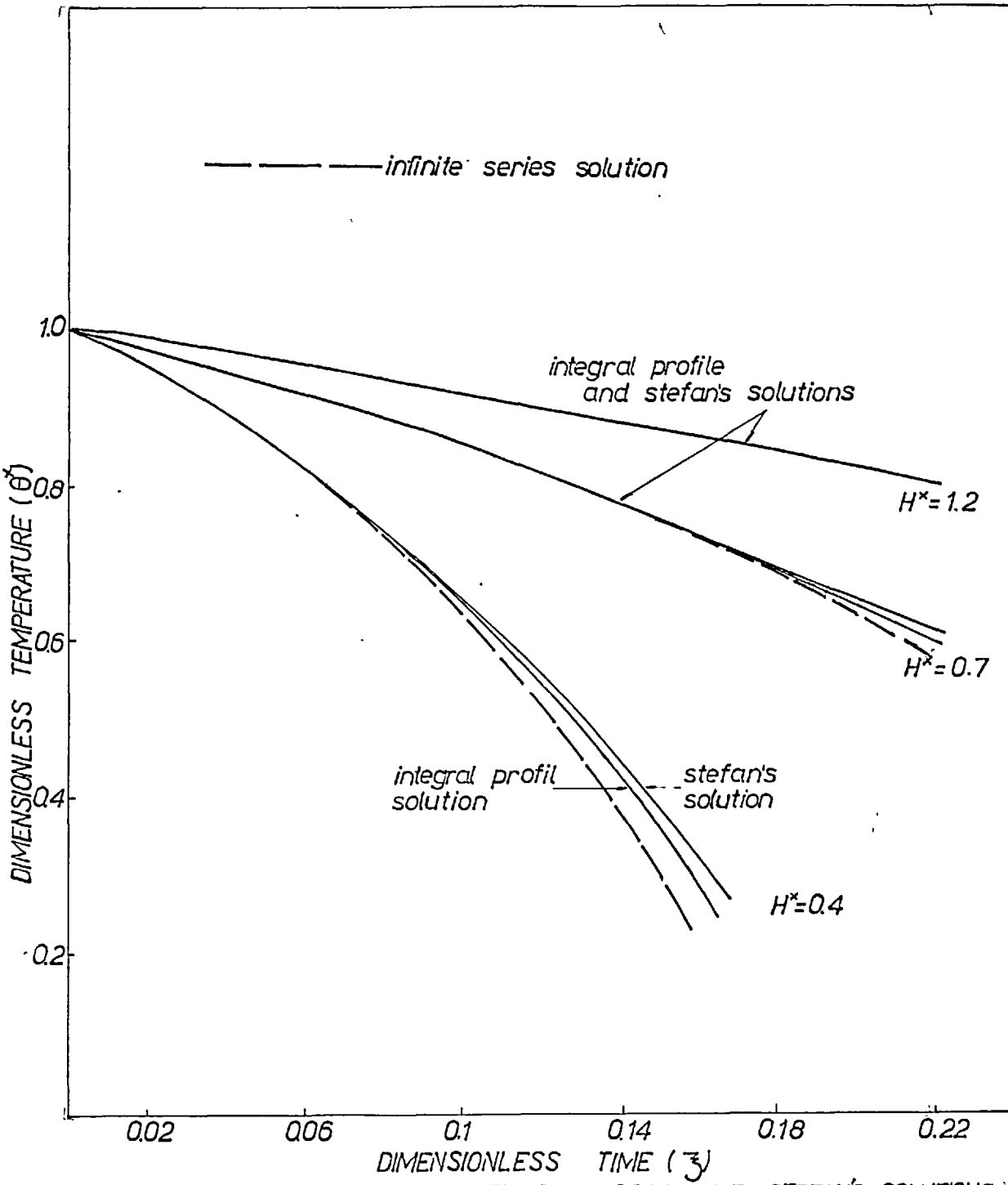

Fig 6.3 COMPARISON OF INTEGRAL FROFILE AND STEFAN'S SOLUTIONS θ^x Vs τ FOR VARIOUS H^x

Stefan showed that the temperature variation in a solid growing from its liquid at a constant rate was given by:

$$\theta = \theta_s - \frac{H}{C_s}\left\{e^{(\alpha m^2 t + mx)} - 1\right\} \qquad (6.5.1)$$

where $\alpha = \frac{K_s}{P_s C_s}$: and $m = \frac{V}{\alpha}$: $v = \frac{dt_s}{dT}$

This equation can be differentiated at x = 0 and written in terms of the variables used in this work to give

$$h^* = \frac{e^{(\xi/H^{*2})}}{1-H^*\left\{e^{(\xi/H^{*2})}-1\right\}} \qquad (6.5.2)$$

In terms of the same variables, equation 6.5.1 also gives

$$\theta^*_o = 1 - H^*\left[e^{(\xi/H^{*2})} - 1\right] \qquad (6.5.3)$$

These two equations are compared with the prediction of the integral profile equations in Figs. 6.2 and 6.3. It can be seen that the two sets of curves agree very closely.

Obviously the exact solutions is easier to use than the integral profile solution. However, since the two sets of vurves agree so precisely, especially in the range $0 < \xi < 0.1$, in which the experiments were carried out, there was no point in repeating the experiments using the values of h* given by the exact solution.

Figs. 6.2 and 6.3 serve to show how closely the integral profile solution can agree with an exact solution.

6.5.3 The experimental results

6.5.3.1 Lead tin eutectic

This eutectic was solidified under conditions of zero superheat and at growth rates varying from 0.25 cm/min to 0.6 cm./min.

This narrow rangeof growth rates did not produce wide structural differences. It can be seen from the photomicrographs that the thickness of the eutectic plates varies with the cooling rates, and the spacing between them changes. This phenomena can be used to explain the mechanical properties, which show a tendency to rise as the growth rate increases. A tendency was also observed for some plates to assume a wave form (plate 14). This comes about when the solidification front encounters impurities (18), causing it to deviate from a plane shape (20).

The transition from plates to rods due to the formation of a curved solid-liquid interface (19) was not observed at the growth rates used in the work reported here.

6.5.3.2 Aluminium - $CUAL_2$ eutectic

The solidification rates with which this eutectic was solidified were 0.33 cm/min, 0.50 cm/min and 0.66 cm/min. From the typical microstructure shown in plates 10 and 11 the eutectic seems to consist of parallel plates or lamellaes. The wider phase is aluminium rich solid solution and the darker plates are the CUAL2 compound.

Different growth rates did not produce differences in the spacing between the lamellaes, or in their width. This is to be expected since a very narrow range of growth was involved in the experiment. In plates 10(a) and 11(a) the mismatched regions can be clearly seen. Similar regions, and the lamellar faults associated with them, have been observed by other workers (34). They have been attributed to the nucleation and growth of an extra plate of one of the phases which in turn causes the automatic growth of a plate of the other phase. This growth being analgous to the growth of edge dislocations.

Banding and a tendency to colony formation are also exhibited by the microstructure. Plate 9, which represents samples solidified unidirectionally, but not at constant growth rates, is an example of these faults. Since no efforts were made to control the impurity content in the alloys investigated, such impurities may precipitate in the metal and nucleat the eutectic phases to produce the faulty structures. Kraft and Albright (34) have concluded in their work on this eutectic that a large ratio between the thermal gradient in the liquid and the growth rate is required in order to create conditions for parallel growth of the two phases. Since in this work a good degree of parallel growth was achieved without maintaing thermal gradients in the liquid, it must be concluded that the thermal conditions, growth rates and impurity level play a more important role together than they do on their own. The increase in mechanical properties with growth rates is probably due more to the different way in which the impurities precipitated at the different growth rates than to the growth rates directly.

6.5.3.3. Aluminium-silicon eutectics

The equilibrium diagram of the aluminium - silicon system is given in Fig. 5.2. Taken from Hansen (2), it gives the composition formally taken as the eutectic at 11.7% si together with a more recent finding at 12.5%si. The alloy used in this work contained 12.7% si. and exhibited a thermal arrest at 577°C. Identical composition and temperatures were recently reported for this eutectic (37). Since this system is similar in the temperatures involved, and hence in heat transfer coefficients that could be achieved, to the AL-cuAL$_2$ system, only the same narrow range of growth rates could be achieved. i.e. $\frac{1}{3}$ - $\frac{3}{5}$ cm/min. The principle

difference between this eutectic and the previous one is that the Al-si eutectic is a typical example of discontinuous microstructure. The Al phase is the continuous matrix and the silicon phase is imbedded in it. Typical microstructures of samples solidified at the various growth rates are given in plates 16 and 17. As in the case of pb-sn and Al-cuAL_2 eutectic systems, the Al-si eutectics' tensile test results show a clear tendency to higher strength with higher growth rates. Similarly, the tensile test bars with axis machinedin the heat flow direction give higher U.T.S. values than the bars whose axis lay normal to the heat flow. The actual level of tensile strength is intermediate between the reported average values for ordinary commercial chill castings and sodium modified chill castings (38). This indicated that the definite improvement in properties can be attributed to the controlled growth.

The directionality of the silicon phase can be seen in the photomicrographs, although some radial growth has taken place. Similar structures were explained before (39) as resulting from the critical value for the ratio between the thermal gradient and the growth rate. The critical value is given as 10^7 $^{o}C.sec./cm^2$. Below this value, the plannar aluminium front is supposed to break down and the silicon is to occur as close packed rods. On the other had tests on very high purity Al-si eutectics (40) have shown that the natural form of the silicon phase should be continuous rods when solidified at slow growth rates. The discontinuity occurs as a result of the impurities causing constitutional undercooling, and hence preferential growth of the aluminium phase. In the work presented here, sufficient data is not available to prove or disprove those hypothesis.

6.5.3.4 Fe-C-p eutectic

Smithells (33) shows the isothermal section of the ternary phase diagram of the iron carbon phosphorous system, taken from the International Critical Tables and presented here in Fig. 5.3. The constituents of the eutectic are Fe_3C, Fe_3p and austenite. The austenite has on subsequent cooling from the eutectic temperature, transformed to pearlite whose presence in the microphotographs (plates 18, 19, 20, 21) reveals the shape and position of the pre-transformation austenite. The directionality is clearly revealed by the structure as is also a slight tendency towards finer structure formation with the higher rates of cooling. As this is a complex eutectic, and a discontinuous one which undergoes a further solid state transformation, it is not possible to impose nucleation and growth conditions by the control of growth rates, thus it is not possible to produce a structure in which the phases will align in a parallel continuous manner in the direction of the heat flow.

The few mechanical properties values obtained are in the same range as those quoted for high phosphorous commercial cast irons.

CHAPTER 7

CONCLUSIONS

CHAPTER 7

CONCLUSIONS

The following conclusions can be drawn from the work described in the preceding chapters.

1) Unidirectional heat flow conditions were achieved. The magnitude of radial heat flow estimated from the thermal balances was small and of the same order as the errors introduced by the theory.

2) The integral profile solution satisfactorily predicts the rates of solidification of pure metals and eutectic alloys with and without superheat, at temperatures up to 1000°C. It also predicts satifactorily the variations in surface temperature of the solidified ingots.

3) Temperature profiles in the ingot at any time, and variations of temperatures at any point inside the ingot throughout the process, were predicted by the theory and found to deviate from measured values by no more than 8%.

4) Good agreement was shown to exist between the theory and experiments in the work on the solidification of binary alloys, over the range of temperatures and compositions studied. The theory using Scheils' equation to develop an effective enthalpy together with the integral profile approach has proved to be valid.

5) It has been shown that the rate of growth of eutectic alloys can be kept constant by controlling the cooling conditions at the cooled surface, although the magnitude of growth rates and the lengths of the ingots produced were limited.

6) It is suggested that further investigation should be undertaken to apply the theory to the solidification of steels and to grow eutectics at higher growth rates using higher heat transfer coefficient values.

APPENDICES

APPENDIX I

The limiting form of $\frac{dt^*_p}{d\xi}$ as t^*_p tends to zero

From equation (3.1.5.11)

$$\lim_{t^*_p \to o}\left|\frac{d\theta^*_o}{d\xi}\right| = \frac{-q^*_L}{K^*_L} \lim_{t^*_p \to o}\left|\frac{dt^*_p}{d\xi}\right| \qquad \text{(AI-1)}$$

rearranging equation (3.1.5.9)

$$\frac{d\theta^*_o}{d\xi} = \frac{2(E^*_L - E^*_o + \frac{q^*_L}{\alpha^*_L} t^*_p + \frac{1}{2}\frac{t^{*2}_p}{\alpha^*_L} g'_t)\frac{dt^*_p}{d\xi} - 6(q^*_o - q^*_L) + \frac{t^{*2}_p}{\alpha^*_L} g'_\xi}{2\, t^*_p \gamma^*_L} \qquad \text{(AI-2)}$$

This equation is indeterminant at $t^*_p = 0$ ($E^*_L = E^*_o$: $q^*_o = q^*_L$)

Applying L'hospital rule

$$\lim_{t^*_p \to o}\left|\frac{d\theta^*_o}{d\xi}\right| = \frac{4\frac{q^*_L}{\alpha^*_L}\left(\lim_{t^*_p \to o}\left|\frac{dt^*_p}{d\xi}\right|\right)^2 - 6\left(f'_\theta \lim_{t^*_p}\left|\frac{d\theta^*_o}{d\xi}\right| + f'_\xi - g'_t \lim_{t^*_p}\left|\frac{dt^*_p}{d\xi}\right| - g'_\xi\right)}{2\gamma^*_L \lim_{t^*_p \to o}\left|\frac{dt^*_p}{d\xi}\right|} \qquad \text{(AI-3)}$$

Using equation (AI-1) to eliminate $\frac{d\theta^*_o}{d\xi}$ from equation (AI-8) and rearranging

$$\lim_{t^*_p \to o}\left|\frac{dt^*_p}{d\xi}\right| = \frac{-(f'_\theta + g'_t \frac{k^*_L}{q^*_L}) \pm \sqrt{(f'_\theta + g'_t \frac{k^*_L}{q^*_L})^2 + 4\gamma^*_L K^*_L \frac{(f'_\xi - g'_\xi)}{q^*_L}}}{2\gamma^*_L} \qquad \text{(AI-4)}$$

Taking the positive root and rearranging

$$\lim_{t^*_p \to o}\left|\frac{dt^*_p}{d\xi}\right| = \frac{2K^*_L(f'_\xi - g'_\xi)}{(q^*_L f'_\theta + K^*_L g'_t) + \sqrt{(q^*_L f'_\theta + g'_t K^*_L)^2 + 4q^*_L \gamma^*_L K^*_L (f'_\xi - g'_\xi)}} \qquad \text{(AI-5)}$$

The two equations, (AI-1) and (AI-5) are two simultaneous equations for the start of the numerical integrations in Mode 1 and Mode 2.

APPENDIX 2

Analytical integration to determine the duration of 1S and 2S

Under Newtonian cooling conditions equation (3.1.5.4) becomes

$$\frac{d\theta^*_o}{d\xi} = - \frac{3\theta^{*3}_o}{2\gamma^*_L K^*_L (\theta^{*2}_m - \theta^{*2}_o)} \qquad (A2\text{-}1)$$

The time elapsing from the start of cooling to the start of mode 1 is:

$$\xi_{1S \to 1} = \int_{\theta^*o=\theta^*m}^{\theta^*o=\theta^*_L} - \frac{2\gamma^*_L K^*_L (\theta^{*2}_m - \theta^{*2}_o)\, d\theta^*_o}{3\theta^{*3}_o} \qquad (A2\text{-}2)$$

hence:

$$\xi_{1S \to 1} = \frac{\gamma^*_L K^*_L}{3} \left\{ \left(\frac{\theta^*_m}{\theta^*_L} \right)^2 - 1 - 2 \ln \left(\frac{\theta^*_m}{\theta^*_L} \right) \right\} \qquad (A2\text{-}3)$$

The thickness of the thermal layer at that time is:

$$t^*_L = \frac{2K^*_L (\theta^*_m - \theta^*_L)}{\theta^*_L} \qquad (A2\text{-}4)$$

If mode 1S is to be followed by mode 2S rather than by mode 1, the temperature of the cooled surface when the change over occurs is from equation (A2-4):

$$\theta^*_{o=} \frac{\theta^*_m}{1 + \frac{D^*}{2K^*_L}} \qquad (A2\text{-}5)$$

Using this temperature as the upper limit of integration in equation (A2-2) yields:

$$\xi_{1S \to 2S} = \frac{\gamma^*_L K^*_L}{3} \left\{ \left(1 + \frac{D^*}{2K^*_L}\right)^2 - 1 - 2 \ln \left(1 + \frac{D^*}{2K^*_L}\right) \right\} \qquad (A2\text{-}6)$$

Mode 2S persists until the temperature of the cooled surface drops to the liquidus temperature. Hence using the liquidus temperature as the

upper limit in the integral, we get:

$$\bar{\xi}_{2S\rightarrow 2} = \frac{\gamma^*_L D^*}{3K^*_L}\,(3K^*_L + D^*)\left[\ln\left(\frac{\phi^*_m}{1+\frac{D^*}{2K^*_L}}\right) - \ln\theta^*_L\right] \qquad \text{(A2-7)}$$

and the thickness of thermal layer at the end of mode 2S is

$$t^*_L \geq D^* \qquad \text{(A2-8)}$$

APPENDIX 3

The partial differentials of the heat flux into the partial layer

Since q^*_L, the heat flux into the partial layer is a function of partial layer thickness or of time or of both, we have:

$$q^*_L = g(t^*_p : \xi) \qquad \text{(A3-1)}$$

and:

$$\frac{dq^*_L}{d\xi} = \frac{\partial q^*_L}{\partial t^*_p}\ \frac{dt^*_p}{d\xi} + \frac{\partial q^*_L}{\partial \xi} = g'_t\ \frac{dt^*_p}{d\xi} + g'_\xi \qquad \text{(A3-2)}$$

Differentiating equation (3.1.3.6) and substituting for $\frac{dt^*_t}{d\xi}$ from equation (3.1.5.13):

$$\frac{dq^*_L}{d\xi} = -\frac{3q^*_L}{t^*_L}\left[\frac{q^*_L}{\gamma^*_L(\theta^*_m - \vartheta^*_L)} - \left(\frac{dt^*_s}{d\xi} + \frac{dt^*_p}{d\xi}\right)\right] \qquad \text{(A3-3)}$$

Comparing coefficients between equations (A3-2) and (A3-3):

$$g'_t = \frac{3q^*_L}{t^*_L} \qquad \text{(A3-4)}$$

and

$$g'_\xi = g'_t\left\{\frac{dt^*_s}{d\xi} - \frac{q^*_L}{\gamma^*_L(\theta^*_m - \vartheta^*_L)}\right\} \qquad \text{(A3-5)}$$

Equations (A3-4) and (A3-5) are to be used in mode 1 and in mode 3.

For the relevant partial differentials to be used in mode 2 and in mode 4, equation (3-1-3-6) is differentiated and substitution is made for $\frac{d\vartheta^*_a}{d\xi}$ from equation (3-1-5-17) to give:

$$\frac{dq^*_L}{d\xi} = \frac{2q^*_L}{D^* - t^*_s - t^*_p}\left(\frac{dt^*_s}{d\xi} - \frac{dt^*_p}{d\xi}\right) - \frac{3k^*_L q^*_L}{\gamma^*_L(D^* - t^*_s - t^*_p)^2} \qquad \text{(A3-6)}$$

comparing coefficients we get:

$$g'_t = \frac{2q^*_L}{D^* - t^*_s t^*_p} \qquad \text{(A3-7)}$$

and

$$g'_{\xi} = \frac{g' t}{2} \left(2 \frac{dt^*_s}{d\xi} - \frac{3K^*_L}{\gamma^*_L (D^* - t^*_s - t^*_p)} \right) \qquad \text{(A3-8)}.$$

APPENDIX 4

Some values of physical and thermal properties

The values of density, thermal conductivity, specific heat and latent heat used in the solution of the equations throughout this work are given in Table (A4-1) together with their source.

Some values were calculated. The calculations for specific heats values of a two phase alloy was done by summing up the specific heat values of the two parent phases in direct proportion to their weight fraction in the alloy.

An identical procedure was used for determining values of thermal conductivity except that the summation was done on a volume basis.

The latent heat value used for the ternary iron-carbon-phosphorous eutectic was determined calorimetrically as follows:

A drop of molten eutectic alloy, at its metling point was introduced into a water calorimeter. The following results were obtained.

Weight of calorimeter + stirrer (gm)	323	323	323
Water equivalent of the calorimeter	30	30	30
Weight of water (gm)	147	152	155
Weight of eutectic metal (gm)	18	28	30
Rise in temperature (^{o}C)	20	30	28
Drop in metal's temperature (^{o}C)	910	899	878
Total heat released (cal/g)	196	192	173
Sensible heat (cal/g)	136	134	112
Latent heat (cal/g)	60	58	61

The value of 60 cal/g was used in the calculation.

Alloy	State	Thermal conductivity cal/cm.S.°C	Specific heat cal/g.°C	Density g/cc	Latent heat cal/g.
AL	Solid liquid	0.505[14] 0.216	0.310[14] 0.282	2.71[14]	90[14]
Al-$CUAl_2$ eutectic	Solid liquid	0.566[4] 0.211	0.219[4] 0.228	3.520[4]	76.5[4]
Al-Si eutectic	Solid liquid	0.422[C] 0.211	0.222[C] 0.230	2.640[4]	110[4]
Fe-C-P eutectic	Solid liquid	0.070[5][C] 0.040	0.170[5][C] 0.150	7.24[5]	60[C]
Pb-Sn eutectic	Solid liquid	0.123[16]	0.052[16]	8.3[16]	8.8[16]
Al-4% Cu	Solid liquid	0.524[14] 0.218	0.268[14] 0.274	2.79[14]	88.9[14]
Al-8%Cu	Solid liquid	0.529[14][4][C] 0.220	0.261[14][4][C] 0.268	2.87[14][4]	86.4[14][4]
Al-30%Cu	Solid liquid	0.561[4][C] 0.236	0.224[4][C] 0.231	3.420[4]	78.2[4]

(C) = calculated

(5)(4)(14)(16) see reference

TABLE A4.1 PHYSICAL AND THERMAL PROPERTIES OF THE ALLOYS

APPENDIX 5

An infinite series solution to variations of heat transfer coefficient with time.

In section 3.3, the differential equations (3.3.6) and (3.3.7) were developed. Those equations are indeterminant at $\xi = 0$ when $t^*_s = 0$.

By expanding as a taylor's series and comparing coefficients, the following are obtained

$$h^* = 1 + \left(\frac{1}{H^*} + \frac{1}{H^{*2}}\right)\xi + \left(\frac{1}{H^{*2}} + \frac{3}{2H^{*3}} + \frac{1}{2H^{*4}}\right)\xi^2 + \left(\frac{1}{H^{*3}} + \frac{2}{H^{*4}} + \frac{4}{3H^{*5}} + \frac{5}{9H^{*6}}\right)\xi^3 + \left(\frac{1}{H^{*4}} + \frac{5}{2H^{*5}} + \frac{29}{12H^{*6}} + \frac{14}{9H^{*7}} + \frac{25}{27H^{*8}}\right)\xi^4 + \left(\frac{1}{H^{*5}} + \frac{3}{H^{*6}} + \frac{15}{4H^{*7}} + \frac{113}{36H^{*8}} + \frac{91}{36H^{*9}} + \frac{115}{21H^{*10}}\right)\xi^5 + \cdots\cdots \qquad (A5\text{-}1)$$

and

$$\theta^* = 1 - \frac{1}{H^*}\xi - \frac{1}{2H^{*3}}\xi^2 - \frac{1}{3H^{*5}}\xi^3 - \frac{5}{2H^{*7}}\xi^4 - \frac{20}{27H^{*9}}\xi^5 \qquad (A5\text{-}2)$$

Neglecting coefficients in ξ^6 and higher.

A comparison between these solutions and others are given in Figs. (6.2) and (6.3)

Difficulties associated with instability, prevented the use of those equations for the starting values in the numerical integration of equations (3.3.6) and (3.3.7) and limiting values have to be used.

The limiting values for the start of integration are determined as follows:

Applying L'hospital rule to equation (3.3.6) gives

$$\lim_{\xi \to 0} \left|\frac{d^*}{d\xi}^o\right| = -\frac{2H^*\theta^* (3H^* + t^*_s) \lim_{\xi \to 0}\left|\frac{dh^*}{d\xi}\right| + 2\theta^* h^* - 1}{H^* (7 + 2 t^*_s h^* + 6H^* h^*)} \qquad (A5\text{-}3)$$

Substituting from equation (A5-3) into equation (3.3.7)

$$\lim_{\xi \to 0} \left|\frac{dh^*}{d\xi}\right| = \frac{4 + h^*(3H^*+t^*_s - \theta^*)}{H^*\theta^*(3H^*+t^*_s)} \qquad \text{(A5-4)}$$

Those two equations are stable when used in the numerical integration at small values of time.

Numerical integration, once started can proceed to equation (3.3.6) for $\frac{d\theta^*}{d\xi}_o$. However, equation (3.3.7) for $\frac{dh^*}{d\xi}$ is unstable even when a successful starting procedure is adopted.

Integrating equations (3.3.6) and (3.3.7) and eliminating $\frac{d^2h}{d\xi^2}$ we get

$$\frac{dh^*}{d\xi} = -\frac{3H^*t^*_s \frac{d^2\theta^*}{d\xi^2} - (8+3h^*t^*_s + 6h^*H^*) - \frac{2\theta^*h^*}{H^*}}{(3t^*\theta^* + 6H^*\theta^*)} \qquad \text{(A5-5)}$$

Differentiating the infinite series (A5-2) twice and neglecting terms in ξ^4 and higher, yields:

$$\frac{d^2\theta^*_o}{d\xi^2} = -\left(\frac{1}{H^*3} + \frac{2t^*_s}{H^*4}\right) \qquad \text{(A5-6)}$$

Equation (A5-6) is substituted into equation (A5-5), which is stable when used in the numerical integration.

APPENDIX 6

SPECIMEN COMPUTED RESULTS

TABLE A6.1 SOLIDIFICATION OF ALUMINUM . . . . IN THE PRESENCE OF SUPERHEAT

KSI	TORMIN	T S STAR	T S CM	THETA STAR	THETA C	MOLTEN PARAM	T M CM	THETA D
0.001	0.1	0.0000	0.00	1.000	660.0	0.0414	3.07	690.0
0.003	0.5	0.0026	0.19	0.997	658.4	0.1197	8.89	690.0
0.004	0.7	0.0044	0.33	0.996	657.3	0.1413	10.49	690.0
0.005	0.7	0.0049	0.36	0.995	657.0	0.1460	10.85	690.0
0.005	0.7	0.0051	0.38	0.995	656.8	0.1483	11.02	690.0
0.005	0.7	0.0051	0.38	0.995	656.8	0.1485	11.03	690.0
THERMAL LAYER HAS REACHED BOUNDARY OF LIQUID REGION								
0.015	2.3	0.0210	1.56	0.980	647.4	1.0265	9.84	676.4
0.025	3.8	0.0381	2.83	0.964	637.9	1.0121	8.57	667.5
0.035	5.3	0.0557	4.14	0.949	628.7	1.0041	7.26	662.5
0.045	6.9	0.0734	5.45	0.935	619.9	1.0008	5.95	660.5
0.055	8.4	0.0908	6.74	0.922	611.8	1.0001	4.66	660.0
0.065	9.9	0.1077	7.99	0.910	604.3	1.0000	3.41	660.0
0.075	11.4	0.1240	9.21	0.899	597.3	1.0000	2.19	660.0
0.085	13.0	0.1400	10.40	0.888	590.7	1.0000	1.00	660.0
0.090	13.7	0.1478	10.98	0.883	587.6	1.0000	0.42	660.0
0.092	14.1	0.1517	11.27	0.881	586.1	1.0000	0.13	660.0

DATA

	SOLID	MOLTEN	UNITS
WEIGHT THERMAL CAPACITY	0.310	0.282	CAL/G.DEG-C
THERMAL CONDUCTIVITY	0.505	0.216	CAL/CM.S.DEG-C
DENSITY	2.710		G/CM(3)
INITIAL TEMPERATURE		650.0	DEG-C
SOLIDIFICATION TEMPERATURE		620.0	DEG-C
DIMENSIONLESS LATENT HEAT		0.468	
INITIAL DIMENSION OF LIQUID		11.4	CM

ABOVE TEMPERATURES ARE SPECIFIED WITH 40.0 DEG-C TAKEN AS ZERO

CALCULATIONS PERFORMED FOR HEAT TRANSFER COEFFICIENT =0.0068 CAL/CM(2).S.DEG-C.

TABLE A6.2 SOLIDIFICATION OF AL/CU EUTECTIC IN THE PRESENCE OF SUPERHEAT

KSI THERMAL	TORMIN LAYER	T S STAR REACHED	T S CM BOUNDARY	THETA STAR OF LIQUID REGION	THETA C BEFORE	MOLTEN PARAM SOLIDIFICATION	T M CM STARTED	THETA D
0.011	2.8	0.0000	0.00	1.000	548.0	1.1130	10.00	605.4
0.021	5.3	0.0063	0.66	0.994	544.8	1.0296	9.34	563.1
0.031	7.8	0.0182	1.91	0.982	539.0	1.0059	8.09	551.0
0.041	10.3	0.0316	3.31	0.970	532.8	1.0006	6.69	548.3
0.051	12.8	0.0449	4.70	0.958	526.8	1.0000	5.30	548.0
0.061	15.3	0.0579	6.07	0.947	521.2	1.0000	3.93	548.0
0.071	17.8	0.0706	7.40	0.937	515.9	1.0000	2.60	548.0
0.081	20.3	0.0830	8.70	0.927	510.9	1.0000	1.30	548.0
0.091	22.8	0.0951	9.97	0.918	506.1	1.0000	0.03	548.0
0.092	22.8	0.0953	9.99	0.917	506.1	1.0000	0.01	548.0

DATA

	SOLID	MOLTEN	UNITS
WEIGHT THERMAL CAPACITY	0.219	0.228	CAL/G.DEG-C
THERMAL CONDUCTIVITY	0.566	0.239	CAL/CM.S.DEG-C
DENSITY	3.520		G/CM(3)
INITIAL TEMPERATURE		608.0	DEG-C
SOLIDIFICATION TEMPERATURE		508.0	DEG-C
DIMENSIONLESS LATENT HEAT		0.688	
INITIAL DIMENSION OF LIQUID		10.0	CM

ABOVE TEMPERATURES ARE SPECIFIED WITH 40.0 DEG-C TAKEN AS ZERO

CALCULATIONS PERFORMED FOR HEAT TRANSFER COEFFICIENT =0.0054 CAL/CM(2).S.DEG-

TABLE A6.3 SOLIDIFICATION OF AL/SI EUTECTIC IN THE PRESENCE OF SUPERHEAT

KSI	TORMIN	T S STAR	T S CM	THETA STAR	THETA C	MOLTEN PARAM	T M CM	THETA D
0.003	0.3	0.0000	0.00	1.000	577.0	0.0931	5.78	627.0
0.005	0.5	0.0006	0.04	0.999	576.7	0.1505	9.34	627.0
0.007	0.6	0.0012	0.08	0.999	576.4	0.1713	10.63	627.0
0.007	0.6	0.0014	0.08	0.999	576.3	0.1760	10.92	627.0
THERMAL LAYER HAS REACHED BOUNDARY OF LIQUID REGION								
0.017	1.5	0.0074	0.46	0.993	573.0	1.0594	10.54	608.9
0.027	2.4	0.0150	0.93	0.985	569.1	1.0368	10.07	596.8
0.037	3.3	0.0235	1.46	0.977	564.8	1.0218	9.54	588.7
0.047	4.2	0.0326	2.02	0.969	560.3	1.0121	8.98	583.5
0.057	5.1	0.0420	2.61	0.960	555.7	1.0062	8.39	580.3
0.067	6.0	0.0516	3.20	0.952	551.2	1.0028	7.80	578.5
0.077	6.9	0.0611	3.79	0.944	546.9	1.0011	7.21	577.6
0.087	7.8	0.0707	4.39	0.936	542.6	1.0004	6.61	577.2
0.097	8.6	0.0801	4.97	0.928	538.5	1.0001	6.03	577.1
0.107	9.5	0.0894	5.55	0.921	534.5	1.0000	5.45	577.0
0.117	10.4	0.0986	6.12	0.914	530.7	1.0000	4.88	577.0
0.127	11.3	0.1077	6.68	0.907	527.0	1.0000	4.32	577.0
0.137	12.2	0.1166	7.24	0.900	523.5	1.0000	3.76	577.0
0.147	13.1	0.1254	7.78	0.894	520.0	1.0000	3.22	577.0
0.157	14.0	0.1342	8.33	0.888	516.7	1.0000	2.67	577.0
0.167	14.9	0.1428	8.86	0.882	513.4	1.0000	2.14	577.0
0.177	15.8	0.1513	9.39	0.876	510.3	1.0000	1.61	577.0
0.187	16.7	0.1598	9.91	0.870	507.2	1.0000	1.09	577.0
0.197	17.6	0.1681	10.43	0.865	504.3	1.0000	0.57	577.0
0.207	18.5	0.1764	10.95	0.859	501.4	1.0000	0.05	577.0

DATA

	SOLID	MOLTEN	UNITS
WEIGHT THERMAL CAPACITY	0.222	0.230	CAL/G.DEG-C
THERMAL CONDUCTIVITY	0.422	0.211	CAL/CM.S.DEG-C
DENSITY	2.640		G/CM(3)
INITIAL TEMPERATURE		587.0	DEG-C
SOLIDIFICATION TEMPERATURE		537.0	DEG-C
DIMENSIONLESS LATENT HEAT		0.923	
INITIAL DIMENSION OF LIQUID		11.0	CM

ABOVE TEMPERATURES ARE SPECIFIED WITH 40.0 DEG-C TAKEN AS ZERO

CALCULATIONS PERFORMED FOR HEAT TRANSFER COEFFICIENT =0.0068 CAL/CM(2).S.DEG-C.

TABLE A6.4

SOLIDIFICATION OF FE-C-P AT ZERO SUPERHEAT WITH H=0.0060 CAL/CM(2).S.DEG-C

KSI	TSTAR	THETA STAR	TIME (MIN)	THICK(CM)	SURFACE TEMP (C)
0.000	0.000	1.000	0.00	0.00	950.0
0.020	0.048	0.957	0.80	0.56	910.7
0.040	0.090	0.924	1.60	1.05	881.0
0.060	0.129	0.897	2.39	1.51	856.7
0.080	0.165	0.875	3.19	1.93	836.1
0.100	0.200	0.855	3.99	2.34	818.1
0.120	0.233	0.838	4.79	2.73	802.2
0.140	0.265	0.822	5.59	3.10	787.8
0.160	0.295	0.807	6.38	3.46	774.8
0.180	0.325	0.794	7.18	3.80	762.8
0.200	0.354	0.782	7.98	4.14	751.7
0.220	0.382	0.771	8.78	4.47	741.5
0.240	0.410	0.760	9.58	4.79	731.8
0.260	0.437	0.750	10.37	5.11	722.8
0.280	0.463	0.741	11.17	5.42	714.3
0.300	0.489	0.732	11.97	5.72	706.3
0.320	0.514	0.724	12.77	6.02	698.7
0.340	0.539	0.716	13.57	6.31	691.4
0.360	0.564	0.708	14.36	6.59	684.5
0.380	0.588	0.701	15.16	6.88	678.0
0.400	0.612	0.694	15.96	7.16	671.7
0.420	0.635	0.688	16.76	7.43	665.6
0.440	0.658	0.681	17.56	7.70	659.8
0.460	0.681	0.675	18.35	7.97	654.3
0.480	0.704	0.669	19.15	8.23	648.9
0.500	0.726	0.663	19.95	8.50	643.8
0.520	0.748	0.658	20.75	8.75	638.8
0.540	0.770	0.653	21.55	9.01	634.0
0.560	0.792	0.648	22.34	9.26	629.3
0.580	0.813	0.643	23.14	9.51	624.8
0.600	0.834	0.638	23.94	9.76	620.4

TABLE A6.5 SOLIDIFICATION OF FE-C-P EUTECTIC IN THE PRESENCE OF SUPERHEAT

KSI	TORMIN	T S STAR	T S CM	THETA STAR	THETA C	MOLTEN PARAM	T M CM	THETA D
0.001	0.0	0.0000	0.00	1.000	950.0	0.0628	0.56	1000.0
0.050	1.2	0.0669	0.77	0.925	882.0	0.4583	4.06	1000.0
0.100	2.3	0.1684	1.49	0.871	832.4	0.5846	5.18	1000.0
0.150	3.5	0.2420	2.14	0.830	795.1	0.6726	5.96	1000.0
0.200	4.6	0.3099	2.75	0.797	765.2	0.7429	6.58	1000.0
0.250	5.8	0.3738	3.31	0.770	740.3	0.8027	7.11	1000.0
0.300	6.9	0.4344	3.85	0.746	718.8	0.8553	7.58	1000.0
0.325	7.5	0.4636	4.11	0.735	709.2	0.8795	7.79	1000.0
0.328	7.6	0.4672	4.14	0.734	708.0	0.8824	7.82	1000.0
0.330	7.6	0.4690	4.16	0.733	707.4	0.8839	7.83	1000.0
0.331	7.6	0.4699	4.16	0.733	707.1	0.8846	7.84	1000.0
THERMAL LAYER HAS REACHED BOUNDARY OF LIQUID REGION								
0.381	8.8	0.5263	4.66	0.714	689.7	1.0514	7.34	996.8
0.431	9.9	0.5804	5.14	0.697	674.2	1.0472	6.86	993.0
0.481	11.1	0.6327	5.61	0.681	660.1	1.0426	6.39	988.7
0.531	12.2	0.6835	6.06	0.667	647.3	1.0375	5.94	984.1
0.581	13.4	0.7332	6.50	0.654	635.5	1.0320	5.50	979.2
0.631	14.5	0.7819	6.93	0.642	624.5	1.0265	5.07	974.1
0.681	15.7	0.8301	7.36	0.631	614.3	1.0209	4.64	969.0
0.731	16.8	0.8778	7.78	0.620	604.6	1.0156	4.22	964.2
0.781	18.0	0.9252	8.20	0.610	595.5	1.0108	3.80	959.8
0.831	19.1	0.9724	8.62	0.601	585.9	1.0067	3.38	956.1
0.881	20.3	1.0194	9.03	0.592	578.8	1.0036	2.97	953.2
0.931	21.4	1.0662	9.45	0.584	571.0	1.0015	2.55	951.4

DATA

	SOLID	MOLTEN	UNITS
WEIGHT THERMAL CAPACITY	0.170	0.150	CAL/G.DEG-C
THERMAL CONDUCTIVITY	0.070	0.040	CAL/CM.S.DEG-C
DENSITY	7.240		G/CM(3)
INITIAL TEMPERATURE		960.0	DEG-C
SOLIDIFICATION TEMPERATURE		910.0	DEG-C
DIMENSIONLESS LATENT HEAT		0.388	
INITIAL DIMENSION OF LIQUID		12.0	CM

ABOVE TEMPERATURES ARE SPECIFIED WITH 40.0 DEG-C TAKEN AS ZERO

CALCULATIONS PERFORMED FOR HEAT TRANSFER COEFFICIENT =0.0079 CAL/CM(2).S.DEG-C.

TABLE A6.6 SOLIDIFICATION OF 4.0 WT.0/0 CU. AL-CU ALLOY WITH SUPERHEAT

TIMESTAR	TIMEMIN	THICKSTAR	THICKCM	PARSOL	PTHICKCM	PARMCL	THLCM	THETSTR	BASTEM	TOPTEM	MODE1
0.002	0.72	0.0000	0.00	0.0000	0.00	0.0682	8.72	1.201	650.0	700.0	1
0.002	0.85	0.0000	0.00	0.0007	0.09	0.0776	9.91	1.199	649.0	700.0	1
0.002	0.92	0.0000	0.00	0.0011	0.14	0.0817	10.45	1.198	648.6	700.0	1
0.002	0.95	0.0000	0.00	0.0013	0.16	0.0837	10.70	1.198	648.4	700.0	1
0.003	0.97	0.0000	0.00	0.0013	0.17	0.0847	10.83	1.197	648.3	700.0	1
THERMAL LAYER HAS REACHED BOUNDARY OF LIQUID REGION											
0.014	5.24	0.0000	0.00	0.0313	4.00	1.2113	7.00	1.168	633.2	655.3	2
0.019	7.38	0.0000	0.00	0.0579	7.40	1.2113	3.60	1.154	626.4	655.3	2
0.025	9.52	0.0000	0.00	0.0841	10.74	1.2113	0.26	1.141	619.6	655.3	2
0.025	9.65	0.0000	0.00	0.0857	10.95	1.2113	0.05	1.140	619.1	655.3	2
0.025	9.67	0.0000	0.00	0.0859	10.98	1.2113	0.02	1.140	619.1	655.3	2
0.025	9.68	0.0000	0.00	0.0860	10.99	1.2113	0.01	1.140	619.0	655.3	2
PARTIAL LAYER HAS REACHED THE REMOTE BOUNDARY											
0.036	13.95	0.0000	0.00	1.1957	11.00	0.0000	0.00	1.092	594.6	647.4	5
0.047	18.22	0.0000	0.00	1.1879	11.00	0.0000	0.00	1.015	555.7	643.5	5
0.048	18.76	0.0000	0.00	1.1867	11.00	0.0000	0.00	1.004	550.0	642.8	5
0.049	18.89	0.0000	0.00	1.1863	11.00	0.0000	0.00	1.001	548.6	642.7	5
0.049	18.92	0.0000	0.00	1.1863	11.00	0.0000	0.00	1.000	548.2	642.6	5
0.049	18.94	0.0000	0.00	1.1862	11.00	0.0000	0.00	1.000	548.0	642.6	5
BASE HAS REACHED EUTECTIC TEMPERATURE											
0.059	23.02	0.0251	3.21	1.0125	7.79	0.0000	0.00	0.978	536.7	554.4	6
0.062	24.09	0.0670	8.56	1.0125	2.44	0.0000	0.00	0.954	524.8	554.4	6
0.063	24.62	0.0852	10.89	1.0125	0.11	0.0000	0.00	0.946	520.5	554.4	6
0.063	24.64	0.0857	10.96	1.0125	0.04	0.0000	0.00	0.946	520.3	554.4	6

SPECIFIC HEAT		THERMAL CONDUCTIVITY		DENSITY		LENGTH	HEAT TRANSFER	PARTITION	FSU	LATENT HEAT	
SOLID	LIQUID	SOLID	LIQUID	ALLOY	EUTECTIC		COEFFICIENT	COEFF.		ALLOY	EUTEC
0.268	0.274	0.524	0.218	2.790	3.520	11.00	0.0041	0.2	0.95	0.659	0.038
CAL/G.DEG-C		CAL/CM.S.DEG-C		G/CM(3)		CM	CAL/CM(2).S.DEG-C		DIMENSIONLESS		

	INITIAL	M.P. SOLVENT	LIQUIDUS	SOLIDUS	AMBIENT(ZERO)
TEMPERATURES(DEG-C)	660.0	620.0	610.0	508.0	40.0

TABLE A6.7 SOLIDIFICATION OF 8.0 WT.0/0 CU. AL-CU ALLCY AT ZERC SUPERHEAT

TIMESTAR	TIMEMIN	THICKSTAR	THICKCM	PARSOL	PTHICKCM	PARMOL	THLCM	THETSTR	BASTEM	TOPTEM	MODEL
0.000	C.0C	C.CCCC	C.CC	C.0000	0.00	0.0000	0.00	1.171	635.0	635.0	7
0.012	2.71	C.CCCC	0.00	C.0866	8.48	0.0000	0.00	1.112	605.1	635.0	7
0.015	3.33	C.CCCC	0.CC	C.1004	9.84	0.0000	0.00	1.105	601.4	635.0	7
0.016	3.64	C.CCCC	C.00	0.1071	10.49	0.0000	0.00	1.102	599.7	635.0	7
0.017	3.80	C.CCCC	0.00	C.1104	10.81	0.0000	0.00	1.100	598.9	635.0	7
0.017	3.88	C.CCCC	C.CC	C.1120	10.97	0.0000	0.00	1.099	598.5	635.0	7
0.017	3.89	C.CCCC	0.00	0.1122	10.99	0.0000	0.00	1.099	598.4	635.0	7
		PARTIAL LAYER HAS REACHED THE REMCTE BCUNDARY									
0.028	6.38	C.CCCC	0.CC	1.1630	11.00	0.0000	0.00	1.073	584.9	630.8	5
0.039	8.87	C.CCCC	0.0C	1.1519	11.00	0.0000	0.00	1.037	566.9	625.2	5
0.045	10.12	C.CCCC	0.CC	1.1450	11.00	0.0000	0.00	1.016	556.C	621.7	5
0.047	10.74	C.CCCC	0.00	1.1411	11.00	0.0000	0.00	1.004	550.1	619.7	5
0.048	10.89	C.CCCC	0.CC	1.1401	11.00	0.0000	0.00	1.001	548.6	619.1	5
0.048	10.93	C.CCCC	C.CC	1.1398	11.00	0.0000	0.00	1.000	548.2	619.0	5
0.048	10.94	C.CCCC	0.00	1.1397	11.00	0.0000	0.00	1.000	548.1	619.0	5
0.048	10.95	C.CCCC	0.CC	1.1397	11.00	0.0000	0.00	1.000	548.0	619.0	5
		BASE HAS REACHED EUTECTIC TEMPERATURE									
0.059	13.27	C.0000	C.CC	1.0544	11.00	0.0000	0.00	1.000	548.C	575.6	6
0.070	15.76	0.0345	3.38	1.0118	7.62	0.0000	0.00	0.969	532.1	554.0	6
0.080	18.08	C.C899	8.81	1.0000	2.19	0.0000	0.00	0.931	513.1	548.0	6
0.083	18.71	0.1047	10.26	1.0000	0.74	0.0000	0.00	0.923	508.8	548.0	6
0.084	19.02	C.1119	10.97	1.0000	0.03	0.0000	0.00	0.919	506.8	548.0	6
0.084	19.03	0.1122	10.99	1.0000	0.01	0.0000	0.00	0.919	506.7	548.0	6

SPECIFIC HEAT SOLID	SPECIFIC HEAT LIQUID	THERMAL CONDUCTIVITY SOLID	THERMAL CONDUCTIVITY LIQUID	DENSITY ALLOY	DENSITY EUTECTIC	LENGTH	HEAT TRANSFER COEFFICIENT	PARTITION COEFF.	FSU	LATENT HEAT ALLOY	LATENT HEAT EUTEC
0.261	0.268	C.529	C.22C	2.670	3.520	11.00	0.0054	0.2	0.84	0.670	0.116
CAL/G.DEG-C		CAL/CM.S.DEG-C		G/CM(3)		CM	CAL/CM(2).S.DEG-C		DIMENSIONLESS		

	INITIAL	M.P. SCLVENT	LIQUIDUS	SCLIDUS	AMBIENT(ZERO)
TEMPERATURES(DEG-C)	595.C	620.0	595.0	508.0	40.0

TABLE A6.8 SOLIDIFICATION OF 30.0 WT.0/0 CU. AL-CU ALLOY WITH SUPERHEAT

TIMESTAR	TIMEMIN	THICKSTAR	THICKCM	PARSOL	PTHICKCM	PARMOL	THLCM	THETSTR	BASTEM	TOPTEM	MODEL
0.010	1.57	0.0000	0.00	0.0000	0.00	0.1618	13.35	1.024	560.0	660.0	1
0.012	1.80	0.0000	0.00	0.0029	0.24	0.1749	14.43	1.017	556.6	660.0	1
0.012	1.85	0.0000	0.00	0.0036	0.29	0.1777	14.66	1.016	555.9	660.0	1
0.012	1.86	0.0000	0.00	0.0036	0.30	0.1780	14.69	1.015	555.8	660.0	1
THERMAL LAYER HAS REACHED BOUNDARY OF LIQUID REGION											
0.015	2.29	0.0000	0.00	0.0080	0.66	1.2046	14.34	1.006	551.2	651.9	2
0.016	2.50	0.0000	0.00	0.0100	0.83	1.1967	14.17	1.002	549.2	647.9	2
0.017	2.61	0.0000	0.00	0.0111	0.91	1.1928	14.09	1.000	548.2	646.0	2
0.017	2.64	0.0000	0.00	0.0113	0.93	1.1919	14.07	1.000	548.0	645.5	2
BASE HAS REACHED EUTECTIC TEMPERATURE											
0.028	4.29	0.0038	0.32	0.0171	1.41	1.1346	13.28	0.996	546.1	616.4	4
0.039	6.00	0.0110	0.90	0.0236	1.95	1.0925	12.15	0.989	542.5	595.0	4
0.050	7.70	0.0201	1.66	0.0329	2.71	1.0625	10.63	0.980	538.1	579.8	4
0.062	9.57	0.0316	2.61	0.0488	4.02	1.0399	8.37	0.970	532.6	568.3	4
0.073	11.28	0.0430	3.55	0.0753	6.21	1.0271	5.24	0.960	527.4	561.8	4
0.083	12.87	0.0543	4.48	0.1135	9.36	1.0236	1.16	0.950	522.5	560.0	4
PARTIAL LAYER HAS REACHED THE REMOTE BOUNDARY											
0.094	14.58	0.0668	5.51	1.0210	9.49	0.0000	0.00	0.939	517.2	558.7	6
0.105	16.29	0.0791	6.53	1.0178	8.47	0.0000	0.00	0.929	512.1	557.0	6
0.116	18.00	0.0914	7.54	1.0142	7.46	0.0000	0.00	0.920	507.3	555.2	6
0.127	19.71	0.1038	8.56	1.0103	6.44	0.0000	0.00	0.910	502.5	553.2	6
0.138	21.41	0.1164	9.60	1.0064	5.40	0.0000	0.00	0.901	497.9	551.2	6
0.149	23.12	0.1294	10.68	1.0030	4.32	0.0000	0.00	0.892	493.2	549.5	6
0.160	24.82	0.1428	11.78	1.0007	3.22	0.0000	0.00	0.883	488.6	548.4	6
0.171	26.54	0.1563	12.90	1.0000	2.10	0.0000	0.00	0.874	484.1	548.0	6
0.183	28.41	0.1710	14.11	1.0000	0.89	0.0000	0.00	0.865	479.4	548.0	6
0.188	29.26	0.1776	14.65	1.0000	0.35	0.0000	0.00	0.861	477.4	548.0	6
0.191	29.69	0.1809	14.92	1.0000	0.08	0.0000	0.00	0.859	476.3	548.0	6

SPECIFIC HEAT SOLID	SPECIFIC HEAT LIQUID	THERMAL CONDUCTIVITY SOLID	THERMAL CONDUCTIVITY LIQUID	DENSITY ALLOY	DENSITY EUTECTIC	LENGTH	HEAT TRANSFER COEFFICIENT	PARTITION COEFF.		FSU LATENT HEAT ALLOY	FSU LATENT HEAT EUTEC
0.224	0.231	0.561	0.236	3.430	3.520	15.00	0.0068	0.2	0.13	0.815	0.602
CAL/G.DEG-C		CAL/CM.S.DEG-C		G/CM(3)		CM	CAL/CM(2).S.DEG-C	DIMENSIONLESS			

	INITIAL	M.P. SOLVENT	LIQUIDUS	SOLIDUS	AMBIENT(ZERO)
TEMPERATURES(DEG-C)	620.0	620.0	520.0	508.0	40.0

TABLE A6.9

SOLIDIFICATION OF AL/SI EUTECTIC AT CONSTANT RATE OF .50 CM PER MIN

TIME (MIN)	THICK(CM)	SURFACE TEMP (C)	HEAT TRANS.COEFF. CAL/CM(2).S.DEG-C	CU.FT/MIN	MM2/C
0.00	0.00	577.0	0.00451	40.5	29.9
0.83	0.41	574.6	0.00455	41.3	30.9
1.66	0.83	572.2	0.00459	42.0	31.9
2.49	1.24	569.8	0.00463	42.7	33.0
3.32	1.65	567.4	0.00468	43.4	34.1
4.15	2.07	565.0	0.00472	44.2	35.3
4.98	2.49	562.5	0.00477	44.9	36.5
5.80	2.90	560.1	0.00481	45.7	37.8
6.63	3.32	557.6	0.00486	46.5	39.1
7.46	3.73	555.2	0.00490	47.3	40.5
8.29	4.15	552.7	0.00495	48.1	41.9
9.12	4.56	550.2	0.00500	49.0	43.4
9.95	4.98	547.7	0.00505	49.9	44.9
10.78	5.39	545.2	0.00510	50.7	46.5
11.61	5.80	542.6	0.00515	51.6	48.2
12.44	6.22	540.1	0.00520	52.6	50.0
13.27	6.63	537.5	0.00525	53.5	51.8
14.10	7.05	535.0	0.00530	54.5	53.7
14.93	7.46	532.4	0.00536	55.5	55.6
15.75	7.88	529.8	0.00541	56.5	57.7
16.58	8.29	527.2	0.00547	57.5	59.9
17.41	8.71	524.6	0.00552	58.6	62.1
18.24	9.12	521.9	0.00558	59.7	64.4
19.07	9.54	519.3	0.00564	60.8	66.9
19.90	9.95	516.6	0.00570	62.0	69.4

DATA

		UNITS
SPECIFIC HEAT	0.222	CAL/G.DEG-C
THERMAL CONDUCTIVITY	0.421	CAL/CM.S.DEG-C
DIMENSIONLESS LATENT HEAT	0.923	
SOLIDIFICATION TEMP.(ZERO=40.0 DEG-C)	537.0	DEG-C
DENSITY	2.64	G/CM(3)

TABLE A6.10

SOLIDIFICATION OF PB/SN EUTECTIC AT CONSTANT RATE OF .20 CM PER MIN

TIME (MIN)	THICK(CM)	SURFACE TEMP (C)	HEAT TRANS.COEFF. CAL/CM(2).S.DEG-C	CU.FT/MIN	MMH2O
0.00	0.00	183.0	0.00170	7.6	1.0
1.25	0.25	182.5	0.00171	7.7	1.1
2.50	0.50	182.0	0.00172	7.8	1.1
3.75	0.75	181.5	0.00174	7.9	1.1
5.00	1.00	181.0	0.00175	8.0	1.2
6.25	1.25	180.5	0.00176	8.1	1.2
7.50	1.50	180.0	0.00177	8.2	1.2
8.75	1.75	179.5	0.00178	8.3	1.3
10.00	2.00	179.0	0.00179	8.4	1.3
11.25	2.25	178.5	0.00180	8.5	1.3
12.50	2.50	178.0	0.00182	8.7	1.4
13.75	2.75	177.5	0.00183	8.8	1.4
15.00	3.00	177.0	0.00184	8.9	1.4
16.25	3.25	176.5	0.00185	9.0	1.5
17.50	3.50	176.0	0.00187	9.1	1.5
18.75	3.75	175.4	0.00188	9.2	1.5
20.00	4.00	174.9	0.00189	9.4	1.6
21.25	4.25	174.4	0.00190	9.5	1.6
22.50	4.50	173.9	0.00192	9.6	1.7
23.75	4.75	173.4	0.00193	9.7	1.7
25.00	5.00	172.9	0.00194	9.9	1.8
26.25	5.25	172.3	0.00196	10.0	1.8
27.50	5.50	171.8	0.00197	10.1	1.9
28.75	5.75	171.3	0.00198	10.3	1.9
30.00	6.00	170.8	0.00200	10.4	2.0

DATA

		UNITS
SPECIFIC HEAT	0.052	CAL/G.DEG-C
THERMAL CONDUCTIVITY	0.123	CAL/CM.S.DEG-C
DIMENSIONLESS LATENT HEAT	1.183	
SOLIDIFICATION TEMP.(ZERO=40.0 DEG-C)	143.0	DEG-C
DENSITY	8.30	G/CM(3)

TABLE A6.11 SOLIDIFICATION OF AL-CUAL2 IN THE PRESENCE OF SUPERHEAT

TIME(MIN)	LAYER THICKNESSES (CM) SOLID	THERMAL	BASE TEMP(C)	TEMPERATURES ABOVE BASE (C) AT HEIGHTS OF- 0.30 CM	1.97 CM	4.02 CM	5.98 CM	8.00 CM	10.00 CM
0.43	0.00	6.92	548.0	552.2	572.4	589.2	597.1	598.0	598.0
0.63	0.02	9.42	547.9	551.1	566.7	581.6	591.3	596.9	598.0
0.68	0.03	9.94	547.8	551.0	565.9	580.3	590.1	596.1	598.0
0.68	0.03	9.97	547.8	551.0	565.3	580.2	590.0	596.1	598.0
THERMAL LAYER HAS REACHED BOUNDARY OF LIQUID REGION									
2.25	0.65	9.35	544.1	545.9	555.2	552.7	566.9	569.3	569.7
3.83	1.56	8.44	538.7	540.5	551.4	554.0	555.6	556.3	556.3
5.40	2.61	7.39	532.8	534.6	544.3	549.9	550.4	550.4	550.5
6.97	3.69	6.31	527.0	528.7	538.3	548.4	548.5	548.4	548.5
8.54	4.77	5.23	521.4	523.1	532.6	543.9	548.0	548.0	548.0
10.12	5.83	4.17	516.1	517.8	527.2	538.4	548.0	548.0	548.0
11.69	6.86	3.14	511.1	512.8	522.1	533.2	543.5	548.0	548.0
13.26	7.87	2.13	506.3	508.0	517.2	528.2	538.4	548.0	548.0
14.84	8.87	1.13	501.8	503.5	512.6	523.5	533.6	543.8	548.0
16.41	9.84	0.16	497.5	499.1	508.2	519.0	529.0	539.1	548.0
16.60	9.96	0.04	497.0	498.6	507.6	518.4	528.5	538.5	548.0
16.65	9.99	0.01	496.8	498.5	507.5	518.3	528.3	538.4	548.0

DATA

	SOLID	MOLTEN	UNITS
SPECIFIC HEAT	0.219	0.228	CAL/G.DEG-C
THERMAL CONDUCTIVITY	0.556	0.239	CAL/CM.S.DEG-C
DENSITY	3.520		G/CM(3)
INITIAL TEMPERATURE		558.0	DEG-C
SOLIDIFICATION TEMPERATURE		508.0	DEG-C
DIMENSIONLESS LATENT HEAT		0.688	
INITIAL DIMENSION OF LIQUID		10.0	CM

ABOVE TEMPERATURES ARE SPECIFIED WITH 40.0 DEG-C TAKEN AS ZERO

CALCULATIONS PERFORMED FOR HEAT TRANSFER COEFFICIENT = 0.0068 CAL/CM(2).S.DEG-C.

TABLE A6.12 SOLIDIFICATION OF AL-CUAL2 IN THE PRESENCE OF SUPERHEAT

TIME(MIN)	LAYER THICKNESSES (CM) SOLID	THERMAL	BASE TEMP(C)	TEMPERATURES ABOVE BASE (C) AT HEIGHTS OF- 0.30CM	1.97CM	4.02CM	5.98CM	8.00CM	10.00CM
0.01	0.00	1.15	548.0	550.3	553.0	553.0	553.0	553.0	553.0
0.47	0.17	9.64	547.4	548.3	549.3	551.3	552.3	552.9	553.0
0.49	0.18	9.81	547.4	548.3	549.3	551.3	552.2	552.8	553.0
0.49	0.18	9.83	547.4	548.3	549.3	551.3	552.2	552.8	553.0
THERMAL LAYER HAS REACHED BOUNDARY OF LIQUID REGION									
4.82	2.05	7.95	540.6	541.7	547.7	548.2	548.3	548.3	548.3
9.14	3.96	6.04	534.1	535.2	541.1	548.0	548.0	548.0	548.0
13.47	5.81	4.19	528.0	529.1	534.9	542.0	548.0	548.0	548.0
17.79	7.62	2.38	522.3	523.4	529.1	536.1	542.6	548.0	548.0
22.12	9.38	0.62	517.0	518.0	523.7	530.6	537.1	543.6	548.0
23.20	9.81	0.19	515.7	516.7	522.4	529.3	535.7	542.3	548.0
23.47	9.92	0.08	515.4	516.4	522.1	528.9	535.4	541.9	548.0
23.61	9.97	0.03	515.2	516.2	521.9	528.8	535.2	541.7	548.0

DATA

	SOLID	MOLTEN	UNITS
SPECIFIC HEAT	0.219	0.223	CAL/G.DEG-C
THERMAL CONDUCTIVITY	0.556	0.239	CAL/CM.S.DEG-C
DENSITY	3.520		G/CM(3)
INITIAL TEMPERATURE		513.0	DEG-C
SOLIDIFICATION TEMPERATURE		508.0	DEG-C
DIMENSIONLESS LATENT HEAT		0.688	
INITIAL DIMENSION OF LIQUID		10.0	CM

ABOVE TEMPERATURES ARE SPECIFIED WITH 40.0 DEG-C TAKEN AS ZERO

CALCULATIONS PERFORMED FOR HEAT TRANSFER COEFFICIENT =0.0041 CAL/CM(2).S.DEG-C.

TABLE A6.13 SOLIDIFICATION OF AL-CUAL2 IN THE PRESENCE OF SUPERHEAT

TIME(MIN)	LAYER THICKNESSES (CM)		BASE TEMP(C)	TEMPERATURES ABOVE BASE (C) AT HEIGHTS OF-					
	SOLID	THERMAL		0.30 CM	1.97 CM	4.02 CM	5.98 CM	8.00 CM	10.00 CM
THERMAL LAYER	REACHED	BOUNDARY OF LIQUID REGION		BEFORE SOLIDIFICATION STARTED					
2.84	0.00	10.00	548.0	551.4	553.4	534.9	596.1	603.1	605.4
5.33	0.66	9.34	544.8	546.3	553.7	558.2	561.1	562.8	563.1
7.82	1.91	8.09	539.0	540.4	549.3	550.2	550.8	551.0	551.0
10.32	3.31	6.69	532.8	534.2	541.9	548.3	548.3	548.3	548.3
12.81	4.70	5.30	526.8	528.2	535.3	545.0	548.0	548.0	548.0
15.30	6.07	3.93	521.2	522.5	530.1	539.2	547.6	548.0	548.0
17.80	7.40	2.60	515.9	517.2	524.7	533.7	542.1	548.0	548.0
20.29	8.70	1.30	510.9	512.2	519.6	528.5	536.8	545.2	548.0
22.79	9.97	0.03	506.1	507.5	514.3	523.6	531.8	540.1	548.0
22.83	9.99	0.01	506.1	507.4	514.7	523.5	531.8	540.0	548.0

DATA

	SOLID	MOLTEN	UNITS
SPECIFIC HEAT	0.219	0.228	CAL/G.DEG-C
THERMAL CONDUCTIVITY	0.556	0.239	CAL/CM.S.DEG-C
DENSITY	3.520		G/CM(3)
INITIAL TEMPERATURE		508.0	DEG-C
SOLIDIFICATION TEMPERATURE		508.0	DEG-C
DIMENSIONLESS LATENT HEAT		0.688	
INITIAL DIMENSION OF LIQUID		10.0	CM

ABOVE TEMPERATURES ARE SPECIFIED WITH 40.0 DEG-C TAKEN AS ZERO

CALCULATIONS PERFORMED FOR HEAT TRANSFER COEFFICIENT =0.0054 CAL/CM(2).S.DEG-C.

ACKNOWLEDGEMENTS

Sincere appreciation is extended to Dr. A.W.D. Hills for supervision and assistance given during the course of this work and for providing facilities at Imperial College initially, and later at the Sheffield Polytechnic. The author wishes to thank Professor A.V. Bradshaw for providing facilities in the John Percy Research Group and Mr. R.J. Tait for useful assistance.

The author is indebted to the Science Research Council for the sponsorship of this project and to Mr. U. Netanel, Urdan Metallurgical Works Ltd., Netanya , Israel and the Israel Central Trade and Investment Co., Tel-Aviv, for the grant of study leave.

Practical help in graphical presentations provided by Mrs. E. Spinat has proved invaluable.

LIST OF SYMBOLS

C	Specific heat at constant pressure
D	Thickness of original liquid metal region
E	Effective enthalpy defined by equation (3.1.2.5)
F_s	Fraction of solid in partial layer
F_{su}	Fraction of solid at the eutectic temperature
G	Growth rate
h	Heat transfer coefficient
H	Latent heat of solidification
k	Partition coefficient
K	Thermal conductivity
m	Defined in equation 6.5.1
$\dot{q}''$	Heat flux
$[\dot{q}''_o]_o$	Heat flux when the cooled surface is at the solidification temperature
R	Thermal resistance
t	Thickness of a layer
T	Time
V	Velocity of liquidus or solidus
x	Co-ordinate in solid layer

GREEK

α	Thermal diffusivity
γ	Thermal capacity
ρ	Density
θ	Temperature
δ	Co-ordinate in partial layer
λ	Co-ordinate in cooled liquid layer
Ω	Functional expression defined by equation 2.1.1.21
Γ	Functional expression defined by equation 2.1.1.22
Λ	Functional expression defined by equation 2.1.1.23
σ	Stefan Boltzman constant
ε	Emmissivity

SUFFICES

a	of air or with air
b	of the crucible base
c	Contact
d	At the insulated top of the ingot
F	For solidification of the pure solvent
L	At the liquidus or in the liquid
L,o	At the boundary of the layer of cooled liquid nearest to the cooled surface
L,t	At the boundary of the layer of cooled liquid furthest from the cooled surface
m	Initial
O	At the cooled surface
P	Within the layer of partially solidified metal
p,o	At the boundary of the partial layer nearest to the cooled surface
p,t	At the boundary of the partial layer furthest from the cooled surface
r	Radiation
S	At the solidus or within the solid layer
s,o	At the cooled surface within the solid layer
s,t	At the boundary of the solid layer furthest away from the cooled surface

DIMENSIONLESS

C*	Specific heat = $\frac{C}{C_s}$
D*	Ingot's height = $\frac{-\left[\dot{q}''_o\right]_o D}{\theta_s K_s}$
E*	Enthalpy = $\frac{E}{\rho_s C_s \theta_s}$
h*	Heat transfer coefficient = $\frac{h}{h(\text{initial})}$
H*	Latent heat = $\frac{H}{C_s \theta_s}$
K*	Thermal conductivity = $\frac{K}{K_s}$

q^* Heat flux = $\dfrac{\dot{q}''}{\left[\dot{q}''_o\right]_o}$

t^* Layer thickness = $\dfrac{-\left[\dot{q}''_o\right]_o t}{\theta_s K_s}$

α^* Thermal diffusivity = $\dfrac{\alpha}{\alpha_s}$

γ^* Thermal capacity = $\dfrac{\gamma}{\gamma_s}$

ξ Time = $\dfrac{\left[\dot{q}''_o\right]_o^2 T}{\theta_s^2 \rho_s C_s K_s}$

PARTIAL DIFFERENTIALS

$$f'_\theta = \frac{\partial q_o^*}{\partial \theta}$$

$$f'_\xi = \frac{\partial q_o^*}{\partial \xi}$$

$$g'_t = \frac{\partial q_L^*}{\partial t^*}$$

$$g'_\xi = \frac{\partial q_L^*}{\partial \xi}$$

REFERENCES

1. Hills A.W.D., TMS-AIME, 245 (1969), 1471.

2. Hansen M.,Constitution of Binary Alloys,
McGraw-Hill, New York, 2nd Edition, (1958).

3. Hills A.W.D. and Moore M.R. TMS-AIME, 245 (1969), 1481.

4. Ruddle R.W. , The Solidification of Castings,
Inst. of Metal,Monograph and report series No.7
Inst. of Metals. London (1957).

5. Hultgreen R., Orr R.L., Anderson P.D. and Kelley K.K.
Selected values of thermodynamic properties of
Metals and Alloys. John Wiley and Sons London (1963).

6. Flemings M.C.
The Solidification of Metals., I.S.I. publication
No. 110. Iron and Steel Institute, London (1968), 102.

7. Brody H.D. and Flemings M.C. TMS-AIME 236 (1966), 615.

8. Bower T.F., Brody H.D. and Flemings M.C. ibid 624.

9. Koump V., Tien R.H., and Perzak T.F. ibid 242 (1968), 1569.

10. Tien R.H. and Geiger G.E.
Journal of heat transfer, Trans-ASME, 90 (1968), 27.

11. Cho S.H. and Sunderland J.E. ibid 91, (1969), 421.

12. Flemings M.C., Porier D.R., Barone R.V. and Brody H.D.
J.I.S.I. April (1970), 371.

13. Carslow H.S. and Jaeger J.C.
Conduction of heat in solids. Oxford University
Press, 1959.

14. Data sheets on thermo physical properties. Thermo
Physical Research Centre (T.P.R.C.) Purdu University.

15. Moore M.R., Ph.D. thesis, University of London (1966).

16. Malhotra S.L., Ph.D. thesis, University of London (1969).

17. Hills A.W.D., Ph.D. thesis, University of London (1966).

18. Hunt T.D. and Chilton J.P., J. Inst. of Metals, 91 (1963), 338.

19. Tiller W.A.
Liquid metal and solidification. Amer.Soc.Metals.
Cleveland, Ohio (1958).

20. Chilton J.P. and Winegard J., J.Inst. of Metals, 89 (1960), 160.

21. Mizikar F.A., TMS-AIME, 239 (1967), 1747.

22. Tien R.H. and Koump V., ibid, 242 (1968) 1283.

23. Tien R.H. and Geiger G.E., J.Heat Transfer, Trans.ASME, 89, (1967), 230.

24. Tien R.H. and Koump V., ibid., 92, (1970), 11.

25. Goodman T.A., ibid., 80 (1958), 335.

26. Campagna A.J., Ph.D. thesis, Massachusetts Institute of Technology (1970).

27. Phelke R.D., Sinnot M.J.
Computer application in Metallurgical Engineering. ASM 1964.

28. Adenis et al., J.Inst. of Metals, 91 (1963), 395.

29. Peel D.A. and Pengally A.E.
London Conference, Iron & Steel Inst. I.S.I. report 123, Feb. (1969).

30. Goodman T.R. and Shea J.J.,
J. Applied Mechanics, Trans.ASME Series E., 82 (1960), 16.

31. Goodman T.R., J. Heat Transfer, Trans.ASME, 89 (1967), 233.

32. Jakson K.A. and Hunt J.D. TMS-AIME, 236 (1966), 1129.

33. Smithells C.,
Metals Reference Book, Butterworths 3rd Edition, London 1962.

34. Kraft R.W. and Albright D.L. TMS-AIME 221 (1967), 95.

35. Chadwick G.A., J.Inst. Metals, 91 (1963), 169.

36. Hunt J.D. and Jakson K.A., TMS-AIME, 236 (1966), 843.

37. Hellawell A., Progress in Materials Science, Pergamon Press, Volume 15, No. 1, (1970).

38. Thall B.M. and Chalmers B.J., J.Inst. of Metals, 78 (1949), 79.

39. Hellawell A. and Day M.G., Proc.Roy.Soc., 305 (1968), 473.

40. Bell J.A.E. and Winegard W.C., J.Inst. of Metals, 93 (1965), 318.

41. Chadwick G.A., Progress in Materials Science, Pergamon Press, Volume 12, No.2.

42. Fullman R.L. and Wood, D.L., Acta.Met., 2 (1954), 188.

43. Sundquist, B.E., Bruscato R. and Modolfo L.F.,
J.Inst. of Metals, 91 (1963), 204.

44. Hunt K.D. and Chilton J.P., ibid. 92 (1963), 21.

45. Chadwick, G.A., ibid. 92 (1963), 18.

46. Sundquist B.E. and Mondolfo L.F., TMS-AIME, 221(1961), 157.